

# Pancreas organoid development, behaviour and structural maintenance: a multiscale analysis

Dissertation

zur Erlangung des Doktorgrades

der Naturwissenschaften

vorgelegt beim Fachbereich Biowissenschaften

der Johann Wolfgang-Goethe-Universität

in Frankfurt am Main

von

Till Seeberger (geb. Moreth)

aus Darmstadt

Frankfurt am Main (2021)

(D30)

vom Fachbereich Biowissenschaften der  
Johann Wolfgang Goethe-Universität als Dissertation angenommen

Dekan: Prof. Dr. Sven Klimpel

Erster Gutachter: Prof. Dr. Ernst H. K. Stelzer

Zweiter Gutachter: Prof. Dr. Maike Windbergs

Datum der Disputation:

## Danksagung

Zuallererst möchte ich mich bei Herr Prof. Dr. Ernst H.K. Stelzer und Dr. Francesco Pampaloni für die Unterstützung und die Betreuung bedanken. Mein besonderer Dank gilt vor allem der wissenschaftlichen Freiheit, die mir stets gewährt wurde und dem mir allzeit entgegengebrachtem Vertrauen. Die Bereitschaft, mir jederzeit mit Rat und Tat beizustehen, empfand ich von Beginn als beruhigend und hat mir in vielen Situationen den nötigen Rückhalt gegeben. Frau Prof. Dr. Maike Windbergs danke ich für die tolle Zusammenarbeit und Hilfestellungen bei der Ausarbeitung der Ergebnisse bei der mit ihrer Arbeitsgruppe entstandenen Kooperation und für die Bereitschaft zur Begutachtung meiner Arbeit.

Ich möchte mich herzlich bei Isabell und Alexander Schmitz, Sabine Fischer, Sven Plath, Heinz Schewe und Nick Austin bedanken. Isabell hat nicht nur Korrektur gelesen, sondern stand mir stets mit Rat und Tat im Labor und der Erstellung dieser Arbeit zur Seite. Ohne Alexanders IT-Wissen und „mal eben nach der Arbeit im Labor vorbeikommen und Probleme lösen“ wäre mir die Auswertung der Bilddaten wohl kaum gelungen. Die Welt der Zahlen und Statistik hätte ich ohne Sabine nur schwer überblicken können und ohne Svens unglaublichem technischem Wissen und Einfallsreichtum wären die Aufnahmen nicht so gelungen. Der Fels in der Brandung stellte Heinz mit seiner unaufgeregten Art für mich dar und wenn es um die Handhabung eines Mikroskops ging, war er immer zur Stelle. Großen Dank geht auch an Nick, der meine Arbeit Korrektur gelesen hat und ihr damit den Feinschliff verleihen konnte.

Ganz besonders möchte ich mich hier auch bei Lotta Hof bedanken. Als mein Projekt-Kollegin wäre ohne sie die Arbeit eine andere gewesen. Alle Ergebnisse dieser Arbeit sind aus dem herausragenden Teamwork mit ihr entstanden und nur so möglich geworden. Michael Koch danke ich ebenso für seine Hilfen in vielen Bereichen. Sein Wissen hat mir immer weitergeholfen und meine Arbeit auf ein anderes Level gehoben. Bei Nathalie Jung möchte ich für ihre Zusammenarbeit im Projekt *Organoid goes Raman* bedanken. Durch ihre Offenheit für Neues und ihr Durchhaltevermögen bin ich viele Schritte vorangekommen.

Ich danke auch allen Praktikanten und Absolventen, die ich betreut habe, dafür, dass sie mir bei der Entwicklung meines Lehrstils geholfen haben. Besonders möchte ich hierbei meinen beiden Masterandinnen Julia Tarnick und Kaja Nicole Wächtershäuser hervorheben. Im Besonderen möchte ich auch Sigrun Becker für die große Unterstützung im Labor und die immer guten Worte Danken. Dem gesamten Arbeitskreis Physikalische Biologie danke ich für die gesamte Zeit. Durch die immer gute Stimmung, die tollen Betriebsausflüge, Grillabende und Ski-Urlaube war es immer eine Freude mit euch zu Arbeiten und Zeit zu verbringen. Auch den Jungs vom HRZ, Kai Richter und Sascha Rodzies möchte ich herzlich dafür danken, den Laden auf virtueller Ebene stets am Laufen gehalten zu haben.

Meinen Eltern Maria und Richard Moreth, meinem Bruder Felix Moreth und meinen Schwiegereltern Micky und Jürgen Seeberger danke ich für die immerwährenden Unterstützungen und das jederzeit für mich da sein. Zum Abschluss danke ich meiner Frau, Johanna Seeberger für die unendliche Geduld, die moralische Unterstützung und die viele Zeit, die sie mit mir bei der Fertigstellung dieser Arbeit verbracht hat. Sie hatte jederzeit ein offenes Ohr für mich und wusste mich moralisch aufzubauen und zu stärken.

## Zusammenfassung

Stammzellen stellen den Grundbaustein des menschlichen Organismus dar. Die Langzeitkultivierung unter Laborbedingungen war bislang jedoch auf embryonale, welche aus der Blastozyste gewonnen wurden, und induzierte pluripotente Stammzellen beschränkt. Seit kurzem rücken vielversprechende Forschungsansätze mehr und mehr in den Focus der Wissenschaft, in denen neben der embryonalen Stammzellkultur induzierte und gewebspezifische adulte Stammzellen in sogenannten Organoiden über mehrere Monate genetisch stabil kultiviert werden können. Diese adulten Stammzellen liegen natürlicherweise im Gewebe und in den Organen vor und werden bei Wundheilung oder regenerativen Prozessen aktiviert. Durch den Einsatz von speziellen Wachstumsbedingungen ist es seit kurzem möglich, die *in vivo* Bedingungen auch im Labor zu simulieren und damit dreidimensionale Organoiden zu züchten. Neben definierten Nährmedien kommen speziell abgestimmte Wachstumsfaktoren und eine extrazelluläre Matrix (EZM) zum Einsatz. Die EZM ermöglicht den Zellen nicht nur miteinander zu interagieren und zu kommunizieren, sondern schafft auch den strukturellen Rahmen, die der Gewebeintegrität des ursprünglichen Organs entspricht. Dadurch proliferieren diese Zellen auch im Labor, behalten ihren Stammzellcharakter und bilden Organoiden. In den vergangenen Jahren hat sich herausdefiniert, dass Organoiden dreidimensionale Zellzusammenschlüsse darstellen, welche in der Lage sind, organspezifische Zelltypen auszubilden und sich in gleicher Weise zu organisieren, wie sie in dem Ursprungs-Organ vorliegen.

Der Einsatz von Organoiden in der Grundlagenforschung verspricht weitreichende Erkenntnisse über das zelluläre Verhalten während der Organogenese, in Wundheilungsprozessen sowie in Medikamentenstudien. Daneben zeigen Organoiden im Besonderen in der personalisierten Zelltherapie enormes Potential. Bei dieser Behandlung werden dem Patienten oder Spender adulte Stammzellen aus dem entsprechenden Organ entnommen, im Labor kultiviert und ggf. gentechnisch korrigiert, differenziert und anschließend reimplantiert. Dort ersetzen oder ergänzen diese die vorhandenen Zellen in ihrer Aufgabe und tragen so zur Heilung des Patienten bei. Personalisierte Zelltherapie birgt unter anderem bei Autoimmunerkrankungen großes Potential. Eine dieser Erkrankungen ist Diabetes Typ 1 (T1D). Hierbei zerstört das körpereigene Immunsystem die  $\beta$ -Zellen der Bauchspeicheldrüse (Pankreas), welche das Hormon Insulin produzieren. Als Folge kommt es zur Deregulierung des Blutzuckerspiegels, was zu stark schwankenden und stark erhöhten Glukose-Konzentrationen im Blut führen kann (Hyperglykämie). Heutige Behandlungsmethoden basieren in erster Linie auf der Insulinersatztherapie. Durch die Transplantation der Bauchspeicheldrüse existiert zwar eine dauerhafte Heilungsmethode, diese ist aber auf Grund der geringen Verfügbarkeit von Spenderorganen nicht massentauglich. Der Einsatz von Organoiden zur personalisierten Zelltherapie von Diabetes Typ 1 verspricht daher großes Potential als eine zukünftige weitere Therapiemöglichkeit. Hierfür sind jedoch im Rahmen der präklinischen Forschung zunächst fundamentale Kenntnisse über die Organoiden zu erlangen.

2013 gelang es erstmalig Matrixell Huch Organoiden aus Pankreas Zellen zu gewinnen. Dazu isolierte Sie diese Zellen aus dem exokrinen, duktalem Bereich und etablierte sie als Organoiden im Labor. Das Erscheinungsbild der Pankreas Organoiden zeigte sich dabei als ballonartige Struktur, die von einer einzelnen Zellschicht gebildet wird und mit Flüssigkeit gefüllt ist.

Weiterreichende Untersuchungen konnten zeigen, dass nach der Transplantation dieser Organoide in immunsupprimierte, an T1D leidende Mäuse, sich diese von ihrer Erkrankung erholen konnten. Dies war möglich, da die Zellen der Organoide sich zu  $\beta$ -Zellen differenzierten, Insulin produzierten und damit die Glukosekonzentration im Blut der Mäuse regulierten. Diese Untersuchungen zeigen das hohe therapeutische Potential der Pankreas Organoide. Aufgrund der Neuartigkeit dieser Kultivierungsmethode fehlt es jedoch an fundamentalen Grundkenntnissen und ausreichend robusten Daten, um diese bereits heute klinisch einzusetzen. Informationen über deren Erscheinungsform, Verhalten und Wachstumseigenschaften sind weitestgehend unbekannt. Verlässliche Methoden zur Beobachtung und Analyse des Wachstumsverhaltens sowie weitreichendes Wissen über die biophysikalischen und biochemischen Prozesse, die zur Ausprägung und Erhalt der Erscheinungsform führen, sind nicht vorhanden. Für klinische Anwendungen sind diese Informationen jedoch unumgänglich und bilden daher derzeit einen bedeutsamen Bereich in der präklinischen Forschung.

Aus diesem Grund war die zentrale Zielsetzung dieser Arbeit, Analysemethoden zu entwickeln, mit deren Hilfe verschiedene Aspekte der Pankreas Organoid Kultur untersucht wurden. Hauptsächlich wurden dabei Hellfeld-, Lichtscheiben- und Fluoreszenzmikroskopie angewendet, sowie halbautomatisierte Auswertungs- und Analyse Pipelines formuliert.

(1) Es wurde ein bestehendes Immunfärbeprotokoll entsprechend der Anwendung für Organoide erstellt, um u.a. die Identität der Organoide zu validieren. (2) Zur Lebendbeobachtung wurde eine halbautomatisierte Hochdurchsatz-Pipeline entwickelt, welche basierend auf der Hellfeldmikroskopie die Analyse des Wachstumsverhaltens hunderter Organoiden erlaubt (Hellfeld-Pipeline). (3) Zusätzlich wurde eine weitere halbautomatisierte Pipeline entwickelt, welche auf Lichtscheibenmikroskopie basiert und die Auswertung zeitlich und räumlich hochaufgelösten Bildern ermöglicht (Lichtscheiben-Prozessierungs-Pipeline). Damit konnte die Analyse von Organoidwachstum und -verhalten auf einem zellulären Level realisiert werden. (4) Des Weiteren wurde ein neuartiger und speziell für den Einsatz in der Organoid-Kultur geeigneter Probenhalter konstruiert. Mit diesem Halter und unter Einsatz der Lichtscheiben-Prozessierungs-Pipeline konnten grundlegende Wachstumseigenschaften identifiziert und definiert werden und eine Vielzahl von verschiedentlichen Verhaltensmustern aufgezeigt werden. (5) Wie beschrieben, benötigen Organoide zur Kultivierung eine EZM. Diese wird aus genetisch veränderten tierischen Krebszellen gewonnen und ist deshalb nicht für den klinischen Einsatz geeignet. Neben der Entwicklung von synthetischen, vergleichbaren Matrices ist eine Reduktion des Einsatzes dieser EZM eine grundlegende Voraussetzung für den klinischen Erfolg. Daher wurde in dieser Arbeit eine alternative Kultivierungsmethode entwickelt, welche den Einsatz von EZM signifikant reduziert und dabei gleichzeitig die Langzeitkultivierung der Organoide fördert. (6) Um den phänotypischen Aufbau der Organoide zu verstehen, wurde eine nicht-invasive chemische Analysemethode herangezogen (Konfokale Raman-Mikroskopie), mit dessen Hilfe erstmalig die Flüssigkeit im Innern der Organoide untersucht werden konnte. (7) Basierend auf diesen Erkenntnissen wurde das weiterentwickelte Immunfärbeprotokoll angewendet, um zelluläre Kanalproteine zu identifizieren, welche an dem Aufbau und dem Erhalt des Organoid-Phänotyps beteiligt sind. (8) Neben der Identifizierung dieser Proteine, wurde die Hellfeld-Pipeline ergänzend angewendet, um die Rolle verschiedener Cytoskelett- und Adhäsions-

assoziierten Proteine zu untersuchen und die Funktion der identifizierten Kanalproteine bei der phänotypischen Entwicklung und Aufrechterhaltung der Organoide zu beleuchten.

Auf Grund des Aufbaus von Pankreas Organoiden als monozelluläre, ballonartige Zellverbände eignen diese sich prinzipiell gut, um mittels Fluoreszenzmarkierung untersucht zu werden. Durch die umgebende EZM sind sie jedoch einerseits von einer physikalischen Barriere umgeben, andererseits beinhaltet die EZM Epitope, an welche die Antikörper bei der Färbung anbinden. Die Folge ist, dass die Antikörper die Organoide nur in geringem Maße erreichen und die EZM eine große Hintergrundfärbung hervorruft. Um das zu vermeiden wurde in dieser Arbeit ein Färbeprotokoll entwickelt, welches mittels geringer Temperatur und mechanischem Kräfteinsatz die Organoide während der Fixierung aus der EZM herauslöst. Damit war die anschließende Färbung mittels Fluoreszenzfarbstoffen ohne Hintergrundfärbung möglich und erlaubte die hochauflösende Darstellung mittels konfokaler Mikroskopie. Die phänotypisch sphärische Struktur konnte dabei weitestgehend beibehalten und abgebildet werden. Dies ermöglicht die Organoide auf ihre Identität hin zu untersuchen und festzustellen, dass sie alle Merkmale aufweisen, die den Stammzellencharakter validieren. Des Weiteren konnten polarisierte Zellskelettstrukturen anhand von Aktin, sowie Adhäsions- und adhäsionsassoziierte Moleküle, wie beispielsweise Cadherine, identifiziert werden. Daraus wurde geschlossen, dass eine klar definierte zelluläre Organisation benötigt wird, um den Phänotyp der Organoide aufrecht zu erhalten.

Sowohl humane als auch murine Pankreas Organoide wachsen in der sie umgebenden EZM zu verschiedenen Größen heran. Hellfeldmikroskopie wurde hierbei genutzt, um weitere dynamische Wachstums- und Verhaltensprozesse zu analysieren. Neben der Formierung der Organoide konnte die Fusion von zwei oder mehreren Organoiden beobachtet werden. Zudem konnte gezeigt werden, dass nicht jedes Organoid eine sphärische Struktur ausbildet, sondern auch kompakt bleiben kann. Daneben wurde deutlich, dass Organoide sehr beweglich in der EZM sind und mehrere hundert Mikrometer migrieren können, nachdem und bevor sie ihre phänotypische Struktur ausbilden. All diese Beobachtungen zeigen, dass Pankreas Organoide eine enorme Heterogenität in ihrem Phänotyp aufweisen. Um trotzdem robuste und valide Daten über das Wachstumsverhalten zu generieren, wurde eine halbautomatisierte Hochdurchsatz-Pipeline entwickelt. Diese basiert auf zeitlich aufgelösten Hellfeldmikroskop-Aufnahmen von mehreren Organoid Kulturen, welche hunderte von Organoiden beinhalten können. Basierend auf diesen Aufnahmen wurde die Größenzunahme pro Zeitintervall der einzelnen Organoide ermittelt. Durch die Analyse von hunderten von Organoiden konnten so trotz großer Heterogenität robuste Daten erhoben werden, welche unter anderem darstellen, dass murine Organoide weitestgehend innerhalb der ersten drei Tage ihre maximale Größe erreichen. Humane Organoide hingegen zeigen eine langsamere, aber konstantere Größenzunahme und benötigten vier bis fünf Tage, um ihr maximale Größe zu erreichen. Der Einsatz der Hellfeld-Pipeline erlaubt die Generierung robuster und valider Daten über das Wachstum bzw. die Größenzunahmen der Organoide aufgelöst über die Zeit. Die Betrachtung und Auswertung einzelner Organoide ist dabei auch möglich, bietet jedoch nur eine limitierte Aussagekraft über das dynamische Verhalten. Des Weiteren erlaubt diese Analyse keine Aussage über zelluläre Abläufe. Um die Pankreas Organoide aber in ihrer Gesamtheit zu erfassen, ist es von größter Wichtigkeit, auch die zelluläre Eben abzubilden und die bereits beobachteten Prozesse genauer zu untersuchen. Dafür wurde ein Probenhalter für die Nutzung in dem kommerziell erhältlichen Zeiss Lightsheet Z.1 entwickelt. Dieser basiert auf

einer speziellen Folie (Tetrafluorethylen-Hexafluorpropylen-Copolymer (FEP)), welche bereits in anderen Lichtscheibenmikroskopen angewendet wird. Dieser Probenhalter erlaubt die zeitlich und räumlich hochaufgelöste Observierung einer Organoid Kultur über mehrere Tage und garantiert gleichzeitig optimale Wachstumsbedingungen. Um die generierten Datensätze auswerten zu können, wurde eine bereits für Sphäroide entwickelte Prozessierungs-Pipeline herangezogen und auf die Auswertung von Organoid-Datensätzen optimiert. Mit Hilfe dieser Auswertung konnten robuste und valide Daten über Zellzahl, Zellkerngröße und Nachbarschaftsverhältnisse der einzelnen Zellen generiert werden. Des Weiteren konnte die Gesamtoberfläche und das Volumen des untersuchten Organoids berechnet werden. Durch die hohe zeitliche Auflösung konnten nicht nur alle bereits beschriebenen Dynamiken des Organoid-Wachstums, sondern auch neue Erkenntnisse über Zellrotation und verschiedenliche Migrationsereignisse von Einzelzellen innerhalb eines Organoids, komplexe zelluläre Umstrukturierungen innerhalb des Organoid-Lumens, sowie die gesamtheitliche Bewegung eines Organoids erlangt werden. Die betrachteten Ergebnisse haben große biologische Bedeutung, um beispielsweise Dynamiken in Epithel-Zellverbänden zu verstehen und Wundheilungsprozesse sowie die Organogenese während der Embryonalentwicklung abzubilden und untersuchen zu können.

Bereits in der Hellfeld-Analyse wurden große Fluktuationen des Organoid Volumens beobachtet (Größen-Oszillation). Dieser dynamische Prozess wurde bisher nur wenig untersucht, zelluläre Abläufe, Häufigkeit und Ausprägung sind dabei so noch nie quantitativ sowie qualitativ ausgewertet worden. Der Einsatz der Hellfeldmikroskopie gepaart mit der Lichtscheibenmikroskopie erlaubte erstmalig eine detaillierte einzelzell-basierende Analyse dieser Dynamiken und erbrachte die Erkenntnis, dass die Frequenz der Größen-Oszillation mit der Größe der Organoid abnimmt. Dies konnte anhand von Zellzahl, Volumen und der Oberfläche der Organoid ermittelt werden. Des Weiteren konnte gezeigt werden, dass nicht alle Organoid die gleiche Zelldichte besitzen. Demnach liegt auch hier eine große Heterogenität vor. Diese Daten wurden in einer Kooperation benutzt, um ein Modell zu erstellen, welches diese Organoid Dynamik abbilden und beispielsweise dazu genutzt werden kann, verschiedene Wachstumsdynamiken zu modellieren, um damit die große Heterogenität abbilden und verstehen zu können.

Alle erbrachten Erkenntnisse zeigen, dass die Pankreas Organoid-Kultur eine hohe Dynamik aufweist. Inwieweit der Einsatz von einer soliden EZM zur Schaffung eines strukturellen Rahmens dabei eine Rolle spielt, war bisher nicht bekannt. Daneben war es ein Ziel dieser Arbeit, den Einsatz eben dieser zu minimieren, um den klinischen Erfolg prinzipiell zu ermöglichen. Aus diesem Grund wurde eine bereits aus der Sphäroid-Kultur bekannte Kultivierungsmethode (Hanging-Drop) zur Kultivierung von Pankreas Organoiden angewendet und soweit optimiert, dass die Langzeitkultivierung unter Einsatz von nur 4 % EZM möglich war. Der geringe Einsatz der EZM führte auch dazu, dass die Organoiden sich nicht mehr in einem soliden, sondern in einem wässrigen Umfeld entwickeln konnten. Da der Phänotyp jedoch erhalten blieb, zeigten diese Experimente, dass die Organoid keine solide Matrix benötigen, um ihren Phänotyp zu entwickeln.

Um zu verstehen, wie der Organoid in der Lage ist seine sphärische Struktur aufzubauen und aufrecht zu erhalten, wurde erstmalig die Lumen Flüssigkeit untersucht. Auf Grund des

Phänotyps und der damit verbundenen Sensibilität der Organoide war eine Entnahme der Lumen Flüssigkeit und eine anschließende Analyse, zum Beispiel mittels Hochleistungsflüssigkeitschromatography (HPLC), nicht möglich. Daher wurde, in einer institutsinternen Kooperation, erstmalig die Konfokale Raman-Mikroskopie adaptiert und angewendet, um die Lumen Flüssigkeit chemisch zu analysieren. Dabei wurden sowohl fixierte als auch lebende Organoide nicht-invasiv untersucht. Neben Erkenntnissen über die Zellschichten selbst, war es dabei möglich das Lumen vom der umgebenden EZM abzugrenzen und dessen chemisch Zusammensetzung zu analysieren. Dabei wurde nachgewiesen, dass der Hauptbestandteil der Lumen-Flüssigkeit Wasser ist, spezifische Molekülverbindungen/-konzentrationen lagen jedoch nicht vor. Des Weiteren wurde gezeigt, dass in der chemischen Zusammensetzung kein Unterschied zwischen der Lumen-Flüssigkeit und der Organoid-umgebenden Flüssigkeit besteht. Dass die Proteine sowie die Bestandteile der EZM im Lumen des Organoids mit zunehmender Größe des Organoids relativ abnehmen, deutet zudem darauf hin, dass der Organoid selbst den Wasser-Einfluss in das Lumen steuert und so den Phänotyp und die observierte Dynamik der Größen-Oszillation bewirkt.

Schlussfolgernd wurden mögliche zelluläre und molekulare Mechanismen untersucht, die den Wassereinfluss in das Lumen steuern und regulieren. Mittels Fluoreszenzmarkierung wurden in der Zellmembran von Pankreas Organoiden erstmalig Aquaporine (1,5 und 8) nachgewiesen. Diese beschreiben eine Gruppe von Kanalproteinen, die den Wasser Ein- und Ausstrom durch die Zellmembran fördern können. Zudem wurden die aus anderen Organoid-Systemen (Lunge und Darm) bekannte Chlorid-Kanal Cystic Fibrosis Transmembrane Conductance Regulator (CFTR) identifiziert und lokalisiert, welche darauf hindeuten, dass der Wassereinstrom durch einen osmotischen Gradienten innerhalb der Epithelzellen begünstigt bzw. reguliert wird. Auf Grund des phänotypischen Erscheinungsbildes und der observierten Dynamik der Pankreas Organoide wurde die Vermutung erhoben, dass mechanische Einflüsse eine große Rolle bei der Regulierung des osmotischen Gradienten spielen könnten. Das am häufigsten vorkommende mechanosensitive Kanalprotein PIEZO-1 konnte mittels Fluoreszenzmarkierung auch in der Zellmembran der Organoid Zellen erstmalig nachgewiesen werden, was die aufgestellte Hypothese verstärkt.

In einer breit angelegten Inhibierungsstudie, bei welcher die vorab entwickelte Hellfeld-Pipeline angewendet wurde, wurden die identifizierten Proteine auf ihre Funktion hin analysiert. Zunächst konnte verifiziert werden, dass die Zytoskelettproteine Aktin und Tubulin einen essenziellen Bestandteil zur Aufrechterhaltung der Struktur der Organoide bilden. Zusätzlich wurde das Aktin assoziierte Motorprotein Myosin 2 als relevantes Protein identifiziert, welches durch die Erzeugung von mechanischer Kraft die Organoid-Ausdehnung verhindert. Weiterhin konnte gezeigt werden, dass der Ionen-Kanal CFTR zum Phänotyp der Organoide beiträgt. Eine Inhibierung dieses Kanals durch die Kombination zweier Wirkstoffe (GlyH-101, CFTRinh-172) führte zu einer signifikanten Verkleinerung der Organoide, welche sich nach Beendigung der Inhibierung als reversibel herausstellte. Neben CFTR wurde auch der Einfluss des mechanosensitive Ionen-Kanalproteins PIEZO-1 untersucht. Dabei stellte sich heraus, dass eine Deaktivierung des Kanals nur in humanen Organoiden zu einer Vergrößerung des Organoid-Phänotyps führte. Dagegen führt eine Aktivierung zu einer signifikanten Größenabnahme sowohl in humanen als auch murinen Organoiden. Auch dieses Verhalten war reversibel, was sich in einer Wachstumskompensation nach Beendigung der Behandlung äußerte. Aus diesen Ergebnissen ging hervor, dass PIEZO-1 zwar in den Organoid-Zellen



vorliegt, jedoch in murinen Organoiden vorwiegend inaktiviert ist. Das beobachtete Verhalten nach Aktivierung des Proteins lässt jedoch auf eine regulatorische Funktion während der Organoid Entwicklung in beiden Spezies schließen.

Die Ergebnisse dieser Arbeit legen den Grundstein für ein weitreichendes Verständnis der Formierung, des Wachstums und der Dynamik von Pankreas Organoid Kulturen. Durch die Entwicklung der Hellfeld- und Lichtscheiben-Prozessierungs-Pipeline konnten robuste Daten gewonnen werden, welche die Definition von Wachstumsparametern für zukünftige klinische Anwendung erlauben. Die Entwicklung einer Kulturmethode, die den Einsatz von tierischem EZM vermindert, ist ein weiterer Schritt hin zur klinischen Übertragbarkeit und zeigt gleichzeitig, dass Pankreas Organoide keine solide EZM benötigen. Neben diesen grundlegenden Erkenntnissen konnten weitreichende Informationen über die Lumen-Flüssigkeit sowie beteiligte Cytoskelett-Komponenten gesammelt und potenzielle Regulationsmechanismen identifiziert werden. Zusätzlich tragen die Ergebnisse dieser Arbeit dazu bei, ein besseres Verständnis von Zellorganisationsverhalten zu erhalten und können als Modell dienen, um beispielsweise Wundheilungsprozesse *ex-vivo* zu untersuchen. Darüber hinaus werfen die Ergebnisse aber auch Fragen über die Rolle der EZM als solide Matrix oder nur als Signalgeber für zelluläre Prozesse auf. Ergänzend bestehen weitere offene Fragen über die Rolle der Aquaporine sowie der intrazellulären Regulationsmechanismen, die zum Aufbau und Erhalt der ballonartigen Struktur der Organoide führen.

## Summary

Until quite recently, stem cell technology mainly focused on pure populations of embryonic stem cells (ES) derived from the inner cell mass of the blastocyst and induced pluripotent stem cells (iPS). Using organoids, a newly established culture technique, it is now possible to culture also organ and patient-specific adult stem (AS) and induced pluripotent stem (IPS) cells *in vitro*. Furthermore, it has been shown that adult stem cells, grown as organoids, are genetically stable, proliferate and maintain their multi-potency (often a bi-potency) for months. This is possible by providing conditions that recapitulate the stem cell niche of the corresponding organ. Particularly, defined growth factors and a physiological scaffold, which is provided by an extracellular matrix (ECM). Because of increasing research activities, organoids became influential in the recent years. Wide-ranging interest also led to a clearer definition: organoids must contain multiple organ-specific cell types, must be able to recapitulate some organ specific functions, and the cells must be spatially organized in a way similar to the organ they are derived from. The excitement about organoids is based on their high potential as a model to understand wound healing, cellular behaviour and differentiation processes in organogenesis. Furthermore, high potential in the drug development and in personalized stem cell therapeutic approaches has been shown. Specifically, for personalized stem cell therapy, one potential application is for chronic autoimmune diseases such as Diabetes type 1 (T1D). T1D is characterized by the immune-mediated destruction of  $\beta$ -cells in the Pancreas that leads to absolute insulin deficiency. In T1D the first-line therapeutic approach is exogenous insulin replacement therapy, which always implicates the risk of high fluctuations in blood-sugar levels and therefore the risk of hypoglycaemia. Another therapeutic approach is the xenotransplantation of islets from human donors. A successful islet transplantation allows patients a years-long insulin independence. However, the therapeutic value of islet transplantation is highly limited by the availability of organ donors and by the need for chronic administration of immune suppressive medication. The use of pancreas organoids offers a promising alternative as a personalized cell therapeutic approach to treat T1D without the hypoglycaemia risks of the established therapies. In 2013 Meritxell Huch and colleagues established for the first-time organoids from the exocrine, ductal part of the pancreas. These pancreas organoids are characterized by a monolayered, spherical cell epithelium which comprises a liquid filled lumen. In addition, they showed that after transplantation of these cells into immunodeficient mice, they differentiate into  $\beta$ -cells and cure T1D. However, basic knowledge of the culture growth behaviour is still lacking: to date, no growth parameters are defined and reliable and robust investigation approaches are still missing. Furthermore, basic knowledge about the organoid development and biochemical/biophysical mechanisms that generate the phenotypic structure are not identified. For a clinical approach these parameters are fundamental and therefore must be defined pre-clinically.

The aim of this study is the preclinical characterization of the hPOs. In order to achieve this, (1) I optimized an existing immunofluorescence protocol for mPOs and hPOs. (2) in cooperation with other members of the team, I developed a brightfield-microscopy-based high-throughput pipeline (in the following named brightfield pipeline) that allows the observation and quantification of size and growth rate for hundreds of organoids. (3) To investigate organoids at a cellular level, I adapted the FEP-foil-cuvette for use in the commercially available Lightsheet microscope Zeiss Lightsheet Z.1. and used it to observe organoid dynamic behaviour on a cellular level. (4) To quantify the light sheet observations I adapted, optimized and used

an existing nuclei segmentation pipeline (in the following named light sheet pipeline). (5) Apart from specific growth conditions, organoids need an ECM that simulates the tissue integrity of the organ they are derived from. The ECM is of animal origin and shows a high batch-to-batch variability, which makes this source of ECM unsuitable for clinical application. To circumvent the variability, I developed a new cultivation method which is based on an existing protocol (hanging-drop culture technique). This method needs only 4 % ECM and supports the long-term cultivation of human and murine pancreas organoids. (6) Because of its spherical and monolayered structure, organoids are highly sensitive. To understand the organoid phenotype and characterize the luminal liquid I initiated a collaboration with the group of Prof. Dr. Windbergs that uses confocal Raman microscopy to investigate the organoid luminal liquid in a non-invasive way in fixed and living organoids. (7) Based on these results and with the use of the optimized immunofluorescence protocol, I identified channel proteins within the cell membrane that presumably guide the maintenance and establishment of the luminal structure of the organoids. (8) To gain more insides in the dynamic regulation of the organoid growth dynamics, I used the developed brightfield pipeline to identify cytoskeletal proteins that are essential for the organoid structure and two additional channel proteins (CFTR and Piezo 1) that control the luminal dynamic of organoid growth.

Because the surrounding ECM hinders the diffusion of the antibodies and offers many epitopes they can bind to, organoids cannot be stained with classic immunofluorescence staining protocols. For this reason, a protocol which extracts the organoids out of the ECM during fixation was developed. This allows for immunofluorescence labelling without altering the phenotypic appearance and without high background noise. Using this technique, the bipotent fate of the organoids were confirmed and polarized cytoskeletal components, such as Actin, and cell adhesion molecules, such as Cadherin, were identified. Using brightfield microscopy, several dynamic behaviours were identified; the fusion of two or more organoids, the formation processes out of cell fragments, the migratory behaviour of the cell fragment prior to formation, and size oscillation events. Furthermore, a high size heterogeneity was identified. To generate robust and reliable data, capable of capturing this heterogeneity, a brightfield microscopy-based and semi-automated high-throughput pipeline was developed. It allows the quantification of hundreds of organoids over time in size increase. With this technique, the growth rate of hPOs and mPOs could be measured. To gain insides not only on the macroscopic, but also on a meso- and microscopic levels, Light sheet microscopy was used. To ensure physiological growth conditions, the FEP-foil cuvette was adapted for use with the commercially available Zeiss Lightsheet Z.1. The FEP-foil cuvette enables high spatial, and temporal resolved images of organoid growth, behaviour, and development. In addition to the aforementioned dynamics, this approach revealed different patterns of migratory cell behaviours, luminal dynamics, fragment migration, and rotational motions. To quantify the organoid observations into usable datasets, a previously developed processing pipeline to segment and track single cell behaviour was adapted and optimized to the use of organoid images. The adapted pipeline allowed for the extraction of cell nuclei numbers, nucleus sizes, cell neighbourhood relations, and the overall organoid geometry (size, volume, surface). Next, it was used to quantify organoid size oscillation events which were already identified with the brightfield pipeline. In contrast to previous findings in intestine organoids, the results showed that smaller organoids tend to rupture more often than big organoids.

All of the described dynamic processes were observed within the surrounding ECM. However, no investigation has ever been conducted as to whether the ECM serves as a physical scaffold or as a signal provider for cellular processes. To reduce the needed amount of ECM and thereby the overall variability, and to investigate its influence in organoid growth, we developed a cultivation technique based on the already established hanging-drop (HD) technique. This new technique allows the cultivation of organoids in only 4 % ECM and simultaneously promotes the long-term culture. The use of 4 % ECM proves that the organoids do not need the ECM as a physical scaffold, because it has no solid phase in the HD-system. This observation led to the question about how organoids are able to develop and maintain their phenotype if they don't need a physical scaffold. We investigated effects due to the luminal liquid using chemically selective confocal Raman microscopy (CRM) – the first time this technique was applied to fixed and living organoids. These experiments revealed that no differences in the chemical composition between the surrounding medium and the luminal liquid exist. Further, CRM showed that no prominent compound is released into the luminal liquid and that it is mainly water. In addition, CRM analysis showed that the organoid volume increase is mainly due to an osmosis-driven water influx, because the concentration of molecules within the organoid liquid decreased with increased volume of the organoid.

In a next step, we investigated possible cellular and molecular mechanisms which could drive and control the observed dynamics by regulating the water influx into the organoid lumen. By the use of the optimized immunofluorescence staining protocol, Aquaporin 1, 5 and 8 were identified in the cell membrane. This observation is in accordance with the *in vivo* situation of ductal cells. Furthermore, aquaporins promote the water in- and out-flux through cells and can endorse the water flux through the organoid epithelium. Next, the ion channel Cystic Fibrosis Transmembrane Conductance Regulator (CFTR) was identified in the cell membrane. CFTR has already been discovered in intestine and lung organoids where it is essential for volume maintenance by controlling the chloride concentration within the cell. The observed highly dynamic behaviours of pancreas organoids led to the hypothesis that mechanical cues play a major role in the regulation and control of organoid growth. The most prominent mechanosensitive channel in mammals is Piezo-1. For the first time, Piezo-1 was identified in pancreas organoids by the use of the improved immunofluorescence staining protocol. To analyse the function of Piezo-1 and CFTR and identify cytoskeletal proteins which promote and facilitate the organoid phenotype, a drug trial was conducted with the developed brightfield pipeline. Next to Actin and Tubulin, the motor protein Myosin 2 was identified to play an essential role in maintaining the organoid luminal structure. In a next step, the function of CFTR was investigated by the use of two inhibitors which revealed the regulatory role of this channel in maintain the luminal phenotype. In contrast, the inhibition of Piezo-1 did not lead to a significant reduction in mPOs but in hPOs. However, Piezo-1 activation led to a significant reduction of the organoid size in both species. In addition, it was compensated by a significant volume increase upon removal of the drug. All of these results suggest that Piezo-1 is present in the pancreas organoid cells and plays a regulatory role in organoid volume dynamics.

Overall, this work identified and characterized pancreas organoid phenotypes on multiple scales. Two processing pipelines were developed that enable the analysis of complete cultures as well as single organoids and their cellular appearances. The thesis revealed a variety of different growth and behavioural patterns of pancreas organoids and addressed possible reasons for it. Another important outcome of this work with clinical implications is that it

challenges the need for an extracellular matrix and illustrates a method to minimize the use of it. This thesis also discovered the cellular presents of the ion channels CFTR and Piezo-1 and addressed their roles in maintaining and developing the phenotypic appearance of pancreas organoids. With the results of this thesis, we have gained a fundamental understanding of biophysical and biochemical requirements of the organoid's appearance and opened questions about the cellular regulatory mechanisms to control the organoids development.

# Table of Contents

Danksagung .....	i
Zusammenfassung .....	ii
Summary .....	viii
Table of Contents .....	xii
List of Figures .....	xviii
List of Tables .....	xix
List of Movies .....	xx
List of Supplemental Figures .....	xxi
List of Abbreviations .....	xxii
1. Introduction .....	1
1.1. The pancreas as a functional unit – The islets of Langerhans .....	1
1.2. Embryonic development and plasticity of the Pancreas .....	2
1.2.1. Morphological development of the pancreas .....	2
1.2.2. Key-regulators of cell differentiation in the development of the pancreas.....	4
1.2.3. Trans-differentiation potential in the adult pancreas .....	5
1.3. Diabetes mellitus – disease, progress and current research.....	6
1.4. Three-dimensional cell culture .....	6
1.5. Organoids as a novel approach .....	7
1.5.1. Stem cell technology .....	7
1.5.2. Organoid technology.....	7
1.5.3. Organoids derived from adult stem cells .....	8
1.5.4. Pancreas derived organoids.....	8
1.5.5. The R-spondin based 3D culture system.....	9
1.6. Physical properties of biological matter .....	10
1.6.1. Internal physical properties of the cell - the cytoskeleton.....	10
1.6.2. Actin .....	10
1.6.3. Intermediate filaments .....	11
1.6.4. Microtubules.....	11
1.6.5. Cell-cell adhesion.....	11
1.7. The extracellular matrix.....	12
1.7.1. Cell-ECM interaction .....	12
1.7.2. Organoids within the extracellular matrix .....	13
1.7.3. Organoids architecture as a liquid filled sphere .....	14
1.7.4. The cystic fibrosis transduction regulator.....	14

1.7.5.	The mechanosensitive channel Piezo-1 and its associated signalling pathways .....	15
1.7.6.	The role of aquaporins in the adult and the embryonic pancreas .....	15
1.8.	Advanced light microscopy .....	16
1.8.1.	Confocal laser scanning microscopy (CLSM).....	17
1.8.2.	Light sheet-based fluorescence microscopy.....	17
1.8.3.	The two different ways to generate the light sheet.....	17
1.9.	Organoids for three-dimensional microscopy.....	18
1.9.1.	General challenges in organoid imaging .....	18
1.9.2.	Immunofluorescence labelling in organoids.....	19
1.9.3.	The ultra-thin FEP-foil cuvette holder for 3D observation of big biological samples.....	19
1.9.4.	The ultra-thin fluorocarbon foil cuvette .....	20
1.10.	Segmenting and tracking the organoids development and behaviour.....	20
1.11.	Main contribution of this thesis.....	21
2.	Material and Methods.....	22
2.1.	Chemicals .....	22
2.2.	Islets of Langerhans culture components .....	23
2.3.	Organoid Culture components.....	23
2.4.	Components for human embryonic kidney (Hek) 293T-HA-R-spondin1-Fc cells.....	25
2.5.	Organoid donor material.....	26
2.6.	Components for immunofluorescence labelling of organoids.....	26
2.6.1.	Blocking solution for immunofluorescence labelling of organoids .....	27
2.6.2.	Antibodies and dyes .....	27
2.7.	Used Microscopes.....	29
2.8.	Clearing solution CUBIC-II.....	29
2.9.	Drugs.....	29
2.10.	Special devices and consumables .....	30
2.11.	Organoid culture method.....	30
2.11.1.	Thawing of organoids.....	30
2.11.2.	Splitting of organoids .....	31
2.11.3.	Freezing of organoids.....	31
2.11.4.	Generation of R-Spondin conditioned medium.....	31
2.12.	Human pancreas organoids .....	32
2.13.	Mouse pancreas organoids .....	32
2.14.	Media components.....	32

2.15.	Hanging Drop .....	32
2.15.1.	Initiation.....	33
2.15.2.	Maintenance.....	34
2.15.3.	Single cell generation .....	34
2.15.4.	Re-culture in a droplet of Matrigel®.....	34
2.15.5.	Freezing/throwing .....	35
2.16.	Immunofluorescence staining of organoids.....	35
2.16.1.	Separation of organoids from Matrigel® or BME .....	35
2.16.2.	Blocking, permeabilization and antibody-incubation of organoids.....	35
2.17.	Preparation of mPOs and hPOs for CRM.....	36
2.17.1.	CRM imaging, spectra analysis and calculations.....	36
2.18.	Fluo-8 AM staining.....	37
2.19.	Pancreas clearing and staining.....	37
2.20.	Immunofluorescence labelling and vitality determination of islets of Langerhans .....	38
2.21.	Brightfield-based analysis pipeline .....	38
2.21.1.	Image processing and organoid segmentation.....	38
2.21.2.	Data processing .....	39
2.22.	Light sheet-based analysis pipeline .....	39
2.22.1.	Fabrication of positive modules for vacuum forming .....	40
2.22.2.	Cuvette fabrication.....	40
2.22.3.	Specimen preparation.....	40
2.22.4.	Image acquisition and single cell analysis .....	40
2.23.	Statistics .....	41
2.24.	Used programs.....	42
2.24.1.	Arivis.....	42
2.24.2.	ImageJ/Fijii.....	42
2.24.3.	SketchUp Make.....	42
2.24.4.	ZEN Blue.....	42
2.24.5.	OpenShot Video Editor, iMovie .....	42
3.	Results .....	43
3.1.	The Pancreas and its functional unit, the islets of Langerhans.....	43
3.2.	The three-dimensional culture system of pancreas organoids.....	44
3.2.1.	Appearance and behaviour of mouse and human pancreas organoids.....	45
3.2.2.	General challenges in organoid imaging – immunofluorescence labelling of organoids.....	47



3.2.3.	Mouse and human pancreas organoid's identity: marker expression and cell polarisation.....	47
3.3.	Organoids at a glance - multiscale analyses of organoids growth behaviour .....	51
3.3.1.	Recording hundreds of organoids and tracking complete organoids on a single cell level – The brightfield and light sheet pipeline.....	51
3.3.2.	Using the brightfield pipeline to understand the phenotypic appearance of pancreas organoids.....	54
3.4.	Understanding organoids dynamics in detail – The light-sheet based segmentation pipeline.....	57
3.4.1.	Recording pancreas organoids <i>in toto</i> for more than 6 days allows detailed visualisation of single cell and individual organoid growth behaviour as well as the dynamic process of organoid morphogenesis .....	57
3.4.2.	Detection of organoids interculture dynamic processes – formation, degeneration, cell division and cell size variability.....	59
3.4.3.	Detection of organoids intercultural dynamic processes – fusion, rotation and cell cluster motion .....	61
3.4.4.	Pancreas organoids vary in their growth behaviour – three representative quantified organoids.....	63
3.5.	The role of the extracellular matrix in pancreas organoid culture .....	66
3.5.1.	Pancreas organoids do not need the ECM as physical scaffold.....	67
3.5.2.	Pancreas organoids are able to grow within solubilized ECM – the hanging drop system.....	70
3.5.3.	Organoids maintain their phenotype and fate in the hanging drop system for more than two years.....	71
3.6.	Human and mouse organoids within the scope of cell-matrix interaction .....	76
3.6.1.	Non-invasive confocal Raman microscopy as a tool to analyse fixed and live organoids.....	76
3.6.2.	The luminal liquid of pancreas organoids consist mainly out of water and the water-protein ratio increases with the organoid size .....	76
3.6.3.	Mouse pancreas organoids express Aquaporin 1, 5 and 8 .....	79
3.6.4.	Organoid lumen maintenance is cytoskeleton dependent – tubulin and the actin-myosin-axis .....	80
3.6.5.	Pancreas organoids express the cystic fibrosis transmembrane conductance regulator CFTR and the mechanosensitive ion channel Piezo-1 .....	82
3.6.6.	The cystic fibrosis transmembrane regulator plays a critical role in luminal dynamics of pancreas organoids.....	84
3.6.7.	The mechanical force translocator Piezo-1 plays a critical role in luminal dynamics of pancreas organoids.....	85
3.6.8.	Piezo-1 activation leads to alteration in the phenotype of pancreas organoids .....	87

4.	Discussion.....	90
4.1.	Islets of Langerhans can be identified by their structure <i>in vivo</i> and used to validate antibodies.....	90
4.1.1.	Antibodies are a valid tool to characterize pancreas organoids.....	90
4.2.	The culture and appearance of human and mouse pancreas organoids .....	91
4.2.1.	Mouse organoids are more suitable to be kept as long-term culture than human organoids .....	91
4.2.2.	Pancreas organoids show high diversity in behaviour and appearance .....	92
4.3.	Characterizing pancreas organoids with immunofluorescence labelling – reasons for the observed expression of Ngn3, Nkx 6.1 and Yap .....	93
4.3.1.	Mouse pancreas organoids show Neurogenin 3 and Nkx 6.1 expression.....	93
4.3.2.	Mouse and human pancreas organoids show variations in Yap expression – possible link to ECM interaction.....	94
4.4.	Multiscale analysis of Organoid growth and behaviour by using light sheet and brightfield microscopy – Part I: the high-throughput pipeline.....	95
4.4.1.	mPOs and hPOs show different growth behaviour – mPOs need less time to reach their final overall volume .....	96
4.4.2.	hPOs are highly DMSO sensitive .....	97
4.5.	Multiscale analysis of Organoid growth and behaviour by using light sheet and brightfield microscopy – Part II: the light sheet pipeline.....	97
4.5.1.	The ultra-thin FEP-foil foil cuvette – adapted for the use in the Lightsheet microscope Z.1 .....	98
4.5.2.	Comparing the light sheet pipeline to other microscope systems .....	98
4.6.	Long-term imaging of pancreas organoids reveals high inter-cultural heterogeneity in growth behaviour .....	99
4.7.	Organoids showed different sized cell nuclei – a classification .....	99
4.7.1.	Identifying dynamic organoid behaviours – fragment migration .....	100
4.7.2.	Identifying dynamic organoid behaviours – fusion of organoids.....	100
4.7.3.	Identifying dynamic organoid behaviours – rotation of organoids .....	101
4.7.4.	Identifying dynamic organoid behaviours – size oscillation.....	101
4.8.	Data handling .....	101
4.9.	Pancreas organoids can be cultivated in Hanging-drops – no ECM is needed.....	103
4.10.	CRM reveals water as the main component of the liquid within organoids .....	105
4.10.1.	Aquaporins are present within the cell membrane and presumably guide the water influx into the lumen .....	106
4.11.	Tubulin and the actin-myosin-axis are the main contributors for the phenotype maintenance of pancreas organoids. ....	107

4.11.1.	Human and mouse organoid volume increase and growth is based on tubulin and the actin-myosin-axis.....	107
4.11.2.	Pancreas organoid luminal dynamics are controlled by the mechanosensitive channel Piezo-1 and dependent on the active regulation of Cl <sup>-</sup> -mediated conductance regulators like CFTR.....	109
4.11.3.	Piezo-1 activation leads to repolarisation of the cell cytoskeleton in pancreas organoids and changes in the expression pattern of Yap.....	110
4.11.4.	Alterations of CFTR and Piezo-1 expression in mouse pancreas organoids cultured in HD – possible CFTR-Piezo-1 coupled mechanism .....	112
4.12.	Two theories emerge from experimental evidence .....	112
4.12.1.	Organoid size oscillation is dependent on the surface-to-volume ratio .....	113
4.12.2.	The organoid size is dependent on the force-equilibrium generated between the organoid lumen and the cytoskeleton .....	113
5.	Outlook and future research areas.....	116
5.1.	Generate a donor bank to analyse donor related differences in the culture of pancreas organoids.....	116
5.2.	Optimize hPO growth conditions for the long-term culture .....	116
5.3.	Validate and establish the HD-culture technique as an alternative to the normal culture .....	117
5.4.	Use the HD-system to develop a fully synthetic hydrogel.....	117
5.5.	Transfer the generated knowledge to organoids of different origin .....	117
5.6.	Use CRM to investigate the organoid luminal liquid .....	118
5.7.	Validating the CRM technique to generate a robust readout which can be used to determine the cell status.....	118
5.8.	Investigating the function of Aquaporins in the organoid phenotype establishment and maintenance .....	118
5.9.	Shed light on the organoid ECM interaction by modulating integrin .....	119
5.10.	Analysing the effect of Myosin-II inhibition .....	119
5.11.	The third cytoskeleton component: the intermediate filaments.....	119
5.12.	Investigating the polarisation dynamics of pancreas organoids .....	120
5.13.	Clarify the influence of GlyH101 and CFTRinh- 172.....	120
5.14.	Clarify the role of Piezo-1 in pancreas organoid development and phenotype maintenance .....	120
5.15.	Treatment of Pancreas organoids with Yoda 1 to initiate EMT-like processes – first step towards optimized $\beta$ -cell differentiation.....	121
5.16.	Universal applicability of the FEP-foil cuvette in different research fields.....	121
6.	Concluding remarks - what we now know .....	123
7.	Publication .....	124

8.	References .....	125
9.	Supplement.....	148
9.1.	Movie description .....	148
9.2.	Supplemental material .....	150
10.	Curriculum Vitae .....	161
11.	Erklärung .....	164
12.	Versicherung.....	164

## List of Figures

Figure 1:	The human Pancreas and its cellular composition. ....	2
Figure 2:	Overview of the embryonic development of the mouse pancreas. ....	3
Figure 3:	The embryonic $\beta$ -cell development from multipotent or bipotent progenitor cells and the corresponding transcription factors. ....	5
Figure 4:	Appearance and generation of pancreas organoids.....	9
Figure 5:	Illustration of integrin and its functions. ....	13
Figure 6:	Overview of the data handling of the brightfield pipeline. ....	39
Figure 7:	Murine pancreas and its islets of Langerhans.....	44
Figure 8:	Illustration of the growth heterogeneity and behaviour of human and mouse pancreas organoids. ....	46
Figure 9:	MPOs show a polarized structure but alter in the expression of differentiation markers.....	49
Figure 10:	HPO organoids show polarized structure but alter in the expression of differentiation markers.....	50
Figure 11:	Illustration of the two processing pipelines – the brightfield pipeline for mass analysis on a macroscale level and the light sheet pipeline to analyse single organoids on a single cell level (meso- and macroscale).....	53
Figure 12:	Ultra-thin FEP-foil cuvette holders for the live recordings of organoids with the Zeiss Lightsheet Z.1 microscope system in physiological conditions. ....	54
Figure 13:	Using the brightfield pipeline to define general growth curves of hPOs and mPOs.....	56
Figure 14:	Using the FEP-foil cuvette in the light sheet microscope allows for detailed visualisation of a live cycle of mPOs from the formation up to the point of shrinkage and degeneration. ....	59
Figure 15:	High temporal and spatial resolved LSFM recordings illustrate dynamic morphological processes in organoid development.....	60

Figure 16: Segmentation and 3D-rendering of high temporally and spatially resolved LSM recordings facilitates a more detailed understanding of the cellular dynamics which underlie the overall organoid dynamic.....	62
Figure 17: Long-term single cell analysis of mPO grown in the FEP-foil cuvette reveals heterogeneity in proliferation capacities and differences in cell density.....	65
Figure 18: Volume analysis of three representative mPOS revealed different size oscillation frequencies dependent on their overall volume.....	66
Figure 19: Pancreas organoids do not need the ECM as a physical scaffold because they are able to grow and maintain their stem cell like characteristics in liquefied 4 % ECM.....	69
Figure 20: Scheme of growing organoids in the hanging drop system.....	71
Figure 21: Three mPO lines grown in the hanging drop system as long-term culture.....	73
Figure 22: Two different hPO lines grown in the hanging drop system as long-term culture..	75
Figure 23: Pancreas organoids imaged with chemically selective confocal Raman microscopy (CRM) illustrate that the lumen of the organoids consists mainly out of water and that the water –protein ratio increases with increasing organoid size.....	78
Figure 24: MPOs express Aquaporin 1, 5 and 8.....	79
Figure 25: Organoid lumen maintenance is dependent on tubulin and the actin-myosin-axis.....	82
Figure 26: MPOs and hPOs express the cystic fibrosis transmembrane conductance regulator (CFTR) and the mechanosensitive ion channel Piezo-1. Mouse pancreas organoids grown in HD showed a basal polarisation of CFTR and apical expression of Piezo-1.....	84
Figure 27: The growth of mPOs is CFTR and Piezo-1 dependent.....	86
Figure 28: The growth of hPOs is CFTR and Piezo-1 dependent.....	87
Figure 29: The activation of Piezo-1 led to repolarisation of the cytoskeleton and alterations in Yap but no differences in the Sox9 expression.....	89
Figure 30: Graphic illustration of organoid growth, heterogeneity and its corresponding detection on multiple scales with the brightfield and light sheet pipelines.....	103
Figure 31: Illustration of the hypothesis of the organoid lumen maintenance based on the results obtained in this work.....	115

## List of Tables

Table 1: List of chemicals used in this thesis .....	22
Table 2: Components of the medium to maintain freshly isolated Islets of Langerhans.....	23
Table 3: Components of the organoid growth media which need to be pre-solved and stored at -20°C .....	23
Table 4: Components of organoid growth media which need to be pre-solved and stored at -4°C.....	23
Table 5: Composition of the basal medium for the culture of organoids.....	24
Table 6: Composition of the basal medium without Phenol red for the use with CRM .....	24

Table 7: Composition of the murine B-27, Nac-stock medium .....	24
Table 8: Composition of the human N2, B-27, Nac-stock medium .....	24
Table 9: Composition of the murine expansion medium .....	24
Table 10: Composition of the human expansion medium.....	25
Table 11: List of components used for the generation of R-spondin conditioned medium .....	25
Table 12: List of the used human organoid lines and their origin .....	26
Table 13: List of the used murine organoid lines and their origin.....	26
Table 14: List of components used for the immunofluorescence labelling of pancreas organoids .....	26
Table 15: List of components to produce the blocking solution for immunofluorescence labelling of pancreas organoids.....	27
Table 16: List of the used primary antibodies used to specify organoid origin .....	27
Table 17: List of the used secondary antibodies used to specify organoid origin .....	28
Table 18: List of organic dyes for fluorescence microscopy .....	28
Table 19: List of used microscopes .....	29
Table 20: Components of the clearing solution CUBIC-II.....	29
Table 21: List of drugs that were used in the brightfield pipeline.....	29
Table 22: List of special devices and consumables .....	30
Table 23: Configuration parameters of the single cell analysis of the light sheet-pipeline .....	41

## List of Movies

Movie 1: Growth of mPOs and hPOs recorded with the brightfield microscope .....	148
Movie 2: MPO growth heterogeneity recorded with the brightfield microscope. ....	148
Movie 3: One mPO that shed presumably dead cells into its lumen, recorded with the brightfield microscope .....	148
Movie 4: MPOs were treated with 5 different drugs and segmented with the brightfield segmentation pipeline. ....	148
Movie 5: Time-resolved observations of mPOs growing in the Z1-FEP- foil cuvette. ....	148
Movie 6: Time-resolved 3D volume rendering of the formation process of mPO. ....	148
Movie 7: Time-resolved 3D volume rendering of the fusion process of two organoids.....	148
Movie 8: Time resolved observation of two mPOs that showed different cell densities and nucleus sizes.....	149
Movie 9: MPOs showed collective cell rotation. ....	149
Movie 10: Alterations in rotational motion of two organoids in close neighbourhood. ....	149
Movie 11: Organoids cell fragment motion prior formation.....	149
Movie 12: MPO development from single, two and three cells within the FEP-foil cuvette..	149

Movie 13: Three representative mPOs processed with the Lightsheet segmentation pipeline.....	149
Movie 14: One Organoid imaged for 48 hours, tracked and segmented in regard to single cells expansion agility and phylogeny. ....	149

## List of Supplemental Figures

Supplemental Figure 1: Illustration of the challenges in organoid imaging.....	150
Supplemental Figure 2: Secondary antibodies controls of immunolabeled islets of Langerhans. ....	151
Supplemental Figure 3: Secondary antibody controls of immunolabeled mPOs. ....	151
Supplemental Figure 4: Secondary antibody controls for immunolabeled hPOs.....	152
Supplemental Figure 5: Secondary antibody control of the immunolabeled channel proteins CFTR and Piezo-1 in mPOs, hPOs and mPOs grown in HD.....	153
Supplemental Figure 6: Secondary antibody control of the immunolabeled channel proteins Aquaporin 1, 3 and 8 in mPOs. ....	153
Supplemental Figure 7: MPO and hPO pre-treatments to identify that the lumen maintenance is tubulin-, actin-myosin, CFTR and Piezo-1-dependent. ....	156
Supplemental Figure 8: Illustration of the Ca <sup>2+</sup> influx in mPO cells upon Yoda 1 (50 μm) treatment measured with Fluo8-AM. ....	157
Supplemental Figure 9: Illustration of the Mann-Whitney-U test of data obtained with the brightfield pipeline for mPOs. ....	158
Supplemental Figure 10: Illustration of the Mann-Whitney-U test of the data obtained with the brightfield pipeline for hPOs.....	159
Supplemental Figure 11: Illustration of the Mann-Whitney-U test for the data obtained with the pipeline for hPOs from the treatment with Yoda 1. ....	160

## List of Abbreviations

A83-01	transforming growth factor-beta type I receptor kinase inhibitor IV
Aabs	islet autoantibodies
ADPKD	autosomal dominant polycystic kidney disease
AED	anti-epileptic drugs
AQP	aquaporins
Arx	aristaless related homeobox
AS cell	adult stem cells
ATP	adenosin triphosphate
BME	basement membrane extract
BMP	bone morphogen protein inhibitor
CaCC	Ca <sup>2+</sup> -dependent Cl <sup>-</sup> conductance
CaCo	colorectal adenocarcinoma cells
CaF2	calcium fluoride
CAM	cell adhesion molecule
cAMP	cyclic adenosine monophosphate
CBMS	carbohydrate-binding modules (specific surface-binding motives)
CFTR	cystic fibrosis transduction regulator
CLSM	confocal laser scanning fluorescence microscopy
CRM	confocal Raman microscopy
DCG	Delaunay cell graph
DMSO	dimethyl sulfoxide
ECM	extracellular matrix (Matrigel® or BME)
EHS	Engelbreth-Holm-Swarm
EMT	epithelial-to-mesenchymal transition
ES cell	pluripotent embryonic stem cells
FAK	focal adhesion kinas
FDA	Fluorescein diacetate
FEP	tetrafluoroethylene-hexafluoropropylene copolymer
FGF10	fibroblast growth factor 10
FIS	forskolin-induced swelling
Foxa2	forkhead box protein 2
GPCR	G protein-coupled receptors
GsMTx-4	amino acid peptidyl toxin from the <i>Grammostola rosea</i> (Chilean rose) tarantula venom, belongs to the huwentoxin-1 family
HD	Hanging drop
Hhex	hematopoietically-expressed homoeobox protein HHEX
HPLC	high performance liquid chromatography
hPO	human pancreatic organoid
IF	immunofluorescence
IKVAV	laminin-derived Ile-Lys-Val-Ala-Val peptide (specific surface-binding motives)
INF	intermediate Filaments
IPS cell	induced pluripotent stem cell
LATS	large tumour suppressor
Lgr5	leucine-rich-repeat-containing G-protein-coupled receptor 5
LIF	Leukemia inhibitory factor receptor



LSFM	Light sheet-based fluorescence microscopy
MafA	V-Maf musculoaponeurotic fibrosarcoma oncogene homolog A
MAPK	mitogen-activated protein kinase
MDCK	Madin-Darby canine kidney cells
mDSLIM	monolithic digital scanned laser light sheet fluorescence microscope
Mnx1	motor neuron and pancreas homeobox protein 1
MPC	multipotent pancreatic progenitor cell
mPO	mouse pancreatic organoid
MST	mammalian Sterile 20-like kinases
MT	microtubules
NC	normal condition (organoid cultivation within a droplet of EMC).
Ngn3	neurogenin 3
Nkx 2.2	homeobox protein Nkx 2.2
Nkx 6.1	homeobox protein Nkx 6.1
Oct1	organic cation transporter 1
Organoid size	In the manuscript, the term “size” describe the organoid volume and surface
Pax4	paired box 4
Pax6	paired box 6
PBS	phosphate buffered saline
PBS-T	phosphate buffered saline supplemented with 1 % Triton-X 100
PCG	Proximity cell graph
PCR	polymerase chain reaction
Pdx 1	pancreatic-duodenal homeobox 1
PenStrep	Penicillin-Streptomycin
PFA	paraformaldehyde (fixative)
PGE2	Prostaglandin E2
PI	Propidium iodide
PSF	point spread function
Ptf1a	pancreatic transcription factor 1 A
RGD	tripeptide Arg-Gly-Asp (Arginin, Glycine, Asparatate)
RI	refraction indices
RT	room temperature
SK-CO	<i>Cellosaurus</i> cell lines
Sox9	SRY-box transcription factor 9
SPIM	single plane illumination microscopes
T1D	type 1 diabetes
T2D	type 2 diabetes
Taz	transcriptional coactivator with PDZ-binding motif
TEA	Tetraethylammonium
TGF- $\beta$	transforming growth factor $\beta$
TNF- $\alpha$	Tumour necrosis factor- $\alpha$
VSORC	volume-sensitive outwardly rectifying Cl <sup>-</sup> conductance
Yap	mechano-reactive transcriptional coactivator Yes-associated protein
Z.1	Zeiss Lightsheet Z.1 microscope
ZO-1	<i>Zona Occludens</i> protein 1
ZO-2	<i>Zona Occludens</i> protein 2

## 1. Introduction

### 1.1. The pancreas as a functional unit – The islets of Langerhans

In the human body the pancreas is located in the abdomen, surrounded by stomach, small intestine, liver, spleen and the gallbladder. It has two regulatory units that control physiological processes. The exocrine part accounts for 98 % of the total pancreas mass and produces and releases digestive enzymes into the *duodenum*, which breaks down carbohydrates, proteins and lipids. The enzymes are produced by acinar cells that are arranged into bulk-like structures, called *acinus*. The *acini* are connected via a network-like structure which is built up by the duct cells. The ductal tree is able to transport the enzymes into the *duodenum* and symbolizes one major source of progenitor cells for the cell-homoeostasis in the organ (Pin et al., 2017). The second regulatory unit in the pancreas is built up by the islets of Langerhans and located within the organ, between the ductal tree and the *acini*. The Islet of Langerhans can be separated from the exocrine part by its different morphology. It is structured as a compact spherical cluster of cells and does not show any luminal areas. The cell cluster is directly connected to the blood stream via a microcapillary network which constitutes 7-8 % of the total islet volume (El-Gohary et al., 2017)(Figure 1). In the human body approximately 3 to 15 million islets make up to 2 % of the adult pancreas mass. The islets control the glucose homeostasis by producing and releasing different hormones into the blood stream. These hormones are produced by five different cell types. Alpha ( $\alpha$ )- and Beta ( $\beta$ )-cells release glucagon and Insulin and account for circa 90 % of the overall cell mass, whereas 60 % are  $\beta$ -cells and 30 %  $\alpha$ -cells (Da Silva Xavier, 2018). Glucagon is able to increase the blood sugar level by converting glycogen into glucose and insulin regulates the uptake of glucose from the liver, fat (white adipose tissue) and skeletal muscles. These two hormones act therefore as counterparts to control the blood sugar level and need to be precisely controlled (Figure 1). For this purpose, delta ( $\delta$ )- and pancreatic polypeptide (pp)- cells are present within the islets of Langerhans and produce and release somatostatin and polypeptides respectively. Both hormones have regulatory functions and mainly control the release of insulin and glucagon and therewith directly influence the activity of  $\alpha$  - and  $\beta$  -cells. The fifth cell type are the Epsilon ( $\epsilon$ )-cells. These cells produce ghrelin, a hormone which has multiple functions and influences directly the blood sugar level by modulating and regulating the food intake. (Bardeesy et al., 2002; Bonner-Weir et al., 2005; DiGrucchio et al., 2016; El-Gohary et al., 2017; Müller et al., 2015).

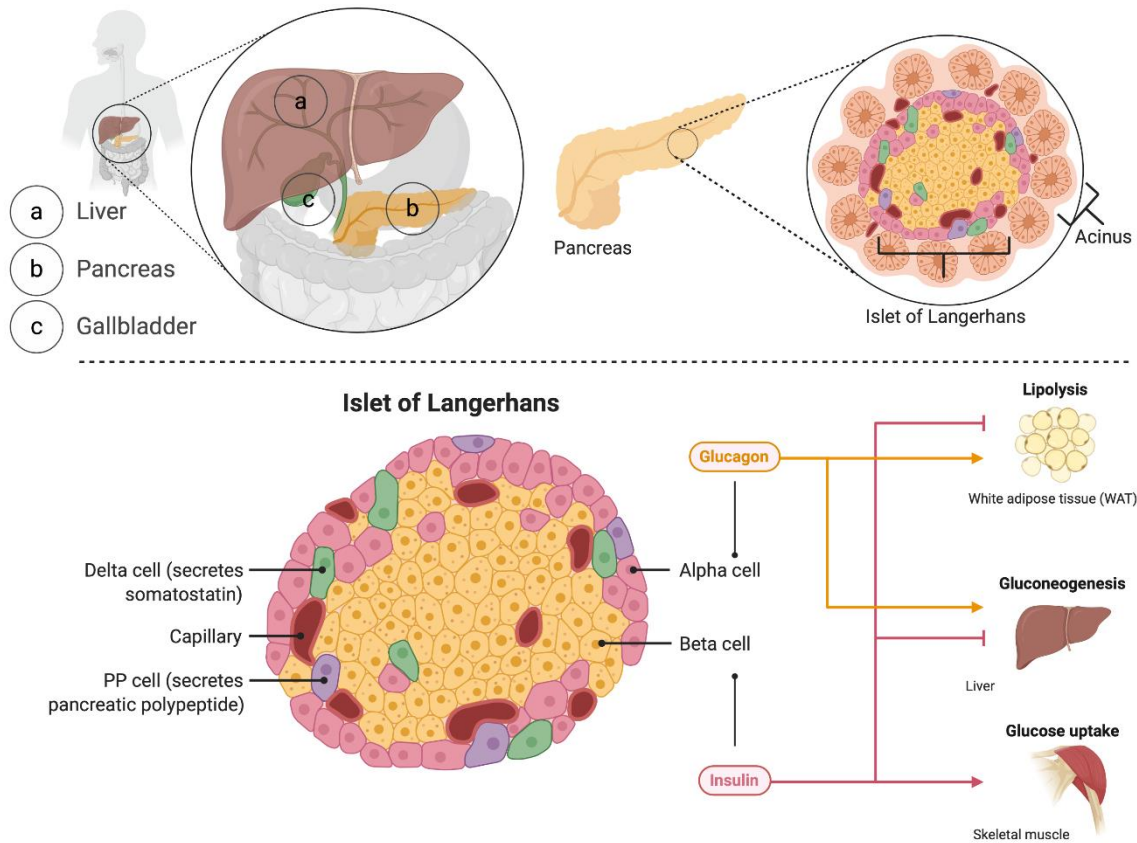


**Figure 1: The human Pancreas and its cellular composition.** The pancreas (b) is located in the abdomen, surrounded by stomach, small intestine, liver (a), spleen and the gallbladder (c). It has two regulatory units that control physiological processes. The exocrine part built up by acinar cells which forms clusters (Acinus), releases digestive enzymes into the duodenum. The second regulatory unit (endocrine) in the pancreas is built up by a compact spherical cluster of cells, the islets of Langerhans. They are directly connected to the blood stream via a microcapillary network which allows the release of hormones to control the glucose homeostasis. These hormones are produced by five different cell types. Alpha ( $\alpha$ )- and Beta ( $\beta$ )-cells release glucagon and Insulin. Glucagon is able to increase the blood sugar level by converting glycogen into glucose (Lipolysis, Gluconeogenesis) and insulin regulates the uptake of glucose from the liver, fat (white adipose tissue) and skeletal muscles. For a tight regulation of these processes, delta ( $\delta$ )- and pancreatic polypeptide (pp)- cells are present within the islets of Langerhans and produce and release somatostatin and polypeptides respectively. Both hormones have regulatory functions and mainly control the release of insulin and glucagon. (Graphic designed with www.BioRender.com)

## 1.2. Embryonic development and plasticity of the Pancreas

The understanding of the pancreas as one organ with two regulatory units requires basic knowledge of its development. However, the analysis of the human pancreas organogenesis during embryonic development remains difficult. Studies from rodents, mostly mice, form the basis of the understanding of pancreas developmental biology. In general, it is divided into three major steps: a primary, secondary and third transition. The primary transition is initiated at embryonic day E5 and lasts until E15, the secondary starts from E15 and lasts until birth and the third transition from birth to weaning (Figure 2).

### 1.2.1. Morphological development of the pancreas

In the first transition the pancreatic progenitor cells, which arise from the endoderm, start to proliferate. It first leads to a thickening of the endoderm and secondly results in an evagination of a dorsal and ventral pancreatic bud. This evagination is accompanied by a transient epithelial stratification which leads to the formation of multiple microlumen. These lumen further

coalesce to form the epithelial plexus, the characteristic tubular structure of the pancreas ((Benitez et al., 2012; Jørgensen et al., 2007; Zaret et al., 2008). During the tube formation a patterning and specification occurs that leads to a bipotent “trunk” and a multipotent “tip” domain. The multipotent pancreatic progenitor cells (MPC) in the tip region can give rise to endocrine and exocrine cells whereas the MPCs in the trunk region are able to differentiate to duct and endocrine cells solely (Benitez et al., 2012). After this primary transition, the epithelium expands to form a branched plexus with multiple tip and trunk regions. In the secondary transition the epithelium undergoes an extensive differentiation process. The tip cells give rise to the exocrine part constructed by acinar and ductal cells and the trunk region can further differentiate to ductal cells and endocrine progenitor cells. The islets of Langerhans are separated regions within the pancreas; thus, the endocrine progenitor cells need to leave the epithelial cell arrangement. Therefore, they underwent an epithelial-to-mesenchymal transition (EMT), leave the epithelium and migrate to distinguished regions where they form clusters of cells. Interestingly this process can happen within a single cell or in complete cell clusters which bud out of the ductal epithelium and migrate to the areas of the islet (Cole et al., 2009; Mastracci et al., 2012; Pan et al., 2014). Finally, in the third transition, these cells differentiate to mature islets with all mentioned cell types (Benitez et al., 2012).

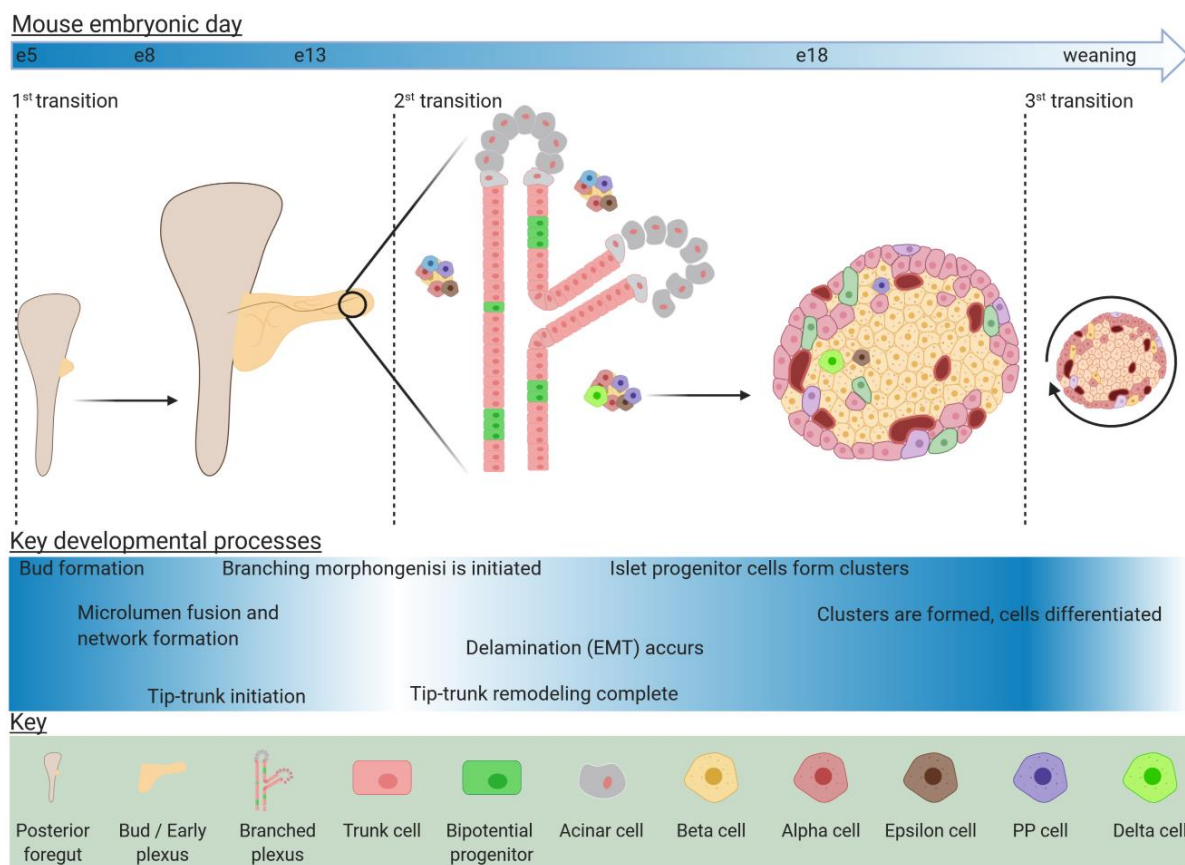


**Figure 2: Overview of the embryonic development of the mouse pancreas.** The first transition: pancreatic progenitor cells start to proliferate which first leads to a thickening of the endoderm and secondly results in an evagination of a dorsal and ventral pancreatic bud. This bud further develops multiple microlumen which fuse to form the epithelial plexus while a patterning in a tip-trunk region of the cells occurs. This further leads to a branched plexus with multiple tip and trunk regions. The second transition: Extensive differentiation processes lead to an exocrine part constructed by acinar and ductal cells and an endocrine part constructed by islet progenitor cells. Subsequently, the islets progenitor cells underwent an epithelial-to-mesenchymal transition (EMT), leave the epithelium and migrate to regions where they form clusters of cells (Islets of Langerhans). Third transition: cells differentiate to all present cell types within the pancreas. (Graphic designed with www.BioRender.com)

### 1.2.2. Key-regulators of cell differentiation in the development of the pancreas

All the above-mentioned processes are tightly regulated and still not completely understood. However, most of the key-regulators, in terms of transcription factors, are identified. In the early development, during the primary transition, Pdx 1 (pancreatic-duodenal homeobox 1) and Ptf1a (pancreatic transcription factor 1 A) are essential regulators of the evagination and bud-formation. Furthermore, the organization of the epithelial plexus is highly regulated by the expression of FGF10 (fibroblast growth factor 10) (Andrei et al., 2020) (Figure 3). In the secondary transition the exocrine compartment becomes functionally distinct from the endocrine compartment whereas the MPCs in the tip region are still able to differentiate to exocrine and endocrine cells. This plasticity is maintained until the acinar gene expression begins, which shows that these processes are spatially and temporally controlled. The Acinar differentiation is characterized by the expression of the transcription factor Ptf1a, Pdx 1 and Oct1 (organic cation transporter 1). The ductal cells can be identified by the expression of Sox9 (SRY-box transcription factor 9) (Huch, Bonfanti, et al., 2013) (Figure3). The endocrine lineage allocation in general is regulated by the pro-endocrine transcription factor Ngn3 (Neurogenin 3), (Gradwohl et al., 2000). Cells that express high levels of Ngn3 ultimately delaminate from the trunk epithelium through an asymmetric cell division. The daughter cell shows an inhibition of E-cadherin which leads to radial migration into the parenchyma (EMT) (Gouzi et al., 2011). In the third transition these cells further develop into the islets of Langerhans with all cell types. In the Islets the  $\beta$ -cell maturation is regulated by dynamic changes in gene regulatory networks and still highly investigated. Beside many others, the expression of Pdx 1, Pax4 (paired box 4), Nkx 6.1 (homeobox protein Nkx 6.1), MafA (V-Maf musculoaponeurotic fibrosarcoma oncogene homolog A ) and Ngn3 is known to play essential roles (Salinno et al., 2019). For  $\alpha$ -cell maturation, temporal alterations in the expression of the transcription factors Arx (aristaless related homeobox), Pax6 (paired box 6), Nkx 2.2 (homeobox protein Nkx 2.2) and Foxa2 (forkhead box protein 2) are essential (Murtaugh, 2007). The differentiation of  $\epsilon$ -;  $\delta$ ; and PP-cells is still poorly understood. Hhex (Hematopoietically-expressed homeobox protein HHEX), 1 Mnx1 (Motor neuron and pancreas homeobox protein) and Pax 4 are known as critical regulators for the differentiation of  $\delta$ -cells (Zhang et al., 2014). The combined absence of Nkx 2.2 and Pax6 leads to an increase in  $\epsilon$ -cell mass in the developing pancreas (Heller et al., 2005; Hill et al., 2009; Sussel et al., 1998). PP-cells develop in the absence of Ngn3 solely (Hecksher-Sørensen et al., 2007; Herrera et al., 1994; Murtaugh, 2007; Salinno et al., 2019) (Figure 3).

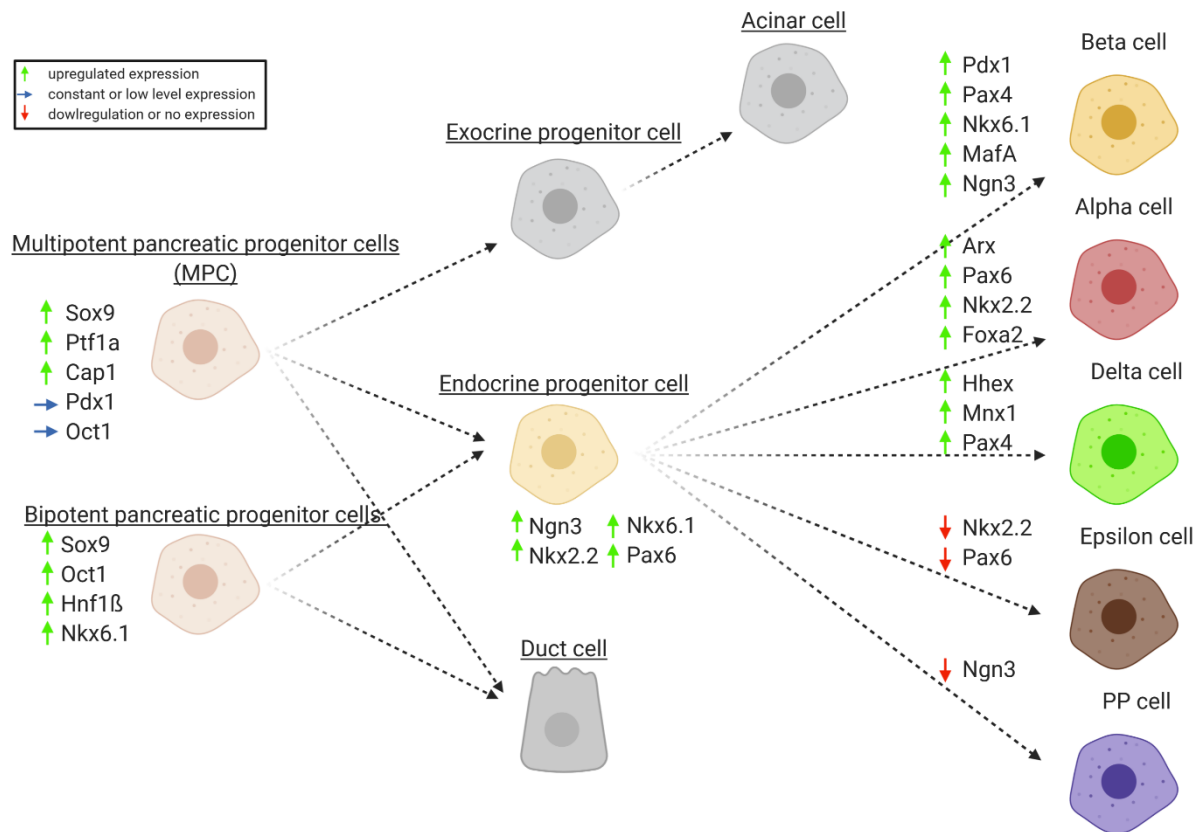


**Figure 3: The embryonic  $\beta$ -cell development from multipotent or bipotent progenitor cells and the corresponding transcription factors.** MPC and bipotent pancreatic progenitor cells differentiate from the endoderm to endocrine progenitor cells by a dynamic and temporal controlled upregulation of Sox9, Ptf1a, CAP1 (MPC) and Oct1, Hnf1 $\beta$  and Nkx 6.1 (bipotent pancreatic progenitor cells) and low expression levels of Pdx 1 and Oct1 (PMC) during the first transition. Upregulation of Ngn3, Nkx 6.1, Nkx 2.2 and Pax6 in the second transition leads to endocrine progenitor cells which then differentiate to beta cells (upregulation of Pdx 1, Pax4, Nkx 6.1, MafA and Ngn3), alpha cells (upregulation of Arx, Pax6, Nkx 2.2 and Foxa2), delta cells (upregulation of Hhex, Mnx1 and Pax4), epsilon cells (downregulation of Nkx 2.2 and Pax6) and PP cells (downregulation of Ngn3) in the third transition. (Graphic designed with www.BioRender.com)

### 1.2.3. Trans-differentiation potential in the adult pancreas

In the recent years it has been shown that the adult pancreas has a high cellular plasticity. It is described by the possibility of fully differentiated cells to undergo a trans-differentiation to another present cell types within the same organ. For example, acinar and ductal cells are able to transdifferentiate into  $\beta$ -cells (Wang et al., 2018; Y. Zhu et al., 2017). Furthermore, it has been shown that terminally differentiated  $\alpha$ -cells can differentiate to  $\beta$ -cells under the control of specific transcription factors like Ngn3, MafA and Pdx 1 *in vivo* and *in vitro* (Zhou et al., 2009; Y. Zhu et al., 2017). Many research groups aim to investigate the underlying processes and the potential application in diseases like diabetes (Aguayo-Mazzucato et al., 2018; Chakravarthy et al., 2017; Gu et al., 1993; Xu et al., 2008). Despite intensive research, which shows that the *in vitro* transdifferentiation into  $\beta$ -cells is possible, the amount of trans-differentiated cells is very low. Further, most of the cells are multi-hormonal and cannot be stimulated with glucagon to produce insulin which shows that they are not fully functional.

### 1.3. Diabetes mellitus – disease, progress and current research

Diabetes is a pandemic chronic disease with more than 463 million affected persons in 2019 and a predicted increase to more than 700 million people in 2045 worldwide. Diabetes comprises two distinguishable diseases. Over 90 % of all cases account for diabetes type 2 (T2D) whereas 10 % for type 1 diabetes (T1D). In both cases the disease is characterized by a high blood glucose level (hyperglycaemia, International Diabetes Federation, 2019). T2D is defined by a decrease in insulin-stimulated glucose uptake, called insulin resistance, which is associated with obesity, ageing and inactivity. In response the pancreatic islets increase their mass of  $\beta$ -cells and the secretion of insulin. In long-term consequence the  $\beta$ -cells cannot produce enough insulin that result into macrovascular complications like atherosclerosis and microvascular complications like retinopathy, nephropathy and neuropathy (Donath et al., 2011). In contrast, T1D is an autoimmune disease characterized by the immune-mediated destruction of pancreatic  $\beta$ -cells that leads to absolute insulin deficiency (V. Pathak et al., 2019). Clinically it is identified by the initial appearance of islet autoantibodies (Aabs) followed by the development of dysglycemia which leads into a hyperglycaemia and ketoacidosis. In T1D the first line therapeutic option is the exogenous insulin replacement therapy. Nevertheless, clinical insights have shown limitations in insulin replacement due to the failure of the full replication of its biological actions (Cohen et al., 2016). Alongside this, the manual administration of insulin always implicates the risk of high fluctuations in blood-sugar levels and therefore the risk of hypoglycaemia (Warshauer et al., 2020). Continuous glucose sensors and insulin pumps as an artificial pancreas may offer a solution but need to be further validated and are associated with high costs (Bekiari et al., 2018). Recent research offers promising results on immune therapies and peptide hormone-based therapies. This field is relatively new, and thus additional research needs to be conducted to evaluate its potential (V. Pathak et al., 2019). So far the xenotransplantation of islets from human donors providing lifelong insulin independence are limited to the availability of donor material and accompanied by life-long administration of immune suppressive medication (Warshauer et al., 2020). In summary, the rising number of T1D cases and the limitations of the treatment highlight the need for alternative approaches such as cellular replacement therapies.

### 1.4. Three-dimensional cell culture

The culture, observation and general use of organic tissue and their response to exogenous substances or stimuli *in vitro* were first established in the nineteenth century (Balls et al., 1995). Until today, two-dimensional (2D) cell culture resembles the foundation of preclinical investigation and is still a powerful tool to understand the biomolecular mechanisms in cells which control biophysical events such as growth, migration and proliferation. Although it is widely used and accepted, *in vivo* studies have shown that cells growing on a flat surface (glass or plastic) do not accurately depict cellular behaviour and resemble tissue-specific architectures with corresponding mechanical and biochemical cues (Pampaloni et al., 2007). To circumvent this and close the gap between cell cultures and physiological tissue, three-dimensional cell culture has been investigated throughout the last three decades (Pampaloni et al., 2007). One widely unnoticed pioneer in the 3D cell culture was Mina Bissell who utilized 3D cell cultures already in the early eighties (Bissell et al., 1982). She predicted the importance of the extracellular matrix (ECM) by providing a physiological environment to the cells. Nowadays 3D-cell cultures can be classified by the system they are derived from. Spheroids are 3D cell aggregates formed by self-aggregation of several cells from one or different origin.

Most of them, but not all, do not need a physical scaffold and are cultured in adhesion free culture conditions (Semino et al., 2003). Dependent on the cellular system, cells can be produced and cultured in low adhesion U-well shaped scaffolds (liquid overlay culture technique), rotating bioreactors or as hanging drops (Pampaloni et al., 2007). More recently, scaffold-based cell systems named organoids gain more and more attention. In this system single cells or cell clusters are seeded in the ECM and self-aggregate into 3D structures and form functional units and cyst like luminal structures (N. Barker et al., 2007; Clevers, 2016; Debnath et al., 2003; Dutta et al., 2017; Sato et al., 2009). In the following sections organoids as 3D cell culture systems will be explained more detailed.

## 1.5. Organoids as a novel approach

The term organoid revealed their first popularity in the mid-sixties until the end of the eighties. Thereby the focus was on the organogenesis of cell clusters which had been dissociated and subsequently rearranged to form the corresponding artificial organ (Clevers, 2016). From then on, the term organoid was not used for more than twenty years, but in the past decade it experienced a comeback in a somehow different guise, the stem cell technology.

### 1.5.1. Stem cell technology

Until quite recently, the stem cell technology focused on pure populations of stem cells or stem cell derived cell types, named progenitor cells (M. a. Lancaster et al., 2014). A stem cell is defined as a cell that is able to develop into any other cell within the organism or organ and is able of a nearly unlimited number of cell divisions (Bonnet, 2002). Stem cells derived from the inner cell mass of the blastocyst are pluripotent embryonic stem (ES) cells and can give rise to all cells existing in all three germ layers of the embryo (Fuchs et al., 2000). Beside embryonic stem cells, also adult stem (AS) cells have been identified. These cells reside in the tissue or organ and have not only the ability to renew themselves, but also the ability to differentiate into distinct cell types of their tissue of origin. Based on that they are multi- or unipotent and maintain and repair the organ they reside in (Prochazkova et al., 2015). Another type of stem cell was introduced in 2006. By the use of a cocktail of transcription factors, already differentiated somatic cells have been re-differentiated into cells. This shows nearly the same expression profile as embryonic stem cells, called induced pluripotent stem cells (IPS) (Shi et al., 2017; Takahashi et al., 2006). All the mentioned types of stem cells can be used to generate organoids.

### 1.5.2. Organoid technology

The term organoid was used in the past more in general to define cells that resemble an organ. This research field became a hot topic in the resent years along with a clearer definition of an organoid (Clevers, 2016): it must contain multiple organ-specific cell types, must be able to recapitulate some organ specific functions and the cells must be spatially organized similar to the organ they are derived from (referred from: M. a. Lancaster et al., 2014). As mentioned above, organoids can be initiated from ES, AS and IPS cells but need to be further separated in organoids derived from pluripotent stem cells (IPSc, ESc) and multipotent stem cells (ASc). While IPSc- and ESc-organoids exploit developmental processes for their generation, organoids derived from AS-cells need to be forced to do so. This is done by providing conditions that



recapitulate the stem-cell niche of the corresponding organ; defined transcription factors and the physiological scaffolds (ECM) (Clevers, 2016).

### 1.5.3. Organoids derived from adult stem cells

Dependent on the organoid origin they can be classified into mesodermal, endodermal and ectodermal/neuroectodermal lineage. To date, organoids can be generated from the mesodermal organs of kidney, bone and fallopian tube. Furthermore, they can be generated from the endodermal lineage like stomach (intestine), liver, lung, gut, thyroid and pancreas. At least, it was shown that organoids can also be generated from ectodermal organs like brain (cerebral), retinal (optic cup) and inner ear (M. A. Lancaster et al., 2019; M. a. Lancaster et al., 2014).

### 1.5.4. Pancreas derived organoids

Until recently the thought was that the  $\beta$ -cell mass within the pancreas is determined from the embryonic development on (Bonnet, 2002). Next to the former mentioned transdifferentiation potential of some islet cells, we now know that there are live long low levels of mature  $\beta$ -cell replicating within the adult pancreas (Bonner-Weir, 2001). This slowly renewing population has its origin in multipotent stem cells located in the pancreatic ducts (Bernard-Kargar et al., 2001). Upon injury, small populations of former quiescence cells start to express Lgr5 (leucine-rich-repeat-containing G-protein-coupled receptor 5), which is a receptor for secreted Wnt-amplifying R-spondins and known as the major driver for activation of epithelial AS-cells (Clevers et al., 2014; Korinek et al., 1998).

Former investigations on liver organoids led to the establishment of a three-dimensional cell culture system that allows long-term clonal expansion of Lgr5+ liver derived cells. Next to other transcription factors, it is based on the mentioned Wnt-agonist R-spondin1 and an ECM which provides a viscoelastic hydrogel as growth environment. Lgr5+ cells grown in that system are able to form transplantable organoids which maintain many characteristics of the original liver epithelial architecture (Huch, Dorrell, et al., 2013). Comparative studies of epithelial cells from liver and pancreas revealed that they have highly similar transcriptomes and share many cell surface markers which indicate a close relationship of these two cell populations (Dorrell et al., 2014). Using the R-spondin-based 3D cell culture system for liver cells, isolated pancreatic ductal fragments from mouse or human biopsies starts to initiate Lgr5 expression. Furthermore, they are able to form budding cyst-like structures, named human or mouse pancreatic organoids (hPO, mPO) (Figure 4). mPOs and hPOs can be expanded for months and keep their ductal morphology, biomarker expression and chromosomal integrity *in vitro* and *in vivo*. Furthermore, they can be clonally expanded from a single Lgr5+ cell and can be induced to differentiate into ducts as well as endocrine cells, which shows their bipotentiality (Boj et al., 2015; Georgakopoulos et al., 2020; Huch, Bonfanti, et al., 2013). Independently of their human or mouse origin, the pancreas organoids phenotype is characterized by a polarized monolayered epithelium that comprises a liquid filled lumen (Figure 4). In general, the organoid growth is characterized by a steady increase of size and an overall roundish and spherical appearance.

### 1.5.5. The R-spondin based 3D culture system

To maintain the organoid bipotentiality over long periods of culture, the 3D culture system relies, next to the previously mentioned R-spondin and the ECM, on several different transcription factors and a precise combination of nutrients (Huch, Bonfanti, et al., 2013, for detail look at: 2.3). In general, mouse and human organoids are grown under the control of the transcription factor FGF 10, the epidermal growth factor (EGF), the bone morphogen protein inhibitor (BMP) Noggin and the hormone Gastrin. The combination of these substances activates a cascade of effects that lead to proliferation, reduced apoptosis and angiogenesis (Debas, 1987; Kang et al., 2017; Pache, 2006). In contrast to mouse organoids, human organoids also need the transforming growth factor  $\beta$  (TGF- $\beta$ ) inhibitor A83 to block EMT-like processes, the cAMP (cyclic adenosine monophosphate) activator Forskolin and inflammatory mediator Prostaglandin E2 (PGE2) for propagation (Boj et al., 2015; Gurung et al., 2015; Morrone et al., 2015; Parker et al., 2015).

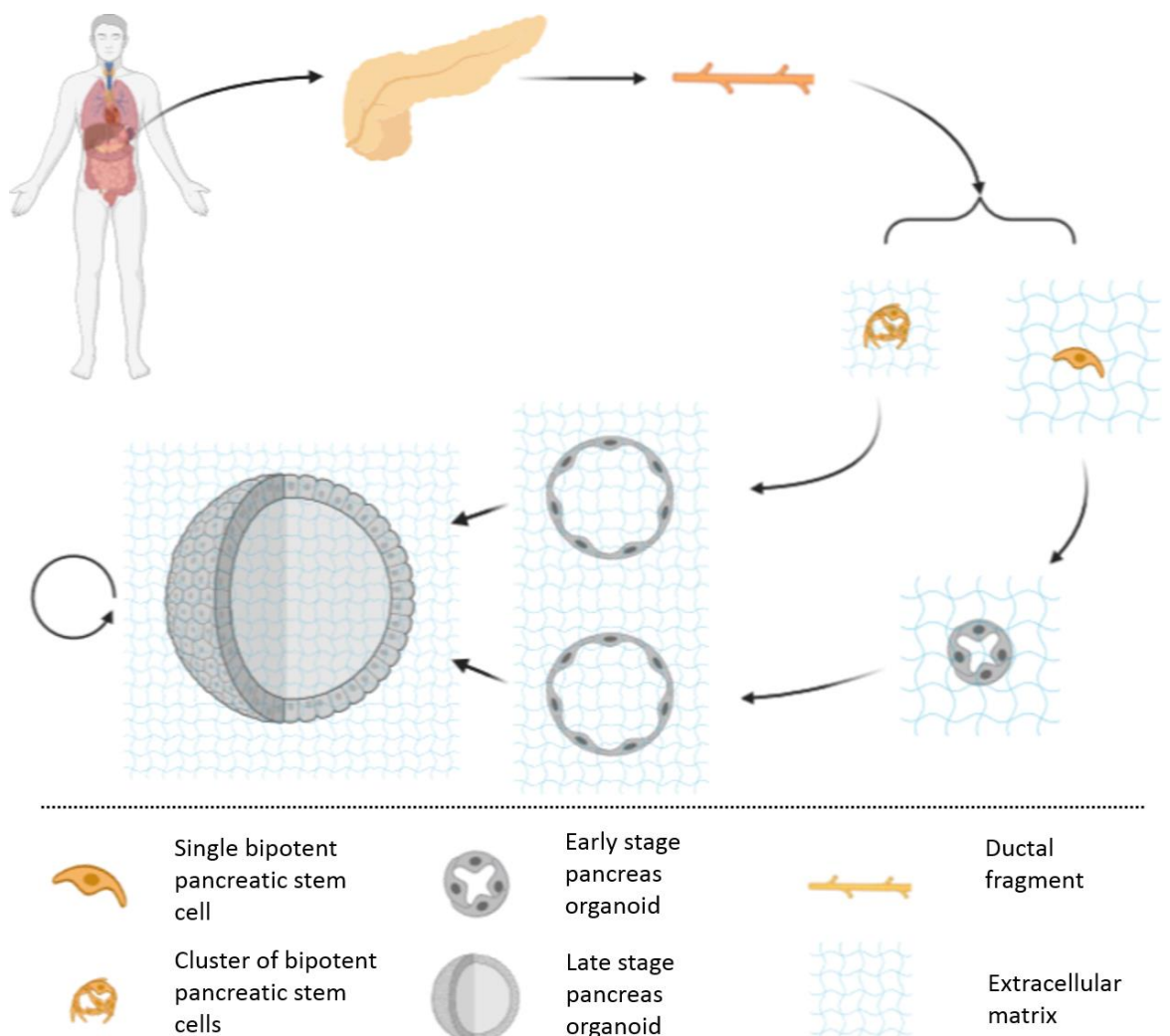


**Figure 4: Appearance and generation of pancreas organoids.** Generation of pancreas organoids from a donor (human as example) biopsy or pancreas transplant. Ductal fragments including bipotent pancreatic stem cells which are able to differentiate into endocrine and exocrine lineage, are cultured in R-spondin based 3D-cell culture and form hollow spherical cell clusters. These pancreas organoids can be clonally expanded and are able to form budding cyst-like structures. They are characterized by a polarized monolayered epithelium enclosing a liquid filled lumen. Pancreas organoids can be expanded over several months without losing their identity. (Graphic designed with [www.BioRender.com](http://www.BioRender.com))

## 1.6. Physical properties of biological matter

As mentioned above, organoids are characterized as a spherical, cyst-like hollow luminal structure, which is embedded in an ECM. Due to its mature appearance as a monolayered epithelium it is on the one hand highly sensitive to mechanical forces and on the other hand it shows a high heterogeneity and flexibility. It is only poorly understood how the cells as a collective are able to maintain and construct this phenotype.

In the early development, comparable luminal, single cell layered epithelial structures, which form hollow spheres or ellipses, are already present. It is a major challenge to investigate the subcellular structures and its properties in relation to the complex physical behaviour of biological matter (Benoit Ladoux et al., 2017; Laurent et al., 2017; Spurlin et al., 2017). Organoids can represent early developmental processes and are therefore a valid tool to understand this mechanisms *ex vivo*. In the following paragraph a summary of the main subcellular structures that cells have and use to transduce, transmit and produce physical forces is given. Next to cell-cell and cell-ECM interaction, it is focused on the cytoskeleton and its major components as a framework of dynamic filaments.

### 1.6.1. Internal physical properties of the cell - the cytoskeleton

The cytoskeleton is the structural basis of each individual cell. It is built up of three main classes of dynamic polymers: Actin, intermediate filaments and microtubules (MT) (Treat et al., 2018).

### 1.6.2. Actin

Actin filaments represent a highly dynamic fibrinous structure because of continuous polymerisation and depolymerisation. Actin monomers (G-actin) are added at one end and detached at the other, and thus building linear polymers (F-actin). The polymerisation process is directly energy dependent in the form of ATP (adenosin triphosphate) consumption and can be regulated by many factors like the rate of ATP hydrolysis and actin polymerisation factors, e.g., formins and capping proteins (Edwards et al., 2014; Paul et al., 2009). Based on these factors, the filament growth can reach orders of micrometres per minute and in connection with filament crosslinking and bundling proteins, it can build up complex geometries. In addition, actin can interact with other molecules and membranes and forms subcellular structures such as filopodia and lamella. Thereby it has numerous functions related to cell shape and movement like cell migration, adhesion and cell division (Edwards et al., 2014; Treat et al., 2018). Next to the dynamic process of filament polymerization, cells are able to actively generate force by pushing and pulling filaments against each other. This is done by the motor protein myosin, which acts as a molecular machine, that uses ATP to move along the actin filaments and is simultaneously connected to another filament (Treat et al., 2018). Thereby it can generate a few piconewtons of force per stroke which can be transmitted to the plasma membrane and control the cell shape and therefore also the intercellular hydrostatic pressure (Mitchison et al., 2008; Newell-Litwa et al., 2015). Actin and myosin build one unit in terms of cell cytoskeleton dynamics, the actomyosin network.

### 1.6.3. Intermediate filaments

Intermediate filaments (INF) symbolize the second class of dynamic polymers and are characterized by a slightly larger diameter than actin, are less dynamic and they do not rely on ATP as an energy source for assembly (Goldmann, 2018; Sanghvi-Shah et al., 2017). The mechanical response of INFs is strongly loading rate dependent and the extensibility is partly determined by a switch from  $\alpha$ -helices to a  $\beta$ -sheet conformation (Trepap et al., 2018). In general, the persistence length of intermediate filaments is much shorter than actin filaments and they are highly extensible. Further, the filaments exhibit strain-induced strengthening without failure. Taken it all together, INFs are important contributors to cells' elasticity, tensile strength and able to define the cell stiffness (Sanghvi-Shah et al., 2017).

### 1.6.4. Microtubules

Microtubules are the largest class of cytoskeletal filament and similar to actin; they form polar filaments. In contrast to actin, the polymerisation and depolymerisation occurs at the same filament and is GTP dependent (Trepap et al., 2018). MTs are formed by the two subunits  $\alpha$ - and  $\beta$ -tubulin. Together they form a tubular structure with  $\beta$ -tubulin exposed to the plus end and the  $\alpha$ -tubulin to the minus end (Benoit Ladoux et al., 2017). The main tasks of MTs are the intracellular vesicle transport. For example, they are critical for the membrane polarity of epithelial cells due to the asymmetric delivery of cellular components to different regions of the plasma membrane. In terms of membranes the basal or apical, MT based delivery of cellular components determine the polarity. In terms of migratory epithelial cells, it defines the front or rear part of the cell. This process is dependent on the motor proteins kinesin and dynein moving and delivering cargo in a directed manner (Muroyama et al., 2017). Therefore, they contribute to cell shape determination and facilitate the chromosome segregation in cell division.

All introduced cytoskeleton components are important to determine the internal mechanical properties of the cell. However, cells in a physiological context are always in close contact to their neighbouring cells or extracellular environment, i.e., they cannot be investigated individually. Consequently, cell-cell and cell ECM interactions need to be considered when investigating the multidimensional cell behaviour.

### 1.6.5. Cell-cell adhesion

A tight cell-cell adhesion is the basis of all epithelial cell arrangements. Tight junctions, adherence junctions and desmosomes are the major players in that system (Trepap et al., 2018).

Tight junctions are intercellular adhesion complexes that control the paracellular permeability and form a border between the apical and the basolateral cell surface domains in polarized epithelia. They are size- and charge-selective and enable the active transport of ions across epithelial layers (Trepap et al., 2018). Furthermore, tight junctions are connected to the adhesion complexes (Zihni et al., 2016).

Adherence junctions are built up by cadherins and comprise adhesion receptors and cytoplasmic proteins including catenin and actin filaments. Thereby a direct transfer of actomyosin forces can be transmitted between cells (B. Ladoux et al., 2015; Takeichi, 2014). With this linkage to the contractile network, adherence junctions are typically under tension and, if clustered, increasing the stability of the epithelial cell arrangement (Treat et al., 2018).

Desmosomes are the third class of cell-cell junctions and essential for maintaining strong intercellular cohesion (Hatzfeld et al., 2017). They are directly coupled with the INFs and by this connection provide a supracellular network that confers mechanical resilience on cell layers (Treat et al., 2018).

## 1.7. The extracellular matrix

Independently of the organoid origin, nearly all of them have in common that they need a 3D matrix for the growth and formation. This is not surprising since in *in vivo* cells make contact with the supporting matrix that confers long lasting form to tissues. Furthermore, it is known that the cell-ECM interaction is essential for the control of morphogenesis, cell fate specification, gain or loss of tissue-specific functions, cell migration, tissue repair and also cell death (Werb, 1997). In general, ECM consists of different protein polymers in different compositions. They can be divided in three classes of molecules: first, the structural (glycol-) proteins (elastin and collagen); second, protein-polysaccharide complexes (proteoglycans); third, adhesive glycoproteins (laminins and fibronectins) (Boyle, 2008). Collagens and laminins are most abundant in many matrices. These polymers exhibit strain-stiffening behaviour depending on their polymer length and are usually differently crosslinked which typically increase the bulk modulus. Thereby the composition and degree of crosslinks determines the elasticity (Storm et al., 2005). Due to the former mentioned subset of matrix proteins, which are heavily glycosylated, and thus hydrated, the ECM usually has a gel-like property (Treat et al., 2018). Beside serving as a physical scaffold, one general task of the ECM is to provide peptides that bind cell surface adhesion receptors, termed adhesion peptides (e.g., Arg-Gly-Asp (RGD) and Carbohydrate-binding modules (CBMs)) (T. H. Barker, 2011; Doxey et al., 2010). These surface binding domains, which can interact with cell surface proteins, are essential for tissue structure as well as cell migration and behaviour.

### 1.7.1. Cell-ECM interaction

One central family of cell-ECM interactions are the heterodimers of integrin (Chang et al., 2016). It is built up by a transmembrane receptor which consists of an  $\alpha$  and  $\beta$  subunit. To date, 24 different integrin receptors have been identified in mammals. Each is specific for a set of ECM ligands (Sun et al., 2016) (Figure 5). With this interaction the cell is able to generate resting forces between itself and the ECM. These forces can be modulated actively from the cell inside as well as is dependent on the engagement of external ECM ligands. Therefore, integrin can modulate the intercellular conformation which leads to changes in cell signalling cascades (Balaban et al., 2001). Further, integrin can be clustered into micrometre scale assemblies forming so called focal adhesions and are capable to generate punctuated high force regions. With the help of different adaptor molecules (e.g., talin, kindlin and migfilin) and filamin, the intracellular part of integrin is coupled to actin (Figure 5). This interaction is essential in the polymerisation process of the cell, because it provides the counterpart of the exerted pushing

force to the plasma membrane (Rosa et al., 2019; Sun et al., 2019; Winograd-Katz et al., 2014). Further, the connection between actin and integrin is tightly regulated by the adaptor proteins, and thus highly dynamic. This leads to different states of actin polymerisation and conformation changes to other associated molecules within the cell. In consequence, it leads to changes in the downstream integrin-linked signalling cascades within the cell (e.g., focal adhesion kinase (FAK)-cascade and mitogen-activated protein kinase (MAPK)-cascade). Furthermore, it manipulates the cell-ECM interaction in a feedback-loop of upstream cascades. This multifarious interaction is termed “mechano-responsiveness” and gained more and more attention in the last years in terms of differentiation potential or stem cell maintenance (Figure 5, (Rosso et al., 2004; Sun et al., 2016; Trepate et al., 2018; Vicente-Manzanares et al., 2011)).

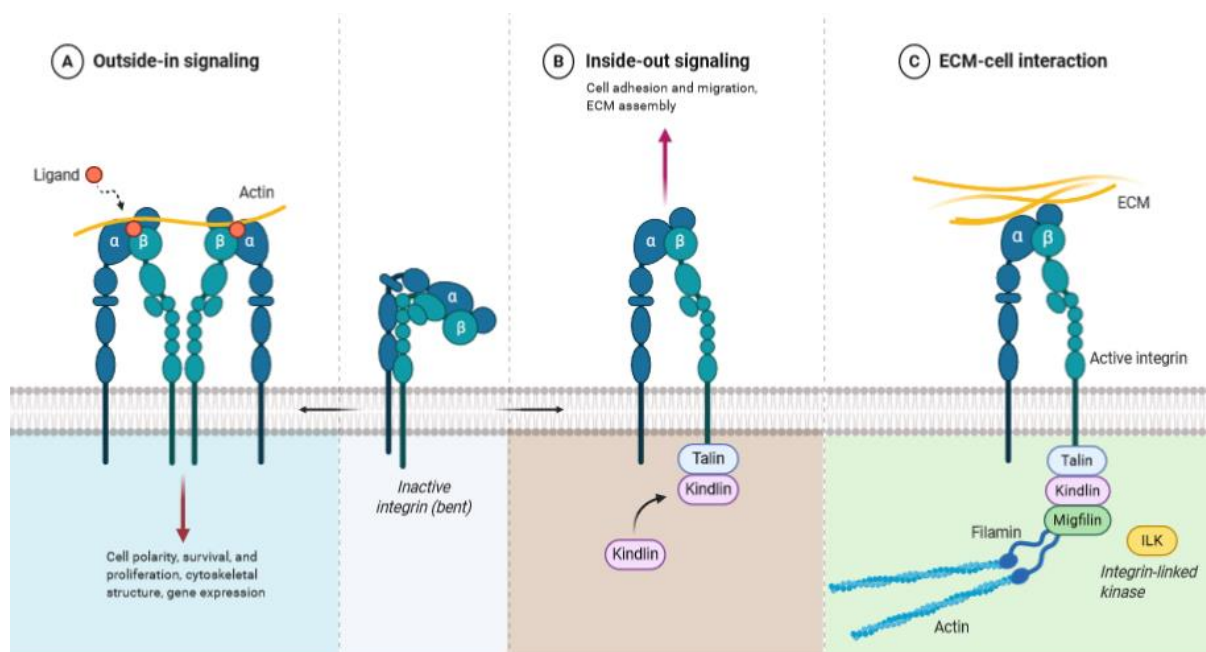


**Figure 5: Illustration of integrin and its functions.** Integrin is one major player of cell-cell and cell-ECM interaction. Depending on the signal it mediates stimuli from the outside to the inside and vice versa, i.e., is connected to the ECM. With these properties it has not only fundamental regulatory properties in cell polarity, survival and proliferation but also generates resting forces with the environment and thereby provides the physical bridge to the circumventing scaffold. (Illustration created with BioRender.com)

### 1.7.2. Organoids within the extracellular matrix

Whether pancreas organoids express ECM-components by their own have never been addressed so far. However, for the culture of pancreas organoids a droplet of ECM surrounding them is needed. The most commonly used matrix is Basement Membrane Extract (BME) or Matrigel®. Both are extracted from Engelbreth-Holm-swarm tumour cell cultures, which are forced to secrete this matrix. One drawback of it is that the cells are of animal origin and therefore bears the risk of xenogeneic contamination when used with human derived organoids. Aside from this, it is poorly defined in its components and can vary in its composition (Hughes et al., 2010). Currently many efforts are made to investigate alternatives to Matrigel® and BME, so called Hydrogels, but for general research Matrigel® it still extensively used (Catoira et al., 2019). Anyway, the interaction of organoid cells with the ECM is poorly investigated. Basic research was conducted in 3D cell cultures and showed that spheroids growing in ECM must overcome some resistance to deformation if they increase their overall cell mass. The resulting pressure can also lead to a limitation of growth or activate cell

mechanism for the remodelling of the surrounding ECM (e.g., release of metalloproteases) (Dolega et al., 2017; Stylianopoulos, 2017; Stylianopoulos et al., 2012). In general, it is known that cells can exert traction by pulling on focal adhesions using their actomyosin machinery. In liquid-filled 3D cell systems the rate of expansion is partly regulated by the osmotic pressure which can be modulated by ion pumps located in the cell membrane (Jaffe et al., 2008). To generate the luminal pressure a coordinated cell polarisation of all cells is needed to ensure a consistent directed transport of solutes. This transport leads to cytoskeleton polarisation which is linked to interfacial tension and epithelial curvature through Laplace's law (Treat et al., 2018).

### 1.7.3. Organoids architecture as a liquid filled sphere

As already mentioned, pancreas organoids are characterized by a polarized epithelium which comprises a hollow, liquid filled lumen. To some degree, this architecture fits to the above-mentioned observations in 3D-cell systems. However, it is completely unknown how pancreas organoids maintain their phenotype. In general, many epithelial cells are able to form fluid-filled spheres. The key player for that behaviour is the cell-cell adhesion, mediated by cadherins and the cell polarity, which is established due to the cell-cell and cell-ECM contact and the corresponding downstream signals (Jaffe et al., 2008). General knowledge of such mechanisms has been generated by the use of cyst-forming immortalized epithelial cell cultures like human epithelial colorectal adenocarcinoma cells (CaCo), Cellosaurus cell lines (SK-CO), Madin-Darby canine kidney cells (MDCK) and autosomal dominant polycystic kidney disease cells (ADPKD) which form cyst-like structures when embedded in a matrix like Matrigel®. Here, it was shown that the cytoskeleton components actin, MT and myosin II play essential roles in cyst formation and maintenance (Ivanov et al., 2008). Aside this knowledge, these investigations revealed that the main driver of cyst formation is the fluid absorption from the basolateral side to the apical side and subsequent active release into the lumen. This water transfer is driven by an active transport of ions ( $\text{Na}^+$  in MDCK,  $\text{Cl}^-$  in ADPKD) across the cell. The generated ion gradient between the matrix and the lumen of the cyst generates a steady liquid flow and drives the luminal size increase. In all of the mentioned cell lines, cAMP was identified as the main regulator of this behaviour (Sharma et al., 2019).

### 1.7.4. The cystic fibrosis transduction regulator

One well known cAMP-dependent ion channel in epithelial cells is the cystic fibrosis transduction regulator (CFTR). It belongs to the ATP-binding cassette (ABC) transporter family and regulates  $\text{Cl}^-$  and therefore water secretion in the cells (Marunaka, 2017). CFTR was already discovered in intestine and lung organoids where it is located at the apical surface and found to be essential for volume maintenance. Organoids derived from humans suffering of cystic fibrosis do not show classic hollow but a dense compact structure which can be restored by using the CFTR activator forskolin (Dekkers et al., 2013). This forskolin-induced swelling (FIS) assay is further used to develop cystic fibrosis drug candidates or for functional studies (Dekkers et al., 2016). As mentioned CFTR is cAMP-dependent and interestingly, insulin regulates cAMP. This regulatory pathway offers a new perspective in future diabetes treatments which can be analysed by using pancreas organoids (Marunaka, 2017).

### 1.7.5. The mechanosensitive channel Piezo-1 and its associated signalling pathways

Another important aspect in organoid volume maintenance and growth behaviour is the conversion of mechanical forces into a biological response, termed mechanotransduction. It is essential for physiological functions in response to extrinsic signals like touch, hearing and also intrinsic signals as blood pressure regulation. However, the molecular mechanisms are largely unknown but activated cation channels seem to play an important role (Montal et al., 2015). In this regard, the mechanosensitive cation channels Piezo-1 and Piezo-2 have been identified to play important roles in vascular development and touch sensing (J. Li et al., 2014; Maksimovic et al., 2014; Ranade, Qiu, et al., 2014; Ranade, Woo, et al., 2014; Woo et al., 2014). Piezo-1 is activated not only upon mechanical stimulation like shear stress and pressure but also shows voltage dependency (Guo et al., 2017; Moroni et al., 2018). It is a non-selective cation channel which consists of a homotrimer that forms a triskelion, a propeller-like structure. The three distal blades comprise a central cap and built-up the extracellular domain whereas several other transmembrane domains bridge into the cytoplasm (W. Li et al., 2017; Ructural et al., 2018). Because Piezo-1 has been identified relatively recently, only less is known about its activation of downstream pathways. In general, Piezo-1 leads to an influx of  $\text{Ca}^{2+}$  which is known as a strong second messenger in many physiological functions like differentiation, cell division, potassium / sodium permeability and cell death pathways like necrosis (reviews: (Carafoli et al., 2016; Fedrizzi et al., 2008). Furthermore, it is known that Piezo-1 is associated to the mechano-reactive transcriptional coactivator Yes-associated protein (Yap) and the transcriptional coactivator with PDZ-binding motif (Taz) (M. M. Pathak et al., 2014). In general, Yap is a primary transcriptional effector of the Hippo signalling pathway, and thus controlling cell proliferation and apoptosis. Moreover, it is involved in multiple pathways ranging from differentiation and proliferation up to cell survival and carcinogenesis (Dobrokhotov et al., 2018; Piccolo et al., 2014). In ES or iPSC, Yap is used as a stem cell marker because it promotes pluripotency and binds directly and stimulates numerous promoters of genes known to be important for stem cells (Lian et al., 2010). In this regard it is not surprising that Yap also promotes stem cell maintenance in developing pancreases and is deactivated in cells undergoing differentiation to the endocrine lineage (George et al., 2012). With these characteristics, Yap has potential as a quality control marker in pancreas organoids and can presumably give further information about force related changes in gene expression.

In summary, the influence of mechanical forces in epithelial organoids is not known yet. Interesting candidates like the ion channel CFTR and the mechanosensitive channel Piezo-1 can give additional insides in the cellular and molecular background. Alongside this, the associated downstream pathways and the corresponding proteins (i.e., Yap) need to be addressed to gain more insides in the phenotypic behaviour of epithelial organoids in general and pancreas organoids in detail.

### 1.7.6. The role of aquaporins in the adult and the embryonic pancreas

The general appearance of organoids as a hollow liquid-filled lumen introduces the question of how the cells are able to build up and maintain this phenotype. Based on the observation of these systems, the most obvious interpretation is that the organoids are able to generate their lumen by simply producing an osmotic gradient that generates a constant influx of liquid.



Further, the most likely liquid is water. In general, most of the biological membranes are reasonably water permeable because of water diffuse through the membrane's lipids. This usually leads to volume equilibrates in a short time in response to an osmotic gradient. In addition, it is known that some organ function (e.g., kidney) needs a high trans-epithelial water permeability to secrete body fluids (Verkman, 2013). In this regard, the exocrine part of the pancreas is able to generate large volumes of isotonic fluids that originate mainly from the ductal system. For this reason, in the recent past, aquaporins (AQP) have been identified to play a major role and facilitate the water transport across epithelial layers (Burghardt, 2003; Leire Méndez-Giménez et al., 2018). Aquaporins are membrane proteins that are organized in a tetrameric structure. Every monomer forms a hydrophilic pore in its centre and each monomer function independently as a water channel. To date, more than twelve AQPs have been identified (the number is dependent on the mammalian species). Their overall function is the water transport across the membrane in response to osmotic gradients which can be created by an active solute transport. However, the water capacity of each monomer is relatively low which shows, that the overall water transport can be regulated by the degree of expressed aquaporin in the membrane (Beall et al., 2012; Verkman, 2013). In the ductal system, AQP1, AQP5 and AQP8 enable the secretion of the fluid from the ductal cells into the ductal tree. In detail, AQP1 is strongly expressed in the apical and basolateral domains, AQP5 only in the apical domains of the intercalated and intralocular duct epithelia and AQP8 in the pole of acinar cells. Furthermore, AQP5 was identified in colocalization to CFTR (Burghardt, 2003). Next to the ductal part of the pancreas, AQP12 is involved in the exocytosis of secretory granules in acinar cells and AQP7 is expressed in  $\beta$ -cells and is known to participate in the insulin secretion (Louchami et al., 2012; L. Méndez-Giménez et al., 2017). Since the pancreas organoids originate from the ductal tree of the adult pancreas, the existence of at least some of them is likely. However, the expression or the role of them have not been addressed so far.

### 1.8. Advanced light microscopy

Just a relatively short time ago (approx. 30 years), most of the data about cells were harvested based on the assumption that two-dimensional monolayers reflect the essential physiology of *in vivo* circumstances. Nowadays it is known that cells lose cell-cell communication and biochemical cues. To close this gap, cells growing *ex vivo* in three dimensions (3D cell culture) and within a scaffold resemble more closely the *in vivo* situation in physiological conditions (Pampaloni et al., 2007). For this reason, 3D cell culture is used in numerous research areas such as cell biology, clinical research and developmental biology. These areas comprise a broad field of model systems ranging from whole animals, organs, organoids and spheroids to monoclonal cysts and simple multicellular cell complexes. However, to analyse 2D cell cultures in its native form, light microscopy is usually used, but becomes more challenging if used to image 3D cell culture systems. With increasing size and density, biological samples become more and more opaque and the penetrating light is more and more scattered (de Souza, 2009; Huisken et al., 2004). In the past decades, specialized microscope systems have been developed to gain high quality information from the inner regions of these specimens. With confocal laser scanning fluorescence microscopy (CLSM) high spatial and with light sheet-based fluorescence microscopy (LSFM) high spatial and temporal resolved images of 3D cell culture can be obtained. In the following a conceptual outline about these two systems is given.

### 1.8.1. Confocal laser scanning microscopy (CLSM)

One major challenge in fluorescence microscopy is to collect the fluorophores that are emitted by the specimens' fluorescence proteins. For that reason, the excitation laser beam is transmitted via the optical axis through one objective to the sample and the emitted photons are collected with the same objective. In CLMS and wide-field epifluorescence only one objective is used. In wide-field epifluorescence microscopes, the sample is illuminated by a point-illumination and all emitted photons are detected (Stelzer, 2014). In contrast, CLMS features a point-detection by which only the emitted photons from the in-focus light within the focal plane of the laser beam is measured. This is due to an adjustable aperture (the pinhole) which facilitates the deletion of the out-of-focus light which results in a lower background to noise ratio in comparison to classical wide-field epifluorescence microscopes (Bayguinov et al., 2018). However, to capture the complete sample, a time-consuming scanning process is indispensable. In this stepwise, pixel-by-pixel scanning process, the sample is illuminated along the entire axial direction. Even though the point-detection eliminates the out-of-focus light, all fluorophores and many endogenous organic components are excited which leads to fluorophore bleaching and in living organisms to photo toxicity (Stelzer, 2014).

### 1.8.2. Light sheet-based fluorescence microscopy

The former mentioned drawbacks in confocal light microscopy were challenged by Ernst Stelzer and colleagues by developing and later improving the LSFM (Huisken et al., 2004; Keller et al., 2008, 2010).

With extensive use in many biological research areas, LSFM is now the single, most effective method for imaging multicellular organisms and allows the analysis of their development over long periods of time (Ovečka et al., 2018). It provides low photo bleaching and photo toxicity, good sample penetration depth and a high image acquisition speed. With the option of multi-view recording, it further improves the axial resolution (Chatterjee et al., 2018; Stelzer, 2014). The mentioned advancements in fluorescence imaging are achieved by two major modifications. First, the illumination path is separated from the detection path by an orthogonal alignment of the objective lenses. That allows the simultaneous detection of the entire focal plane and the subsequent record of a two-dimensional image along different positions within the specimen (Pampaloni et al., 2013). Second, the sample is moved, in respect to the detection path, through a thin cuboid of laser light, so called light-sheet which results in a stack of images in z direction, termed z-stack. The construction of the LSFM provides a true axial resolution, which is dependent of the thickness of the generated laser light sheet, and optical sectioning of the sample because it illuminates only the focal plane of the detection optics and generate no out-of-focus fluorescence (Huisken et al., 2004).

### 1.8.3. The two different ways to generate the light sheet

The laser light sheet can be generated in two different ways. The first developed light sheet-based microscope is called single plane illumination microscopes (SPIM). It generates a sheet of light by focusing a collimated laser beam with a cylindrical lens to a static sheet of light (Huisken et al., 2004). However, in the monolithic digital scanned laser light sheet fluorescence microscope (mDSLMS) the light sheet is produced by a line-scanned, diffraction limited Gaussian beam which enables the modulation and synchronisation of the power of the laser beam with

the beam movement (Azzarelli et al., 2018; Baumgart et al., 2012; Keller et al., 2008). In microscopy, spatial resolution is determined by two resolution capacities. On the one hand it is dependent on the lateral resolution which is, in LSM, identical to CLSM, and on the other hand determined by axial (along the optical axis, “z”) resolution. In LSM the axial resolution is determined by the thickness of the illuminating beam as a result of the three-dimensional point spread function (PSF). For the additional improvement of the axial resolution, the image stacks can be generated along different view angles and subsequently fused to one image, termed multi-view image fusion (Huisken et al., 2004; Keller et al., 2010).

Next to the optical properties of microscope system itself, the image quality of the region of interest depends on several factors: first, on the optical properties of the specimen itself, second, on the media the specimen is embedded in (mounting medium) and third, of the general positioning of the illumination and detection objectives (within the mounting media or as an air objective). Dependent on these three factors, the light sheet and the generated photons need to cross several different refraction indices (RI) along the optical axis. This further reduces the quality of the resulting images. Finally, the specimen itself is the limiting factor. Dependent on its size, optical properties, the needed resolution to identify targets and the needed temporal resolution to image dynamic processes, the light sheet-type should be chosen. The static light sheet can be produced in one step which leads in a lower acquisition time in comparison to the scanned light sheet. However, the scanned light sheet provides a better axial resolution, has a much higher illumination efficiency (96 % in comparison to 3 % with a static light sheet) and a reduced light scattering due to the option of structured illumination (Keller et al., 2008).

## 1.9. Organoids for three-dimensional microscopy

In this work, the focus is laid on organoids. As already mentioned, organoids arise from single cells or small clusters of cells forming monolayered liquid-filled three-dimensional spheres and are therefore suitable for microscopic analysis in terms of optical properties. The monolayer of cells does not scatter the light in a reasonable manner. The circumventing matrix consists, as mentioned mainly of water, consequently, shows only small deviations to the circumventing liquid interface. Whether the luminal liquid has a water comparable RI is not really known, but several studies on other organoids systems suggest that it has comparable optical properties like the circumventing medium (Broutier et al., 2017; Dekkers et al., 2019; Held et al., 2018; Mahe et al., 2013). However, organoids show a high sensibility in terms of physical stability and, because of their stem cell-ness, are highly sensitive to phototoxic damaging. For this reason, handling and imaging of organoids need to be adapted which is discussed in the following section.

### 1.9.1. General challenges in organoid imaging

In theory, organoids display an optimal microscopic sample in terms of optical properties. In practical terms, imaging of organoids is challenging. First, organoids are highly sensible to physical deformation. Due to their phenotype, they are not able to resist physical forces which can lead to deformation or bursting and subsequent loss of their phenotype. Because they are embedded in an ECM, deformation of the circumventing ECM is also transferred to the organoids. Second, in terms of their stem cell-ness and their high cell proliferation activity it

makes them highly sensitive for DNA damage due to extrinsic factors like photo toxicity, changes in the pH-value of the growth medium, starvation due to high metabolic turnover rates or in general temperature fluctuations (Kenyon et al., 2007). Third, their highly dynamic growth behaviour requires short recording intervals which is usually accompanied with a high photo toxic exposure. The last two former mentioned properties are only important for the live imaging under physiological condition. The physical deformation can be partly solved by fixing the organoids and the circumventing ECM.

### 1.9.2. Immunofluorescence labelling in organoids

In general, Immunofluorescence imaging (IF) is a widely used method to study protein distribution *in situ*. Antibodies with high epitope binding specificity are able to bind to corresponding proteins within the cell. The combination of various antibodies with fluorophores allows the labelling of different proteins within cells (Coons et al., 1950). Usually, IF is performed after the fixation and if the target is localized within the cell, permeabilization of the samples is necessary to allow the antibody to enter. Therefore, IF usually illustrates the endpoint of an experiment. Although extensive progress has been made by developing methods and antibodies to target and label epitopes in living cells, their usability and adaptability to organoid cultures need to be addressed (Reviews: Fernández-Suárez et al., 2008; Hanson et al., 2008; Terai et al., 2008)

However, existing protocols for the IF of 3D cell cultures need to be adapted. Huch and colleagues published a protocol for the histological analysis of mouse and human liver organoids. They utilize the widely used fixative paraformaldehyde (PFA) and recommend whole-mount staining for the best results (Broutier et al., 2016). One major drawback of staining the organoid within the ECM is that antibodies are relatively large (dependent on the antibody  $\approx$  150kDA) and carry charged amino acid residues which may affect the diffusion of the antibodies through the ECM because of steric and physical hindrance. Since the ECM is a complex mixture of various proteins, which offer many epitopes, the unspecific binding of the antibody within the gel is highly possible and can lead to a high background noise.

### 1.9.3. The ultra-thin FEP-foil cuvette holder for 3D observation of big biological samples

Imaging living 3D cell systems is always challenging. Because of the size of the sample, many microscopes soon reach their limitations in terms of penetration depth. In CLSM, the use of culture plates with a glass culture surface is needed to generate high resolved images and reduce light scattering. Beside the use of ultra-thin glasses (e.g., borosilicate glasses with a thickness of 1.5 mm), flat and optimized culture well designs can help to increase the working distance in scales of micrometres. However, the only microscope systems which are able to image large living specimens are the above-mentioned LSFM systems. In contrast to conventional brightfield and CLSM systems, the sample needs to be mounted on a specific sample holder to be inserted and imaged within the chamber inside the LSFM (Huisken et al., 2004; Pampaloni et al., 2013). Because of its transparency and biocompatibility, mainly agarose and other hydrogels have been used to immobilise and place the living specimen during the image acquisition (Huisken et al., 2004; Pampaloni et al., 2013; Strobl et al., 2015; Susaki et al., 2015). Agarose-gel embedding is mainly used for mounting embryos of model organism like

drosophila or zebrafish but not useable to mount hollow 3D cell cultures like organoids. The embedding of organoids in agarose deforms the ECM that surrounds the organoid and also deforms the organoid itself.

#### 1.9.4. The ultra-thin fluorocarbon foil cuvette

To circumvent this issue, we recently developed the ultra-thin FEP-foil cuvette (further referred as FEP-foil cuvette) for the use in the mDSLIM. This multi-faceted cuvette is based on an ultra-thin fluorocarbon (FEP) foil (10-12  $\mu\text{m}$  thickness) which can be shaped by heat and a vacuum. It is gas permeable but impermeable to liquids, stable but flexible, inert and durable, and subsequently illustrates a small chamber within the microscope chamber. In addition, FEP-foil has nearly the same RI as water. With these properties it is optimally suitable for the imaging of living 3D cell cultures (Hötte et al., 2019). Moreover, it has been shown that organoids can grow within this FEP-foils cuvette within the cell culture incubator. Up to now, the immunofluorescence labelling, and microscopic visualisation was only possible after fixation and staining. Possible adaptations need to be performed and more research needs to be conducted to validate that the organoids can be grown and imaged within the light sheet microscope.

#### 1.10. Segmenting and tracking the organoids development and behaviour

Organoid systems have the potential to recapitulate organ-specific developments and diseases (Dutta et al., 2017; Fatehullah et al., 2016; Kretzschmar et al., 2016; M. A. Lancaster et al., 2019) which can lead to a breakthrough in personalized (Broutier et al., 2017; de Winter-De Groot et al., 2018) and regenerative medicine approaches (Okamoto et al., 2020; Takeda et al., 2013). However, quantitative as well as qualitative reference parameters are still missing. Nowadays, advanced molecular biology ranges from the analysis of single cell transcriptomics to large-scale omics data of complete organoid populations. Even though these analyses identified rare populations or trajectories of cell population it does not comprise a comprehensive overview of single cell or whole organoid behaviour and global morphological changes. In contrast, time-resolved advanced microscopy allows the analysis of whole organoid populations and still provides data of single cell behaviour. Sebrell and colleagues used time resolved brightfield image analysis to quantify the growth of human gastric epithelial spheroids. By manually measuring the diameter of developing organoids they were able to generate growth curves. However, only a small number of organoids were analysed at that point (Sebrell et al., 2018). A step forward was made by Kassis and colleagues. They developed a deep convolutional neural network implementation (termed OrgaQuant) that identifies, locates and quantifies the size distribution of human intestinal organoids. As mentioned, it is based on brightfield images but equipped with an automated computational analysis (Kassis et al., 2019). In contrast, Dekkers and colleagues developed a more advanced forskolin swelling assay by using calcein green-labelled intestine organoids imaged with fluorescence confocal microscopy and subsequently measured size changes (Dekkers et al., 2013). More recently, Bolhaquero and colleagues were able to use a confocal spinning disc microscope and observed single mitotic events in single organoids and associated them with chromosomal segregation errors (Bolhaquero et al., 2019). At the same time, Serra and colleagues were able to analyse the development of multiple organoids arising from a single cell. With image parallelisation,

they were able to image multiple drops that contain organoids by the use of an inverted LSMF (Serra et al., 2019).

All the above-mentioned investigations illustrate that unlike single cell cultures, no method is existing that captures and quantifies organoid systems *in toto*. Because every microscope and the developed technics have their limitations, the use of different types and the combination of the obtained data to one comprehensive result may offer a solution to identify the multi-cellular self-organisation parameters that determine the organoid behaviour and morphology. This technique enables the analysis at a macroscale (complete organoid droplets) at a mesoscale (single organoid) and at a microscale (organoid on a single cell level).

### 1.11. Main contribution of this thesis

Pancreas organoids as a recently developed cell culture system gained enormous potential for clinical applications and disease research. However, basic knowledge of the culture growth behaviour is still missing. For this reason, this study aims to assess first the development of reliable methods to track and analyse organoid behaviour, development and heterogeneity by using light microscopy and second, investigate how organoids maintain and build their hollow spherical phenotype on a cellular level.

The question addressed in this work are:

- Is it possible to generate valid and reliable growth parameter and what kind of analysis is needed to obtain them?
- To understand the organoid phenotype as a hollow liquid filled lumen:
  - o Do the organoids need the ECM as a physical scaffold, as ligand provider for their surface binding proteins or both?
  - o What are the components of the luminal liquid and are specific substances released in it?
  - o What drives the organoid lumen maintenance on a cellular / biophysical / biochemical level?

The tasks addressed in this work are:

- Develop and adjust present experimental setups for the imaging of 3D cell aggregates in brightfield, confocal and Light sheet microscopy to the use in organoid culture.
- Assess and generate a complete overview of the organoid's heterogeneity and appearance.
- Combine present evaluation methods and develop new methods of light microscopy image evaluation to analyse pancreas organoids on multiple scales (*in toto*).
- Generate robust and valid data of organoid growth and behaviour for the future clinical application.
- Develop or adjust new methods to reduce or circumvent the employment of Matrigel® or BME as ECM.
- Develop or adjust present methods to investigate the organoid luminal phenotype.

## 2. Material and Methods

### 2.1. Chemicals

Table 1: List of chemicals used in this thesis

<b>Material</b>	<b>Manufacturer</b>
10xCB (pH 7.2)	Cellendes GmbH
Advanced DMEM/F12	Life Technologies
RPMI 1640 Medium	Thermo Fisher Scientific
SILAC Advanced DMEM/F12 Fex Media without Phenol red	Thermo Fisher - Gibco
Recovery™ Cell Culture Freezing Medium	Thermo Fisher Scientific
B-27 Supplement	Life Technologies
Albumin Fraction V	Carl Roth
FBS	Thermo Fisher Scientific
HEPES 1M	Life Technologies
Hyaluronidase Type IV-S (H4272)	Sigma-Aldrich
Hyaluronidase Type IV-S (H3884)	Sigma-Aldrich
Gastrin I Human	Sigma-Aldrich
GlutaMax (100x)	Life Technologies
Glycine	Carl Roth
Goat serum	Life Technologies
Hellmanex-II	Thermo Fisher Scientific
Lysozyme	Carl Roth
Matrigel® Matrix, Phenol Red-free	Corning
N-Acetylcysteine	Sigma-Aldrich
Nicotinamide	Sigma-Aldrich
PBS	Life Technologies
Paraformaldehyde (PFA)	Sigma-Aldrich
Penicillin/Streptomycin	Life Technologies
Recombinant Mouse EGF	Peprtech

Recombinant Human FGF10	Peprotech
Recombinant Human Noggin	Peprotech
Recombinant Mouse EGF	Peprotech
RGD Peptide	Cellendes GmbH
SG PVA #788	Cellendes GmbH
HA-SH #242	Cellendes GmbH
Triton X-100	Carl Roth
Tween-20	Carl Roth

## 2.2. Islets of Langerhans culture components

Table 2: Components of the medium to maintain freshly isolated Islets of Langerhans

Growth Medium	RPMI Medium
	10 % FBS
	1 % Penicillin-Streptomycin (PenStrep)

## 2.3. Organoid Culture components

Table 3: Components of the organoid growth media which need to be pre-solved and stored at -20°C

Pre-solved compounds stored at -20 °C	Stock solution
N-Acetylcysteine	500 mM in PBS
Nicotinamide	1 mM in PBS
Recombinant Human FGF10	1 mg/ml in PBS+0,1 % BSA
Recombinant Human EGF	500 µg/ml in PBS+0,1 % BSA
Recombinant Mouse EGF	500 µg/ml in PBS+0,1 % BSA
Gastrin I Human	100 µM in PBS
TGF-β inhibitor (A83-01)	5 mM in DMSO
Forskolin	10 mM in DMSO
Recombinant Human Noggin	100 µg/ml in PBS+0,1 % BSA
PGE2	10 mM in DMSO

Table 4: Components of organoid growth media which need to be pre-solved and stored at -4°C

Pre-solved compounds stored at 4 °C	Stock solution
Human EGF	5 µl (100 µg/ml) + 45 µl Basal Medium



Gastrin	10 $\mu$ l (100 $\mu$ M) + 30 $\mu$ l Basal Medium
Noggin	10 $\mu$ l (100 $\mu$ g/ml) + 90 $\mu$ l Basal Medium

Table 5: Composition of the basal medium for the culture of organoids

Basal Medium	485 ml Advanced DMEM/F12 / const.
	5 ml HEPES / final 10 mM
	5 ml Penicillin-Streptomycin
	5 ml GlutaMax

Table 6: Composition of the basal medium without Phenol red for the use with CRM

Basal Medium for CRM	10 ml SILAC Advanced DMEM/F12 FEX Media without Phenol red / const.
	32 mg D-Glucose
	62,91 $\mu$ l Arginin / final 0,69 mM
	44,87 $\mu$ l Lysin / final 0,49 mM
	100 $\mu$ l HEPES / final 10 mM
	100 $\mu$ l Penicillin-Streptomycin
	100 $\mu$ l GlutaMax

Table 7: Composition of the murine B-27, Nac-stock medium

Murin B-27, Nac-stock medium	9.6 ml Basal medium
	400 $\mu$ l B-27 supplement
	50 $\mu$ l N-acetylcysteine (final 2.5 mM)

Table 8: Composition of the human N2, B-27, Nac-stock medium

Human N2, B-27, Nac-stock medium	9.6 ml Basal medium / const.
	400 $\mu$ l B-27 supplement
	200 $\mu$ l N2 supplemental
	50 $\mu$ l N-acetylcysteine / final 2.5 mM

Table 9: Composition of the murine expansion medium

Murine pancreas expansion medium	5ml 2x B27Nac stock medium / const.
	4.5 ml Basal medium
	5 ml R-spondin condition Medium
	100 $\mu$ l Nicotinamide / final 10 mM

10 µl recombinant mouse EGF / final 50 ng/ml
10 µl recombinant human FGF10 / final 100 ng/ml
10 µl recombinant Noggin / final 25 ng/ml
10 µl Gastrin / final 10 nM

Table 10: Composition of the human expansion medium

Human pancreas expansion medium	5ml 2x B27Nac stock medium / const.
	9.5 ml Basal medium
	10 µl recombinant R-Spondin / final. 1 ng/ml)
	100 µl Nicotinamide / final 10 mM
	10 µl recombinant mouse EGF / final 50 ng/ml
	10 µl recombinant human FGF10 / final 100 ng/ml
	10 µl recombinant Noggin /final 25 ng/ml
	10 µl Gastrin / final 10 nM
	10 µl A83 / final 5 µM
	10 µl Forskolin / final 10 µM
	3 µl PGE2 / final 3 µM

#### 2.4. Components for human embryonic kidney (Hek) 293T-HA-R-spondin1-Fc cells

Table 11: List of components used for the generation of R-spondin conditioned medium

Component's growth medium	Concentration	Origin / Cat. Nr
DMEM 31053	-	Gibco / 1797322
Fetal bovine serum (FBS)	10 %	Gibco / 42F5561K
Glutamax	1 %	Gibco
100X Penicilin-Streptomycin	1 %	Gibco
<b><u>Components conditioned medium</u></b>		
DMEM 31053	-	Gibco / 1797322
Fetal bovine serum (FBS)	10 %	Gibco / 42F5561K

Glutamax	1 %	Gibco
100X Penicilin-Streptomycin	1 %	Gibco
Zeocin	300 µg/ml	Invitrogen / 1771480

## 2.5. Organoid donor material

Table 12: List of the used human organoid lines and their origin

Name of human pancreas organoid line	Origin / Reference
Human Donor 25	Metrixel Huch / (Georgakopoulos et al., 2020)
Human Donor 37	Metrixel Huch / (Georgakopoulos et al., 2020)
Human Donor 1803	Lorenza Lazzari / (Dossena et al., 2020)
Human Donor 1804	Lorenza Lazzari / (Dossena et al., 2020)
Human Donor 1805	Lorenza Lazzari / (Dossena et al., 2020)

Table 13: List of the used murine organoid lines and their origin

Name of murine pancreas organoid line	Origin / Reference
Mouse Donor NHBSI16	Metrixel Huch / (Huch, Bonfanti, et al., 2013)
Mouse Donor C230316	Metrixel Huch / (Huch, Bonfanti, et al., 2013)
Mouse Donor MHOW 21C - RFP-Gt(ROSA)26Sortm1(CAG-tdTomato*, -EGFP*)Ees	Metrixel Huch / (Huch, Bonfanti, et al., 2013)
Mouse Donor C22814 - NGN3-YFP	Metrixel Huch / (Huch, Bonfanti, et al., 2013)

## 2.6. Components for immunofluorescence labelling of organoids

Table 14: List of components used for the immunofluorescence labelling of pancreas organoids

Material	Origin
PBS	Life Technologies
Triton X-100	Carl Roth
Tween-20	Carl Roth
Fetal bovine serum (FBS)	Sigma-Aldrich
Penicillin/Streptomycin	Life Technologies
Paraformaldehyde (PFA)	Sigma-Aldrich

## 2.6.1. Blocking solution for immunofluorescence labelling of organoids

Table 15: List of components to produce the blocking solution for immunofluorescence labelling of pancreas organoids

Blocking solution components	Amount for 10 ml solution
PBS	7533,4 µl
Triton X-100 (3 % in PBS stock-solution)	666.6 µl (0,2 %)
Tween-20 (1 % in PBS stock solution)	500 µl (0,05)
Bovine serum albumin (BSA) (10 % in MilliQ)	100 µl (0,1)
Penicillin/Streptomycin	200 µl (2 %)
Fetal bovine serum (FBS)	1000 µl (10 %)

## 2.6.2. Antibodies and dyes

Table 16: List of the used primary antibodies used to specify organoid origin

Primary antibody	Dilution	Species	Isotype	Origin / Cat. Nr.
α-Sos9	1:50	rabbit	IgG	Millipore / AB5535
α-ZO-1 (DO114)	1:100	goat	IgG	Santa Cruz / sc-8146
α-E-cadherin (DECMA)-1	1:100	rat	IgG1	Abcam / ab11512
α-Pdx 1	1:100	goat	IgG	Abcam / ab47383
α-Muc1	1:200	hamster	IgG	Thermo Fisher Scientific / HM-1630-P1ABX
α-β-catenin (H-102)	1:100	rabbit	IgG	Santa Cruz / sc-7199
α-Yap	1:50	mouse	IgG2A	Santa Cruz / sc-101199
α-Krt19	1:100	rabbit	IgG	St. John's Lab / STJ24355
α-Ezrin	1:100	Mouse	IgG1	Santa Cruz / sc-58758
α-Neurogenin 3	1:50	rabbit	IgG	Abcam / ab38548
α-Nkx 6.1	1:50	goat	IgG	R&D Systems / AF5857
α-CFTR	1:50	mouse	IgM	Abcam / ab2784
α-Piezo-1	1:50	rabbit	IgG	Novus Biologicals / NBP1-78537
Aquaporin 1	1:200	rabbit	IgG	Bioss Antibodies / 1506R-TR
Aquaporin 5	1:200	rabbit	IgG	Bioss Antibodies / 1554R-TR

Aquaporin 8	1:200	rabbit	IgG	Bioss Antibodies / 6786R-TR
-------------	-------	--------	-----	-----------------------------

Table 17: List of the used secondary antibodies used to specify organoid origin

Secondary antibody	Dilution	Species	Target	Origin / Cat. Nr.
$\alpha$ -mouse Alexa Fluor 488	1:400	goat	IgG2A	Thermo Fisher Scientific / A21131
$\alpha$ -mouse DyLight 550	1:400	goat	IgM	Abcam / 97008
$\alpha$ -mouse Alexa Fluor 568	1:400	donkey	IgG	Thermo Fisher Scientific / A10037
$\alpha$ -mouse Cy5	1:400	goat	IgG	Thermo Fisher Scientific / A10524
$\alpha$ -rabbit Alexa Fluor 488	1:400	goat	IgG	Thermo Fisher Scientific / A11008
$\alpha$ -rabbit Alexa Fluor 568	1:400	goat	IgG	Thermo Fisher Scientific / A11011
$\alpha$ -rabbit Alexa Fluor 633	1:400	goat	IgG	Thermo Fisher Scientific / A21070
$\alpha$ -goat Alexa Fluor 488	1:400	donkey	IgG	Thermo Fisher Scientific / A11055
$\alpha$ -hamster Alexa Fluor 546	1:400	goat	IgG	Thermo Fisher Scientific / A21111
$\alpha$ -rat Alexa Fluor 633	1:400	goat	IgG	Thermo Fisher Scientific / A21094

Table 18: List of organic dyes for fluorescence microscopy

Dye	Dilution	Target	Origin / Cat. Nr.
DAPI 405	1:200	Nucleus	Invitrogen
Draq 5	1:500	Nucleus	Thermo Fisher / 62251
Alexa Fluor 546 Phalloidin	1:200	Actin	Mol Probes / A22283
Alexa Fluor 647 Phalloidin	1:200	Actin	Mole Probes / A22283
FLUO-8 AM	5 $\mu$ M	Ca <sup>2+</sup>	Abcam / C50H50N2O23)
FDA (Fluorescein diacetate)	5 $\mu$ g/ml	Cell viability	Merck / 8F7378
Promidium iodide	1 mg/ml	Dead cells	Merck / P4170

## 2.7. Used Microscopes

Table 19: List of used microscopes

Description	Origin / Cat. Nr.
Confocal laser scanning Microscope Zeiss LSM 780	Carl Zeiss AG
Brightfield Microscope Zeiss Cellobserver Z.1	Carl Zeiss AG
Stereo Microscope Zeiss Stereo Discovery V.8	Carl Zeiss AG
Light sheet-based fluorescence microscope Zeiss Lightsheet Z.1	Carl Zeiss AG
Light sheet-based fluorescence microscope mDSLM	Physical Biology, BMLS, Goethe University Frankfurt

## 2.8. Clearing solution CUBIC-II

Table 20: Components of the clearing solution CUBIC-II

Chemicals	Concentration	Origin / Cat. Nr.
Sucrose	50 wt%	Carl Roth / 4621
Urea	25 wt%	Sigma / U1250
2,2',2''-nitrilotriethanol (Triethanolamine)	10 wt%	Sigma / 90279
Water (ultra-pure)	15 wt%	Physical Biology, BMLS, Goethe University Frankfurt

## 2.9. Drugs

Table 21: List of drugs that were used in the brightfield pipeline

Name	Origin / Cat. Nr.
Cytochalasin D	Enzo / ALX-380-031
Para-(nitro)-Blebbistatin	Optopharm / DR-N-111
Paclitaxel	Merck / T1912
Nocodazole	Merck / M1404
GlyH-101	MedChemExpress / Hy-18336
CFTRinh-172	Sigma / C2992
GsMTx-4	Alomone / STG-100
Yoda 1	Merck / SML1558

## 2.10. Special devices and consumables

Table 22: List of special devices and consumables

Description	Origin / Cat. Nr.
FEP-foil (50 µm thickness) to form the cuvette	Lohmann Technologies
JT-18, thermal vacuum forming machine	Jin Tai Machining Company, Yuyao, PR of China
3D-printed the positive moulds to form the FEP-foil cuvette	Shapeways (Eindhoven, The Netherlands)
glass capillary (borosilicate glass 3.3) to connect the FEP-foil cuvette with the micropipette	Hilgenberg, material # 0500
flame retardant polyolefin tube, size 3, to connect the FEP-foil cuvette with the glass capillary	G-APEX
200 µl micropipette to place the FEP-foil cuvette in the Zeiss Lightsheet Z.1 sample holder	Blaubrand intraMark
TipOne 10/20 µl Bulk to fill the FEP-foil cuvette	Starlab
1.5mm borosilicate Lap-Tek II culture plates	Lap-Tek
Suspension culture plate (non-coated) 24-well	Greiner / 662102
Suspension culture plate (non-coated) 48-well	Greiner / 677102
Suspension culture plate (non-coated) 96-well	Greiner / 655185
Square Petri Dish	Greiner / 688161
Biobanking and Cell Culture Cryogenic Tubes	Fisher scientific / 10577391

## 2.11. Organoid culture method

All cell culture work has been carried out under sterile conditions. MPO were cultivated as described in Huch, Bonfanti, et al., 2013 and hPO as described in Georgakopoulos et al., 2020. The organoids were cultured in a Heracell™ 150i CO<sub>2</sub> Incubator at 37 °C and 5 % CO<sub>2</sub>. HPO and mPO were handled and processed in the same way. Differences in the medium compositions were considered (look at: 2.3) and mPOs were cultured in a droplet of Matrigel® and hPOs in BME.

### 2.11.1. Thawing of organoids

Already isolated organoids were received as frozen samples. The cells were defrosted in a 37°C heated water bath, transferred in 10ml pre-warmed basal medium and centrifuged at 250 rpm for 45 minutes at 8°C. The supernatant was discarded, the droplet of cells resolved in freshly thrown ECM (Matrigel® for murine and BME for human organoids), placed as droplets in a 37°C pre-heated multi-well plate (12 µl droplet for 96 well-plate, 25 µl droplet for 48 well-plate, 50 µl droplet for 24 well-plate) and transferred in an incubator for solidification. After 10 minutes, the droplets were covered with pre-warmed (37°C) expansion medium (125 µl for 96

well-plate, 250  $\mu$ l for 48 well-plate and 500  $\mu$ l for 24 well-plate) and the surrounding wells filled with the same amount pre-warmed PBS. Afterwards, the multi well-plate was retransferred into the incubator. After the first 24 hours, the medium was changed, followed by a frequent exchange of medium ever two to three days. In the first three days of cultivation, Rock-inhibitor Y-27632 (1:100) was added to the medium.

#### 2.11.2. Splitting of organoids

After at least 7 days of growth the organoids were passaged as followed (all steps were process on ice, the ratio depends on the amount of organoid within one droplet, general ratio is 1:4 – 1:6). For each well, 3 ml ice cold basal medium was added into a 15 ml falcon, 1 ml of it was added to each well containing the organoids. The organoids within the ECM were detached from the well-bottom by scratching with the pipette tip and pipetting up and down. Subsequent, the organoid suspension was transferred into the falcon and centrifuged at 200 g for 5 minutes at 8 °C. After the centrifugation the supernatant was discarded, leaving ~500  $\mu$ l organoid-medium-mixture in the tube. To further disrupt the organoid into fragments the organoid-medium-mixture was pipetted up and down by using a 200  $\mu$ l tip. Alternatively, Pasteur pipettes made from glass with a flame narrowed tip were used. Afterwards, 3 ml ice cold basal medium per organoid droplet was added and the tube centrifuged at 250 g for 5 minutes at 8 °C. Afterwards the supernatant was discarded, the organoid fragments re-suspended in freshly defrosted ECM (Matrigel® for murine and BME for human organoids) and placed as droplets (12  $\mu$ l droplet for 96 well-plate, 25  $\mu$ l droplet for 28 well-plate, 50  $\mu$ l droplet for 24 well-plate) into a multi-well plate. The Multi-well plate was then carefully transferred into an incubator (37 °C and 5 % CO<sub>2</sub>) and the ECM solidified for at least 10 minutes. Afterwards the droplets were covered with the corresponding amount of pre-warmed expansion medium (125  $\mu$ l for 96 well-plate, 250  $\mu$ l for 48 well-plate and 500  $\mu$ l for 24 well-plate) and the surrounding wells filled with pre-warmed PBS. The Multi-well plate was then carefully transferred into an incubator (37°C and 5 % CO<sub>2</sub>). Every 2 to 3 days, or when the medium turns yellow, the medium was exchanged and after 7 to 10 days the organoids were splitted again.

#### 2.11.3. Freezing of organoids

To freeze organoids, the normal splitting procedure was processed up to the point of re-suspending the organoid fragments into the fresh ECM. Instead of that the fragments are transferred in ice-cold Recovery Freezing Medium (250  $\mu$ l per 25  $\mu$ l droplet) within a cryovial and placed for 24 hours in a cryo-container at -80°C. Afterwards the cryovial was placed in liquid nitrogen for long term storage. A maximum of two 25  $\mu$ l droplets were frozen in one cryovial.

#### 2.11.4. Generation of R-Spondin conditioned medium

To produce R-spondin condition medium, human embryonic kidney (Hek) 293T-HA-R-spondin1-Fc cells (Culturex) were used. They were maintained in DMEM 31966 (GIBCO) which was supplemented with 12 % fetal bovine serum (FBS) (GIBCO), 1 % GlutaMax (GIBCO), 1 % penicillin/streptomycin (GIBCO) and 300  $\mu$ g/ml Zeocin (Invitrogen) until confluency. Then, the growth medium was replaced with organoid basal medium and cells were incubated for 7 to 10 days without media change. For the use in organoid growth medium, the conditioned



medium was centrifuged, filtered (0.22 µm PES filter) and subsequently the R-Spondin activity was determined by a TOPFlash assay (performed by Lotta Hof, Physical Biology, working group of Prof. Dr. Stelzer, BMLS, Goethe-University Frankfurt)

### 2.12. Human pancreas organoids

Human adult pancreas-derived organoids have been generated and initiated from two different cooperation partners:

(1) The lab of Dr. Metrixel Huch at The Wellcome Trust/ Cancer Research UK Gurdon Institute, University of Cambridge from patients collected during surgery performed at Cambridge Biorepository for Translational Medicine & Department of Surgery, University of Cambridge and NIHR Cambridge Biomedical Research Center (UK).

(2) The lab of Dr. Lorenza Lazzari at Laboratory of Regenerative Medicine – Cell Factory, Department of Transfusion Medicine and Hematology, Fondazione IRCC Ca'Granda Ospedale Maggiore Policlinico (IT).

Independent from the lab, all lines have been proven to be bi-potent ductal cells and suitable for the culture as pancreas organoid (Dossena et al., 2020; Huch, Bonfanti, et al., 2013). All used lines are listed here: 2.5

### 2.13. Mouse pancreas organoids

Murine adult pancreas-derived organoids have been generated and initiated from the lab of Metrixel Huch at The Wellcome Trust/ Cancer Research UK Gurdon Institute, University of Cambridge. All used lines are listed here: 2.5

### 2.14. Media components

Basal Medium was pre-mixed and used within 4 weeks. N2, B-27, Nac-stock medium and pancreas expansion medium were mixed freshly and used within 2 weeks. All components were stored at -20 °C before and after dissolved in the recommended solvent. For the use, the components were defrosted on ice. Recombinant EGF, Gastrin and Noggin were pre-solved in basal medium and stored at 4°C up to 2 weeks. BME and Matrigel® as ECM, were defrosted slowly on ice short before usage.

### 2.15. Hanging Drop

The hanging drop culture technique was initially established to form and culture spheroids out of a cluster of loose cells (Kelm et al., 2003). Here, this technique was adapted to the use with pancreas organoids to reduce the amount of ECM within the organoid culture system. A graphical abstract is illustrated in Figure 20.

### 2.15.1. Initiation

To initiate the pancreas hanging drop system, an already existing organoid culture can be used. Theoretically, the HD-system can be initiated out of fresh donor material (e.g., from a biopsy) but due to the unavailability of fresh donor material, it was not possible to test this option.

Pancreas organoids embedded in a droplet of ECM were splitted as mentioned (2.11.2). After the organoids were fragmented and centrifuged at 250 rpm at 8°C, the fragments were resolved in ice cold expansion medium containing 4 % dissolved Matrigel® and 10 µM Rock inhibitor Y-27632. The Matrigel®-medium-mix has already been prepared on ice short before usage. To ensure a homogeneous distribution and no clumping of the Matrigel®, the mixture is pipetted up and down at least 10 times. The Matrigel®-medium was always prepared fresh and cannot be stored. After the organoid fragments were resolved in the Matrigel®-medium-mix, 25 µl drops were smoothly placed on the inner side of a squared petri dish. The drops were placed beginning at the middle of the dish towards the outside. Depending on the size of the used squared petri dish, the number of drops varied. As a guiding principle, drops were placed at least in a distance of 1 cm from each other whereas the gap between the drop and the edges of the squared petri-dish should be as big as possible. After the 25 µl drops were placed on the lid, the lid was turned up-side-down (180°) in one smooth and constant move and placed on the bottom of the squared petri dish which has been pre-filled with pre-warmed (37°C) PBS. Dependent on the size of the squared petri dish, the amount of PBS varied. However, the complete bottom should be covered with pre-warmed PBS. After the lid with the drops was placed on the bottom, the complete construct was transferred into an incubator (37°C, 6 % CO<sub>2</sub>, 95 % humidity). After 24 hours, 10 µl of organoid expansion medium containing 4 % solved Matrigel® without Rock-inhibitor Y-27632 was added to each drop. Therefore, the lid of the squared petri dish was turned again down-side-up (180°) in one smooth move and the 10 µl were added carefully to the drops. As a guiding principle, the expansion medium was added by penetrating the drop softly at the surface and not by a drop that falls onto it. After the medium has been added to each drop, the lid was durned up-side-down, placed on the bottom of the lid and transferred back to the incubator. From now on, every 48 hours 10 µl of expansion medium containing 4 % Matrigel® was added to the drops.

After at least 7 days in culture, the organoids need to be splitted (2.11.2). Depending on the organoids growth rate, the time for the first split after HD-culture initiation varied between 7 and 12 days. As a guiding principle, the organoids were always splitted after they stop increasing their overall size.

In theory, the HD-culture system should be feasible for the use of fresh isolated ductal material. Therefore, the protocol published from Huch and colleagues can be used (Broutier et al., 2016). Instead of seeding the ductal fragments into droplet of ECM they should be seeded into a hanging drop containing 4 % of solved Matrigel®.

### 2.15.2. Maintenance

After the HD-culture system is initiated (2.15.1) the organoids need to be splitted regularly to maintain their growth potential and increase the overall cell mass. The general setup of that process is similar to the culture of organoids in ECM droplets.

The initiated HDs were taken out of the incubator, the lid was turned down-side up, and the drops were collected in a 15ml Falcon tube. Per 3 drops an amount of 1 ml ice cold basal medium was added and the falcon was centrifuged at 200 rpm and 8°C for 5 minutes. The supernatant was discarded leaving ~ 1ml basal medium containing the organoids. The organoids were then disrupted into cell fragments by up and down pipetting with a 200 µl tip. Alternatively, a glass Pasteur pipettes with a flame narrowed tip were used. Afterwards, 1 ml ice cold basal medium was added per HD and centrifuged at 250 g for 5 minutes at 8 °C. After the last centrifugation step the supernatant was discarded carefully until only a small drop of organoid fragments was left. The fragments were then dissolved in 4°C cold medium containing 4 % solvated Matrigel®. Depending on the amount of material, the amount of medium need to be chosen. As a rough guideline a 1:3 ratio can be used. Depending on the number of organoids within one HD, the ratio was adapted every time. The medium-Matrigel®-cell-fragment-mix was then placed as 25 µl drops on the inner side of a squared Petri dish lid. The lid was then turned smoothly 180° and placed on the Petri dish bottom which was filled with 37°C pre warmed sterile PBS beforehand. The Petri dish was then placed in an incubator (37°C, 6 % CO<sub>2</sub>, 95 % humidity). After the first 24 hours 10 µl of Medium containing 4 % Matrigel® was added to each drop. From then on, every 48 hours 10 µl of Media with 4 % Matrigel® was added to each drop until the organoids reached their desired size or days in culture. This procedure is repeated ever 7 to 12 days.

### 2.15.3. Single cell generation

To generate a HD-culture from single organoid cells, two different approaches were conducted. First, organoids which were already in the HD-culture were splitted as described until the first disruption step. The supernatant was discarded, and the organoids were incubated for 5 minutes at 37°C with 200 µl PBS supplemented with 0.05 % Trypsin. During the 5 minutes incubation the falcon tube was softly inverted a couple of times. To stop the trypsinization 1ml pre-warmed Basal medium was added and the falcon centrifuged at 250rpm for 5 minutes at 8°C. Afterwards, the organoids were seeded in 25 µl drops as described. The second approach is to generate single organoid cells out of a droplet of ECM containing organoids. Therefore, the same procedure was performed like mentioned before but with 500 µl PBS supplemented with 0.05 % Trypsin and incubated for 10 minutes 37°C. Afterwards, 1.5 ml pre-warmed Basal medium was added to stop the trypsinization and the droplets were handled as described.

### 2.15.4. Re-culture in a droplet of Matrigel®

To test whether the cells grown in the HD-system are able to be re-cultured in a droplet of Matrigel®, organoids in HD were splitted as described and after the last centrifugation step transferred into freshly defrosted drop of pure Matrigel® and placed as 25 µl droplets in a 24-well plate.

#### 2.15.5. Freezing/throwing

The same protocols as described in 2.11.1 and 2.11.3 was used to freeze or thaw organoids growing in the HD-culture system. As a guiding principle, 3 drops reflect on 25 µl ECM droplet in the amount of containing organoids.

### 2.16. Immunofluorescence staining of organoids

Pancreas organoids and organoids in general are usually grown in a droplet of ECM. For the immunofluorescence staining of them, the ECM need to be removed to avoid a high background noise, unspecific antibody binding and in general the accessibility of the antibodies to the organoids. However, the removal of the ECM can be accompanied with alterations in the organoid appearance.

#### 2.16.1. Separation of organoids from Matrigel® or BME

To minimize the impact of the isolation procedure to the organoids, they were fixed within the multi-well plate. Therefore, 4 % PFA solved in PBS was used. ECM in general and Matrigel®/BME in detail de-polymerizes at low temperature to a certain degree. Therefore, the fixation step was performed on ice and to further support the de-polymerization process, the complete multi-well plate was shaken slowly on a shaker (Polymax 1040 Shaker&Mixer). Dependent on the size of the ECM droplet, the time, the organoids needed to be fixed varies between 20 minutes and 2 hours. Subsequently, the 4 % PFA solution was removed, and the organoids incubated for one hour with Cell Recover Solution to further remove the ECM. This step was performed on ice and under continuously shaking. After the incubation, the organoids were carefully pipetted up and down by the use of a 1ml pipette at which the tip was cutted. The pipetting was continued until the organoids were freely floating around. Subsequently, the organoid-Cell Recovery solution was transferred to a 15ml falcon and washed twice with ice-cold PBS.

#### 2.16.2. Blocking, permeabilization and antibody-incubation of organoids

To avoid losing organoids, all following steps were performed under a Stereo microscope. Because isolated organoids tend to stick on surfaces, all tips and Eppendorf tubes were pre-coated with 10 % BSA in PBS solution. To reduce contamination risk PBS was always dosed with 2 % Penicillin and Streptomycin. In addition, all substances were used at room temperature (RT) and did not need any special handling.

The fixed organoids solved in PBS were transferred into a 0.5ml Eppendorf tube and washed twice with PBS. The organoids were then washed three times with 200 µl 150 mM Glycin in PBS for 10 minutes, followed by additional three incubation times of permeabilization with 200 µl PBS dosed with 1 % Triton-X 100 (PBS-T). Afterwards, the organoids were blocked over night at 37 °C while continuously shook at 300 rpm with 300 µl blocking solution (0). Directly before it was used, 10 % FBS or goat serum was added to the blocking solution. To avoid dehydration of the sample, the 0.5ml Eppendorf tube was sealed with Parafilm during the blocking. At the following day, fresh blocking solution (+ 10 % FBS or goat serum) was prepared and mixed with the primary antibodies. The blocking solution containing the sample was discarded and exchanged with the fresh prepared, antibody containing solution. Thereafter,

the sample was incubated at 37°C for 24 hours continuously shaking (300 rpm) and sealed with Parafilm. After the incubation the organoids were washed 3x 1 minute and 3x 5 minutes with PBS-T. In the meanwhile, 200 µl of fresh prepared blocking solution (+ 10 % FBS or goat serum) was mixed with the corresponding secondary antibodies. After the last washing step, PBS-T was replaced with the blocking solution that contains the secondary antibodies and incubated at 27°C for 2 hours under continuously shaking (300rpm) and protected from light. After the incubation, the organoids were washed with PBS-T, stored at 4°C in PBS + 2 % Penicillin and Streptomycin and protected from light until further use.

## 2.17. Preparation of mPOs and hPOs for CRM

The CRM imaging of organoids within a droplet of ECM need some adaptations to guarantee optimal imaging conditions. Because all purchase options of the Basal medium DMEM/F12 contain Phenol red which can lead to aberrations in CRM, SILAC Advanced DMEM/F12 Fex Media without Phenol red were used as expansion medium and pre-prepared by hand as shown in Table 5 (2.3). For the Raman analysis of fixed organoids, 4 % PFA with 1 %/Vol formaldehyde were used to fix (10 minutes at RT without shaking) the organoids and to preserve the ECM droplet. After the fixation, the organoids were carefully detached from the multi-well plate and collected in PBS containing 1 % Penicillin-Streptomycin and stored at 4°C.

To avoid transients during CRM analysis of living organoids, the ECM droplets that contain the organoid fragments, were seeded on CaF<sub>2</sub>-glass slides which were sterilised in 90 % ethanol beforehand and placed within a 9-well plate and covered with 2ml of the expansion medium (prepared for CRM). Short before the CRM analysis, the organoid droplets were taken out of the incubator, transferred to the CRM and immediately imaged.

### 2.17.1. CRM imaging, spectra analysis and calculations

All CRM imaging, analysis and calculations were done by Nathalie Jung, Institute of Pharmaceutical Technology located in the Buchmann Institute for Molecular Life Sciences.

CRM was performed by using an Alpha300R+ system (WITec GmbH, Germany) which was equipped with a 532 nm laser. The laser power was adjusted to 40 mW and a 63x water emersion objective (1.0 NA, Epiplan Neofluar, Zeiss) was used for single cell measurements and an 10x objective (0.25 NA, Epiplan Neofluar, Zeiss, Germany) for complete organoid measurements. To capture the full spectrum, the range was chosen from 400 to 3700cm<sup>-1</sup> with a spectral resolution of 4 cm<sup>-1</sup>. The acquired spectral datasets were processed with WITec ProjectFOUR in terms of a cosmic ray removal and a background subtraction by using the "shape" function. The false-colour Raman images were created by a hierarchical cluster analysis to illustrate the different compartments of the organoid. With this technique the spatial distribution of the average Raman spectra for the different organoid/droplet components (cell nuclei, lumen, ECM) were illustrated. To calculate the protein-water ratio of the organoids lumen, a spectrum of the organoid lumen and of an ECM droplet without organoids (blank) were conducted. Like before, a cosmic ray removal of the data sets was performed. The resulted datasets were further processed in Excel by extracting the Raman peak for proteins (2939 cm<sup>-1</sup>) and water (3280.5cm<sup>-1</sup>). To analyse the water-protein-ratio, the Raman signal intensities of protein and water from the blank gel were subtracted from the

calculated ratios of the lumen of every organoid. The results of the calculations were plotted against the diameter of the measured organoids.

### 2.18. Fluo-8 AM staining

For the staining with Fluo-8 AM mPOs were seeded and cultivated in Lab-Tek II #1.5 borosilicate bottom plates at least for 3 days. At least 20 minutes before the experiments started, the incubation system of the microscope (Confocal laser scanning Microscope Zeiss LSM 780) were activated (37°C, 95 % humidity, 5 % CO<sub>2</sub>) and controlled towards its function. The experiment started with the incubation (37°C, 95 % humidity, 5 % CO<sub>2</sub>) of the organoid droplets with freshly prepared and pre-warmed 5 µM Fluo-8 AM solved in DPBS for one hour. DPBS was used because of its transparency and its defined Ca<sup>2+</sup> amount. The use of DPBS guaranteed a standard of Ca<sup>2+</sup> availability which was not dependent on the amount of solved and available Ca<sup>2+</sup> within the growth media. After one hour of incubation, the solution was discarded and replaced with pre-warmed DPBS. The plate was then transferred into the microscope by using an obscured plastic box to avoid bleaching. After the plate was placed the areas of interests within the organoid droplets were defined and imaged. After the image was taken, the DPBS medium was replaced with 50 µM Yoda 1 containing medium and directly imaged again.

Differences of Fluo-8 AM signal was detected first by eye and second by creating an intensity blot (ImageJ/Fiji) along a defined line through the image before and after the treating with Yoda 1.

Because Yoda 1 must diffuse through the ECM droplet, the impact of it can differ depending on the position of the imaged organoid. To circumvent that and to generate more valuable data, mPO cells were seeded directly on the glass surface of the Lap-Tek plate that was pre-coated with a thin layer of ECM. After at least 7 days, a monolayer of cells had grown on top of the ECM. This 2D cell culture was then treated and imaged as described.

### 2.19. Pancreas clearing and staining

For the clearing of the complete pancreas piece, CUBIC-II was used. Before the pancreas was cleared it was permeabilized for 24 h (2 % Triton X-100 in PBS, 37°C, continuously shaking) and stained with Draq 5 (Draq5 1:500 in PBS, 12 h, 4°C continuously shaking) to visualize the cell nuclei. The CUBIC-II solution was prepared beforehand as followed (2.8). The water and the sucrose were mixed and simultaneously heated up to 68°C. During the heating period, it was mixed with the help of a magnetic stirrer and a magnetic stir bar until the sucrose was completely solved. In the next step, the urea was added, and the solution was mixed until it was solved as well. Before Triethanolamine was added, the solution was cooled down to RT overnight while continuously mixing. At the next day and after the Triethanolamine was added, CUBIC-II was ready to use.

The pancreas piece was covered with CUBIC-II and placed in a thermos-block at 37°C, 400 rpm shaking and protected from light. After 2 days the CUBIC-II was replaced with fresh CUBIC-II. This procedure was done for 7 days before the pancreas piece was subsequently imaged.

## 2.20. Immunofluorescence labelling and vitality determination of islets of Langerhans

To validate the specificity of the used primary antibodies, isolated and fixed islets of Langerhans were used. The fixation was performed with 4 % PFA in PBS at RT for 30 minutes. The immunofluorescence labelling was performed like described in 2.16.2.

Living islets of Langerhans were cultured in RPMI-medium supplemented with 10 %FBS and 1 % PenStrep up to three weeks. Ever two days, the islets were picked by the use of a 1000  $\mu$ l pipette and transferred into a new well containing fresh medium.

To label the cell nuclei, Hoechst 33342 were used. A stock concentration of 5mg/ml was added in a ratio of 1:12000 into the medium containing the islets and incubated for 30 minutes at 37°C in the incubator. Afterwards, the islets were washed with fresh pre-warmed medium three times. To determine the vitality of the islets Fluorescein diacetate (FDA) staining for living cells and a Propidium iodide (PI) staining for dead cells was conducted. Islets were incubated for 2 minutes with FDA (5  $\mu$ g/ml) and PI (5  $\mu$ g/ml) in PBS and subsequently washed 2 times with PBS. Thereafter, organoids were imaged in 96 wells plates (Grainer) by using the LSFM 780 microscope (equipped with an incubation chamber and under controlled physiological conditions).

## 2.21. Brightfield-based analysis pipeline

For the analysis of hundreds of organoids grown in multiple droplets of ECM, the brightfield microscope Carl Zeiss Cell Observer Z.1 was used. It was equipped with an incubation system to guarantee optimal growth conditions (37°C, 5 % CO<sub>2</sub>, 95 % humidity). Organoids were seeded in 25  $\mu$ l ECM (Matrigel® or BME) droplets in suspension culture plates and overlaid with 250  $\mu$ l expansion medium. Because the brightfield-based analysis pipeline (in the following named brightfield pipeline) is configured to detect hollow and luminal objects, the organoids were cultured for 12 h before imaging because at this point most of them had a lumen established. To image one complete droplet a Plan-Apochromat 5x/0.16 objective with a pixel size of 1.29  $\mu$ m x 1.29  $\mu$ m was used and configured to a tile scan of 3x3 tiles. To image the drop in the z-direction, a z-stack was calculated to capture a total distance of 1200  $\mu$ m within 10 slices (distance between the slices 120  $\mu$ m). The temporal resolution was set to a 30-minute interval. All the data which is shown in this work was produced with this configuration.

### 2.21.1. Image processing and organoid segmentation

For the semiautomatic segmentation of the organoid growth rate a custom-made pipeline in python was designed and equipped with a general user interface. This was mainly done by the master student Julia Tarnick under the supervision of Lotta Hof and me and further optimized by Tim Liebisch (Frankfurt Institute for Advanced Studies, working group of Prof. Dr. Franziska Matthäus, for further details, take a look at: Hof et al., 2021).

Prior segmentation, the recorded time-laps images stacks were processed with ImageJ/Fiji to reduce the dimensionality from 3x3 tiles and 10 z-slices per time point to one stitched image. It was done by using the function Average Intensity Z-Projection, combined with a Background

subtraction (Rolling ball radius: 700 pixels, light background, sliding paraboloid, Disable smoothing) and subsequent stitching with Grid/Collection (Preibisch et al., 2009). The resulting image stacks were further filtered (Median, Radius: 5 pixels), again background subtracted (Rolling ball radius: 500 pixels, light background, Sliding paraboloid) and finally the projected luminal areas extracted by using the ImageJ/Fiji plugin MorphoLibJ (Legland et al., 2016). Border Image, Tolerance mPOs: 12, Tolerance hPOs: 7, Calculate dams: true, Connectivity: 6). After this step, missegmented organoids were manually corrected and the resulting projected luminal areas measured by the function Region Morphometry (incorporated in MorphoLibJ).

### 2.21.2. Data processing

The results from the brightfield pipeline are defined as the number of pixels of the projected luminal area of each segmented organoid per time point. To validate the overall growth of all segmented organoids in a droplet per time point, additional processing steps were performed. The pixel numbers of each organoid were normalized to the median pixel number of all segmented organoids at a defined time point. In the first 24 h of observation (pre-treatment) the 5<sup>th</sup> time point and at all following intervals (treatment, recovery, all 5 (mPO) and 6 (hPO) following days at the general growth evaluation) the first observed time point was used. This resulted in a relative growth rate of each segmented organoid per time point in regard to the overall size at the defined time point. In the next step, the median and the mean value of the relative growth rate of all organoids per time point were calculated. The result was one value that reflects all segmented organoids within the analysed well per time point in regard to the defined time point (For an overview take a look at Figure 6). The results were plotted and statistically evaluated.

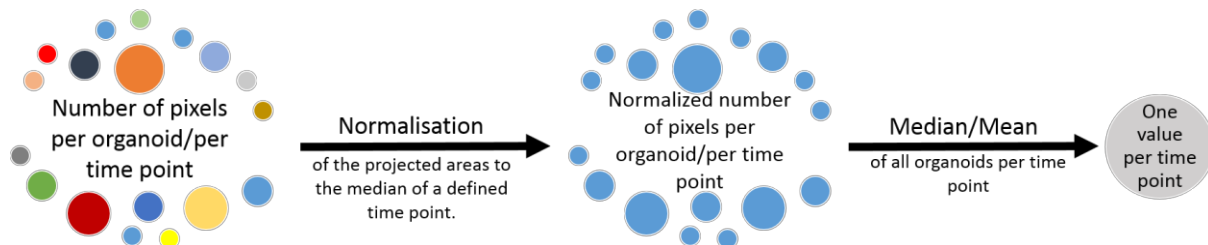


*Figure 6: Overview of the data handling of the brightfield pipeline.* From left to right: The raw data from the brightfield pipeline, in terms of the number of pixels of the projected luminal area of each organoid at each timepoint, was normalized to the median of all projected luminal areas at a specific time point. In the first 24 h (pre-treatment) timepoint 5 and all following 24 h recording intervals the timepoint 1 was used. In a next step the median or mean of the normalized values over all organoids at each time point was calculated. The resulted value reflects the growth behaviour of all detected organoids within the well at the corresponding time point.

### 2.22. Light sheet-based analysis pipeline

To image organoids in the Zeiss Lightsheet Z.1 the previous published ultra-thin FEP-foil cuvette was used (Hötte et al., 2019). Because it was design for the use in the mDSLML, slight modifications were necessary.



### 2.22.1. Fabrication of positive modules for vacuum forming

Because the FEP-foil cuvette is produced by thermoforming, a positive mould was designed (Figure 12). Therefore, the free CAD software “123D Desing” (Autodesk Inc., version 2.2.14) was used. The mould was 3D-printed by the service of the company Shapeways (Eindhoven, The Netherlands, [www.shapeways.com](http://www.shapeways.com))

### 2.22.2. Cuvette fabrication

The general procedure is already published at Hötte et al., 2019, and done as described. Instead of the mould designed for the mDSLIM, the newly designed Lightsheet Z.1-mould was used. In brief, a 10 cm x 10x cm squared patch of FEP-foil (50 µm thickness, Lohmann Technologies, batch # GRN069662) was insert into the vacuum forming machine (JT-18, Jin Tai Machining Company, Yuyao, PR of China) and heated up to 280°C. Once the foil was heated it was pressed onto the positive mould that is equipped with a glass capillary (borosilicate glass 3.3, Hilgenberg, material # 0500). The glass capillary was cut to a length of 15 mm beforehand (Figure 12 D). After the formation and cool down of the construct, the cuvette, supported by the glass capillary was released from the squared FEP-foil patch and connected with a shrinking tube (flame retardant polyolefin tube, size 3, G-APEX, cat # E255532) The tube served as a linker to the capillary (Blaubrand intraMark 200 µl micropipette, Brand, cat # 708757) which can be inserted into the holder of the Lightsheet Z.1. Before use, the capillary was removed in order to pipette the sample into the FEP-cuvette and cleaned with a detergent (1 % Hellmanex-II in ultrapure water), sterilised with 75 % Ethanol for at least two hours and washed twice with sterile PBS.

### 2.22.3. Specimen preparation

Organoids were cultured as described (2.11). During the splitting procedure 20 µl of Matrigel® containing pancreatic organoid fragments were filled slowly into the cuvette. For optimal image results, air bubbles need to be avoided. Therefore, the use of a 20 µl pipette tip is recommended (Starlab TipOne 10/20 µl Bulk). Subsequently, a glass capillary (Blaubrand intraMark 200 µl Micropipette, Brand GmbH & Co KG, REF:708757) was connected. The capillary need to be filled with Expansion Medium beforehand. To avoid leakage, the connections between the mentioned parts were wrapped with Parafilm.

At least 10 minutes before the FEP-foil cuvette was inserted into the Lightsheet Z.1 the camber was filled with DMEM (without phenol red) dosed with 2 % Penicillin and Streptomycin and HEPES (1:100) and heated up to 37°C. In the meanwhile, the FEP-foil cuvette attached to the capillary, was inserted first into the Zeiss Lightsheet Z1 sample holder and then into the Zeiss Lightsheet Z.1 microscope. During the time of observation, the medium exchange was conducted every two days. The medium change was performed under semi-sterile conditions directly at the microscope with a 10 µl microloader tip (Eppendorf Microloader Tip 0,5-10 µl / 2-20 µl, Eppendorf AG) which was inserted from the top.

### 2.22.4. Image acquisition and single cell analysis

For the imaging of the entire FEP-foil cuvette containing the organoids, the Carl Zeiss Lightsheet Z.1 was used. The z-stack was configured to capture the complete FEP-foil cuvette

in z-direction and tiles were made to capture the complete FEP-foil cuvette in x- and y-direction. For visualisation the tiles were fused manually after the z-stack was processed to a maximum projection. The mPO cells express SRm160-tdTomato and were excited with a 561 nm laser, dual-sided illuminated with a Carl Zeiss LSM 10x/0.2 objective and the signal detected with two Carl Zeiss W Plan-Apochromat 20x/1.0 UV\_VIS objectives. At least 10 minutes before use, the microscope chamber was filled with pre-warmed (37°C) DMEM containing 2 % Penicillin and Streptomycin and HEPES (1:100) and the temperature was set. For single organoid segmentation, the image z-stacks were cropped towards the corresponding region (Fiji/ImageJ) and the single slices were segmented per time point with the previously published multiscale image analysis pipeline (Schmitz et al., 2017). All organoids were segmented and post-processed with the same configuration (Table 22). The segmentation results were displayed as the number of detected cell nuclei, their volume, surface area, the minimum and maximum counted pixels of a cell nuclei, the PCG neighbourhood count (with minimum, maximum, mean and standard derivation), the DCG neighbourhood count (with minimum, maximum, mean and standard derivation) and the coordinates of the centroid of the complete organoid, per time point. The results of all time points per collected subsequently in one Excel sheet and plotted as showed. To evaluate the nuclei segmentation performance of the image analysis pipeline the previously published validation tool was used (Schmitz et al., 2017). With this tool a ground truth data set was generated and compared to the segmentation results (for the results and details, take a look at Hof et al., 2021).

*Table 23: Configuration parameters of the single cell analysis of the light sheet-pipeline*

Segmentation settings		Post processing settings	
NucleiFilterRange	2	NucleiSeedDetectionMaxRadius	4
NucleiThresholdRange	10	NucleiSeedDilation	1
NucleiMeanFactor	1	Alpha	150
NucleiStandardDeviationFactor	0	OutlierDistanceThreshold	50
NucleiBackgroundFactor	0.9	EdgeDistanceThreshold	50
HoleFillingRange	1	NucleiMinCount	50
MaxDetectionRange	0.12	NucleiMaxCount	10000
NucleiSeedDetectionMinRadius	1		

### 2.23. Statistics

For all statistic calculation OriginPro 64bit was used. To test the results generated by the brightfield pipeline all acquired data from each trail were used. Because the raw data is the number of pixels per organoid and time point, the data was first normalised over all measured organoids per trail to the fifth time point in the first 24 hours of observation (pre-treatment) and afterward normalized to the first time point of observation (treatment, recovery). The resulting values of all measured organoids from all trails were then analysed towards normal distribution (trail showed normal distribution) and subsequent tested towards the DMSO-control group per measured time point by using the Mann-Whitney-U test.

## 2.24. Used programs

### 2.24.1. Arivis

For three-dimensional visualisation and rendering of the data acquired with the Carl Zeiss Lightsheet Z.1 the program Arivis Vision4D (Version: 3.2.1) was used. For better segmentation results the image stacks were filtered with “Particle Enhancement” (Diameter: 10, Lambda: 1) prior segmentation with “Blob Finder” (Segment Value: 500  $\mu\text{m}$ , Threshold: 5, Watershed Level: 1.303, Normalize per Frame: true, Split Sensitivity: 82 %) and subsequent tracked with “Segment Tracker” (Motion type: Brownian Motion (centroid), Max distance: 5  $\mu\text{m}$ , Track: Fusion false – Divisions true, Weighting: Multiple). For visualisation, movies of the developing organoids and the tracked cell nuclei were made by the use of the inbuilt program “Storyboard”.

### 2.24.2. ImageJ/Fiji

For image processing the open-source program ImageJ/Fiji for win64Bits (v.1.51n) was used. For optimal visualisation but not for measurements, the following tools were used: Maximum Intensity Projection, Montage creation, Enhance contrast (Saturated pixels: 0.3), Subtract Background (rolling ball radius: between 20-80 pixel); Filters: Minimum (0.5 pixels), Maximum (0.5 pixels), Unsharp Mask (Radius 1.0-2.5, Mask Weight 0.6-0.8); Noise: Remove Outliers (Radius: 0.5-2.0, Threshold: 50-150, Bright). If mentioned, the organoid sizes and the cell nucleus sizes were measured by hand, the “line” tool were used after the properties were adjusted in terms of pixel size in all dimension. To generate movies the “Save as AVI” (compression: PNG, frame rate: 5 fps) function was used.

### 2.24.3. SketchUp Make

To visualize the basic setup of the Carl Zeiss Lightsheet Z.1 with all components and the custom-made sample holder the program SketchUp Make 2017 (version 17.2.2555 64 Bits) was used. All components, beside the Objectives, were designed by my own. The objectives were taken from the “3D Warehouse”.

### 2.24.4. ZEN Blue

All acquired images from Carl Zeiss microscope systems were exported by the use of ZEN 2012 blue (version 1.1.2.0). By the use of the “export” function the subsets were defined, and the single z-slices were exported in the “tagged Image File Format” (tiff) for further usage.

### 2.24.5. OpenShot Video Editor, iMovie

To cut, connect, change the movie speed and insert arrows or titles, the free programs OpenShot Video Editor (version: 2.5.1) and iMovie (version 10.1.15) was used.

### 3. Results

#### 3.1. The Pancreas and its functional unit, the islets of Langerhans

In the human body the pancreas unites two functions within one organ. On the one hand, the exocrine part of the pancreas, namely the acinar and ductal cells, is part of the digestive unit of the organism. On the other hand, the endocrine cells, joint within islets of Langerhans, secrete hormones and regulate the blood sugar level, and thus they are a part of the circulatory system (Valdez et al., 2015).

Figure 7 (A) shows a Cubic II-cleared tail-part of a murine pancreas. Because the cleared pancreas is stained with Dapi, the nucleus of all cells is visible. The islets of Langerhans can be identified because they showed a clearly separated dense structure (close-up). They can be separated by a digestion protocol (not shown, isolated living islets provided by Nikola Dolezalova, University of Cambridge) and immunostained to illustrate their composition. Figure 7 (B) and (C) show a five-day old isolated murine Islet of Langerhans *ex vivo* stained with Fluorescein Diacetate (FDA) to illustrate the active cells and PI the dead cells. The PI staining revealed a necrotic core which is surrounded by living cells. The staining illustrates that the isolated islets were alive, but already showed signs of cell death after 5 days in culture. The generation of islets of Langerhans is basically a digestion of the complete pancreas. Because the islets of Langerhans are more compact and denser, they resist longer against the enzymatic digestion, and in this way, they can be separated from the surrounding tissue. This process is accompanied by a digestion of the capillary system of the islets. Without this capillary system the cells within the core of the islets can suffer from nutrient and oxygen supply which causes the necrotic core. To further identify the different cell types and confirm the functionality of the used antibodies, isolated and fixed islets of Langerhans were immunolabeled for: Insulin to indicate mature  $\beta$ -cells, Sox9 to indicate bi-potent stem cells, Pdx 1 to indicate cells which are in the early process of  $\beta$ -cell maturation, Ngn3 to indicate cells which are on the next developing step towards  $\beta$ -cells and Nkx 6.1 to indicate cells which are in the late state of  $\beta$ -cell maturation (Figure 7, D). Because the expression of Pdx 1 and Ngn3 was not constant and showed some fluctuations over time of  $\beta$ -cell maturation only some of the cells showed Pdx 1 and Ngn3 expression. However, a separate and clear signal of all the mentioned antibodies were detected and confirmed the presence of the mentioned cells within the islets of Langerhans and, in addition, showed the functionality and sensitivity of the used antibodies.

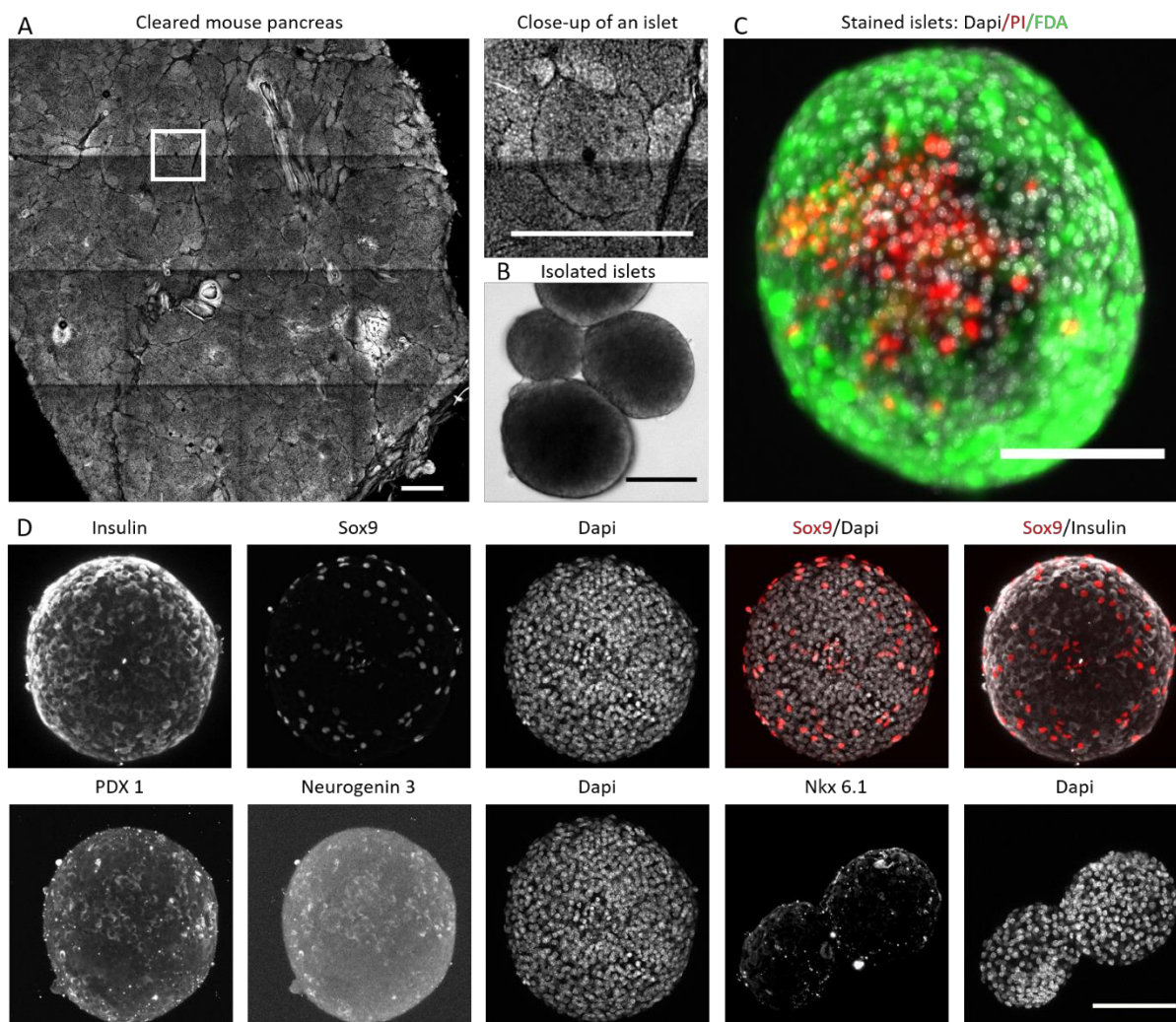


**Figure 7: Murine pancreas and its islets of Langerhans.** (A) CUBIC II-cleared and nuclei-stained tail-part of a murine pancreas (Image reconstructed from 16 tiles). The red rectangle points out an Islet of Langerhans. It appears as a dense packed and separated structure. (B) After the isolation of the islets of Langerhans from the pancreas, the roundish and dense structure becomes more clearly. (C) After the isolation, islets of Langerhans are still vital (indicated by the FDA staining in green) and have an area of dead cell in the inner cell mass (indicated by PI staining in red). (C) Isolated and immunolabeled Islands of Langerhans. Top, from left to right: Insulin to indicate  $\beta$ -cells, Sox9 to indicate bi-potent stem cells, Dapi to indicate cell nuclei of all cells within the Islet of Langerhans. In red Sox9 merged with Dapi to indicate the position of the bi-potent stem cells throughout the Islet of Langerhans and merged with insulin expressing cells to indicate that Sox9 positive cells do not express insulin. Bottom, from left to right: PDX 1 staining to indicate cells, which are in the early process of  $\beta$ -cell maturation, Neurogenin 3 to indicate cells, which are on the next developing step towards  $\beta$ -cell, and Nkx 6.1 staining to indicate cells, which are in the late state of  $\beta$ -cell maturation. (For secondary Antibody controls take a look at Supplemental Figure 2) Microscope: (A,C,D) Zeiss LSM780, (B) Zeiss Cell Observer. Objectives: (A) Plan-Apochromat 10x/0.3, (B) LD Plan-Neufluar 20x/0.4 cor. Ph 2, (C) W-Plan Apochrimat 20x/1.0 UV-VIS, (D) EC-Plan Neufluar 40x/0.75 Ph 2. Ex/Em: Dapi 405/462; FDA 488/553; PI, Sox9, Neurogenin, Nkx 6.1 3 561/633; Insulin, Pdx 1 633/699. All images are maximum projections of z-stacks. . Scale bars: (A) 500  $\mu$ m, (B)(C)(D) 100  $\mu$ m. Murine pancreas islets kindly donated from Nikola Dolezalova, Department of Surgery, University of Cambridge, Box 202, Addenbrooke's Hospital, Hills Road, Cambridge, UK

### 3.2. The three-dimensional culture system of pancreas organoids

The availability of pancreatic islet donors is limited, and a lifelong medication is needed to treat patients that suffer from Diabetes type I. Therefore, one aim in cell based therapeutic research is the *in vitro* generation of insulin-producing  $\beta$ -cells and the subsequent transplantation into the patient. However, the most promising way to generate  $\beta$ -cells is the use of bi-potent ductal cells which are able to grow in a droplet of ECM under specific medium conditions to organoids

(Huch, Bonfanti, et al., 2013; Huch, Dorrell, et al., 2013). However, the organoid culture is known to represent the ductal part of the pancreas, relatively low knowledge has been generated about its appearance and phenotypic behaviour so far.

### 3.2.1. Appearance and behaviour of mouse and human pancreas organoids

In this work, hPOs and mPOs were used. Because human and mouse organoids grow in an ECM-droplet and have the same cellular origin, the appearance and behaviour are basically the same. Figure 8 shows the development of mPOs and hPOs over time within a droplet of ECM imaged with a stereo microscope (left side) and a brightfield microscope (right side). One result of the observation was that mPOs usually developed faster than hPOs. Alongside this the development of the organoids varied, because it depends on several parameters like cell age, seeding density and the re-activity of the added transcription factors. The general time frame the organoids of both origins needed to grow, was between six to eleven days. Figure 8 and Movie 1 show the appearance of mPOs and hPOs grown in a droplet of ECM over one live cycle of seven and ten days respectively. The typical roundish, spherical like character of the organoids became visible after two to three days. After the organoids had formed, a steady increase of size, up to a point of maximum expansion, was visible. Dependent on their seeding density the organoids grew up to a size of several millimetres in diameter, but usually reached between 200 and 1500 micrometres (measured by hand). The first step in organoid growth is the formation and establishment of the phenotype. Depending on the splitting procedure, organoids are able to form out cell clusters which are characterized at first by a conglomeration of cells and secondly, by the establishment of a phenotypic luminal structure with one layer of cells. The formation out of single cells in general is possible, but hard to visualize in brightfield microscopy, and thus not illustrated at this point of the work. Because the final size is dependent on several mentioned factors, every droplet showed a high heterogeneity in organoid size and appearance. However, Figure 8 and Movie 2 illustrate some exemplary organoids that demonstrated high heterogeneity in behaviour patterns and differences in their general appearance. The fusion of two or more organoids was a common phenomenon in pancreas organoid culture. Some of the organoids demonstrated organoid motion within the ECM which was manifested in the travelling of hundreds of micrometres (measured by hand). Another frequent behaviour was that organoids did not develop a hollow lumen but showed a roundish structure which was filled with - presumably - dead cells. Movie 3 shows that during the development of an organoid cells were shed from the organoid apical side inside the lumen which leads to the assumption that these cells were dead. Taken all of this into account, the results show that human and mouse pancreas organoids have a high heterogeneity in terms to appearance and behaviour.

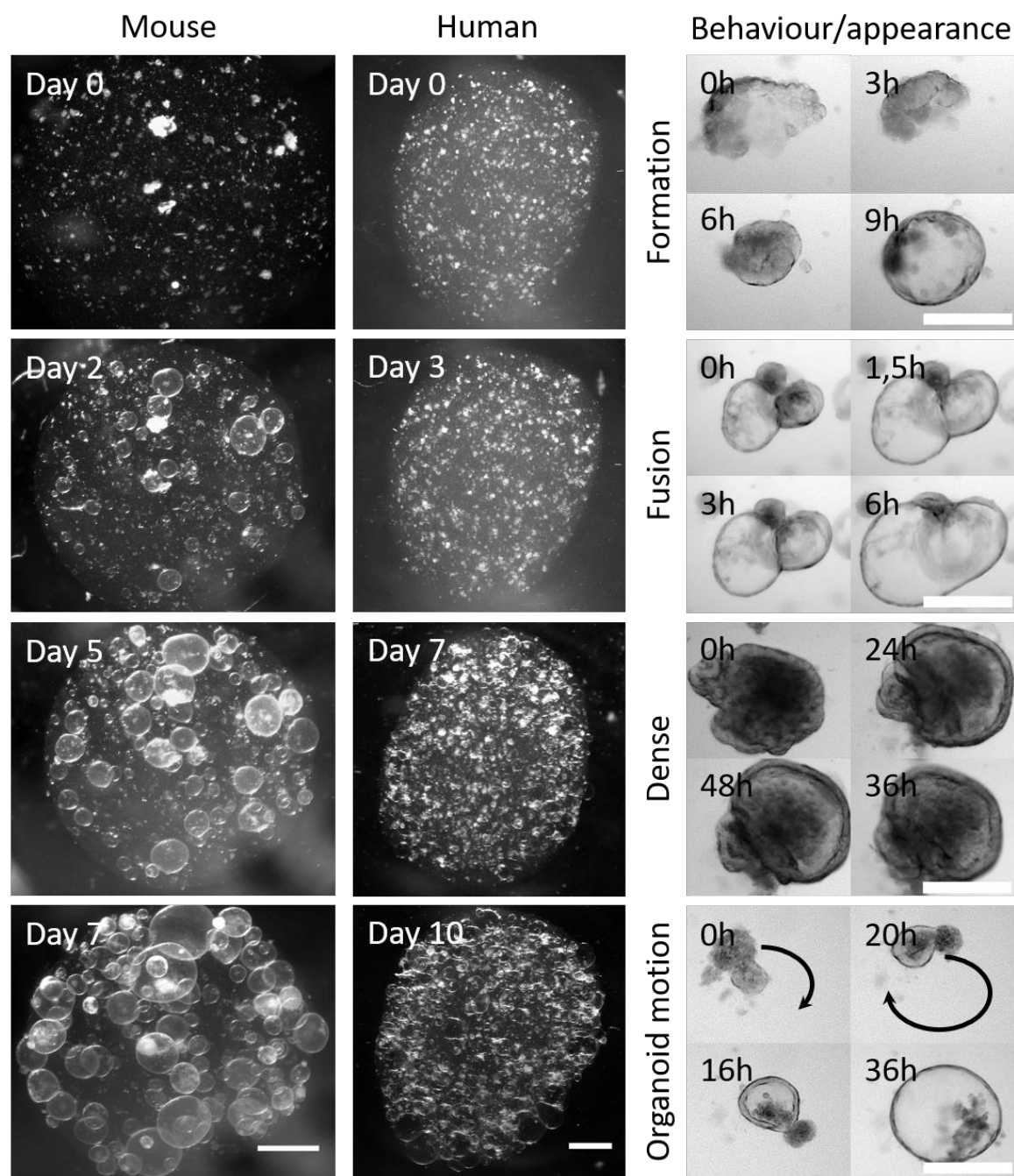


**Figure 8: Illustration of the growth heterogeneity and behaviour of human and mouse pancreas organoids.** On the left side representative darkfield images of one droplet of ECM with the embedded growing organoids over multiple days is shown. Mouse pancreas organoids grew faster and needed to be splitted every 7 days whereas human pancreas organoids reached the maximum growth capacity after 10 days. On the right side, representative brightfield images are shown that illustrate phenotypic behaviour of pancreas organoids during growth. Next to the fusion of multiple organoids to one, some organoids demonstrate organoid motion during the initial formation. Dependent on the splitting procedure, organoids are able to form out of cell clusters, which is characterized by first, a conglomeration of cells, and second, the establishment of a phenotypic luminal structure with one layer of cells. In addition, organoids can also show a dense multi-layered structure and no detectible size increase (see also Movie 1 and Movie 2) Microscope; left: Zeiss Stereo Discovery V8, Objective: PlanApo S 0.63 (2,5x). right: Zeiss CellObserver, Objectives: Plan-Apochromat 5x/0.16. Scale bar: Human and Mouse: 1000  $\mu$ m, Behaviour: 100  $\mu$ m

### 3.2.2. General challenges in organoid imaging – immunofluorescence labelling of organoids

Immunofluorescence labelling of organoids in their native surrounding is challenging. Huch and colleagues developed a protocol which allows the labelling of organoids within the ECM as well as after isolation (Broutier et al., 2016). Supplemental Figure 1 shows organoids immunolabeled within the droplet of ECM. In (A), organoids were stained with the nuclei marker Dapi and the actin marker Alexa Fluor® Phalloidin 488. A clear staining with background noises is shown. In contrast, (B) shows the same organoids indirectly immunolabeled with an antibody against ZO-1, a component of the tight junctions. The signal was detectable but a high background noise from the surrounding Matrigel® was detected which was also present when labelled solely with the secondary antibody (“primary antibody control”). This result shows that organoids can be fluorescently stained (Dapi) and labelled with dyes, directly conjugated with a fluorophore within the ECM by using the referenced protocol. However, the labelling with a primary antibody followed by a secondary antibody led to a high background noise and none or unspecific labelled cellular parts. To circumvent this problem Huch and colleagues recommend isolating the organoids from their surrounding ECM. Because Matrigel® and BME can be destabilized by cooling down close to 0°C they recommend isolating organoids by using multiple washing steps with ice cold PBS and pipetting the organoids up and down to break the ECM. Supplemental Figure 1 (B) shows the results of three washing steps prior IF. Next to an unchanged Dapi and Alexa Fluor® Phalloidin 488 staining, a specific fluorescence signal was detected but still a strong background noise surrounded the organoid. By increasing the brightness of the image, it becomes clear that parts of the ECM were still attached to the organoid. Alongside this, the washing steps led to an altered appearance in terms of a collapsed or disrupted organoid. Usually, cells are fixed at 37°C which increases the fixation and reduces the needed time. During the experiments, the observation was made that the fixation itself can lead already to a partly dissolving of the ECM that surrounds the organoid. To further support the ECM degradation the organoids were fixed on ice continuously shaking for 30 to 60 minutes. After the fixation, the organoids were washed with Cell Recovery solution on ice continuously shaking. Supplemental Figure 1 (C) shows the results of the improved protocol. The organoids maintained their hollow spherical appearance, Dapi and Alexa Fluor® Phalloidin 488 staining was not altered, and IF was possible without increased background noise. All following IF images were made with the mentioned steps prior IF.

### 3.2.3. Mouse and human pancreas organoid’s identity: marker expression and cell polarisation

Aberrations in mouse and human organoids cell fate is possible because they are generated from different donor sources. As already illustrated, organoids show a high heterogeneity in terms of size, behaviour and appearance. However, it is of great importance to define and characterize their identity as bi-potent stem cells for further research. Therefore, IF is a valid tool. Figure 9 shows pancreas organoids which were isolated from the ECM and stained against different markers for characterization. Human and mouse organoids need to be polarized to maintain their spherical and luminal character. A cytoskeleton marker, or components of it, displays a valid tool to illustrate that the cells show polarisation. Actin, as the major component of the cytoskeleton and ezrin as a linker between the cytoskeleton and the plasma membrane showed an apical localization. E-Cadherin,  $\beta$ -Catenin and ZO-1 as cell-cell adhesion molecules



showed a lateral localization in mouse (Figure 9) and human (Figure 10) organoids. In conclusion, the expression patterns of the mentioned cytoskeleton components and interaction molecules point towards a strong polarisation of the pancreas organoid cells. Furthermore, the cell nucleus staining revealed a palisade-shaped arrangement which additionally supports this result.

To validate the cell fate of the organoids, several markers were used. In mouse and human organoids, Sox9 and Pdx 1 are the most common markers to proof their bi potency (Georgakopoulos et al., 2020; Huch, Bonfanti, et al., 2013; Huch, Dorrell, et al., 2013). Figure 9 (B) and 10 (B) shows a homogeneous expression of Sox9 in the nucleus of all cells in mouse and human organoids, indicating that the cells were in a bi-potent state. Pdx 1 was also observed in the cytosol of human organoids but was not detected in mouse organoids whereas Keratin 19 (Krt19) was expressed in mPOs but not in hPOs. During the development of the ductal cells to  $\beta$ -cells, the transcription factors Ngn3 and Nkx 6.1 are temporally activated (1.2). In mouse pancreas organoids some of the cells showed Ngn3 and Nkx 6.1 expression but none were detected in human organoids. Yap plays a critical role in the mechanotransduction by cross-talking with the ECM and f-actin. Depending on this interaction it is expressed in the nucleus as an active transcription factor or inactive located in the cytosol (Pećina-Šlaus, 2003). Mouse and human organoids demonstrated alteration in the expression of Yap. Mouse organoids mainly expressed Yap in the nucleus and only single cells showed none, or cytosolic expression (Figure 9 (B), close-up) whereas the cells of human organoids demonstrated more frequent alterations of Yap expression in the cytosol and in the nucleus (Figure 10 (B) close-up).

These results disclose that mouse and human organoids show comparable expression patterns of cytoskeleton components and interaction molecules but alterations in the expression of stem cell and differentiation markers. It shows that the pancreas organoid culture is highly heterogenic and need to be intensively analysed.

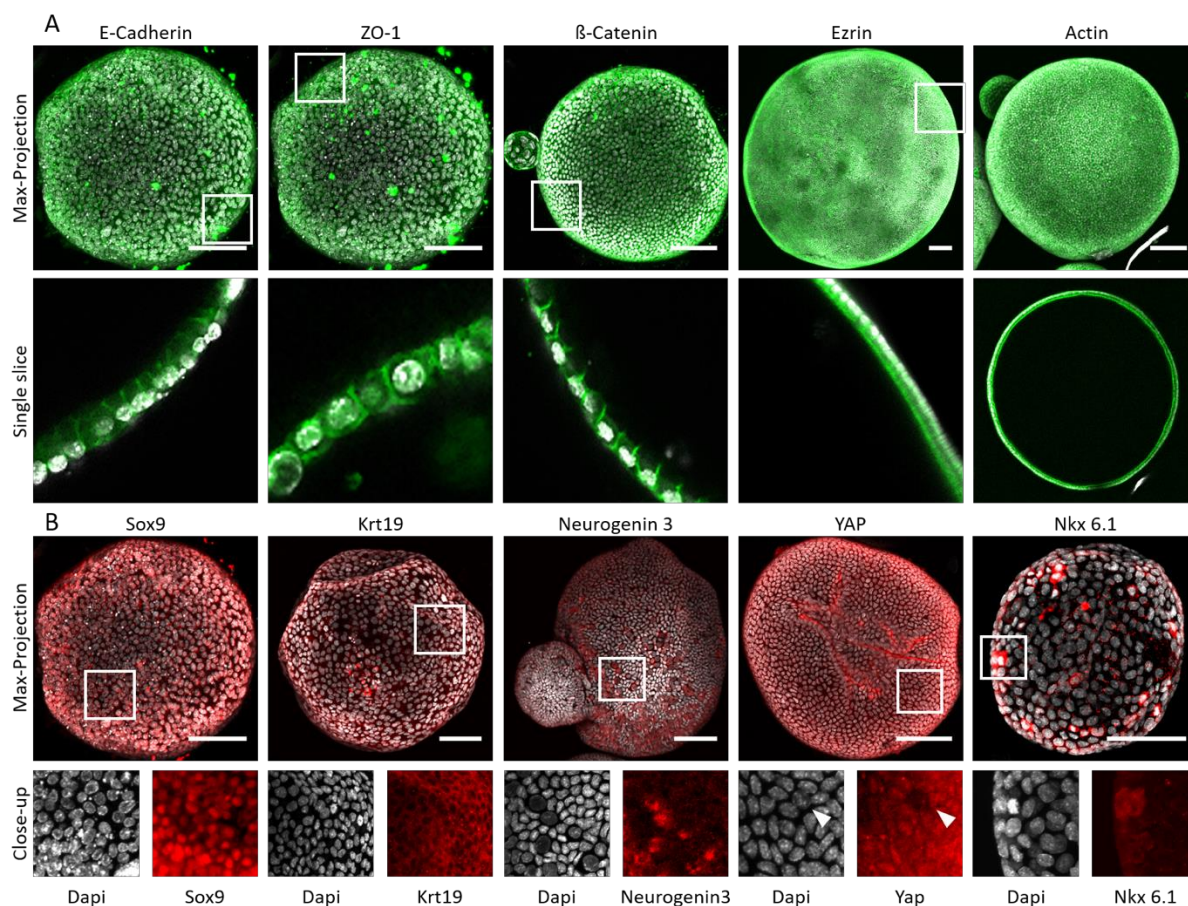


**Figure 9: MPOs show a polarized structure but alter in the expression of differentiation markers..** (A) Max-projection (top) and single slices (bottom) of immunolabelled mPOs. Dapi (grey) illustrate the cell nuclei, E-Cadherin, ZO-1 and  $\beta$ -Catenin shows phenotypical lateral polarisation, ezrin and actin phenotypical apical polarization (green). (B) Max-Projection and close-ups of immunolabelled mPOs against phenotypic stem cell and differentiation markers (red, from left to right). Homogeneous nucleus localized expression of Sox9 as the phenotypic marker for bi-potency indicates the stem cell and Krt19 illustrates the endothelial character of the organoids. Alterations on the cytosolic Neurogenin3 and Nkx 6.1 expression indicates possible differentiation patterns of some of the cells. Absent Yap (cytosolic expression of yes-associated protein 1) expression is also visible and may indicates alterations in the differentiation status of single cells. (For secondary Antibody controls take a look at Supplemental Figure 3) Microscope: Zeiss LSM780, Objectives: Plan-Apochromat 20x/0.8, Plan-Apochromat 10x/0.3 (Ezrin, CXCR4). Ex/Em: Dapi 405/462; CXCR4, ZO-1, Yap 488/553; Sox9, Ezrin, Actin 6.1 3 561/633; E-cadherin,  $\beta$ -catenin 633/699. Scale Bar: 100  $\mu$ m

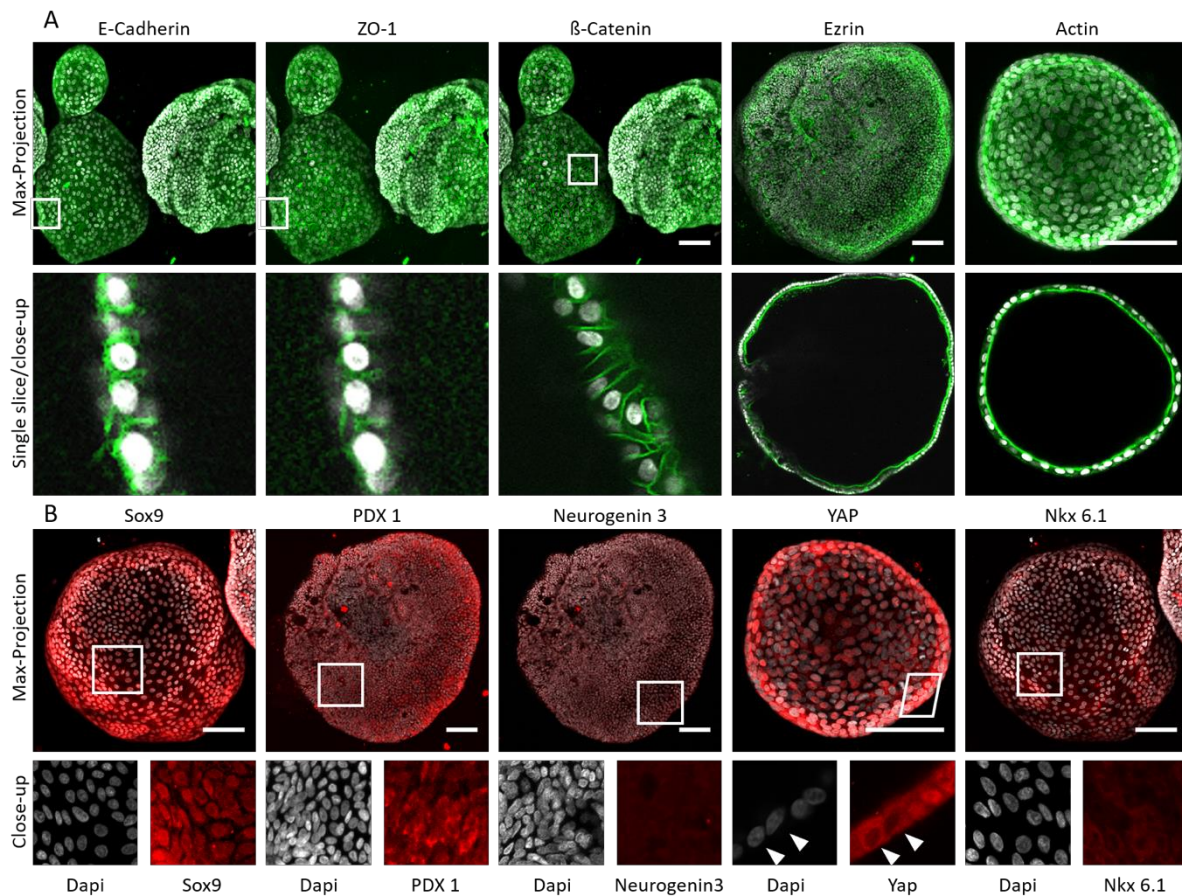


**Figure 10: HPO organoids show polarized structure but alter in the expression of differentiation markers.** (A) Max-projection (top) and single slices (bottom) of immunolabelled Human organoids. Dapi (grey) illustrate the cell nuclei, ZO-1 and β-Catenin shows phenotypical lateral polarisation, ezrin and actin phenotypical apical polarization (green). (B) Max-Projection and close-ups of immunolabelled mouse organoids against cell nuclei (grey) and phenotypic stem cell and differentiation markers (red, from left to right). Homogeneous nucleus localized expression of Sox9 as the phenotypic marker for bi-potency indicates the stem cell and Pdx 1 expression illustrates the pancreas progenitor status. Alteration on the cytosolic Nkx 6.1 expression indicates possible differentiation patterns of some of the cells. Presents or absents of nucleus localized expression of YAP (yes-associated protein I) are also visible and may indicates alterations in the differentiation status of single cells. Ngn3 expression cannot be detected. Tilted rectangles illustrate a close-up of a single slice, non-tilted rectangles a close-up of a Max-Projection. (For secondary Antibody controls take a look at Supplemental Figure 4) Microscope: Zeiss LSM780, Objectives: Plan-Apochromat 20x/0.8, Plan-Apochromat 10x/0.3 (Ezrin, CXCR4). Ex/Em: Dapi 405/462; CXCR4, ZO-1, Yap 488/553; Sox9, Ezrin, Actin 6.1 3 561/633; E-catherin, β-catenin 633/699. Scale bar: 100 μm

### 3.3. Organoids at a glance - multiscale analyses of organoids growth behaviour

Pancreas organoids show a high heterogeneity not only in their appearance, but also in their behaviour dynamics. To understand the general heterogeneity, a multi-scale investigation is necessary (micro-, meso-, macroscopic). For these reasons, two multidimensional analysis pipelines were developed. On the one hand, a brightfield-based analysis pipeline (in the following named brightfield pipeline) that enables the measurement of the size development of hundreds of organoids over time (developed by the Master student Julia Tarnick under supervision of Lotta Hof and me and optimized by myself and Tim Liebisch). On the other hand, a light sheet-based analysis pipeline (in the following named light sheet pipeline) that enables the tracking of complete organoids on a single cell level in a high spatial and temporal resolution (developed by me and based on a former developed and published segmentation pipeline from Schmitz et al., 2017). The combination of both pipelines allows the *in toto*, multiscale analysis of pancreas organoids and helps to understand core regulatory principles of organoid behaviour and heterogeneity.

#### 3.3.1. Recording hundreds of organoids and tracking complete organoids on a single cell level – The brightfield and light sheet pipeline

To generate robust and valid data about the growth behaviour of pancreas organoids, the brightfield pipeline was developed. Figure 11 (green background) shows the basic principle of this pipeline (for detailed description look at 2.21). In brief, organoids embedded in an ECM-droplet, were seeded in a multiwell plate and placed in a brightfield microscope that needs to be equipped with an incubation chamber. At physiological conditions (37°C, 5 % CO<sub>2</sub>, 95 % relative humidity), the organoid-droplets were then entirely imaged. To acquire this, images stacks and tile scans were generated over time. The temporal resolution was chosen according to the temporal dynamic of the process that wanted to be observed, and thus can range from seconds to hours and days. A regular medium exchange was conducted every two days. After the experiments, the data needed to be exported and pre-processed. Therefore, the tiles were stitched, and the stacks were projected to one slide. The single time points were then segmented using the ImageJ/Fiji plugin “MorphoLibJ”. As result, the obtained data displays the projected luminal areas (in pixels) which were derived from the equatorial plate of the organoids. At first, the results were normalized over the median pixel number of all segmented organoids at the 5<sup>th</sup> timepoint of the first 24 hours (1 day) of observation (pre-treatment) and secondly normalized over the first time point of each following day (treatment, Recovery). As results, the data were plotted as the overall median or mean growth rate of all measured organoids relative to the timepoint of normalisation. The resulted values describe the size increase; a change from the value one to the value two means a doubling of the overall size of all organoids within the analysed well. To statistically evaluate the results, the Mann-Whitney-U test was used because the data sets did not show a normal distribution (Supplemental Figure 9, Supplemental Figure 10, Supplemental Figure 11). This setup enables the macroscale investigation of organoid cultures.

Because the heterogeneity of pancreas organoids cannot be explained entirely on the macroscale level, the investigation of single organoids (mesoscale) as well as the single cells comprising an organoid (microscale) is necessary. Figure 11 (blue background) illustrates the

basic setup of the light sheet pipeline which enables the tracking of complete organoids on a single cell level (for detailed description look at 2.22). In brief, organoids were splitted and seeded in a FEP-foil cuvette that has been produced for the use in the Lightsheet Z.1 beforehand. Because the FEP-foil is thermo-formable, the cuvettes were fabricated by the use of a vacuum-forming machine in which the 280°C heated foils were clamped into and pressed onto the square cross-section positive mould (Figure 12, E). After several cleaning and drying steps, the cuvette was filled with the organoid fragments and connected to the Z.1 sample holder (D, G). The sample holder connected to the FEP-foil cuvette was then transferred into the microscope (A, B). An included incubation unit guaranteed physiological conditions (37°C, 5 % CO<sub>2</sub>, 95 % relative humidity). The FEP-foil cuvette was then completely imaged. Z-stacks, tiles and views from multiple directions were generated. The temporal resolution was chosen according to the temporal dynamic of the processes to be imaged and can range from seconds to hours and days. Regular medium exchange was ensured by a semi-sterile exchange directly at the microscope every two days by the use of a 10 µl micro-loader tip. After the experiment, the corresponding data were exported and segmented separately per time point. The segmentation was calibrated, as previously described (Schmitz et al., 2017), and the batch-processing option was used to analyse all time points at once. Afterwards, the obtained data per time point was collected to one document, plotted and analysed.

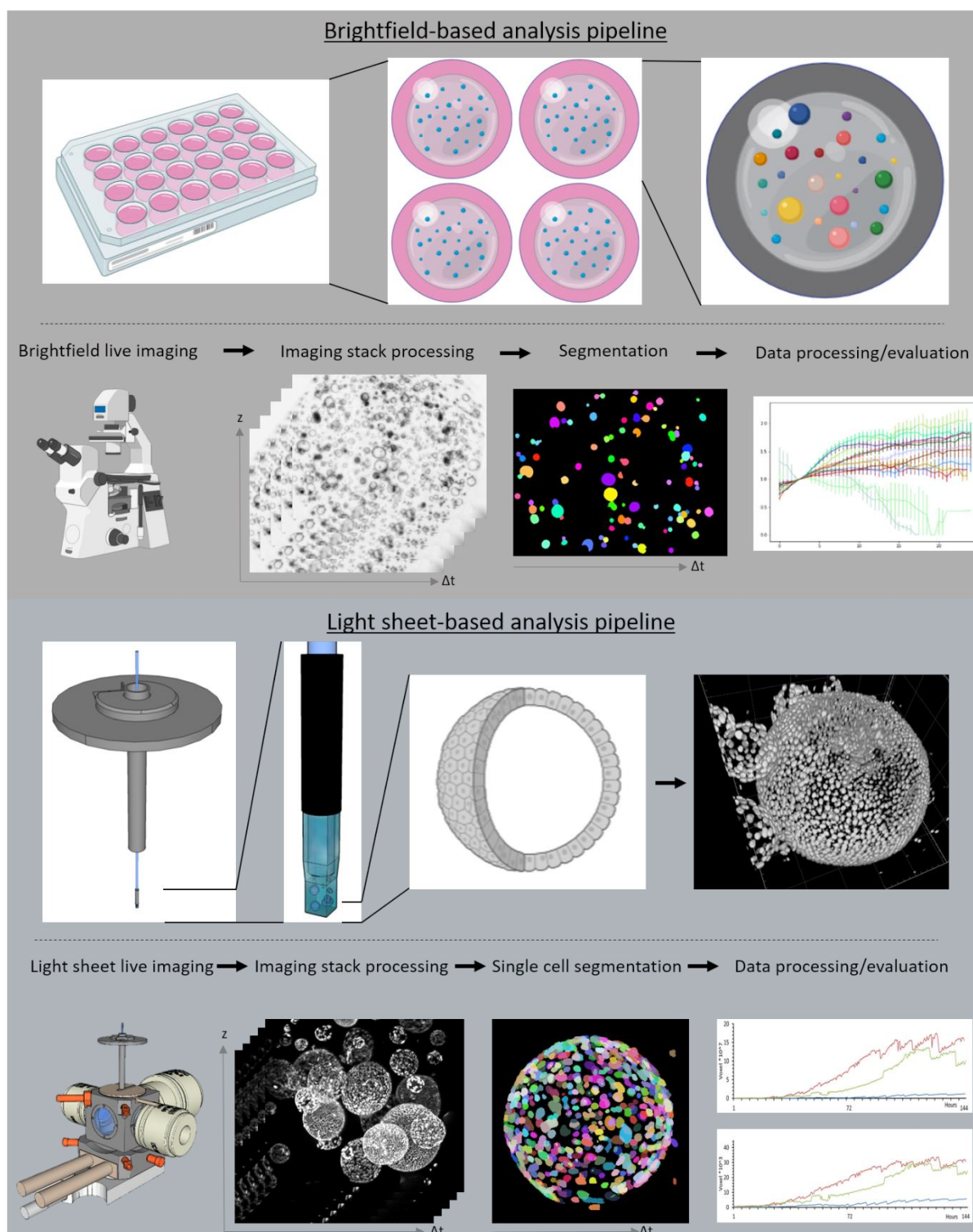


**Figure 11: Illustration of the two processing pipelines – the brightfield pipeline for mass analysis on a macroscale level and the light sheet pipeline to analyse single organoids on a single cell level (meso- and macroscale).** In green, the basic setup of the brightfield pipeline is shown. Organoids seeded in a multi-well plate, were placed in the brightfield microscope and imaged in physiological conditions over multiples days. To image the complete ECM-droplet with all organoids, tiles and z-stacks were used. After the image acquisition, a semi-automated pipeline was used to first stitch the tiles and second project the z-stacks to one image (“image stack processing”). By the use of the ImageJ/Fiji (MorphoLibJ), the organoids were then segmented, and miss segmented once manually corrected (“Segmentation”). Finally, the projected luminal areas of the organoids were evaluated (“Data processing/evaluation”). In blue, the light sheet pipeline is shown. Organoids which expressed a cell nuclei fluorophore, either stained or stable transfected, were seeded in a FEP-foil cuvette that was produced beforehand. The FEP-foil cuvette was then placed in the light sheet microscope which was equipped with an incubation system to guarantee

physiological conditions. To image the complete FEP-foil with all organoids, tiles, multiple views and z-stacks were used. After the image acquisition, in a first image processing step, organoids of interest were extracted from the dataset (“image stack processing”). In a second step, organoids were segmented on a single cell level by using a Mathematica-script (“single cell segmentation”) (Schmitz et al., 2017). Finally, the data of all segmented cells that build-up the organoid were evaluated (Data processing/evaluation).

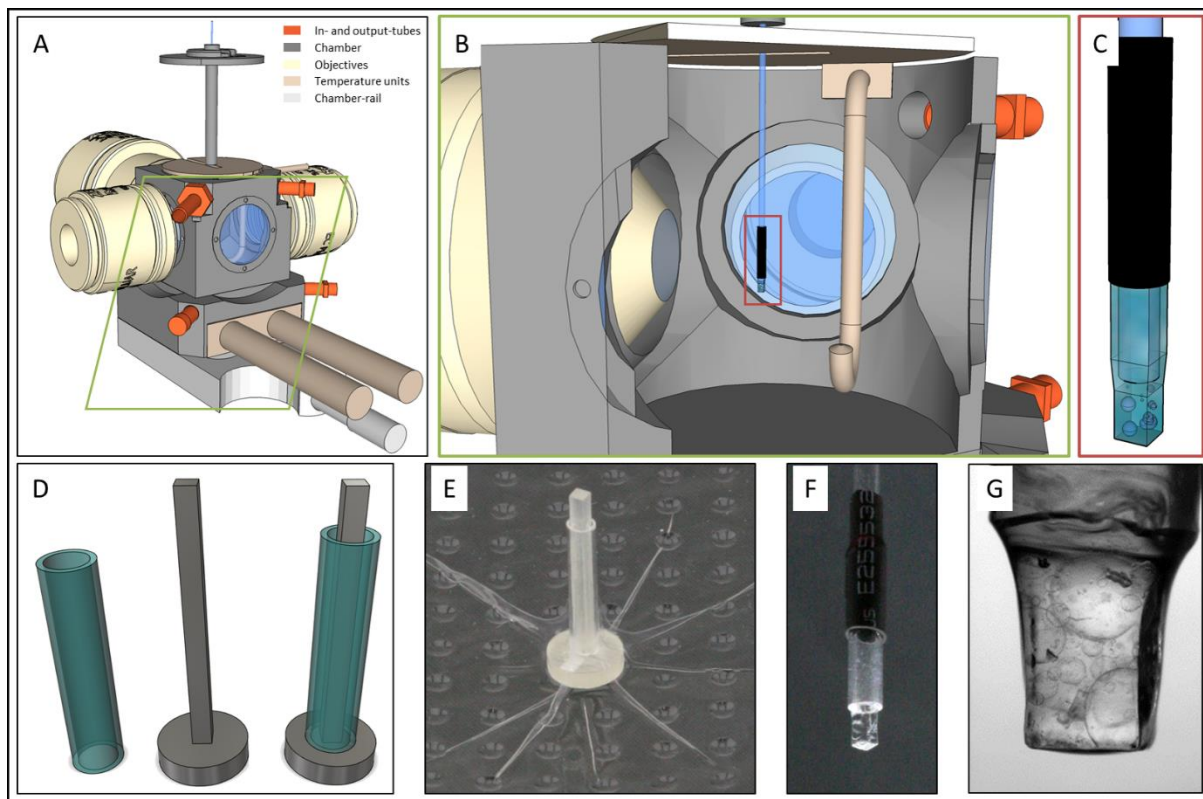


**Figure 12: Ultra-thin FEP-foil cuvette holders for the live recordings of organoids with the Zeiss Lightsheet Z.1 microscope system in physiological conditions..** In (A) a 3D model of the general setup of the Zeiss Lightsheet Z.1 microscope is shown. In (B) a close-up of the microscope chamber with the downwards directed ultra-thin FEP-foil cuvette holder enclosing the organoids (red rectangle illustrates the close-up of (C)) is illustrated. In (C) a close-up of the sample holder is shown. The shrinking tube that seals the FEP-foil cuvette and connects it with the glass capillary is depicted in black. Spheres within the holder illustrate the organoids. In (D) the CAD-derived drawings of positive moulds of the FEP-foil cuvette and the surrounding glass capillary to produce the Lightsheet Z.1 FEP-foil cuvette holder are illustrated. In (E) the printed mould with a surrounding glass capillary, which is used to form the ultra-thin FEP-foil cuvette holder in the vacuum forming process, is shown. One empty and ready-to-use Lightsheet Z.1-adapted FEP-foil cuvette holder is shown in (F). In (G) mPOs grown for 7 days in the ultra-thin-FEP-foil cuvette holder within their ECM are illustrated. Adapted from Hof et al., 2021.

### 3.3.2. Using the brightfield pipeline to understand the phenotypic appearance of pancreas organoids

Human and murine pancreas organoids show a heterogeneous behaviour in their development. The most effective way to generate organoids is by disrupting them into cell fragments and place them into a fresh droplet of ECM. This procedure is made by hand and depends on the dexterity of the operator. It results in different sized cell fragments and therefore favours organoid size heterogeneity. To generate robust data that pictures the culture heterogeneity, hundreds of organoids need to be analysed.

Figure 13 shows the growth of human and murine pancreas organoids tracked and segmented with the bright field segmentation pipeline. In (A) the median- and mean-size of all tracked mouse pancreas organoids over five days in culture is shown. The organoids doubled their overall size in the first 24 hours (blue-dotted line, median), followed by a 0.5-fold increase rate

at the second day (red line, median). From the third day on, only a slight size increase ( $<0.25$ -fold, median) over all organoids was measured (green-dashed, purple-dashed and black-dotted line). Human pancreas organoids differed in their growth behaviour compared to murine organoids. In (B) the median- and mean-size of all tracked human pancreas organoids over six days in culture is shown. The most prominent median size increase was detected from day two to four (red line, green interrupted line and purple dashed line) with a value of 0.5 times. At day one and five a 0.25-fold increase and at day six less than 0.2-fold median size increase was observed.

The segmentation of murine and human organoid growth show that the size increase did not follow classic linear or exponential growth. However, it shows that the brightfield pipeline was able to measure the organoid growth and that it is suitable for further research.

Based on the aforementioned growth observation, additional analysis of human and murine organoid size development was conducted focusing at the first three days of culture. Therefore, murine and human pancreas organoid growth is displayed in detailed in Figure 13 (A) and (B) in the second row. The blue-dashed lines show the overall mean growth of the organoids under normal conditions with its standard error. It is shown that mouse organoids had an overall 1.25-fold growth of the normalized projected area at day one, a 0.75-fold at day two and a 0.5-fold growth at day three. Slightly different, but more consistent growth rates became visible for human organoids, with a 0.6-fold growth at day one, a 0.75-fold at day two and again 0.6-fold at day three. To investigate the influence of drugs to the organoid growth behaviour, the substances are usually solved in DMSO. This solvent is in general cytotoxic which means that it can influence the vitality of the organoids. To address this, human and murine organoids were treated with 1 %/vol of DMSO at the second day (red line), because this is the maximum recommended amount of DMSO in cell culture (Pal et al., 2012; Santos et al., 2003). To guarantee the normal growth of the organoids, the first day of growth was always measured (pre-treatment) and used as a quality parameter. Organoid cultures that did not show a comparable (within the standard error of the mean) growth rate at day one was not used for further analysis. At day two DMSO was added to the medium (treatment) and the size increase was measured. To confirm the vitality after the treatment, or observe possible long-term effects, the DMSO-treated medium was exchanged with fresh non-treated medium after 24 hours (day 2) and the organoids size increase was analysed for additional 24 hours (day 3, recovery). In mPOs, DMSO did not show any effect towards the size increase rate, neither during the treatment nor in the recovery phase. However, hPOs showed a significant (Mann-Whitney:  $p \leq 0.01$ ) lower mean size increase when treated with 1 %/vol DMSO (Figure 13 (B), Treatment). In the recovery phase, the DMSO-treated organoids were able to grow again and had a slight, but not significant higher growth than in the control group (Figure 13 (B), Recovery) which shows that the DMSO treatment led to a growth delay but to a long-term effect in hPOs growth.

In conclusion, the brightfield pipeline was able to measure the size of organoids embedded in a droplet of ECM over time. Moreover, the analysis revealed that organoids had the most prominent size increase within the first three (murine) and four (human) days in culture and that human organoids were significantly altered when treated with DMSO.



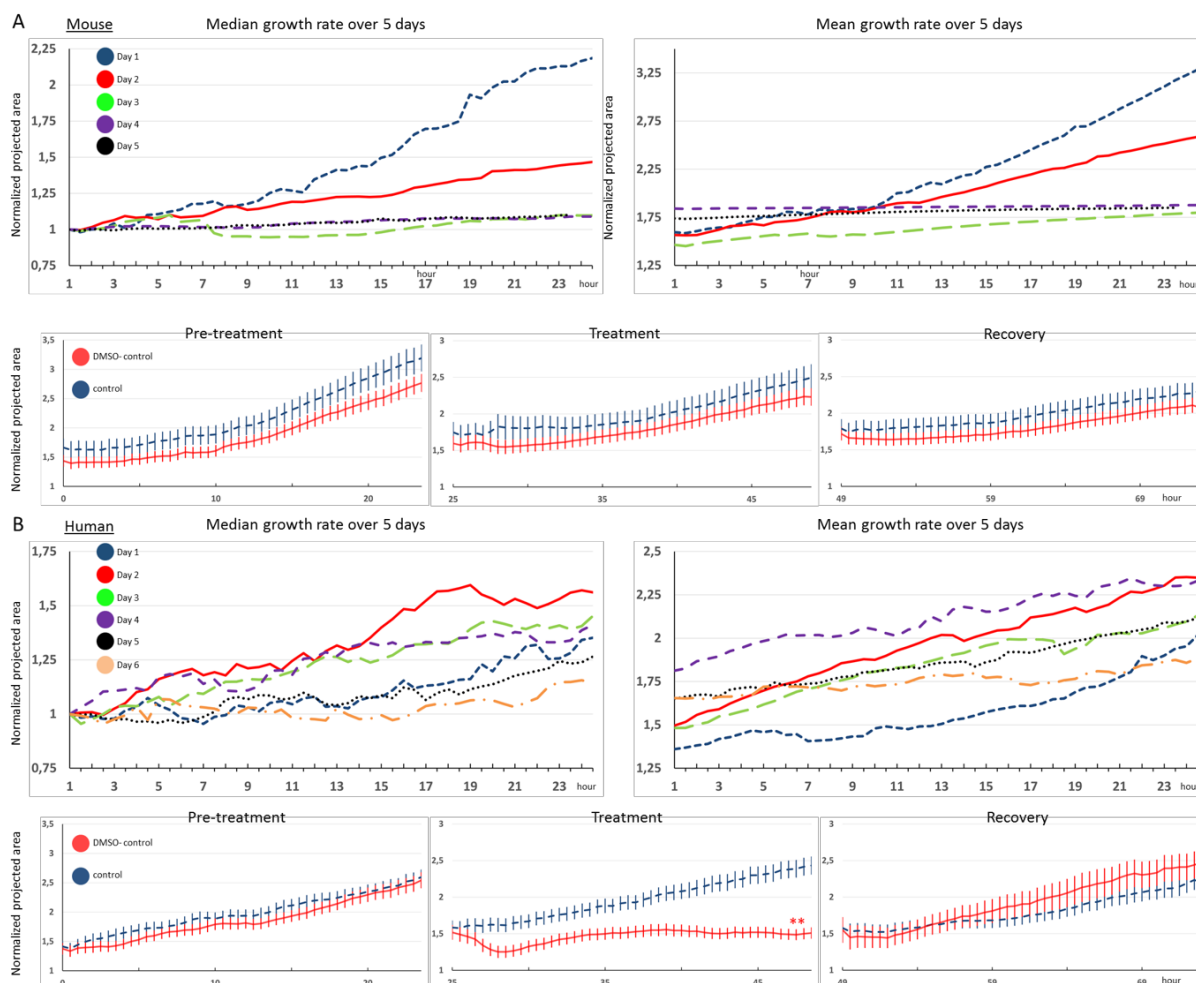


**Figure 13: Using the brightfield pipeline to define general growth curves of hPOs and mPOs** In all graphs, the normalized projected area is plotted against the observed time. The growth curves show the median or mean of the normalized projected areas over all imaged organoids. The results were obtained by normalizing over the median pixel number of all segmented organoids at the 5<sup>th</sup> time point of the first 24 hours (1 day) of observation (pre-treatment) and subsequent over the first time point of each following day (treatment, Recovery, day 4-6). To statistically evaluate the results, the Mann-Whitney-U test was used because the data sets did not show normal distribution. In (A) mPOs are shown. In the upper row the colour indicates the day after seeding. In total 5 days were analysed because after day 5 no more size increase was detectable. At day 1 and 2 a doubling and 0.5-fold increase of the median organoid size was detected respectively. At day 3, 4 and 5 non, or only a minor size increase was detectable. In the lower row, a close up of the first three days of the mean organoid growth rate is shown (termed as Pre-treatment, Treatment and Recovery). In blue organoids in normal culture medium and in red organoids in normal culture medium supplemented with 1 % DMSO are shown. Error bars indicate the standard error of the mean. The growth curves of both conditions did not differ significantly in the first three days of growth. Because a clear growth was detected only within these days, they were defined as meaningful for drug treatment experiments. In (B) hPOs are shown. In the upper row, the colour indicates the day after seeding. In total 6 days were analysed because after day 6 no more size increase was detectable. The most overall organoid increase was detected at day 2, 3 and 4 with a  $\approx$  0.5-fold median size increase. At day 1 and 5 the organoids showed a  $\approx$  0.25-fold and at day 6 less than 0.2-fold median size increase. In the lower row a close up of the first three days of the mean organoid growth are shown (termed as pre-treatment, treatment and recovery). In blue organoids grew in normal culture medium and in red organoids in normal culture medium supplemented with 1 %/vol DMSO are shown. Error bars indicate the standard error of the mean. The growth curves of both conditions did not differ significantly before and after the application of DMSO. At day two the organoids were treated with DMSO and showed a significantly lower size increase than the control group (Mann-Whitney  $p \leq 0.01$ ). Based on the influence of DMSO to the growth rate of the organoids, all drug treatment experiments have been evaluated in respect to the DMSO treated organoids as the control group. Number of analysed organoids: (A) mPO 5 days analysis: 80, mPO 3 days analysis: 500; (B) hPO 6 days analysis: 150, hPO 3 days analysis: 460

### 3.4. Understanding organoids dynamics in detail – The light-sheet based segmentation pipeline

The growth behaviour of entire pancreas organoid cultures can be investigated by the presented brightfield pipeline. However, differences in single organoids are measurable, but the obtained data is limited. To investigate single organoids on a single cell level (micro- and mesoscopic) and with a high spatial-temporal resolution, light sheet microscopy is the tool of choice.

#### 3.4.1. Recording pancreas organoids *in toto* for more than 6 days allows detailed visualisation of single cell and individual organoid growth behaviour as well as the dynamic process of organoid morphogenesis

To understand the growth behaviour of pancreas organoids *in toto*, single organoids need to be analysed on a single cellular level (microscale) in the context of the complete organoid (macroscale) surrounded by the ECM. Therefore, the Zeiss Lightsheet Microscope Z.1 in combination with the custom-made holder was used. Figure 14 and Movie 5 illustrate mPOs (expressing Rosa26-nTnG as nuclei marker) that grew over a period of six days in the microscope (organoids were initiated from an adult pancreas of the Rosa-nTnG mouse line, transgenic mouse was created and provided by the lab of Metrixell Huch, Gordon Institute, University of Cambridge). To capture the complete FEP-foil cuvette, two image stacks were made and subsequently fused. Each image stack contained 871 z-slices with a z-distance of 2  $\mu\text{m}$  between the light sheets. With this setting, a total volume of approximately 5mm<sup>2</sup> was imaged. The FEP-cuvette contained more than 100 organoids which were imaged every 30 minutes. The medium was exchanged once after 24 hours and left untouched until the end of the recording to initiate the starvation process. This setup was used to simulate one life cycle of an organoid culture with an initial seeding phase, followed by an expansion and plateau phase and subsequent overall shrinkage of the organoids (because of starvation) accompanied with nuclei condensation and fading nuclei signal as hallmarks of organoid degeneration (Figure 15, “Degeneration”).

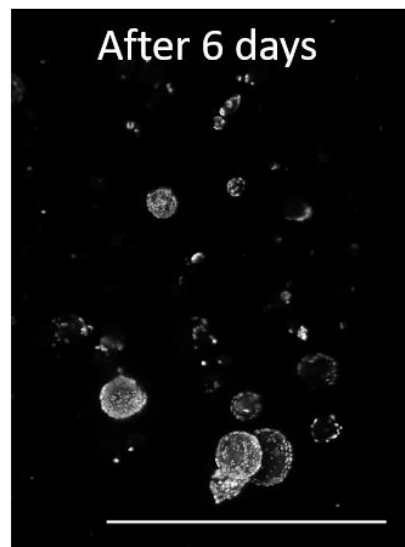
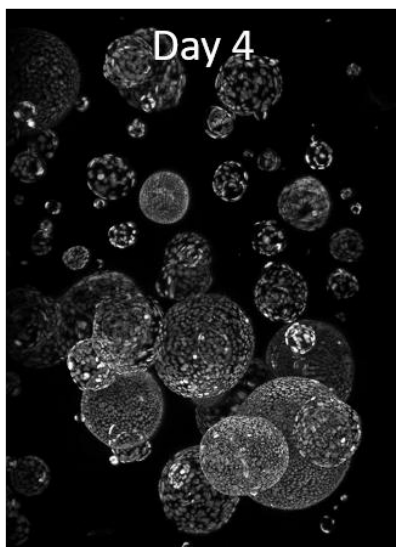
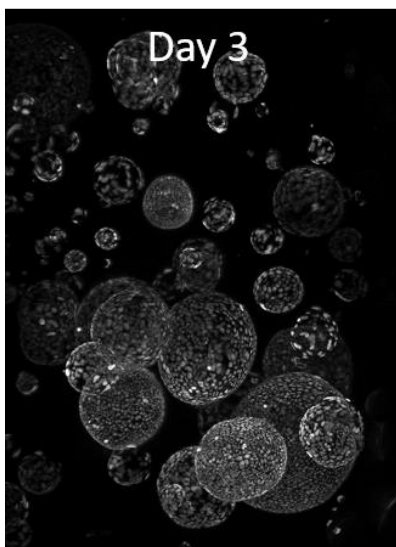
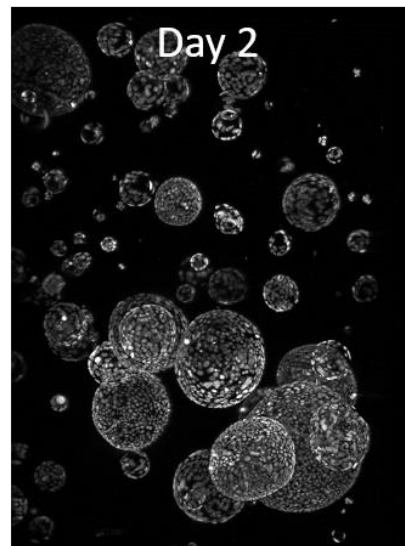
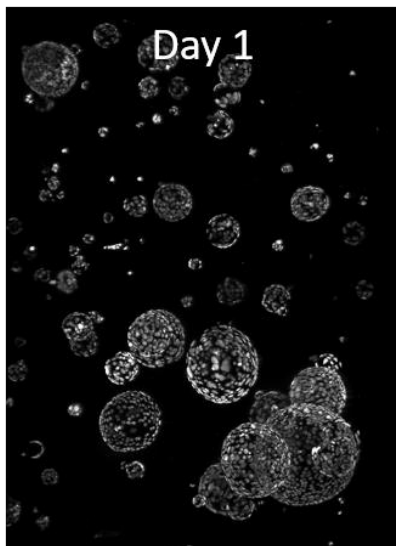
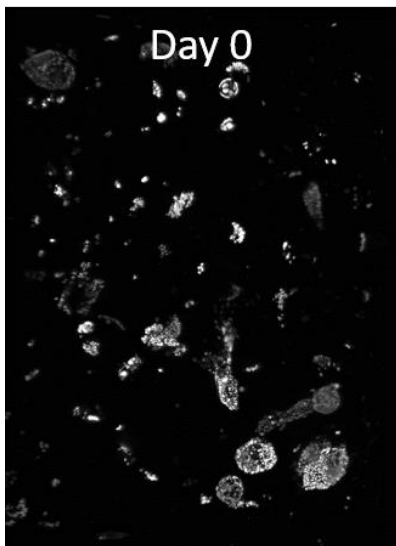
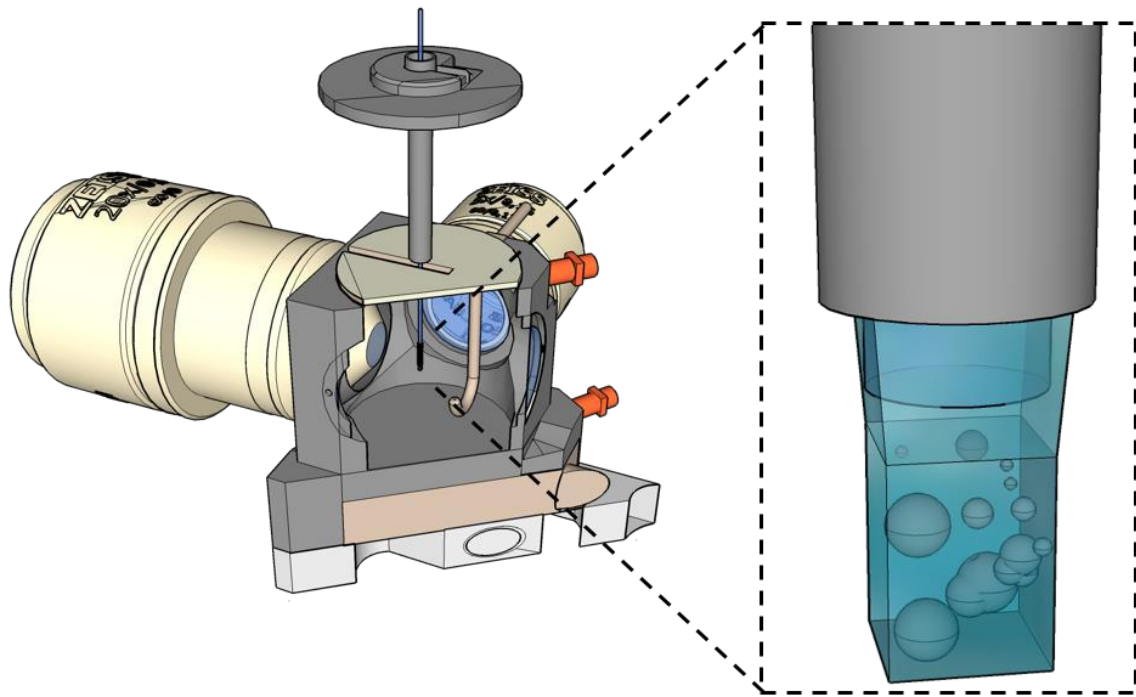


**Figure 14: Using the FEP-foil cuvette in the light sheet microscope allows for detailed visualisation of a live cycle of mPOs from the formation up to the point of shrinkage and degeneration.** The upper part of the illustration visualizes the Z.1 microscope chamber setup with the inserted sample holder equipped with the FEP-foil cuvette. The close-up illustrates the FEP-foil cuvette which containing already formed organoids. The lower part shows 6 representative images of a six-day observation series of mPOs expressing Rosa26-nTnG (nuclei marker, grey). The FEP-foil cuvette contains approximately 100 organoids imaged in a total volume of approximately 5mm<sup>3</sup> (871 z-slices with 2 µm spacing, two tiles fused to one image) and imaged every 30 minutes (288 time points). The organoid growth started with the formation and initial fast expansion which reached a maximum after approximately three days and finally ended with the shrinkage of the organoids accompanied with nuclear condensation and a fading nuclei signal as hallmarks of organoids degeneration (see also Movie 5). Microscope: Zeiss Lightsheet Z.1; objective lenses: detection: W Plan-Apochromat 20x/1.0, illumination: Zeiss LSM 10x/0.2; laser lines: 488 nm, 561 nm; filters: laser block filter (LBF) 405/488/561; voxel size: 1.02 x 1.02 x 2.00 µm<sup>3</sup>; recording interval: 30 min; scale bar: 1000.

### 3.4.2. Detection of organoids interculture dynamic processes – formation, degeneration, cell division and cell size variability

Figure 15 and 16 points out the overall heterogeneity, which was manifested by differences in the process of accumulation and formation, the overall sizes (in this manuscript the term “size” describes the organoid volume and surface) and rotation speeds, fusion of multiple organoids, differences in size oscillation frequencies and the movement of cell clusters within the gel. In the beginning of a life cycle of an organoid, the cells needed to accumulate and initiate a spherical structure. The acquired images allowed the detailed visual inspection and observation of this process. Figure 15 and Movie 6 show one cluster of cells that contracted and accumulated before the cluster started to rearrange and formed the spherical structure. In the illustrated organoid, the process took approximately seven hours and revealed the high dynamic of the formation process. However, the time of the formation process varied within the cell culture because the initial cell cluster size was highly diverse (for a comparison look at Movie 5 which additionally illustrates the general heterogeneity within one organoid culture in terms of size and formation time). Next to cell clusters, organoids can be seeded as single cells. With a recording interval of 30 minutes the setup allowed the visual tracking of division events of single cells (see “single cell division” and Movie 12) as well as in the organoids (see “single cell division within an organoid”). In both cases one cell division took approximately 2.5 hours and was accompanied by a rearrangement of the daughter cells within the organoid. After the division event, the daughter cells stood in close contact to each other. In addition to the overall heterogeneity in size and appearance of the organoids, the observation of the organoids on high spatial and temporal resolution combined with the possibility to observe cultures *in toto* revealed that organoids differed also in cell nuclei size. Figure 15 “cell size variability” and Movie 8 illustrate two organoids from the initial seeding up to 4 days. It is shown that they differed in the initial number of cells but reached the overall same size after 4 days. However, one organoid showed much bigger cell nuclei sizes (diameter between 5 µm and 10 µm) than the other (between 10 µm and 20 µm) which further illustrates the high heterogeneity of the system.

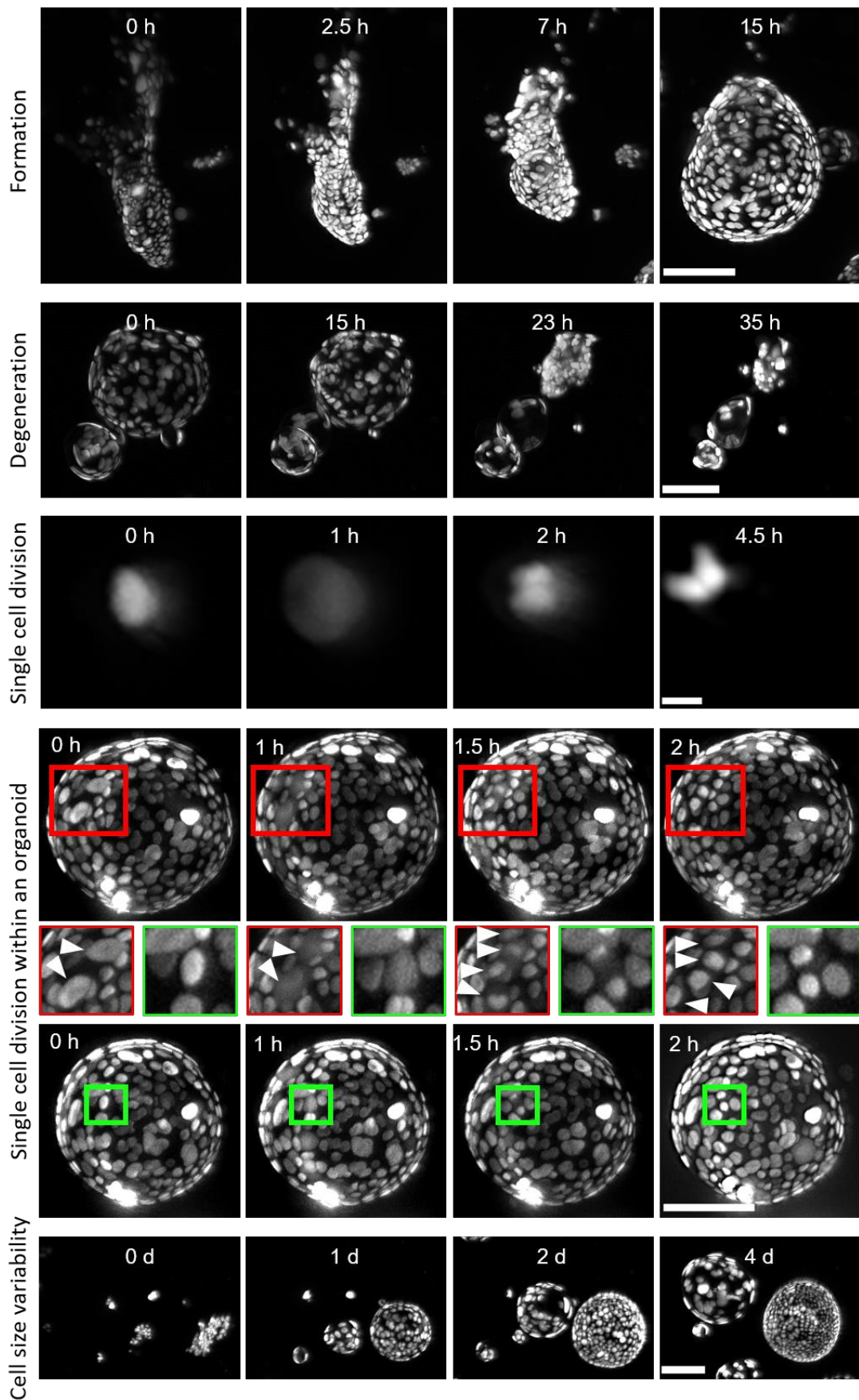


*Figure 15: High temporal and spatial resolved LSM recordings illustrate dynamic morphological processes in organoid development.* MPOs expressing Rosa26-nTnG in the nucleus (grey) were seeded in the FEP-foil cuvette and imaged over several

days in the Z.1 microscope. The figures show excerpts of maximum intensity z-projections of around 100 organoids imaged in stacks (up to 900 planes) over 7 days. Beside the formation and degeneration of organoids, cell divisions of single cells within organoids (green and red rectangle) are illustrated. Further, two organoids are shown which demonstrated the high heterogeneity in nuclei size within a culture. Microscope: Zeiss Lightsheet Z.1; objective lenses: detection: W Plan-Apochromat 20x/1.0, illumination: Zeiss LSM 10x/0.2; laser lines: 488 nm, 561 nm; filters: laser block filter (LBF) 405/488/561; voxel size: 1.02 x 1.02 x 2.00  $\mu\text{m}^3$ ; recording interval: 30 min; scale bars single cell division: 10  $\mu\text{m}$ , all others 100  $\mu\text{m}$ .

### 3.4.3. Detection of organoids intercultural dynamic processes – fusion, rotation and cell cluster motion

The high-resolution images allow the imaged-based segmentation and three-dimensional (3D) volume rendering of the acquired data. It allows a detailed inspection and reveals even more features in the highly dynamic organoid system.

The 3D rendering facilitates a more detailed understanding of the cellular dynamics which underlie the overall culture dynamic (Figure 16). The observation of the fusion of at least two organoids have already been mentioned in a former part of this work (see 3.2.1). With the help of 3D rendering, this process can be described in more detail. The fusion started with the touch of the epithelial monolayer of the organoids, continued with the formation of a small opening which connected both organoid lumen and rapidly expanded while cells migrated into one connected monolayer (Figure 16, “Fusion”, Movie 7). In Figure 16 the differently sized cell nuclei were already described. In addition to that observation, volume rendering illustrates that the organoids with big, large nuclei demonstrated fewer divisions over the time of observation (observed by eye) and were less densely packed, which further underlies the heterogeneity of pancreas organoids (Movie 8).

The acquired images allowed the quantitative feature extraction by the use of feature tracking tools (Arivis Vision4D, “Blob-finder” and “Tracking”). With single cell tracking, it was possible to observe the rotatory migration of the single cells and that the cells within an organoid demonstrated a collective rotatory motion. (Figure 16, “Rotation”, Movie 9). Aside from this observation, a detailed look at the single cells revealed that the expansion agility of single cells is not homogeneous distributed throughout the organoid. Areas with faster expansion went along with areas with slower expansions resulting in an elliptic sphere (Movie 13, first part). Along with this observation, the single cell tracking over the complete time of organoid development furthermore revealed that most of the mother and daughter cells stayed in closed contact during the complete time of development. It results in cluster of cells derived from one adult stem cell (Movie 14, second part). However, not all organoid cells demonstrated rotation behaviour, but in general high dynamics in regard to cell behaviour during organoid expansion (Figure 14 and Movie 10). Prior organoid formation, some cell clusters migrated through the ECM. One example is shown in Figure 16 “Organoid motion” and Movie 11. A cluster of cells (approximately 15 cells) travelled at an average speed of 10  $\mu\text{m}$  and a maximum speed of 23  $\mu\text{m}$  per hour through the ECM. In total, they covered a distance of approximately 250  $\mu\text{m}$  before they stopped and started to develop a spherical structure. Beside the directed movement, it becomes clear that the front cell guided the cluster to a specific point. However, this kind of behaviour was observed only a couple of times. Most of the cell cluster showed only minor travel activity prior formation (compare Movie 1 and Movie 5).

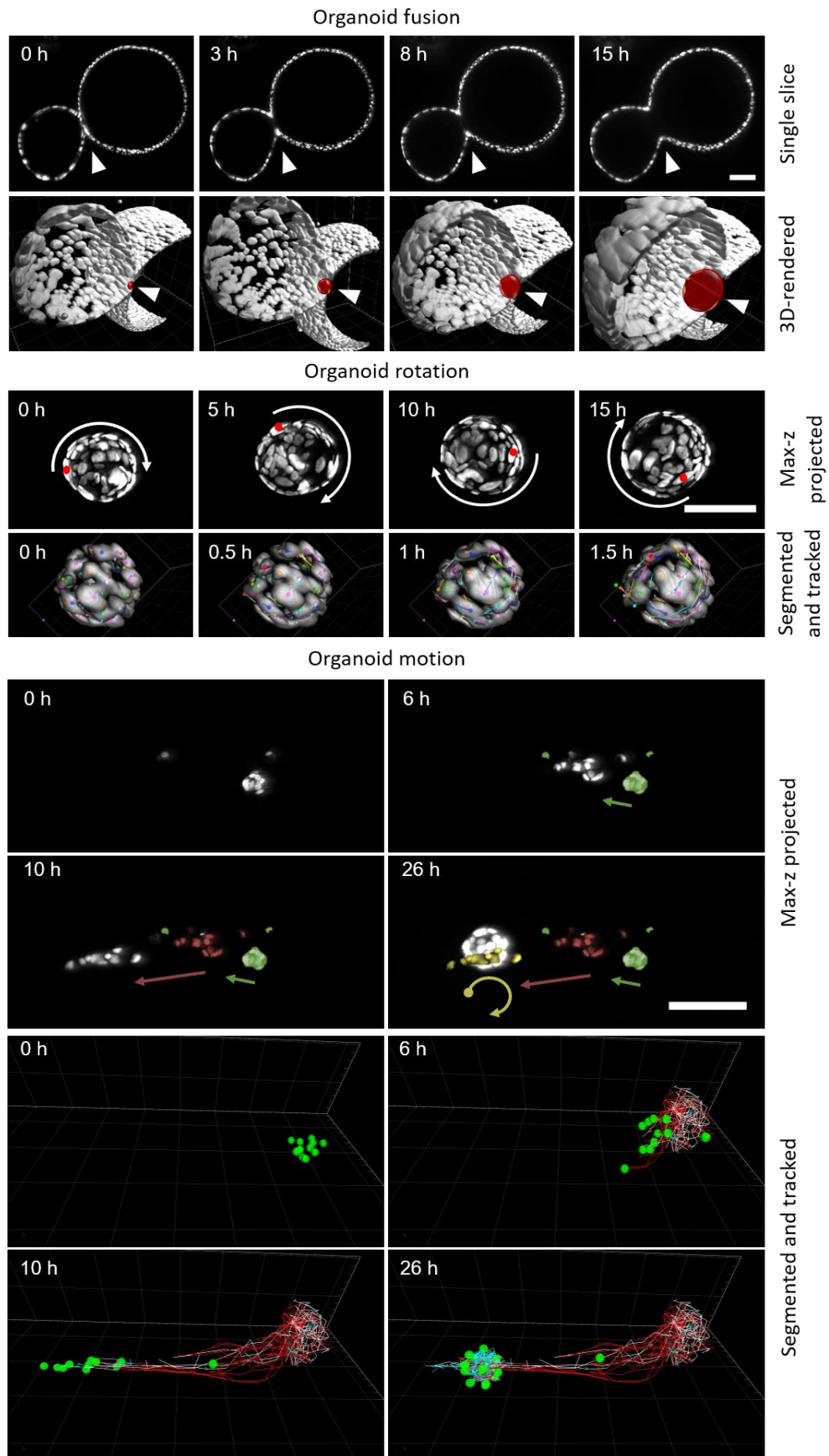


*Figure 16: Segmentation and 3D-rendering of high temporally and spatially resolved LSM recordings facilitates a more detailed understanding of the cellular dynamics which underlie the overall organoid dynamic. Highly dynamic processes were visualised*

by 3D rendering and elucidate the luminal dynamics in a spatial context. The fusion of two murine pancreas organoids expressing Rosa26-nTnG (grey) is shown in a single slice as well as a 3D rendered illustration. The processes of the fusion became clear and can be described as a first touch of the epithelial layers, followed by the formation of a small opening (red sphere) and a rapid expansion while cells migrated into one connected monolayer. Beside the fusion, the cell movement within an organoid was visualized and tracked by single cell segmentation. It is shown that all cells within the organoid rotated within one direction (red dot and coloured lines). Further, the cell cluster migration prior the organoid was formed is visualized and tracked (Max-Projection: the white cell nuclei illustrate the present time point and the coloured nuclei the former showed time point. Segmented and tracked: green illustrate the tracked cells and the lines the tracked movement of it, from white to red they travelled distance per time point.). Segmentation, tracking and 3D rendering was performed with Arivis Vision4D. Microscope: Zeiss Lightsheet Z.1; objective lenses: detection: W Plan-Apochromat 20x/1.0, illumination: Zeiss LSM 10x/0.2; laser lines: 488 nm, 561 nm; filters: laser block filter (LBF) 405/488/561; voxel size: 1.02 x 1.02 x 2.00  $\mu\text{m}^3$ ; recording interval: 30 min; scale bar 100  $\mu\text{m}$

### 3.4.4. Pancreas organoids vary in their growth behaviour – three representative quantified organoids

To quantify the acquired LSM data, our previously published cell nuclei segmentation pipeline was used (Hötte et al., 2019). With some adaptations the collected data can be semi-automatically segmented and enables the quantitative feature extraction over multiple days of acquisition (2.22). The provided, time-resolved data on cell nuclei numbers, organoid volume, surface area, number of neighbouring cells for each cell, as well as the cell density, can be further used to investigate basic principles of the organoid behaviour. With a 30-minute interval, a total number of 288 time points were analysed. Figure 17 and Movie 13 show three murine pancreatic organoids expressing Rosa26-nTnG (nuclei marker) grown in the ECM in the same cuvette and therefore in the same environment and under the same conditions. The three organoids have been investigated because of their representative character: one organoid, which was built from a small number of cells, one organoid which was built from a big number of cells and one organoid which was built from a large number of cells but was smaller than the other big organoid. With these three organoids, it became clear that the number of cells increase at different rates even if they had the similar starting cell number. It is illustrated that the small organoid had a cell number of eight directly after the seeding and that it increased its number at a low rate on average with 0.65 cells per hour. It reached a maximum number of 107 cells after six days, whereas another organoid that had started with nine cells and had a high cell increasing rate (7.41 cells per hour) ended up with 1077 cells after six days (Figure 17, blue and green organoid). As already mentioned, the splitting procedure results in different sizes of cell clusters. In order to meet this variability an organoid that started with 37 cells and reached a total number of 644 after six days had been analysed (averaging 4.12 cells per hour) (Figure 17, red organoid).

Next to the cell number, basic features can be quantified with the light-sheet segmentation pipeline. From the tracked cells, the volume and surface can be approximated. Furthermore, corresponding neighbourhood relation, e.g., number of cells in a defined distance to each other, can be calculated based on the segmented cell nuclei. (Figure 17, B). Taken these parameters into consideration, the organoid with the highest final number of cells did not show the largest volume and surface area. The mean distance of neighbouring cell nuclei in that organoid was smaller in comparison to the organoid that showed the largest volume and surface area. Alongside the neighbouring distance, it displayed a higher number of neighbouring cells which led to the result that firstly, this organoid had smaller cells in general and secondly, had a higher cell density.



Furthermore, frequent size oscillation is common in organoid culture (Sebrell et al., 2018). Therefore, the size oscillation based on the organoid volume was analysed. (Figure 18). As a threshold, a volume reduction of more than 5 % over three consecutive time points was defined as a size-oscillation event. All segmented organoids demonstrated frequent size oscillation events. On the one hand, the two bigger organoids conducted two (green) and three (red) events, on the other hand, the small organoid passed through seven collapse events at the same time of observation (blue). No patterns were identified that this behaviour correlated with cell density or any synchronised size oscillation events. In the first 80 hours no size-oscillation event of any of the segmented organoids was detected, but the small organoid demonstrated a general higher size oscillation frequency in comparison to the two big organoids.

On a single cell level, different phenotypes of organoids concerning volume, surface area, cell density and size oscillation events were identified. These observations help to understand and interpret the high intercultured heterogeneity in the growth behaviour of pancreas organoids and proves the usability of the system for the analysis of pancreas organoids.

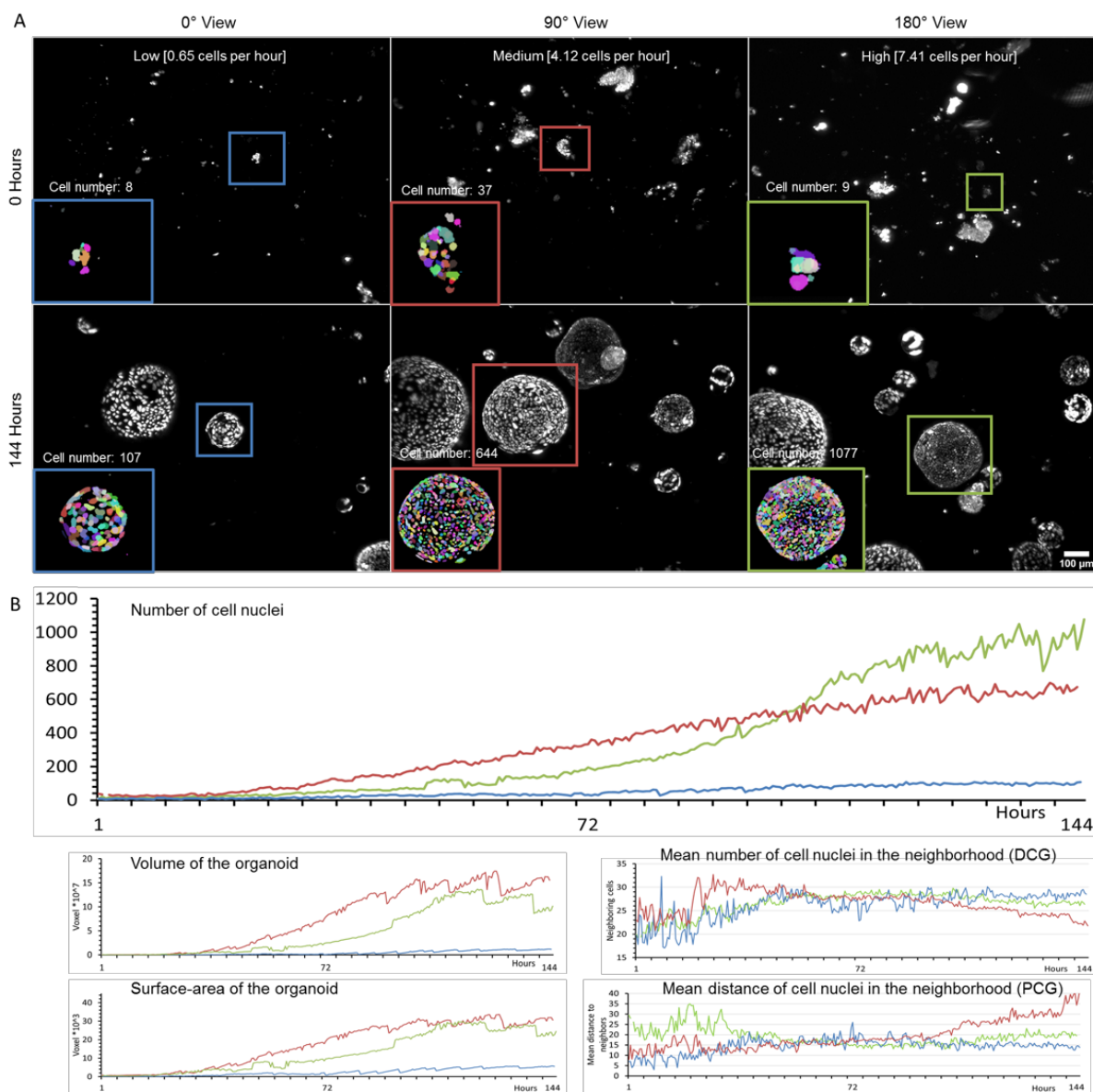


**Figure 17: Long-term single cell analysis of mPO grown in the FEP-foil cuvette reveals heterogeneity in proliferation capacities and differences in cell density.** Three representative pancreatic organoids, expressing Rosa26-nTnG (nuclei marker), imaged every 30 minutes over 6 days were analysed with the light sheet pipeline. (A) Pancreatic organoids are shown directly after seeding (0 h, upper rows) and after 6 days (144 h) of growth (lower row). Because all displayed organoids grew in the same environment every row shows one view of the same ultra-thin FEP-foil cuvette. The close-ups display the segmentation of the organoid at the corresponding time point. The single segmented cells are coloured randomly. The coloured edgings indicate the position of the segmented organoids with different growth behaviours. In green an organoid with a high rate in cell proliferation, in blue a low and in red the medium proliferative organoid is illustrated. (B) From top to bottom, corresponding evaluation of the volume, surface area and neighbourhood relations as a function of time. The corresponding graphs illustrate that all three organoids differed in their cell number, volume and surface-area. In addition, the measurement of the neighbourhood relations revealed that the organoid with more than 1000 cells (red) was more densely packed compared to the two other organoids (blue, green). (see also Movie 13) (DCG: Delaunay cell graph; PCG: Proximity cell graph); Cell Line: Mouse pancreatic organoids, microscope: Zeiss Lightsheet Z.1, objective: W Plan-Apochromat 20x/1.0, voxel size:  $1.29 \times 1.29 \times 4 \mu\text{m}^3$ ; fluorophore: SRm160-tdTomato. Adapted from Hof et al., 2021.

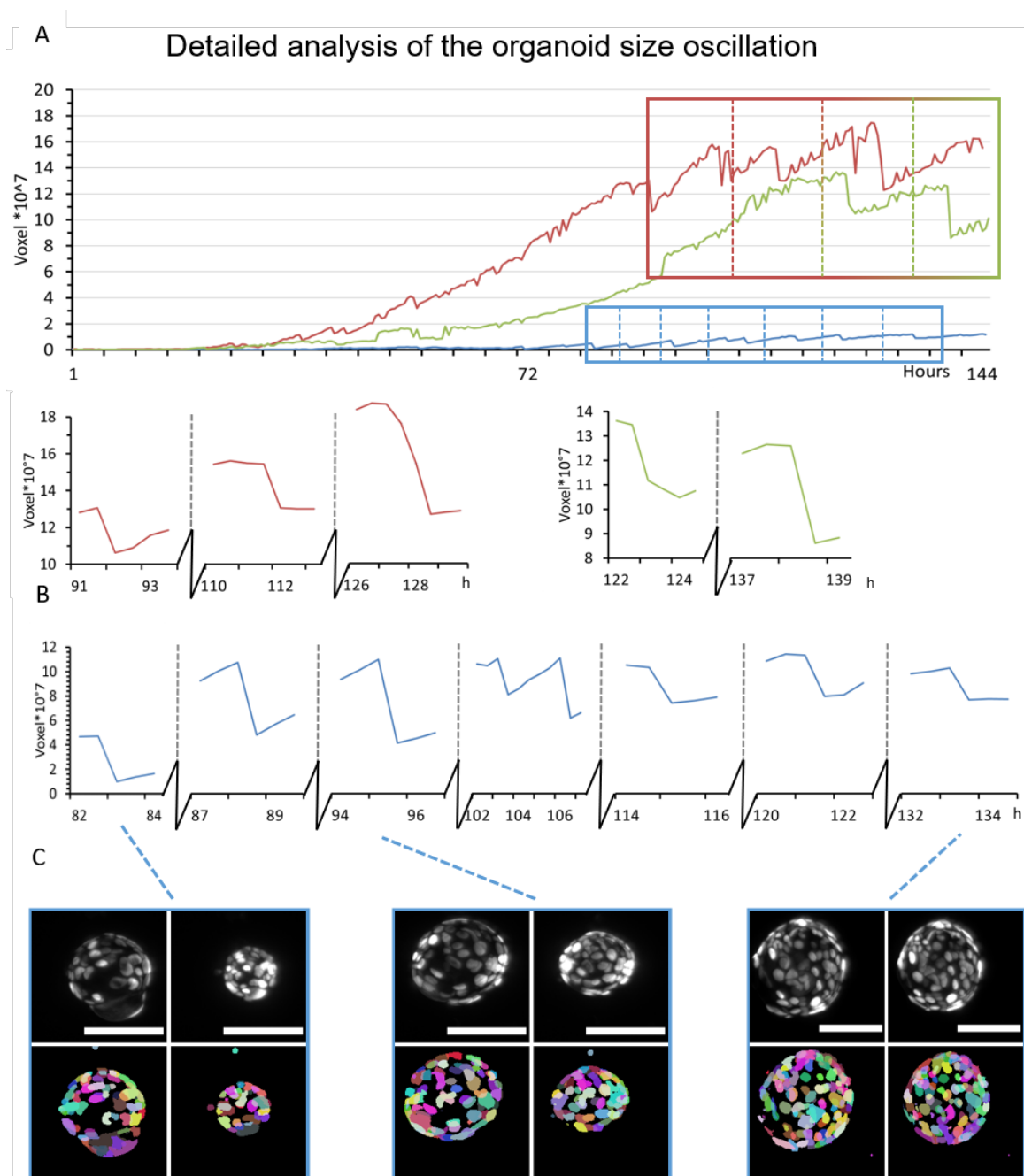


**Figure 18: Volume analysis of three representative mPOS revealed different size oscillation frequencies dependent on their overall volume.** Three representative Rosa26-nTnG (nuclei marker) expressing pancreatic organoids were imaged every 30 minutes over 6 days and analysed regarding the volume as a function of time. The frequencies of size oscillation did not follow a defined pattern or show any other similarities. A size oscillation event took between 30 minutes and two hours and occurred more often in the small organoid. (A) Plotted volume of three representative organoids approximated from the cell nuclei segmentation. (B) Detailed analysis of three (red) two (green) and seven (blue) pumping cycles in terms of significant reduction (more than 5 % volume reduction within 3 measured time points) of the organoid volume respectively. (C) Exemplary images of the organoids pumping behaviour. The upper row shows the nuclei in grey in the raw image, the lower row the segmented cell nuclei, respectively. Each colour illustrates a single cell nucleus. Cell Line: Mouse Pancreas Organoids, Microscope: Zeiss Lightsheet Z.1, Objective: W Plan-Apochromat 20x/1.0, voxel size:  $1.29 \times 1.29 \times 4 \mu\text{m}^3$ , 1 voxel =  $4,16 \mu\text{m}^3$ ; Fluorophore: SRm160-tdTomato H2B. Adapted from Hof et al., 2021.

### 3.5. The role of the extracellular matrix in pancreas organoid culture

The aforementioned *in toto* observation revealed, for the first time, a high heterogeneity in pancreas organoid behaviour and phenotype. It can be partly explained by the organoid cell

origin because the organoid generation rely on a selection process, based on the transcription factors, but do not include cell sorting procedures. However, one major source of heterogeneity is the ECM. In combination with specific growth conditions the ECM mimics the stem cell niche, and the cells can stay in their stem cell-ness. In the here presented study, mPOs and hPOs were grown in Matrigel® or BME-droplets, respectively. Both ECMs can vary in their composition from batch to batch. Whether this heterogeneity is one reason for the high organoid growth and appearance variability has never been addressed. Aside from this and of greater importance for clinical applications, the cell culture needs to be completely defined and reproducible. To meet this requirement reduced application or a replacement of ECM is inescapable. Therefore, this work tries to generate fundamental knowledge about the interaction of the organoid cells with the ECM.

### 3.5.1. Pancreas organoids do not need the ECM as physical scaffold

It is yet unclear whether organoids need all components of the ECM for growth or only certain motifs that are presented by distinct (glyco)proteins. In classic organoid cultures, the cell-clusters are seeded in a droplet of ECM and surrounded by medium. Thereby a separation of the solid ECM and the surrounding medium is ensured. To test whether the organoids are also able to grow only in a liquid phase, Matrigel® was dissolved at low concentration in medium without polymerisation into a gel. The solved ECM provides the needed surface proteins which can serve as binding motives but not a physical scaffold. This setup eliminates the physical force related interaction of the organoid cells with its environment. By this reason, a cell-ECM interaction is restricted to its influence of activation or deactivation of possible downstream pathways. However, to guarantee the absence of polymerized ECM particles, the cultivation and splitting procedure was adapted.

The pancreas organoid culture is based on frequent splitting intervals (passages) to guarantee the maintenance of the cells. During the splitting procedure the Matrigel® droplet and its enclosed organoids is disrupted and due to a stepwise washing and centrifugation procedure the organoid cell clusters are released from the ECM. Nevertheless, parts of the ECM are always attached to the organoid cell clusters and transferred into the new droplet of ECM. With the transfer of the organoids into a liquid culture system it needs to be ensured that no solid ECM parts are attached to the cell clusters. The splitting procedure itself is critical for the survival of the organoids which means no modifications can be made. To ensure the absence of solid ECM parts in the culture, organoids need to be kept in liquid culture at least for 3 passages. Then, the stochastic probability is given that no solid ECM piece is still attached to cell clusters and transferred into the new culture.

Figure 19 (A) shows murine pancreas organoids grown in four different concentrations of solved Matrigel®. Organoids grown in two and three percent of solved Matrigel® were not able to form organoids already in the first passage whereas in four and five percent of solved Matrigel® the majority of cell clusters were able to form phenotypic organoids from the beginning on and continued to grow after three passages. That shows that organoids need at least four percent solved Matrigel® within the media to survive and grow. Furthermore, Figure 19 (B, Passage 3) illustrates that organoids, growing in four percent solved Matrigel®, showed phenotypic polarisation patterns in terms of an apical actin and a lateral E-Catherin localization. In addition, the expression of Sox9 as the bi-potent marker and no detectible signal from Nkx

6.1 showed that cells maintained their bi-potentiality and did not differentiate. To investigate whether the cells maintained their phenotype also in long-term culture, organoids were kept in liquid culture conditions over more than two years and did not show any signs of alteration in their phenotype (Passage 64).

These results show that pancreas organoids are able to grow, survive and maintain their phenotype over a long time without a solid ECM. It is also shown that the ECM in general is necessary for the survival and growth of organoids, but not as a physical scaffold.

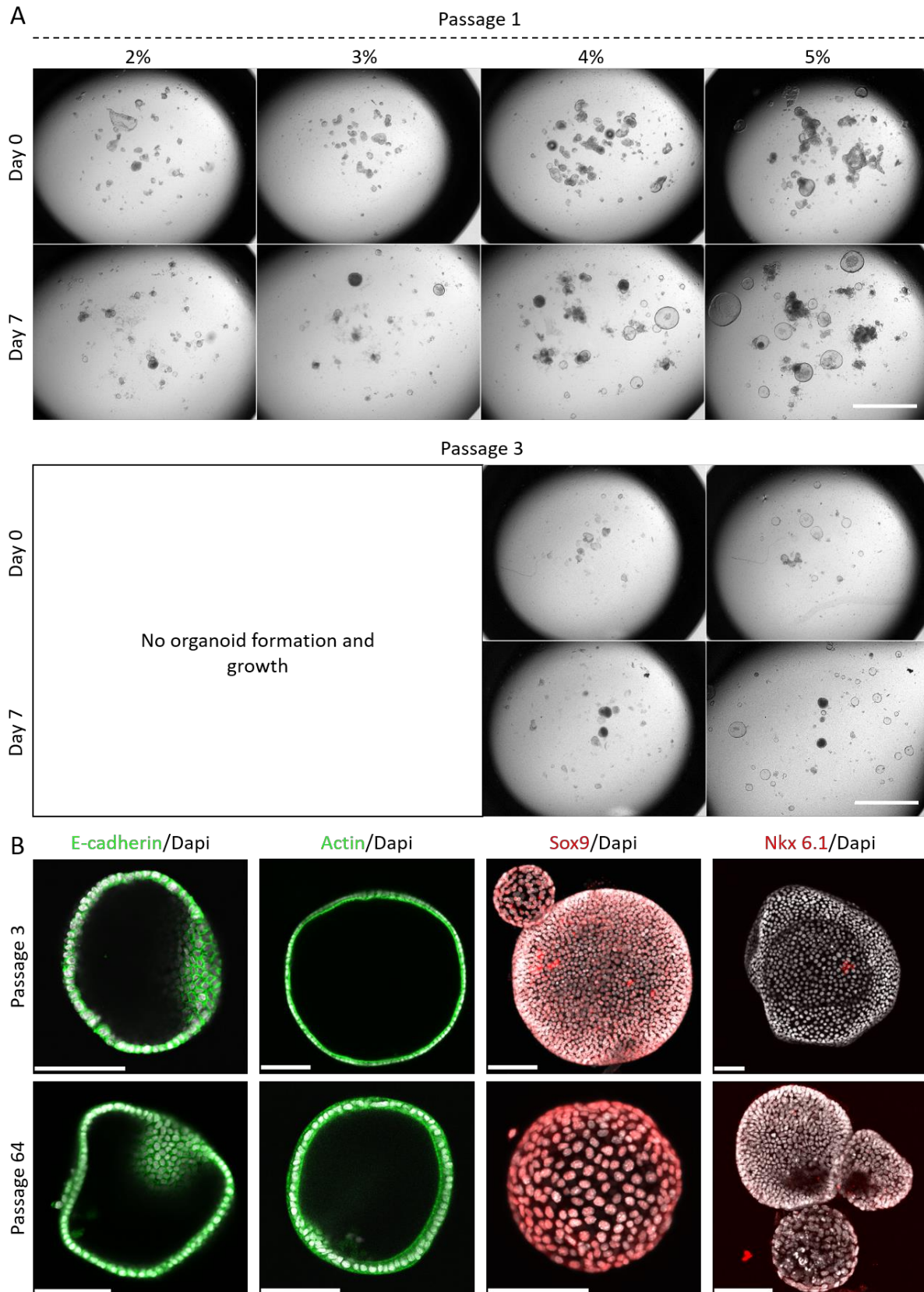


**Figure 19: Pancreas organoids do not need the ECM as a physical scaffold because they are able to grow and maintain their stem cell like characteristics in liquefied 4 % ECM.** (A) Representative brightfield images of murine pancreas organoids growing in different concentrations of liquefied Matrigel® as ECM. The top row shows organoids directly after the transfer from a solid droplet into different concentrations of liquefied Matrigel® (Passage 1). The second row shows the same organoids after 7 days in culture. In two and three percent liquefied Matrigel® only a limited number whereas in four and five percent a

reasonable number of organoids were formed. After one additional splitting procedure and after 7 days of growth no phenotypic organoids have been observed in two and three percent but in four and five percent liquefied Matrigel® (Passage 3). (B) Representative IF labelled organoids that have been grown in four percent liquefied Matrigel® for three passages (one month) and 64 passages (two years) respectively. Phenotypic expression of polarisation markers (E-cadherin, actin) homogenous expression of stem cell marker Sox9 and no signal of the differentiation marker Nkx 6.1 proof their phenotypic stability over a long time of cultivation. (For secondary Antibody controls take a look at Supplemental Figure 3) Microscope: (A) Zeiss Stereo Discovery V8, (B) LSF780, Objectives: (A) PlanApo S 0.63 (2,5x), (B) Plan-Apochromat 20x/0.8. Ex/Em: Dapi 405/462; Nkx 6.1488/553; Sox9, Actin 6.1 3 561/633; E-cadherin 633/699. scale bars: (A) 1000 µm, (B) 100 µm.

### 3.5.2. Pancreas organoids are able to grow within solubilized ECM – the hanging drop system

It has been shown that pancreas organoids are able to grow without a solid ECM surrounding them. However, it was not possible to cultivate organoids in liquefied Matrigel® per se. After the organoids were placed in the culture well, the cell-cluster tended to settle down due to gravity and started to grow on the bottom of the well. Without a solid scaffold, organoids tended to lose their three dimensionalities by growing as a flat, 2D cell layer on the bottom of the culture plate. It is already proved that stem cells growing as a 2D-layer start to lose their cell fate and tend to differentiate (Pampaloni et al., 2007). To circumvent this and to keep the cells in their stem-cell like fate a new culture system was developed.

The hanging drop culture principle was initially established to form and culture spheroids out of a cluster of loose cells (Foty, 2011). Figure 20 shows the scheme of the hanging drop culture technology adapted for the use with organoids (for detailed description take a look at 2.15). In short: starting with raw material from a biopsy or an already established organoid culture (Figure 20, A), the organoids were splitted into fragments as recommended in the standard protocol. After the last centrifugation step the organoid pieces were then placed in the 4°C cold medium containing 4 % pre-solved Matrigel® (Figure 20, B). Depending on the amount of material, the amount of medium need to be chosen. As a rough guideline a 1:3 ratio of solid Matrigel® droplet to liquid drop can be given. Depending on the number of organoids within a droplet, the ratio needs to be adapted. The medium-Matrigel®-cell-fragment-mix was then placed as 25 µl drops on the inner side of a squared Petri dish lid (optional, round petri dishes can be used if needed). The lid was then turned smoothly 180° upside-down and placed on the Petri dish bottom which has been filled with 37°C pre warmed sterile PBS. The Petri dish was then placed in an incubator. After the first 24 hours 15 µl of the medium containing 4 % solved Matrigel® was added to each drop. From then on, every 48 hours 10 µl of Media with 4 % solved Matrigel® was added to each trop until the organoids reached the desired size or days in culture and the splitting protocol was repeated.

The presented protocol to culture pancreas organoids in a hanging drop system illustrates a technique to keep organoids in their native state without the use of solid ECM (in this case Matrigel®). Aside from this and due to gravity, it guarantees that no organoid cell can attach to the well surface and form a 2D cell layer. This technique enables a long-term culture of organoids with a reduced amount of ECM.

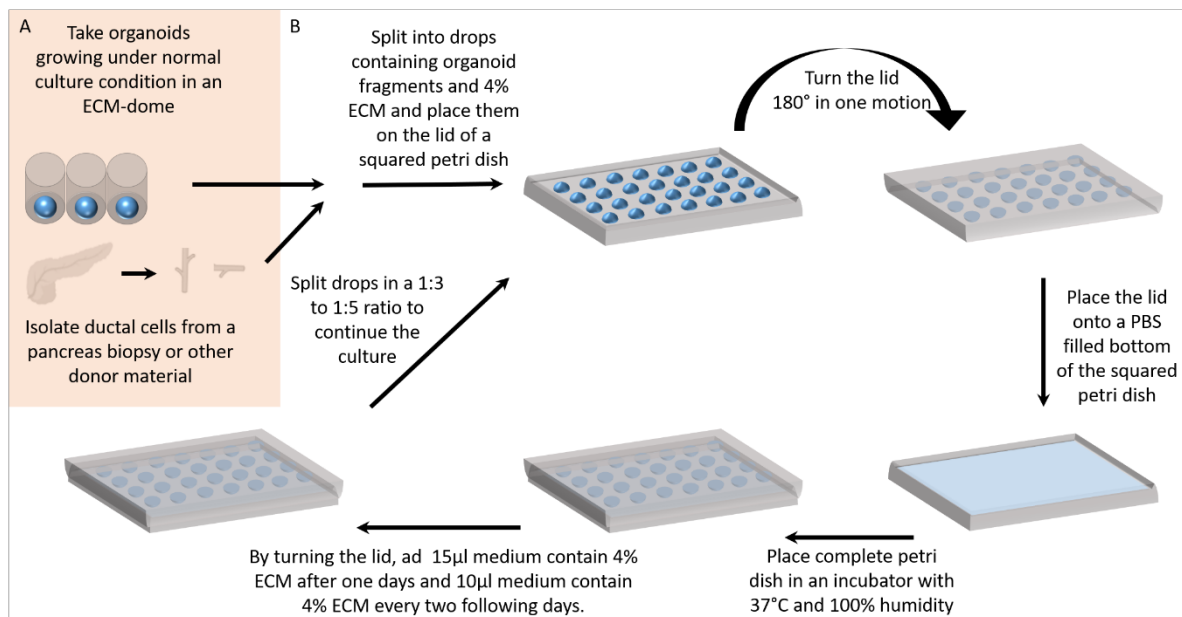


**Figure 20: Scheme of growing organoids in the hanging drop system..** The scheme describes a procedure that is initiated by taking already established organoids from a classic ECM-droplet culture or fresh isolated ductal donor material (A). Independent from the starting material, (B) organoid cell clusters, ductal fragments or single cells need to be placed in 4°C cold growth medium that comprises of at least 4 % Matrigel®. The solution is then gently mixed and placed as 25 µl drops on the lid of a squared petri dish. Depending on the number of drops, the petri dish size and type (squared or round) can be chosen. The lid is then turned up-side-down (180°) in one gentle movement and placed on the corresponding petri dish bottom which is filled with pre-warmed (37°C) PBS. The closed petri dish is then incubated at 37°C and 95 % relative humidity in an incubator. After 24 h 15 µl 4°C cold growth medium, containing 4 % solved Matrigel®, is added to the drops by turning the lid down-side-up, gently pipette the 15 µl into the drops and turn it again up-side-down on the bottom of the petri dish. This procedure is repeated with 10 µl 4°C cold growth medium, containing 4 % solved Matrigel® every two days and in total for at least seven days or as long as the organoids need to grow into the desired size. A new splitting procedure start with splitting the hanging drops in a ratio of 1:3 to 1:5 drops.

### 3.5.3. Organoids maintain their phenotype and fate in the hanging drop system for more than two years

The organoid hanging-drop (HD) culture system was developed to understand the interaction of ECM with the cells, reduce the amount of ECM in the culture but also to minimize the influence of uncontrolled parameters due to the ECM's animal origin and its batch-to-batch variability. However, for the validation of the system, it is necessary to analyse the growth of the organoid over long periods of time and with different donors. Only the long-term culture proves the replication potential and thereby the stem cell-ness of the organoids. Figure 19 (B) already proved that the organoids showed polarisation and bi-potency after two years in the hanging-drop culture. Figure 21 (A) illustrates that two murine organoid cultures generated from two different donor mice grew in the hanging drop system for several passages. In fact, all lines grew more than five passages ( $\approx$  5 weeks) whereas organoids from donor #2 were kept in culture for more than 15 passages ( $\approx$  4 month) and from donor #1 for more than 90 passages ( $\approx$  2 years) before they were transferred in liquid nitrogen for long term storage. Figure 21 (B) shows the organoids from donor #1 after fourteen, three and one month of culture in the hanging-drop system. At all ages, the organoids demonstrated the same phenotype. In comparison to the normal grown organoids, the organoids in the HD-system appeared with increased time more homogeneous in terms of size and structure. This indicate that the HD-system provides stable and constant conditions.



The multiplication rate of organoids can be validated in terms of the splitting ratio because it describes the number of drops that can be generated out of one drop. To validate the growth of mPOs in HD, the splitting ratio of donor #1 is plotted against the passage number (Figure 21, C). It is shown that the splitting ratio varied between one and six with an average of three new generated drops from one single drop over all 80 passages which indicates a constant proliferation activity of the organoid's cells. For clinical applications or for molecular analysis of organoids, a large amount of cell material is needed. Therefore, it is necessary to culture the organoids from cell fragments instead of single cells. One drawback in this procedure is that single cell counting is not possible. For that reason, the only option to generate valid and robust data is to use the splitting ratio for theoretical considerations of the number of organoids that can be produced. Figure 21 (D) shows the theoretical calculation of the number of HDs over the days of culture based on real splitting ratios of Donor #1 (termed "increasing rate") (Supplemental table 1). A clear linear increase of the drop number illustrates that the system is suitable to generate a large amount of cell material independently of the amount of starting cell material. This consideration is essential, because the amount of donor material is usually the limiting factor (Georgakopoulos et al., 2020; Huch, Bonfanti, et al., 2013). In addition, the culture of organoids out of a single cell is important, because it is needed to generate transfected cell lines, investigate single cell behaviour or generate defined numbers of organoids. For this reason, the culture of organoids in the HD-system out of single cells was also tested. Figure 21 (E) shows one drop contained hundreds of small organoids which grew from single cells. As mentioned, organoids grown out of a single cell show less survival rate, this observation further validates the HD system to provide optimal growth conditions. In addition, the organoids were still able to grow in normal culture conditions (Figure 21, D). Alongside this, it confirms that murine organoids conserved their phenotype when grown in the hanging-drop culture system.

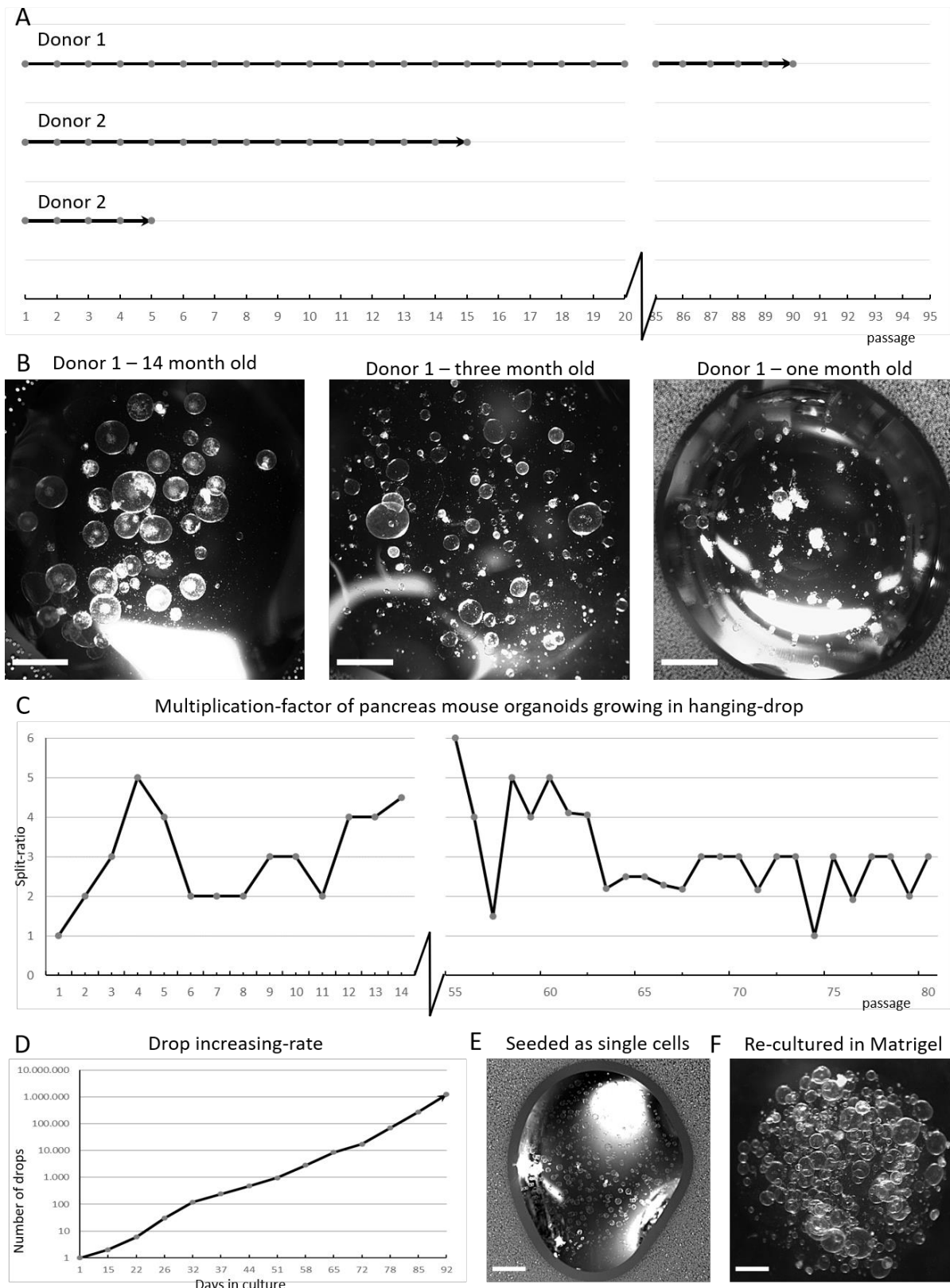


**Figure 21: Three mPO lines grown in the hanging drop system as long-term culture.** In (A) three murine pancreas organoid lines (generated from two donors) are shown that grown for more than 5 passages in the HD system before they were frozen for long term storage. In (B) Donor #1 is shown after 14 months, three and one month in the HD system. At all ages, the organoids show the hollow phenotype. In (C) the splitting ratio of donor #1 for more than 80 passages are shown. With an average of 3 drops generated out of one drop a constant proliferation activity of the organoid's cells is demonstrated. In (D) the drop increasing rate of Donor #1 is plotted against the days in culture and shows a linear increasing rate of organoid drops in time.

It illustrates the theoretical calculation of the number of drops that can be generated from one single drop based on the splitting ratios shown in (C). In (E) organoids derived from single cells and grown in the HD system are shown. In (F) organoids grown in the HD-system and placed back into the normal ECM droplet system are shown. Microscope: Zeiss Stereo Discovery V8, Objectives: PlanApoChromat S 0.63. Scale bar: 1000  $\mu$ m

Human pancreas organoids suffer from lower reproduction rates, higher sensibility to external stimuli and cannot be cultured for an unlimited time (compare (Huch, Bonfanti, et al., 2013) and (Georgakopoulos et al., 2020)). Because of this fact the culture of human pancreas organoids needs to be optimized to generate robust and reliable data. Furthermore, the use of animal originated ECM restricts the use of hPOs to pre-clinical investigations. For this reason, the culture of hPOs in the HD-system was tested. Figure 22 shows that hPOs were able to grow in the HD-system. A comparison between human organoids, grew over twelve days in the hanging-drop culture system, to the normal system illustrates that the organoids in the HD-system tended to be smaller but the size of all organoids were more homogeneous (Figure 22, A). To validate the system, two pancreas organoid lines, that derived from two different human donors, were grown in the hanging-drop system for more than ten passages simultaneously to the normal culture (NC, Figure 22, B). Donor #1 showed the same number of possible passages (10) grown in HD in comparison to organoids grown in normal conditions (NC). Organoids from donor #2 grew for more than 15 passages ( $\approx$  6 month) in the hanging-drop system before they were stored for long term, whereas the control group stopped growing after 11 passages ( $\approx$  4 month). The human organoids maintained their phenotypic appearance over the complete time of culture (Figure 22, B). In addition, it was possible to re-culture them in the normal culture system (Figure 22, C). These results demonstrated that human pancreas organoids can be maintained in the hanging-drop system presumably longer than under normal culture conditions and still maintain their phenotype. These further proofs that the HD-system provides stable and constant growth conditions which favours the homogeneous growth and the long-term culture of hPOs.

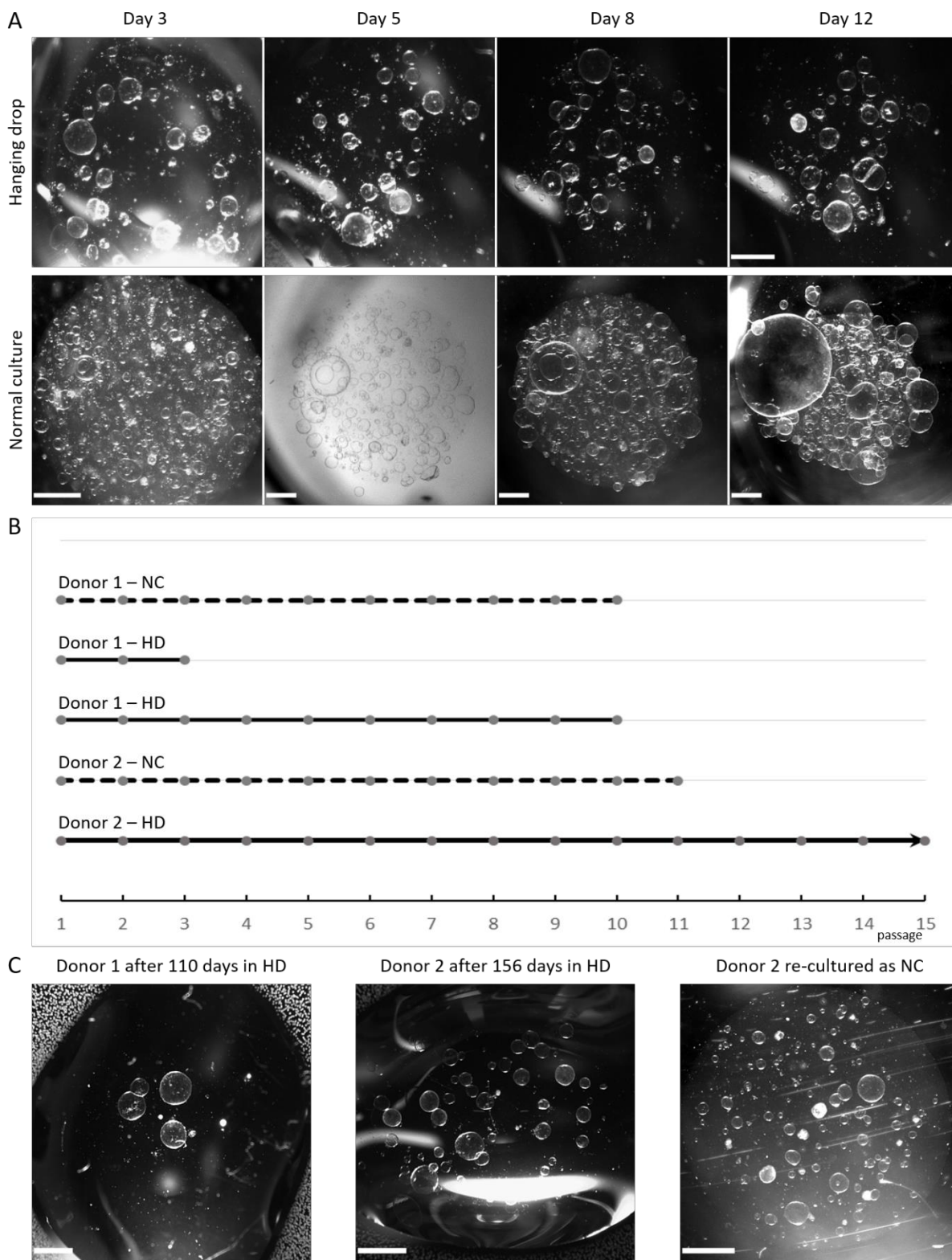


**Figure 22: Two different hPO lines grown in the hanging drop system as long-term culture.** In (A) one representative human pancreas organoid line grown in the hanging drop system and under normal Matrigel®-droplet culture conditions over twelve days. In both culture conditions the organoids demonstrated their phenotype of a hollow liquid-filled lumen. In (B) three human pancreas organoid lines (generated from two donors) grew in the hanging drop system (HD) and the corresponding Matrigel®-droplet culture as a control (NC, dashed lines). After ten passages (~ 3 month) the Matrigel®-droplet and HD culture of donor #1 stopped growing. Organoids from donor #2 were frozen for long term storage after 15 (~ 6 month) passages in the hanging-drop system whereas the culture in Matrigel®-droplets stopped growing at passage eleven (~ 4 month). (C)

Organoids from donor #2 showed the hollow phenotype after 110 days as well as after 156 days and could be re-cultured in the Matrigel®-droplet culture system. Microscope: Zeiss Stereo Discovery V8, Objectives: PlanApo S 0.63. Scale bar: 1000  $\mu\text{m}$

### 3.6. Human and mouse organoids within the scope of cell-matrix interaction

Pancreas organoids have been developed less than a decade ago because of this novelty basic knowledge is still missing. It was already shown that mPOs and hPOs do not need an ECM as a physical scaffold per se, but presumably as a provider of extracellular binding domains. This leads to the question how organoids maintain their spherical like structure without a surrounding physical scaffold. Next to the polarized cytoskeleton components which can provide physical strength up to a certain degree, it can be hypothesized that the liquid filled lumen of organoid is needed to construct the phenotype and that it is generated by an influx of water from the basal towards the apical side.

#### 3.6.1. Non-invasive confocal Raman microscopy as a tool to analyse fixed and live organoids

While the here-presented fluorescence and phase contrast microscope images yielded information about phenotypic appearance and growth behaviour, a more chemically selective analysis is needed to gain information about the composition of the luminal liquid and the exchange with the organoid surrounding. Furthermore, the interaction of the organoid cells with the ECM can also be more target-aimed analysed by preserving the native state of the organoids embedded within the ECM. For this reason, alternatives need to be found that do not affect or influence the organoids. Raman microscopy was considered as a non-invasive technology which fulfill these criteria. In a cooperation with the research group of Maike Windbergs, Nathalie Jung and myself adapted Raman spectroscopy, combined it with confocal imaging (confocal Raman microscopy, CRM) and adapted the organoid culture for a non-invasive analysis of live and fixed organoid cultures (Jung and Moreth 2020, in preparation). Raman spectroscopy, as a label-free and yet chemically-selective technique, has been used to characterise three-dimensional cell cultures but has never been applied to organoid cultures. It allows the analysis of the chemical composition of the analysed sample and holds great potential for a comprehensive analysis of organoids embedded in ECM.

#### 3.6.2. The luminal liquid of pancreas organoids consist mainly out of water and the water-protein ratio increases with the organoid size

As described above, CRM was adapted and used to analyse mPOs. Figure 23 (A) shows the results of a CRM scan at the equatorial plate of a chemically fixed organoid. A false negative coloured picture shows that the organoid is formed out of a layer of cells (grey) that separate the ECM (cyan) from the volume (blue) of the organoid. In (B), the full spectra of the corresponding areas of (A), marked in the same colours, were plotted in regard to its intensity. Highlighted are the regions for lipids/DNA (around  $2900\text{ cm}^{-1}$ ) and water (around  $3280\text{ cm}^{-1}$ ). It shows that the luminal liquid and the surrounding ECM/media had a comparable water content whereas the cell layer had a smaller amplitude of water but stronger peaks in lipids and DNA. The fingerprint region ((B), lower row, spectrum from  $400\text{ to }1800\text{ cm}^{-1}$ ) enables a closer look towards the measured compositions of the depicted region of the organoid. Specific peaks for chemical bonds such as cytochrome C, as a hallmark of apoptosis, polysaccharides

and proteins (increased concentration can be used to identify cellular components) allowed a detailed analysis of the chemical composition of the different compartments of the organoid. Both presented graphs illustrate that the spectra of the lumen and the surrounding did not differ in its water content but within peaks of lipids, proteins and polysaccharides. The lower levels of these chemical bonds, within the organoid lumen illustrates that mainly water was transferred through the monolayer during the growth of the organoid. Nonetheless, ECM components were detected within the organoid as well. Furthermore, it points out that the organoid cells separated the apical from the basal side and by this fulfil their native function as a cellular barrier (Edelblum et al., 2015).

Single-spectrum CRM measurements allowed a rapid analysis of individual living organoids within a droplet of ECM (Figure 23, C). The single spectrum was made in the middle of the corresponding organoid and in organoids of different sizes. The results were then analysed in regard to the intensity ratio of water to protein. This setup detects the differences of the water-protein ratio and helps to understand the mechanism the cells use to increase the overall organoid size. Therefore, organoids were plotted against their diameter (every blue circle represent one measured organoid). The corresponding graph proved the former made observation that the organoid lumen is filled with a water-protein mixture. Additionally, it illustrates that the water-protein ratio correlates with increasing diameter of the organoids (red punctuated line, correlation line). In conclusion, this data shows that the organoids increase their size by increasing the water content within its lumen.

In summary, CRM scans revealed that the general composition of the lumen liquid reflects the circumventing liquid in terms of its chemical composition. Further, it proves that all components of the ECM are also present within the organoid liquid and that the cells do not secrete any specific substance into its lumen. The CRM analyses of living mPOs revealed that the organoid size increase is accompanied with an increase in the water-protein ratio. The made observations further promote the aforementioned hypothesis that the water influx into the lumen is needed to construct and maintain the organoid phenotype and that it is mainly caused by an osmotic gradient produced by the cells and not by any specific substances within the lumen.

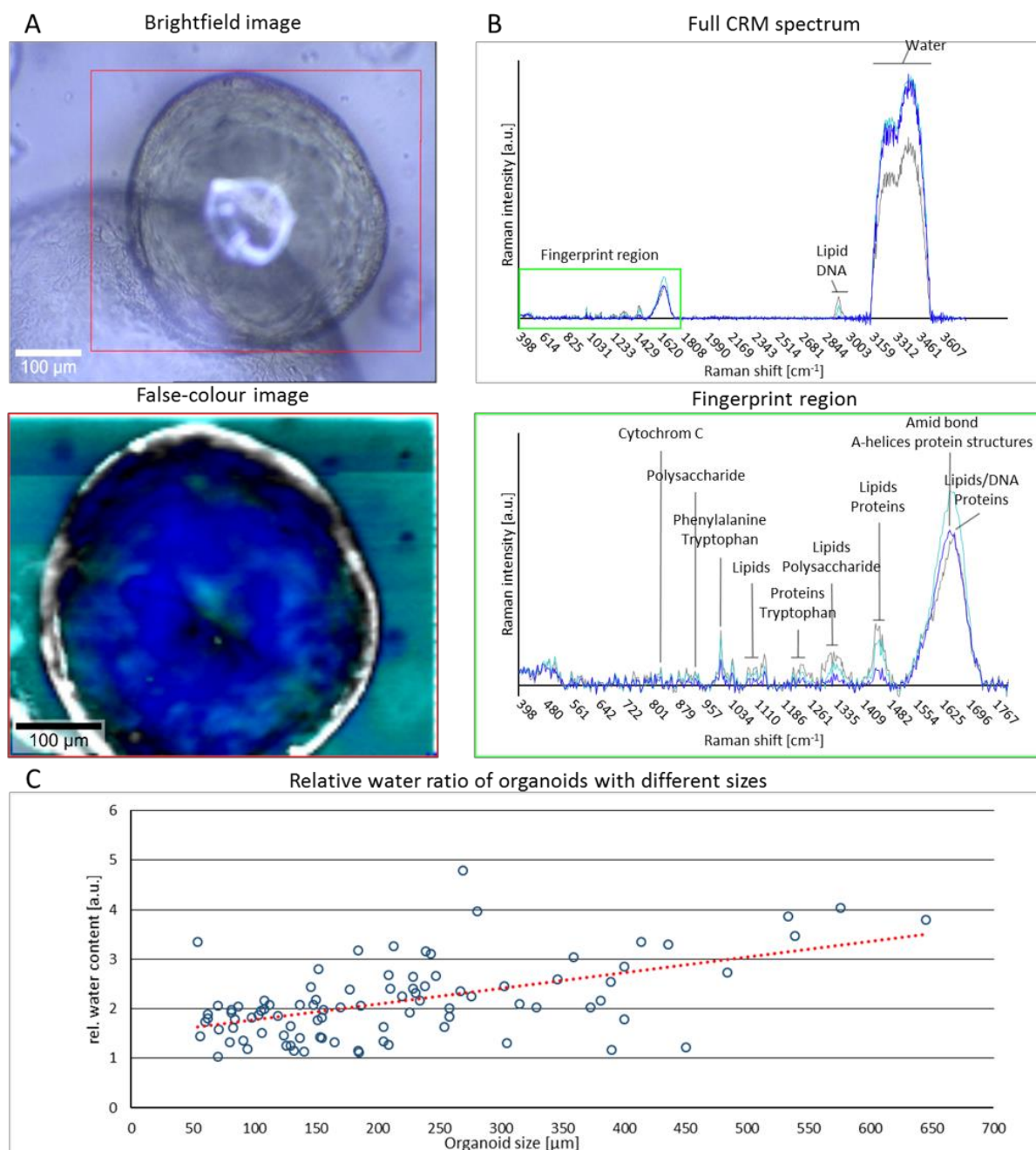


**Figure 23:** Pancreas organoids imaged with chemically selective confocal Raman microscopy (CRM) illustrate that the lumen of the organoids consists mainly out of water and that the water–protein ratio increases with increasing organoid size. In (A) and (B) the result of a full spectra measurement of the equatorial area of a fixed pancreas organoid is shown. In (A), a brightfield (top) and the corresponding false colour picture (bottom), generated from the CRM measurement, are shown. The colours illustrate that the organoid surrounding (cyan), the cell layer (grey) and the inner luminal area (blue) was distinguishable with CRM. In (B), the full spectra of the corresponding areas in the same colours are shown (top). Next to the characteristic peaks of water (peak around 3280,5  $\text{cm}^{-1}$ ), characteristic regions for Lipids and DNA are illustrated. The lower graph (highlighted in green) illustrates the fingerprint region of the full spectra measurement, which showed the detection and characterisation of peaks of specific chemical bonds such as cytochrome C, polysaccharides and proteins in general. Both graphs illustrate that the spectra of the lumen and the surrounding did not differ in its water content. Differences were detected within areas of lipids, proteins and polysaccharides which are characteristic for the ECM and the surrounding media. In (C) the measurement of multiple living mPOs (blue circles) in regard to the CRM spectral data of the water to protein ratio is shown. The red line shows a linear regression and illustrate that the water to protein ratio increased with increasing size ( $R^2$ : 0.2913). Microscope: Alpha300R+ system (WITec GmbH, Germany), Objectives: Epiplan Neofluar 63x/1.0, Epiplan Neofluar 10x/0.3, spectral range: 400-3700 $\text{cm}^{-1}$ , spectral resolution: 4  $\text{cm}^{-1}$ .

### 3.6.3. Mouse pancreas organoids express Aquaporin 1, 5 and 8

Based on the above-mentioned results, the presence of channel proteins that foster and increase the transport of water from the basal to the apical side is highly likely. In the adult pancreas, the presence of Aquaporin 1, 5 and 8 in the ductal epithelial cells has been proven (Burghardt, 2003; Leire Méndez-Giménez et al., 2018). Whether these channels are also expressed in pancreas organoids is not known. To investigate the presents of these channels, immunofluorescence staining was performed.

Single mPOs that were immunolabeled with antibodies against Aquaporin 1, 5 and 8 in a maximum intensity projection and as a single slice in a close-up are shown (Figure 24). It becomes clear that all three channels were expressed at the membrane but slight differences between the channels could be detected. Aquaporin 1 was homogenously expressed at the basal, basolateral as well as apical side and showed a general diffuse expression in the cytosol. Aquaporin 5 showed a slight tendency towards the apical and basal side and a high cytosolic expression but only low expression at the cell connections (lateral). A clear expression at the apical side and low expression in the cytosol was detected for Aquaporin 8

These results illustrate that murine pancreas organoids expressed all three Aquaporin channels within their cell membranes. The observed polarized expression fits to the mentioned expression patterns *in vivo* (Burghardt, 2003). Whether they are responsible or at least support the water transfer through the cell inside the lumen is probable but need to be additionally addressed.

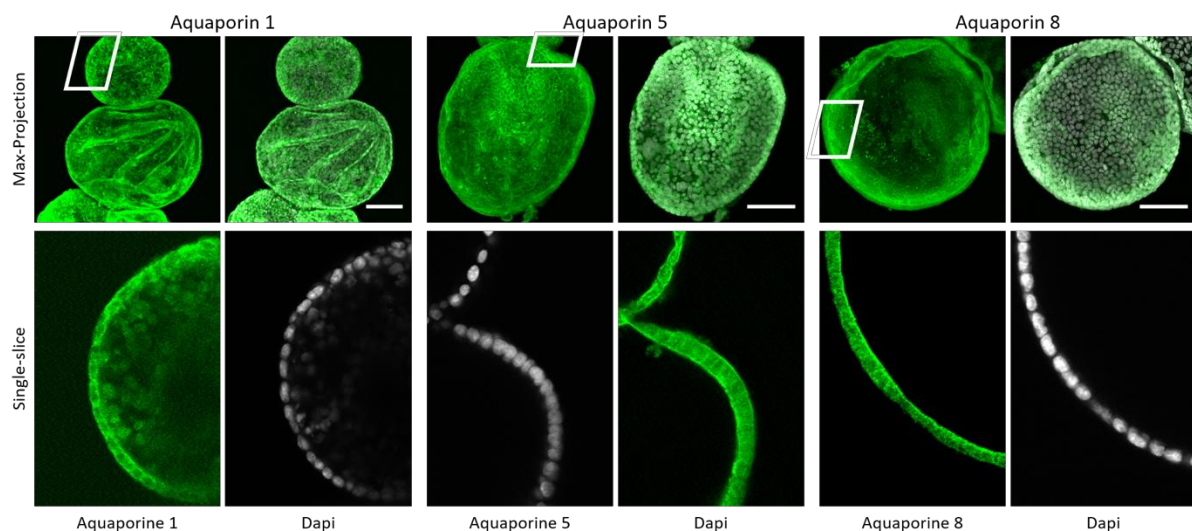


**Figure 24: MPOs express Aquaporin 1, 5 and 8.** Mouse pancreas organoids were stained against Aquaporin 1, 5 and 8 (green) and the nucleus (Dapi, grey). The top layer shows a Maximum Intensity Projection of multiple z-slices of the corresponding Aquaporin (left) and a merge of it with Dapi (right). The bottom layer show on z-slice from the above shown projection as a close-up. All three Aquaporin channels showed a polarized expression but slightly differ in their profile. Aquaporin 1 was homogeneous expressed at the cell membrane, Aquaporin 5 showed a tendency for a lateral and basal expression whereas Aquaporin 8 was mainly expressed at the apical side. (For secondary Antibody controls take a look at Supplemental Figure 6) Microscope: Zeiss LSM780, Objectives: Plan-Apochromat 20x/0.8. Ex/Em: Dapi 405/462; Piezo-1 488/55. Scale bar: 100  $\mu$ m



### 3.6.4. Organoid lumen maintenance is cytoskeleton dependent – tubulin and the actin-myosin-axis

The cellular mechanisms that are responsible for the generation and maintenance of the organoid's phenotype are not understood well. In the course of this work, it has already been shown that the organoid luminal liquid consists mainly out of water and that specific water channel proteins (AQP) are present in the cell membrane of the cells. In accordance with these observations, it has been shown that organoids have a polarized cytoskeleton. Thus, the hypothesis was made that the interplay between the generated internal pressure (due to water influx) and the polarized cytoskeleton components alongside with force generating proteins are responsible or at least support the organoid phenotypic structure. One well known force generating mechanism is the molecular machinery of Myosin 2. Furthermore, and due to its molecular structure, MTs provide mechanical support (Muroyama et al., 2017). Whether and how actin, MTs and myosin 2 are involved in the maintenance of the phenotypic structure were addressed below.

To confirm the hypothesis, human and mouse pancreas organoids were treated with different active ingredients that target the cytoskeletal components. The organoids reactions were imaged and analysed with the brightfield pipeline. All of the organoids were also imaged and measured 24 hours before the treatment (pre-treatment) to guarantee normal growth conditions. Because all of the presented measured organoids demonstrated the same growth behaviour before treatment, only the treatment and the recovery of the analysis is shown (for the pre-treatment curves take a look at: Supplemented Figure 7).

The results of the treatment and the recovery potential of mPOs (treatment for 24 hours followed by additional 24 hours of recovery) are shown in Figure 25 (A) and Movie 4. Because of the potential influence of DMSO (Figure 13), all tests and measurements refer to the DMSO control group (red line,  $n \approx 500$ ). All used drug concentrations were first evaluated by applying different concentrations to the organoid cultures and then the organoids' reaction was observed by eye (data not shown). Finally, the lowest concentration was chosen at which all organoids showed a reaction. Because the organoids are embedded in ECM droplets which presumably act as a physical or electro statical barrier all drugs in a relatively high concentration were used.

To destroy and inhibit dynamic maturation of the major cytoskeleton component actin, the inhibitor Cytochalasin D (10  $\mu\text{M}$ ) was used. The measurement of  $\approx 100$  treated murine organoids showed a significant reduction in the overall size of the organoids (black dotted line, Mann-Whitney  $P < 0.01$ ). Because none of them demonstrated any growth after the treatment, no recovery was measurable, and no recovery line is shown. Another major component in the cytoskeleton of cells is the heterodimer tubulin. It consists of alpha- and beta-tubulin that builds up the MTs. It is involved in many other essential dynamic processes like the cell division as well as the intracellular vesicle transport. For the inhibition of the dynamic assembly of the tubulin subunits Paclitaxel (100  $\mu\text{M}$ ) was used. By binding to the N-terminus it stabilizes the MTs and prevents dynamic assembly processes (Alqahtani et al., 2019). Paclitaxel showed a significant reduction in the organoid size but no differences in the recovery of the organoids (blue interrupted line, Mann-Whitney  $P < 0,5$ ,  $n: \approx 65$ ). To test whether the MTs are needed at all to maintain the luminal structure, Nocodazole was used (1  $\mu\text{M}$ ). It binds to the  $\beta$ -tubulin

subunit, and thus inhibits and disrupts the MTs. It is shown that the treatment leads to a significant reduction in the overall size of all analysed organoids and that none was able to recover after the treatment (purple dashed-interrupted line, (Mann-Whitney:  $p < 0,01$ ,  $n: \approx 15$ ). In contrast to actin and MT, the inhibition of the motor protein myosin 2, with the inhibitor Para-Nitro-Blebbistatin (in the following named Para-Blebbistatin,  $50 \mu\text{M}$ ) showed that the overall organoid size increased significantly (green dashed line, Mann-Whitney  $P < 0,001$ ,  $n: \approx 260$ ). No significant alteration to the DMSO control group was detected in the recovery phase, but a slightly lower growth was visible.

The above-mentioned results were obtained with mPOs. In course of this investigation, it was already shown that hPOs can react differently, are more sensitive and cannot be cultured as long as mPOs. Thus, the similar experimental setup for human pancreas organoids as it was carried out for mouse organoids was conducted (Figure 25). Similar to this experiment, all measurements are compared to the DMSO control group (red line,  $n: \approx 460$ ). The inhibition of actin with Cytochalasin D ( $10 \mu\text{M}$ ) led to a significant reduction of the overall size of the human organoids and no recovery (black dotted line, Mann-Whitney  $p < 0,001$ ,  $n: \approx 40$ ). The inhibition of the dynamic assembly of the  $\beta$ -tubulin subunits with Paclitaxel ( $100 \mu\text{M}$ ) showed a temporal significant reduction in the overall size of the organoids. This reduction became only visible within 30 and 40 hours of observation. After 40 hours no difference between the treated organoids and the DMSO-control group was detected and none were measured during the recovery phase (blue interrupted line, Mann-Whitney  $P < 0,001$ ,  $n: \approx 189$ ). The inhibition of the MTs with Nocodazole led to a significant reduction of the organoid sizes and no recovery was detectable (purple dashed-interrupted line, Mann-Whitney:  $p < 0,001$ ,  $n: \approx 120$ ). The inhibition of the motor protein myosin 2 Para-Blebbistatin ( $50 \mu\text{M}$ ) showed a significant increase of organoid size (green dashed line, Mann-Whitney  $P < 0,001$ ,  $n: \approx 115$ ) which was stronger than the reaction of mPOs.

In conclusion, it has been shown that actin, MTs as well as myosin play a significant role in maintaining the organoid phenotype in human as well as in murine organoids (in the following, only named "tubulin and the actin-myosin-axis"). Further it has been proven that the dynamic assembly and disassembly of MTs are important not only for the luminal appearance, but also for the survival of the organoids in general.

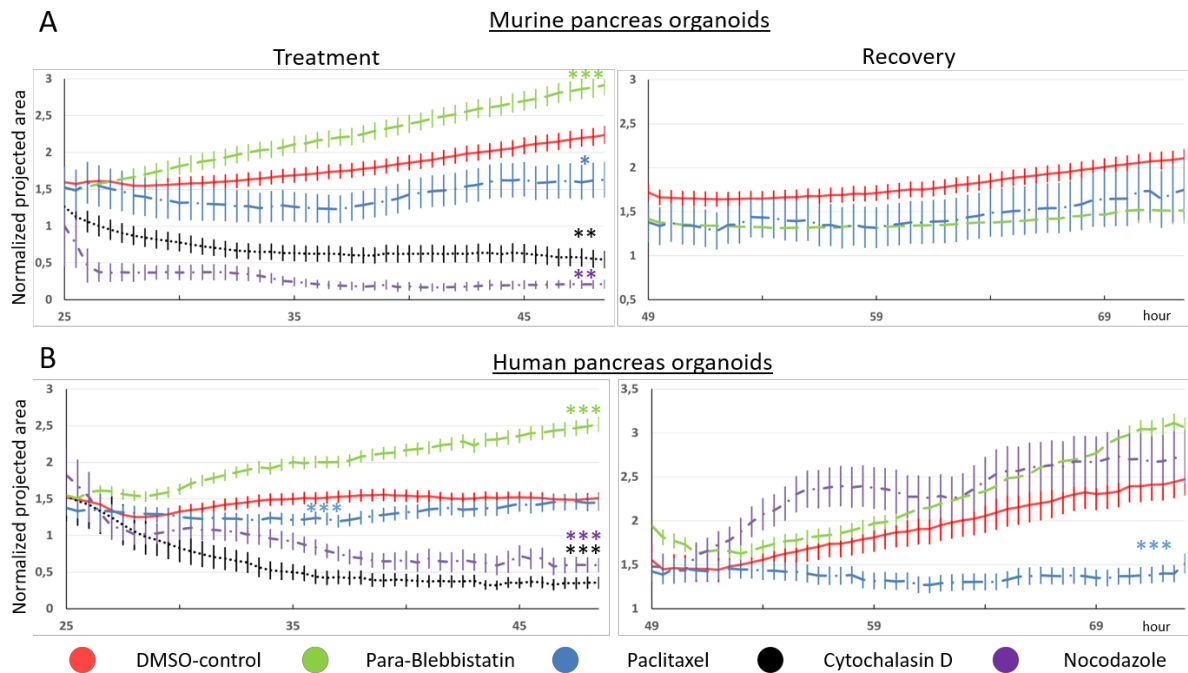


**Figure 25: Organoid lumen maintenance is dependent on tubulin and the actin-myosin-axis.** Illustrated is the treatment of murine and human organoids with different inhibitors and their recovery potential after the treatment. MPO and hPO behaviour was analysed with the brightfield pipeline in regard to their overall size over time of 24 hours during the treatment as well as 24 hours after the treatment with non-treated medium (recovery). All statistical evaluations were made in regard to the DMSO-control group (red line, mPO:  $n \sim 500$ , hPO:  $n \sim 460$ ). (A) MPOs size increase is MT- and actin-dependent which was indicated by a significant reduction in the size if the MT or actin was inhibited. No size recovery after the removal of the drugs was detected (Treatment: Nocodazole ( $1 \mu\text{M}$ ), purple dashed line ( $n \sim 15$ ), Cytochalasin D ( $10 \mu\text{M}$ ), black pointed line ( $n \sim 100$ ), Mann-Whitney  $p < 0,01$ , Recovery: no line is shown since no organoid has been recovered). The inhibition of the motor protein myosin 2 led to a significant increase but no significant alterations in the recovery of the organoids size compared to the control (Para-Blebbistatin ( $50 \mu\text{M}$ ) green interrupted line ( $n \sim 260$ ), Mann-Whitney  $p < 0,001$ ). The inhibition of the dynamic assembly and disassembly of the tubulin subunits led to a slightly reduced size and no significant alterations in the recovery phase of the organoids size (Paclitaxel ( $100 \mu\text{M}$ ) dashed blue line, Mann-Whitney  $p < 0,05$ ,  $n \sim 65$ ). (B) hPO size increase is MT and actin dependent which was indicated by a significant reduction in the size during the treatment with MT or actin inhibitors. Further, no size recovery was detected after the treatment was replaced with untreated medium (Treatment: Nocodazole ( $1 \mu\text{M}$ ) the purple dashed line ( $n \sim 120$ ), Cytochalasin D ( $10 \mu\text{M}$ ) the black pointed line ( $n \sim 40$ ), Mann-Whitney  $p < 0,001$ , Recovery: Nocodazole Mann-Whitney  $p > 0,001$ ). The inhibition of the motor protein myosin 2 led to a significant increase but no significant alteration in the recovery of the organoids size (Para-Blebbistatin ( $50 \mu\text{M}$ ) green interrupted line ( $n \sim 115$ ), Mann-Whitney  $p < 0,001$ ). The inhibition of the dynamic assembly and disassembly of the tubulin subunits led to a temporary and only slightly reduced size during treatment (t33-t42). In the recovery phase no growth of the organoids was detected which was a significant difference to the control group (Paclitaxel ( $10 \mu\text{M}$ ) dashed blue line, treatment: Mann-Whitney  $p < 0,05$ , recovery: Mann-Whitney  $p < 0,001$ ,  $n \sim 189$ ).

### 3.6.5. Pancreas organoids express the cystic fibrosis transmembrane conductance regulator CFTR and the mechanosensitive ion channel Piezo-1

One of the major tasks of epithelial cells in the mammalian body is to line and separate lumen or parts from each other. However, the phenotypic appearance of organoids in general, and of pancreas organoids in detail, as a monolayer, liquid filled luminal structure cannot be answered by its origin solely. Up to this point in this work, it was known that the luminal liquid is mainly water; that AQPs are present which can support the directed osmotic water flux into the lumen; that tubulin and the actin-myosin-axis are needed for to maintain the structure. However, the regulatory mechanisms which balance the interplay of all of these components are not known. In the following, this question was addressed.

One already known important protein in other organoid cultures is the Cystic Fibrosis Transmembrane conductance regulator (CFTR). Whether this channel is also expressed in pancreas organoids and if it is also able to modulate the luminal dynamics of the organoids has never been investigated.

In pancreas organoids, the liquid filled lumen seems to be necessary to maintain the organoid structure. Because of the apical polarized cytoskeleton component actin (Figure 9), the assumption can be made that the lumen generates a pressure which counteracts with the force that is generated by the cytoskeleton. Both forces are then in a steady interplay to ensure the luminal structure of the organoids. How this interplay is regulated, is completely unknown. On a cellular level and in the mammalian system the most common mechanosensitive protein is the ion channel Piezo-1. If this channel is expressed in pancreas organoids has never been observed.

The presence of CFTR and Piezo-1 in mouse and a human pancreas organoid were investigated by immunolabelling (Figure 26, A and B). Both candidates were identified in pancreas organoids, whereas CFTR was expressed cytosolic and in the nucleus with a tendency towards the apical/luminal side and Piezo-1 mainly in the cytosol. Moreover, Piezo-1 was not detectable within the nucleus. No clear differences between human and murine pancreas organoids were observed. Because both proteins did not show a clear polarisation, it was not ensured whether they are actively involved in the maintenance of the luminal phenotype. Therefore, mPOs cultured in the HD-system were stained against both proteins to see if the expression profile was changed: CFTR showed a clear polarisation on the basal side and only a weak overall cytosolic and nuclear expression, Piezo-1 showed a less cytosolic but a punctuated appearance at the apical side (Figure 26, C). This observation pointed towards a role of both proteins within the growth and maintain of the organoid phenotype. Moreover, it demonstrated that the absence of the ECM leads to direct cellular reactions which need to be further investigated.

In conclusion, it was shown that human and murine pancreas organoids expressed CFTR and Piezo-1. Furthermore, the expression patterns differ with the surrounding environment. Whether these channel-proteins are directly involved in the maintenance of the luminal character of pancreas organoids was not answered at this point. Nevertheless, the knowledge of the presence and the alteration of their expression in regard to the environment, demonstrates the need for further investigations.

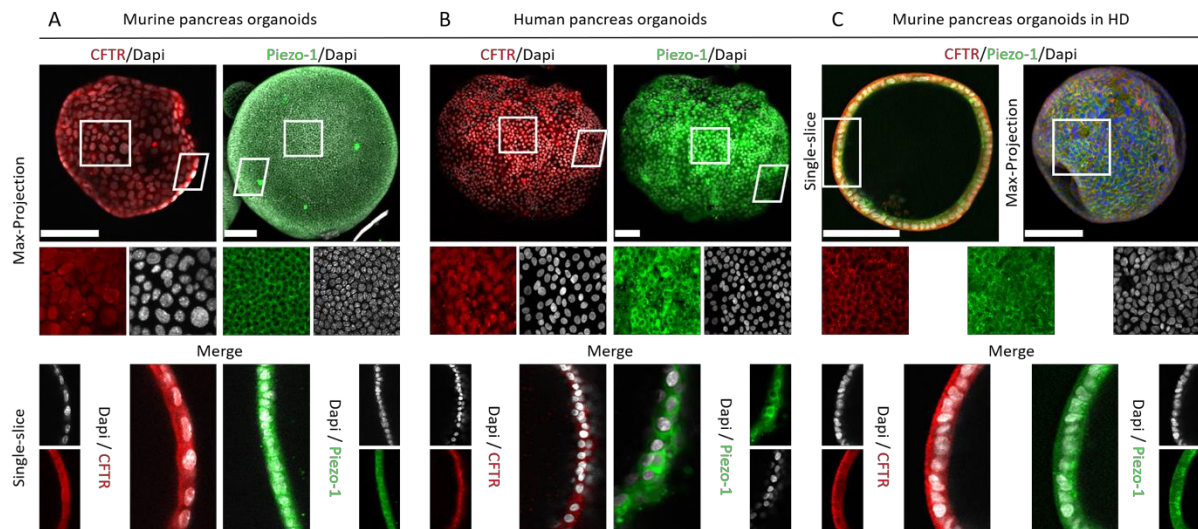


**Figure 26:** MPOs and hPOs express the cystic fibrosis transmembrane conductance regulator (CFTR) and the mechanosensitive ion channel Piezo-1. Mouse pancreas organoids grown in HD showed a basal polarisation of CFTR and apical expression of Piezo-1. In (A) mPOs were stained against CFTR and Piezo-1. CFTR was homogeneous expressed in the cytosol and nucleus with a tendency towards the apical/luminal side. Piezo-1 was expressed only in the cytosol and didn't show polarisation tendencies. In (B) hPOs were stained against CFTR and Piezo-1 and showed similar expression patterns like mPOs. In (C) mPOs grown in HD showed a homogeneous basal and no nucleus expression of CFTR. Further, Piezo-1 was punctuated polarised towards the apical side and less expressed in the cytosol in general. (For secondary Antibody controls take a look at Supplemental Figure 5) Tilted rectangles illustrate a close-up of a single slice, non-tilted rectangles a close-up of a Max-Projection. Microscope: Zeiss LSM780, Objectives: Plan-Apochromat 20x/0.8. Ex/Em: Dapi 405/462; Piezo-1 488/553; CFTR 561/633. Scale bar: 100  $\mu$ m

### 3.6.6. The cystic fibrosis transmembrane regulator plays a critical role in luminal dynamics of pancreas organoids

The luminal characteristic of pancreas organoids cannot be maintained by one monolayer of cells per se. Based on the results obtain so far in this study, the hypothesis was made that a steady interplay between the cell cytoskeleton alongside with the force generating proteins maintain the luminal hydrostatic pressure which enables the luminal structure. Furthermore, the presents of CFTR as a potential regulator of the luminal dynamics has been shown but the influence of it needs to be addressed.

To check the regulatory function of the CFTR channel, the brightfield pipeline was used. Therefore, MPOs were imaged and analysed while treated with different substances to test the influence of CFTR (Figure 27 B, Movie 4). The same setup as it is already described in Figure 27 (A) was used. The voltage independent inhibition with CFTRinh-172 (50  $\mu$ M) led to a slight increase in the overall size of the organoids (green interrupted line,  $n$ :  $\approx$ 250) whereas the inhibition with GlyH-101 (50  $\mu$ M) that blocks the channel in a voltage depend way demonstrated a significant reduction in the organoid size after 22 hours (blue interrupted line, Mann-Whitney  $p > 0,01$ ,  $n$ :  $\approx$  220). To guarantee a complete inhibition of the CFTR-channel (mechanical and voltage dependent) a combination of both inhibitors (50  $\mu$ M each) was analysed and showed a significant reduction in the overall size of the organoids (black dotted line,  $p > 0.01$ ,  $n \approx$  200). In all conditions, the organoids were able to recover from the treatment. The CFTRinh-172 treated organoids demonstrated a similar behaviour as the control group whereas the GlyH-101 treated organoids still showed a reduced overall size during the first 10 hours of recovery. The combination of both inhibitors showed the most prominent effect in

the recovery phase. It led to a significant reduction in size in the first 10 hours before the organoids start to increase again.

To investigate the reaction of hPOs upon CFTR inhibition, the same setup as described before was used (Figure 28, B). In strong contrast to the mPOs, the voltage independent inhibition with CFTRinh-172 (50  $\mu$ M) led to a significant increase in the overall size of the organoids (green interrupted line, Mann-Whitney:  $p > 0.01$ ,  $n \approx 210$ ). Comparable to mPOs, the inhibition with GlyH-101 (50  $\mu$ M) that blocks the channel in a voltage dependent way showed a significant reduction in organoid size after 22 hours (blue interrupted line, Mann-Whitney  $p > 0.01$ ,  $n \approx 160$ ). The combination of both inhibitors (50  $\mu$ M each) showed significant reduction in the overall size of the organoids (black dotted line,  $p > 0.01$ ,  $n \approx 170$ ). In all conditions, the organoids were able to recover from the treatment. The CFTRinh-172 and GlyH-101 treated organoids demonstrated similar behaviour as the control group whereas the organoids that were treated with both inhibitors simultaneously showed a significantly higher size increasing rate after 15 hours of recovery ( $p > 0.01$ ).

In conclusion, it was shown that the CFTR-channel is not only expressed in hPOs and mPOs, but also that it is able to regulate the luminal dynamics. Furthermore, the high impact of a voltage dependent inhibitor and the low reaction upon the mechanical inhibitor in mPOs demonstrated that the organoid luminal dynamic is highly dependent on the electro statical conditions of the organoid membrane. Whether this is the only regulatory unit of the luminal dynamic needs to be addressed.

### 3.6.7. The mechanical force translocator Piezo-1 plays a critical role in luminal dynamics of pancreas organoids

In the course of this work, the presence of the mechanosensitive channel Piezo-1 in pancreas organoids has already been shown. Due to the phenotypic appearance of the pancreas organoids as a hollow spherical like structure, it was hypothesised that Piezo-1 is in an activated state.

The same setup as used for the inhibition of CFTR was used to analyse the reaction of mPOs upon treatment with the Piezo-1 inhibitor GsMTx-4 (10  $\mu$ M) and the activator Yoda 1 (10  $\mu$ M and 50  $\mu$ M, Figure 27 C and Movie 4). The inhibition did not lead to any differences in the size of the organoids (green interrupted line,  $n \approx 240$ ). In contrast and depending on the concentration, the treatment with the activator Yoda 1 led to a significant reduction in organoid size (blue interrupted line (10  $\mu$ M), Mann-Whitney  $p > 0.05$ ,  $n \approx 100$ ; back dotted line (50  $\mu$ M), Mann-Whitney  $p > 0.001$ ,  $n \approx 50$ ). In all conditions, the organoids were able to recover from the treatment, whereas the treatment with 50  $\mu$ M Yoda 1 led to a slight delay of size increase in the recovery phase but reached the same values after 24 hours as the control group.

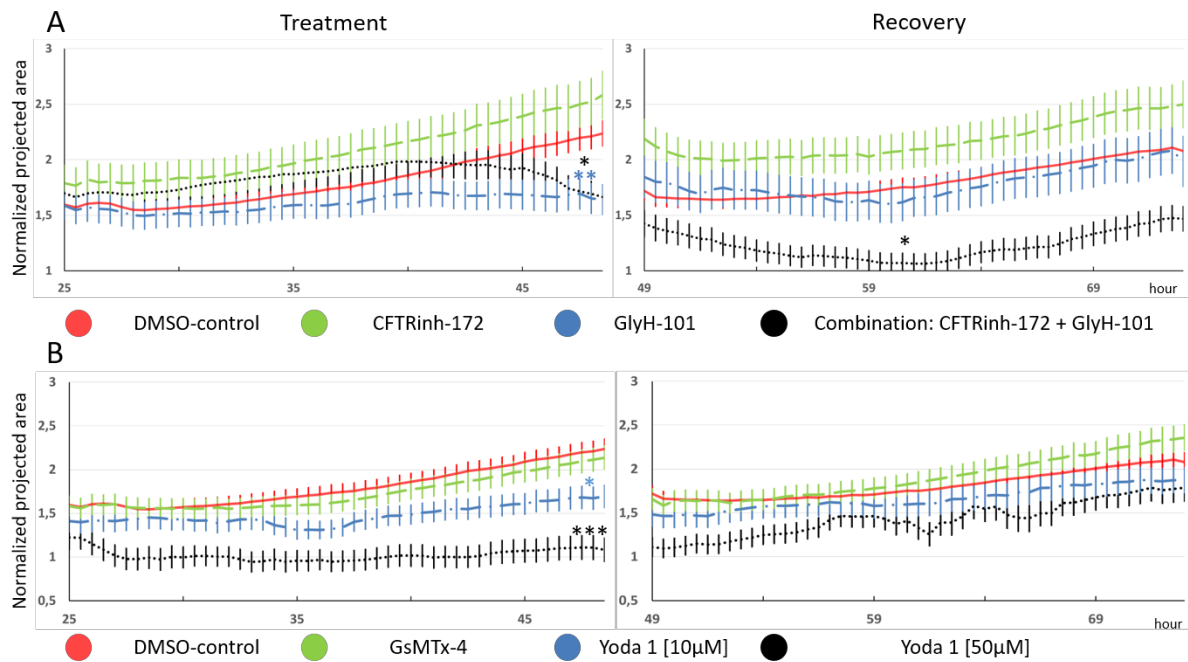


**Figure 27: The growth of mPOs is CFTR and Piezo-1 dependent.** The mPO behaviour was analysed with the brightfield pipeline in regard to their overall size over time of 24 hours during the treatment as well as 24 hours after the treatment and with non-treated medium (recovery). All statistical evaluations were made in regard to the DMSO-control group (red line,  $n \sim 500$ ). (A) mPOs that were treated with two CFTR-inhibitors. In green the influence of the CFTR-172 (50  $\mu\text{M}$ ), in blue of GlyH-101 and in black the influence of the combination of both inhibitors are shown. Only GlyH-101 and the combination of both inhibitors showed a reduction in the size of the organoids during the treatment. In addition, a significant reduction in the organoid size was detected in the recovery phase when both inhibitors were used in combination (CFTR-172: 50  $\mu\text{M}$  ( $n \sim 250$ ), GlyH-101: 50  $\mu\text{M}$  ( $n \sim 220$ ), Combination: 50  $\mu\text{M}$  CFTR-172 + 50  $\mu\text{M}$  GlyH-101 ( $n \sim 200$ ). Mann-Whitney; Treatment: Combination  $p > 0,05$ ; GlyH-101  $p > 0,01$ . Recovery: Combination  $p > 0,05$ ). (B) mPOs were investigated in regard to the influence of the mechanosensitive channel Piezo-1. To inhibit the channel GsMTx-4 (10  $\mu\text{M}$ , green line,  $n \sim 240$ ) and to activate Yoda 1 (blue line 10  $\mu\text{M}$  ( $n \sim 100$ ), black line 50  $\mu\text{M}$  ( $n \sim 50$ )) were used. Upon an inactivation of Piezo-1 no significant alteration in the organoid size was detected (green line) but the activation of the channel led to a significant size reduction compared to the control. Upon treatment removal, a complete recovery to the previous size of the organoids was detected (blue line, Mann-Whitney  $p > 0,05$ ; black line, Mann-Whitney  $p > 0,001$ ).

The results of the Piezo-1 experiment with mPOs already illustrate that the channel is present in an inactive form but can be activated which led to a reversible luminal shrinkage. To investigate this mechanism also in hPOs, the same setup was used (Figure 28, C). To inhibit Piezo-1 in hPOs the same concentration of GsMTx-4 was used (10  $\mu\text{M}$ ). In contrast to mPOs, it led to a significant increase of the organoid size (green interrupted line, Mann-Whitney  $p > 0.001$ ,  $n: \approx 345$ ). The opposite effect was observed when the hPOs were treated with the activator Yoda 1 (10  $\mu\text{M}$ ). It led to a significant reduction in organoid size which was temporally determined and started after 5 hours of treatment and ended after additional 10 hours (blue interrupted line (10  $\mu\text{M}$ ), Mann-Whitney  $p > 0,001$ ,  $n: \approx 110$ ). A higher concentration of Yoda 1 (25  $\mu\text{M}$ ) led to a significant reduction over the complete observed time of 24 hours (back dotted line, Mann-Whitney  $p > 0.001$ ,  $n: \approx 60$ ). In all conditions, the organoids were able to recover from the treatment. Depending on the concentration of Yoda 1 during the treatment phase and in contrast to mPOs, the organoids showed a significant increase of their overall size in the recovery phase. Organoids treated with 10  $\mu\text{M}$  Yoda 1 showed a triplication of their normalized projected area in the 24 hours of recovery. Moreover, organoids treated with 25  $\mu\text{M}$  Yoda 1 demonstrated an increase of their size of more than seven times when they recovered from the treatment (blue interrupted line (10  $\mu\text{M}$ ), Mann-Whitney  $p > 0,001$ ,  $n: \approx 110$ , back dotted line (50  $\mu\text{M}$ ), Mann-Whitney  $p > 0.001$ ,  $n: \approx 60$ ).

The results of the treatments of Piezo-1 in mPOs and hPOs showed that in mPOs the Piezo-1 channel is present in an inactive configuration and that upon activation the organoid lose its ability to maintain the luminal pressure. A different picture was generated for hPOs. Here the deactivation of Piezo-1 already led to a significant increase of the organoid volume, which illustrates that Piezo-1 was present in a partly active form. The additional activation upon treatment with Yoda 1 led to a significant decrease in the overall size of the organoids, but a significant compensatory mechanism in the recovery phase.

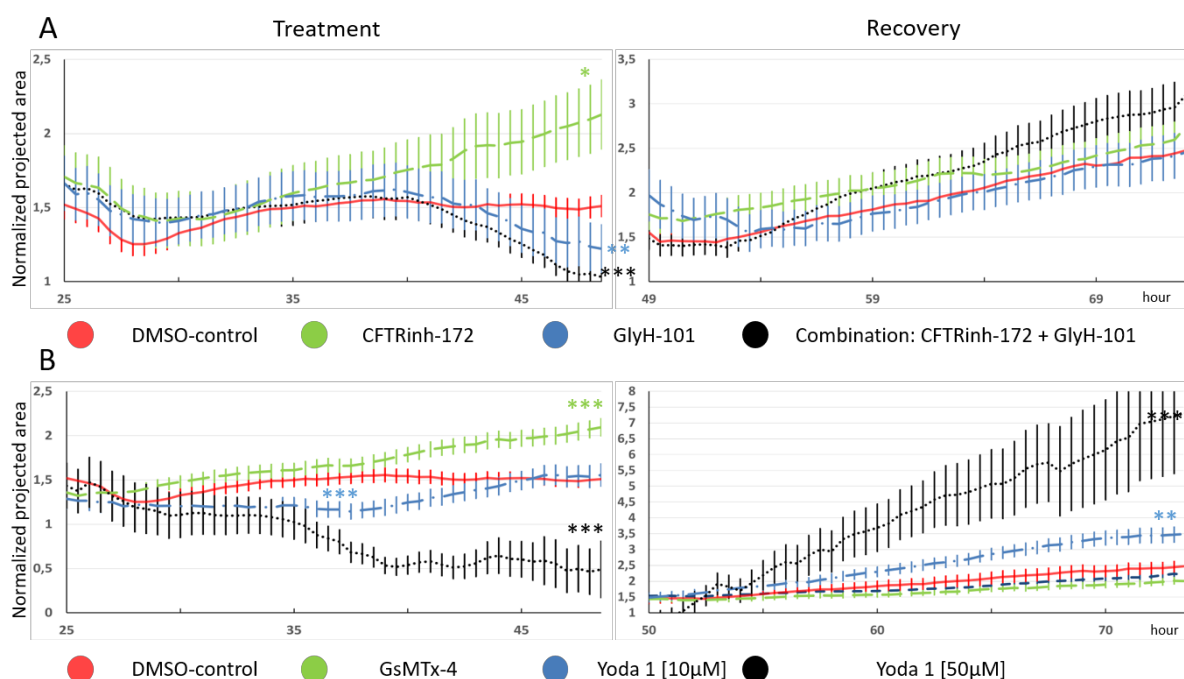


**Figure 28: The growth of hPOs is CFTR and Piezo-1 dependent.** The hPO behaviour was analysed with the brightfield pipeline in regard to their overall size over time of 24 hours during the treatment as well as 24 hours after the treatment and with non-treated medium (recovery). All statistical evaluations were made in regard to the DMSO-control group (red line,  $n \sim 500$ ). (A) hPOs that were treated with two CFTR-inhibitors. In green the influence of the CFTR-172 (50  $\mu\text{M}$ ), in blue of GlyH-101 and in black the influence of the combination of both inhibitors are shown. GlyH-101 and the combination of both inhibitors showed a reduction in the size of the organoids during the treatment whereas CFTR-172 enhanced the organoid size significantly. None of the treatments showed any influence on organoid size in the recovery phase. (CFTR-172: 50  $\mu\text{M}$  ( $n \sim 210$ ), Mann-Whitney:  $p > 0.05$ ; GlyH-101: 50  $\mu\text{M}$  ( $n \sim 160$ ), Mann-Whitney:  $p > 0.01$ ; Combination: 50  $\mu\text{M}$  CFTR-172 + 50  $\mu\text{M}$  GlyH-101 ( $n \sim 170$ ), Mann-Whitney:  $p > 0.001$ ). (B) hPOs were investigated in regard to the influence of the mechanosensitive channel Piezo-1. To inhibit the channel GsMTx-4 (10  $\mu\text{M}$ ,  $n \sim 345$ ) and to activate Yoda 1 (blue line 10  $\mu\text{M}$  ( $n \sim 110$ ), black line 25  $\mu\text{M}$  ( $n \sim 60$ )) were used. The inactivation of Piezo-1 led to a significant increase (green line) and the activation to a significant reduction (blue and black line) in the organoid size. The reduction in size upon Piezo-1 activation led to a significant size increase in the recovery phase (black line). No alteration in the size was detected in the recovery phase after the inhibition of Piezo-1. (Treatment: GsMTx-4 Mann-Whitney  $p > 0.001$ , Yoda 1 25  $\mu\text{M}$  Mann-Whitney  $p > 0.01$ ; Recovery: Yoda 1 10  $\mu\text{M}$  Mann-Whitney  $p > 0.01$ , Yoda 1 25  $\mu\text{M}$  Mann-Whitney  $p > 0.01$ );).

### 3.6.8. Piezo-1 activation leads to alteration in the phenotype of pancreas organoids

In the course of this work, we identified the cytoskeleton as a major player in maintenance of the luminal phenotype of pancreas organoids and that at least, CFTR and Piezo-1 are involved in this process. However, the activation of Piezo-1 showed a direct dynamic and reversible shrinkage of the organoid. These results illustrate that this mechanosensitive channel is able to actively modulate the luminal structure of pancreas organoids. However, its functionality needs to be addressed. Piezo-1 is a cation selective channel that regulates the influx of  $\text{Ca}^{2+}$ .



To measure the  $\text{Ca}^{2+}$  level in the cell cytoplasm, Fluo-8 AM was used. This fluorescent dye is cell-permeable and once it is in the cytoplasm the lipophilic blocking groups are cleaved by cellular esterase. This results in a negatively charged configuration of the dye which stays in the cell and shows only a low fluorescence signal. Upon calcium binding, the fluorescence signal increases significantly. In the cellular context a stronger fluorescence signal of Fluo8-AM can be detected upon an increase of the intracellular calcium level. MPOs which were loaded with Fluo-8 AM in normal conditions showed a low fluorescence signal. After the activation of Piezo-1 with 50  $\mu\text{M}$  Yoda 1, a strong fluorescence signal was detected and measured (Supplemental Figure 8). This result confirmed that Yoda 1 activates Piezo-1 and that this subsequently led to an increase of  $\text{Ca}^{2+}$  within the cell.

The activation of Piezo-1 led not only to an increase of the intracellular  $\text{Ca}^{2+}$  level, moreover a reversible shrinkage of the organoids was detected. Figure 29 shows representative fixed and immunolabeled human pancreas organoids after the treatment for 24 hours with the Piezo-1 activator Yoda 1 (25  $\mu\text{M}$ ). In (A) two slices of a drop of ECM that contains several organoids and stained with Dapi for cell nuclei (grey) and against actin (green) are shown. It becomes clear that none showed the classic phenotype of a hollow, luminal structure which is build-up of one layer of cells. Most of the organoids showed a dense structure that is defined by multiple lumen which were surrounded by multiple layers of cells. Moreover, the actin staining revealed that the organoids showed mainly a basal polarisation after the treatment. In contrast, apical polarisation at the regions of the lumen became visible as well.

The change from a mono-layered to a multi-layered epithelium can be associated with a change in the cell fate (Boj et al., 2015; Broutier et al., 2017). To determine the organoid cell fate upon Piezo-1 activation and to ensure that the shrinkage is only due to the  $\text{Ca}^{2+}$  influx, the expression of Sox9 and Yap was investigated. Figure 29 (B, left) shows a comparison of the Sox9 expression of non-treated (control) and treated organoids. In both conditions Sox9 was homogeneously expressed in all cell nuclei (close-ups) and did not show any differences in the expression pattern. Piezo-1 is directly associated with the mechanosensitive protein Yap. Whether an activation of Piezo-1 leads to an alteration in the expression pattern of Yap is not known. Figure 29 (B, right) compares the expression of Yap with and without the treatment with Yoda 1. It becomes clear that Yap was expressed in the nucleus as well as in the cytosol without a treatment. After the treatment with Yoda 1, the expression pattern differed. Yap was then exclusively expressed in the cytosol and no expression was detected in the nucleus (close-up). The differences in the Yap expression indicates that Yap1 might be transcriptionally active in the cells after Piezo-1 activation.

In summary, the treatment of Piezo-1 with the activator Yoda 1 led to an increase of  $\text{Ca}^{2+}$  within the cytoplasm of the organoid cells and subsequently to a shrinkage of the organoid which was associated with a re-localisation of the actin cytoskeleton and changes in the expression of Yap.

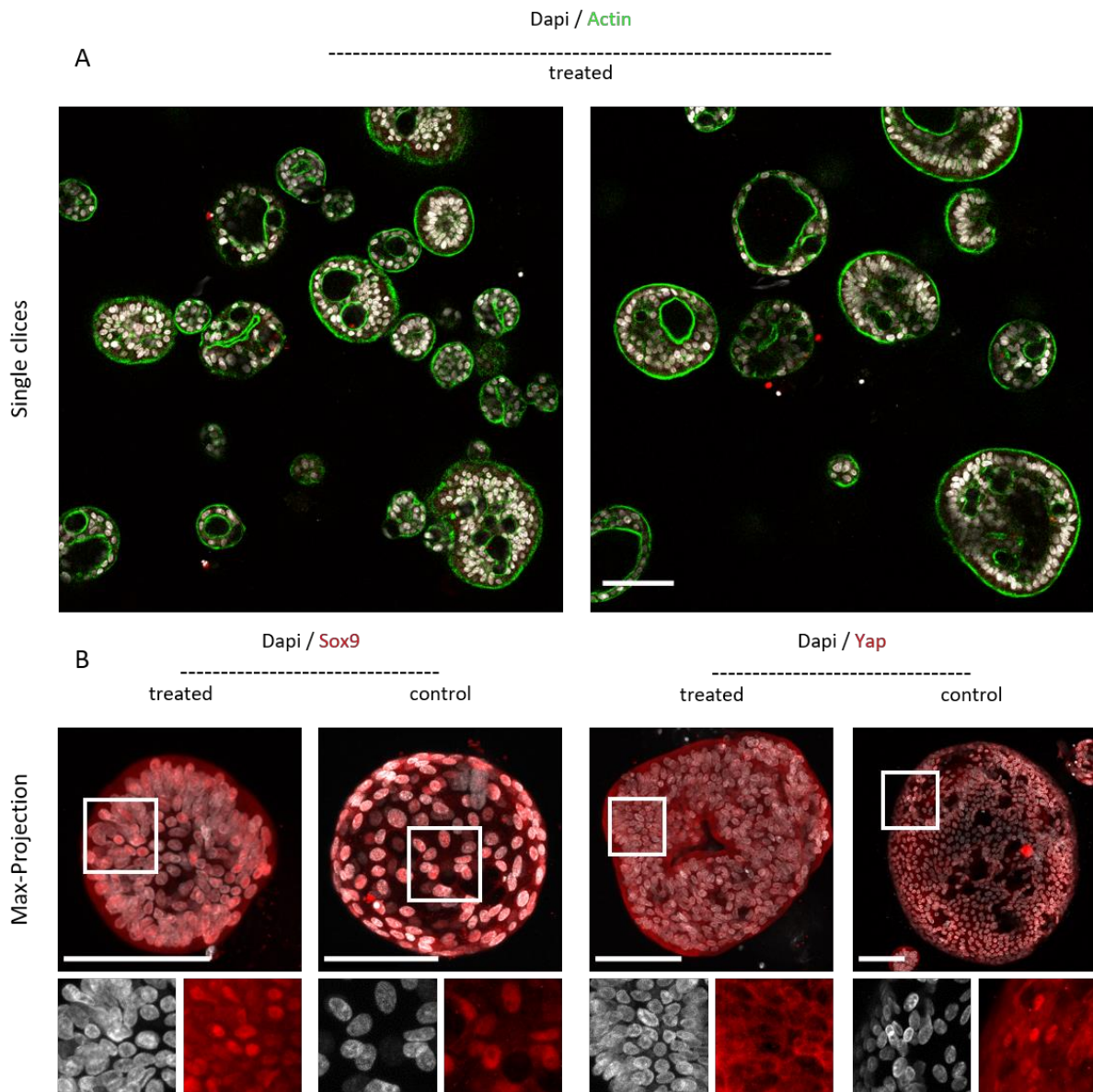


**Figure 29: The activation of Piezo-1 led to repolarisation of the cytoskeleton and alterations in Yap but no differences in the Sox9 expression.** (A) Two exemplary slices of a z-stack of human pancreas organoids grown in a droplet of ECM. Organoids were treated with 25  $\mu$ M Yoda 1 for 24h to activate the mechanosensitive cation channel Piezo-1 and stained against actin (green) and the nucleus (grey). The treatment led to several alterations in the phenotypic appearance of the organoids: organoids showed mainly a basal polarisation in comparison to the apical polarisation in normal conditions, the development of multiple instead of one lumen and a higher cell density that was manifested in multiple cell layers instead of a single cell layer. (B) one human organoid treated with 25  $\mu$ M Yoda 1 and stained against Sox9 (left) and Yap (right) and its untreated counterpart. The green rectangles show the position of the close-ups respectively. No clear alterations were observed in the expression of Sox9, but the expression of Yap shifted from the nucleus to the cytosol. Microscope: Zeiss LSM780, Objectives: Plan-Apochromat 20x/0.8. Ex/Em: Dapi 405/462; Yap/Sox9 488/553; Actin (Phalloidin) 647/747. Scale bar: 100  $\mu$ m

## 4. Discussion

### 4.1. Islets of Langerhans can be identified by their structure *in vivo* and used to validate antibodies

The pancreas unites two functions, the exocrine and the endocrine part. Both functions are essential, need to be tightly regulated, and are spatially separated within the organ. Besides the pancreas homogeneous structure, it was shown that the islets of Langerhans can be distinguished from the surrounding tissue by their separated roundish and compact appearance. To investigate islets *in vitro* and for medical approaches (e.g., Diabetes 1 treatment), they can also be separated from the surrounding tissue by a specific digestion protocol (D. S. Li et al., 2009). This Protocol results in various-sized isolated and living islets of Langerhans which can be further used. One major aspect in this process is that it leads to the digestion of the blood vessels within the islets which results in a lack of nutrition and oxygen supply within the core of the islets. Thus, the cell vitality and the general architecture of the islets is altered which results in cell death, generally lower survival rates and lower success rates in islets transplantation approaches (Ryan et al., 2001). However, basic information about the suitability of antibodies or functionality of the different cell types can be given by the use of isolated islets of Langerhans.

#### 4.1.1. Antibodies are a valid tool to characterize pancreas organoids

The need to validate IF's is often underestimated. The quality of immunofluorescence staining in 3D-cultures is highly dependent on several extrinsic factors like temperature and incubation time and intrinsic factors like antibody specificity and concentration. Furthermore, the density and general appearance in terms of cellular composition influence the diffusion kinetics of the antibody. This fact shows that it is highly important to validate the used antibodies prior using them in the target sample.

The antibodies used in this work were validated using isolated islets of Langerhans obtained from Nikola Dolezalova (University of Cambridge). Sox9 and Insulin were identified throughout the islets. Pdx 1, Ngn3 and Nkx 6.1 were identified but did not show a comparable clear signal like Sox9 and Insulin. Because Pdx 1 is mainly expressed in the first transition of the embryonic pancreas development, during the invagination and bud formation, the observed low expression pattern is not surprising and can be explained by the general postnatal pancreatic plasticity (Zhou et al., 2009; Y. Zhu et al., 2017). In the development of the islets of Langerhans, high Ngn3 expression can be observed when cells delaminate from the trunk epithelium (Gouzi et al., 2011). Although Ngn3 plays a critical role in all maturation processes of  $\beta$ -cells it is known to show fluctuations in its expression level. This observation can explain the low levels of detected expression in pancreas organoids. The expression of Nkx 6.1 can be found in the early development of pancreas and is later restricted to  $\beta$ -cells. However, different temporal expression levels within the  $\beta$ -cell maturation can lead to the observed low levels of expression in mature islets of Langerhans (Dassaye et al., 2016). In conclusion, all tested antibodies showed a positive signal in the isolated islets of Langerhans and were further used to validate the differentiation and stem cell state of pancreas organoids.

## 4.2. The culture and appearance of human and mouse pancreas organoids

In the last decade, personalized cell therapeutic approaches have garnered more attention because it could be shown that most of the human organs contain regions with cells that have stem cell characteristics and are able to rebuild the organ either partially or in its entirety. These cells can be cultured as organoids (M. A. Lancaster et al., 2019). In 2013 Huch and colleagues demonstrated that the pancreas contains ductal cells which are able to form organoids and recover Diabetes 1 in mice after the transplantation. To use these cells in therapeutic applications, significant basic research needs to be done to validate, identify and characterize organoids *in toto* (Broutier et al., 2016).

### 4.2.1. Mouse organoids are more suitable to be kept as long-term culture than human organoids

The general phenotype of pancreas organoids is similar in mouse and human organoids. Roundish, liquid-filled spheres are built by one layer of epithelial (ductal) cells within a matrix. This is the most observed phenotype. However, we observed some general differences. Human organoids usually need around 7 to 10 days to grow to their final size whereas mouse organoids usually reached their growth-plateau already after 7 days in culture. Interestingly, mouse organoids can be kept in culture longer (> 40 weeks) than human pancreas organoids (<20 weeks), (Referred from (Broutier et al., 2016)). Reasons for this observation are not clear yet. The embryonic development of a human pancreas is partly delayed in comparison to mouse. Further, it is known that the mouse pancreas has higher recovery rates after injury (Jennings et al., 2013, 2015). However, the results of this work point towards a general higher proliferation rate of mouse pancreas cells, but whether this is also the reason for the observed longer culture potential *ex vivo* needs to be clarified. Another major reason might be that the currently used medium composition misses some components or needs some concentration adjustments to keep the fate of the bi-potent stem cells for long term. One difference between the medium for human and mouse is the concentration of Wnt-agonist R-Spondin1. Because R-Spondin is produced in-house by 293-HA-Rspol-Fc-cell lines, the final concentration varies between batches. However, the final concentration in human organoid medium should be doubled in comparison to the mouse. As described in 2.3, human organoids were finally kept in a medium which was supplemented with recombinant R-spondin (1ng/ml) to avoid the mentioned fluctuations in the concentration. However, human organoids cannot be kept in culture for more than twelve passages. Next to R-spondin, the human pancreas organoid medium is supplemented with A83 which acts as a TGF- $\beta$  inhibitor and the cAMP activator Forskolin. Both substances are used to inhibit EMT-processes which is the main step in the first transition in the embryonic development of the pancreas. A closer look into the obtained datasets can lead to the assumption that organoids in late passages show denser than hollow, luminal structures. This phenotype could suggest to an EMT-like state and may be avoided by using higher concentration of the mentioned inhibitors.

In conclusion, it is not clear why human organoids show a less long-term culture potential in comparison to mouse organoids. However, adaptations in the corresponding media may increase the long-term culture potential.

#### 4.2.2. Pancreas organoids show high diversity in behaviour and appearance

Apart of the general growth differences in human and mouse organoids, the performed experiments demonstrate diverse behaviours and appearances in both species. In addition to the dense structure, frequent fusion events of two or more organoids were common. Fragment migration and complete organoid movement within the ECM was also detected.

The fact that not all organoids showed the same behaviour patterns can be partly explained by their origin. During the generation of pancreas organoids, pancreas ducts are picked, or complete pieces of pancreas are digested, and placed into the ECM. No purification or sorting step is performed (Broutier et al., 2016; M. A. Lancaster et al., 2019). Because only cells with proliferation potential are able to survive for long term, an additional sorting step is not needed. Dependent on the cell line, primary cell cultures are able to survive several weeks which means that organoids should be kept in culture long term to guarantee purity in terms of stem cell-ness. However, the cells that survive do not necessarily have the same age, status and differentiation state. As an example, the recorded organoids which demonstrated a high versatility had an elongated phenotype with a leading region. During the early embryonic pancreas development, in the tube formation, a tip and trunk region is present, which leads the development of the ductal tree. As discussed, in later developmental stages, cell clusters or single cells migrate from the epithelium towards the region of islets of Langerhans (Cole et al., 2009; Mastracci et al., 2012; Pan et al., 2014). The observed organoid behaviours may partly mimic these processes and illustrate different developmental stages of the cells that built up the organoid. To validate this hypothesis, single cell and next generation sequencing of the corresponding organoids can be used to identify the existence of variations in the differentiation status of the cells (Brazovskaja et al., 2019). The ECM as another major parameter in the growth and appearance of organoids needs to be considered. Because the ECM (Matrigel® or BME) is generated by the use of Engelbreth-Holm-Swarm (EHS) tumour cells it is not completely defined (Prestwich, 2007; Serban et al., 2008). It consists of multiple protein polymers which provide a physical scaffold and also interaction regions (epitopes). During the splitting procedure, organoids are placed in liquid ECM and transferred as a droplet into a well. By increasing the temperature from 0°C to 37°C the ECM polymerises. Because this polymerisation is a dynamic process and depends on many factors other than temperature (e.g., dilution, pH-level), variation in the stiffness or the distribution of cell-ECM-ligands can be expected (T. H. Barker, 2011; Doxey et al., 2010; Storm et al., 2005; Trepap et al., 2018). The influence of these variable factors has not been investigated so far and can be one possible reason for the high variations in the dynamic behaviour and also in the different phenotypes of organoids. Optimisations in the splitting and production procedure of organoids may lead to more robust behaviour patterns, and thus helping to identify factors which lead to the behaviour variations. To circumvent the general variability of the ECM compositions, fully defined synthetic hydrogels should be considered.

In summary, the high diversity in behaviour and appearance of pancreas organoids can be partly explained by intrinsic and extrinsic factors. Most likely, the combination of both leads to the mentioned variations. However, the results obtained in this work illustrate that the culture of organoids need additional research to understand its variability. Alongside this, the results push the need to a multiscale analysis to understand the core regulatory principles of organoid behaviour.

### 4.3. Characterizing pancreas organoids with immunofluorescence labelling – reasons for the observed expression of Ngn3, Nkx 6.1 and Yap

Despite the high heterogeneity in the behaviour and appearance, mPOs and hPOs can be characterized by the use of fluorescence markers. The conducted experiments revealed that the organoids showed polarisation patterns of ZO-1 and actin and defined expression regions of ezrin,  $\beta$ -catenin and E-Cadherin which point towards a high level of cytoskeleton and cellular organisation. The homogeneous expression of Sox9 in all cells showed that they were in a bi-potent ductal fate which was further confirmed by the expression of Pdx 1 in hPOs. It remains unclear why a detection of Pdx 1 was not possible in mPOs. In any case, Pdx 1 is only expressed in early embryonic developmental stages of the pancreas which might be an explanation for the low or no expression in the AS cell derived mPOs and hPOs. Recent publications support this explanation by showing that the expression of Pdx 1 in general is low in mPOs and hPOs (Andrei et al., 2020).

#### 4.3.1. Mouse pancreas organoids show Neurogenin 3 and Nkx 6.1 expression

The conducted experiments revealed that Ngn3 and Nkx 6.1 were not detected in human organoids. It confirmed that the cells didn't show a tendency towards  $\beta$ -cell differentiation, and thus illustrating their AS cell fate (Gradwohl et al., 2000). In contrast to the hPOs, Ngn 3 and Nkx 6.1 were detected in some but not all cells of mPOs.

These observations can be explained in two ways; First, Rukstalis and Habener demonstrated that the expression of Ngn3 in the organogenesis of the murine pancreas show successive waves with peaks in the first and second transition. These peaks were associated with a downregulation of E-Cadherin and upregulation of EMT-like cytoskeletal rearrangement processes (Rukstalis et al., 2009). The observed upregulation of Ngn 3 in mPOs can point in a similar direction where the cells start to differentiate towards an unknown direction. Second, In the mouse pancreas, the Wnt signal is strongly upregulated upon pancreas injury. This upregulation is involved in transdifferentiation processes and leads to the proliferation activity of the former quiescent adult stem cells. This healing mechanism is used in the mPO culture by applying R-spondin into the growth medium which activates the Wnt-signalling, and thus keep the cells in a proliferative state. *In vivo* studies demonstrated that the upregulation of these proliferation and remodelling processes upon injury are associated with a higher Ngn3 expression. (Huch, Bonfanti, et al., 2013; Rukstalis et al., 2009). Whether this Ngn3 upregulation is also present in the mPOs *in vitro*, has never been investigated but is highly likely.

Next to Ngn 3, some mPO cells showed also Nkx 6.1 expression. In the process of  $\beta$ -cell differentiation Nkx 6.1 is one key regulator. However, it is known that it is already expressed in the early development (first transition) of the pancreatic bud (Cerf et al., 2005). The mPOs that were used in this work were derived from the ducts of the pancreas. By the use of specific growth factors and an ECM, the biochemical and biophysical circumstances mimic the stem cell niche which leads to the proliferation activity of the AD cells and subsequently to organoid growth. However, the given circumstances of the organoid culture may partly mimic also the

circumstances in the embryonic development, and thus be responsible for the observed Nkx 6.1 expression.

#### 4.3.2. Mouse and human pancreas organoids show variations in Yap expression – possible link to ECM interaction

Immunofluorescent labelling revealed the expression of Yap in mPOs and hPOs. Furthermore, fluctuations in the expression patterns were observed. It was expressed only in the nucleus, combined in the cytosol and the nucleus and in the cytosol solely. However, the observed expression of Yap can be used as a quality control for stem cells and further confirms the AS cell characteristic of the organoids (Lian et al., 2010). Besides this, yap expression is also linked to the physical milieu that circumvent the cells.

##### Box 1: Yap association to the physical milieu

Yap and its transcriptional coactivator Taz respond directly to the physical milieu surrounding the cell either by sensing changes in cell-cell contacts (“canonical signalling”) or by cell-ECM interaction differences, namely the rigidity of the ECM (“non-canonical signalling”). The canonical signalling is based on MST and LATS, the two kinases of the mammalian Hippo pathway. They are known to interact with membrane receptors (G protein-coupled (GPCR and LIF receptors)), the protein complexes tight and adherent junctions and the cell adhesion molecule (CAM) E-cadherin (see review Low et al., 2014). Since LATS binds Yap/Taz within the cytosol, LATS deactivation leads to nucleus translation and a subsequent activation of Yap/Taz. The non-canonical pathway does not necessarily involve MST and LATS but act directly on Yap/Taz. How the cells sense changes in the geometry and in their environment is not fully understood, but raising evidences show that the actin-myosin and their corresponding tensile forces can directly regulate the translocation of Yap/Taz from the nucleus into the cytosol. On the one hand it can be regulated by RhoA after GPCR or focal adhesion activation via Yap phosphorylation from a jet unknown serine kinase. On the other hand, a non-kinase pathway via the Amot protein which is driven by the actin-myosin tensile forces has been indentified to regulate the Yap translocation. Furthermore, the regulation via junction proteins such  $\alpha$ - and  $\beta$ -catenin and Zona Occludens proteins (ZO-2) have been shown (Dupont et al., 2011; Thomasy et al., 2013). Reviewed in: (Low et al., 2014).

The link between Yap and the circumventing physical milieu (see Box 1) and the variability in the expression patterns of Yap along both organoid species rises some questions. Theoretically and based on the organoid phenotype as a monolayered spherical shaped sphere, all cells of the organoid expert the same signals from their neighbouring cells and the same impact from the ECM. Practically, several factors can vary. The rigidity of the ECM is dependent on its composition, which means that it can vary within the droplet containing the organoids due to the dilution during the mixing of the organoid cell fragments with the ECM. Further, multiple organoids grow in one droplet which can lead to deformation within the surrounding of the organoids. These possibilities can partly explain the different expression patterns of Yap. In addition, one important factor is the modulation ability of the organoids itself. Because cells can release enzymes like metalloproteases, they can modulate their surroundings, and thus changing physical parameters like the rigidity (Turunen et al., 2017). In recent publications, it was shown that liver organoids stiffness-sensitivity is highly Yap dependent but in contrast to

intestine organoids independent of acto-myosin contractility. Moreover, they demonstrated that a shift in the matrix stiffness leads to a shift to a progenitor phenotype, illustrated by a compromised proliferative activity (Gjorevski et al., 2016; Vinet et al., 2019). The results of these investigations show that no general statement can be given to explain the observed expression patterns. A conceptual analysis of the interaction between the ECM and the organoid cells which include investigations regarding the cell differentiation status need to be performed to shed light on the observed Yap expression differences.

In summary, the experiments illustrate that the human and mouse pancreas organoids can be characterized by the use of immunofluorescence. Nevertheless, fluctuations in the expression of differentiation and stem cell markers need to be addressed and clarified to validate the organoid stem cell character. Additionally, the results show the need to address the phenotype of the organoids on multiple scales to include all modalities and aspects which may influence the organoid appearance.

#### 4.4. Multiscale analysis of Organoid growth and behaviour by using light sheet and brightfield microscopy – Part I: the high-throughput pipeline

In order to understand both the nature of organoids as well as the heterogeneity and behaviour in detail, high numbers of organoids need to be analysed. For this reason, one main part of this work was to develop and establish analysis and processing pipelines to record and measure organoids under physiological conditions on multiple scales (macro-, meso-, microscale, Figure 30). An important consideration is that organoids should be observed and studied under the same conditions in which they are cultured (multi-well plates and physiological conditions). A high-throughput processing pipeline fitting these criteria was developed by the master's student Julia Tarnick under the supervision of Lotta Hof and me and finalized with the help of Tim Liebisch, a cooperation partner from Frankfurt Institute for Advanced Studies (FIAS, working group Franziska Matthäus).

In brief, a classic brightfield microscope (Zeiss Cell Observer) was used to record the droplets of ECM containing the organoids via image tiling and z-stack recording. After the image acquisition, one image per time point was processed over all tiles and all z-stacks. The result is one picture per time point which was then segmented in regard to the surface area of the equatorial plate of each organoid. The term *organoid size changes* therefore describes the change of the surface area of the organoid per measured time point. For feature extraction a Python script was used that process the obtained data sets. For detailed description see Hof et al., 2020.

In this work, the pipeline was used to investigate and define pancreas organoid growth in general and their size changes upon drug treatment. Although the system produced reliable results, there were still some disadvantages related to the segmentation efficiency and robustness. As mentioned, the organoids were imaged as tile scans and in z-stacks. In the first processing step, the z-stacks per time point were projected to one single image plane per time point. This processing step can lead to the overlapping of multiple organoids which subsequently leads to mis-segmentations. Although it is possible to correct these mistakes by



hand, it is highly time-consuming. The seeding of the organoids within a thinner droplet of Matrigel® can reduce this issue, because it reduces the overlapping of organoids in z-direction. Another disadvantage is the process of the medium change. It needs to be conducted under a sterile hood to avoid contaminations. Therefore, the plate was taken out of the microscope and after the medium change placed back into it. This process was always accompanied by a shift in the acquired images and often led to the need for a new adjustment of the tiles and stacks. To avoid this issue or at least reduce it, the medium amount per well can be increased to the maximum volume of the well (e.g., 48 well plate: from 250 µl to 1ml), and in this way avoiding regular medium exchange processes. If this leads to different growth behaviour of the organoids due to the accommodation of waste products, changes in the pH-value or due to inactivity of the medium supplements (e.g., FGF 10, EGF has a limited time of activity at 37°C) needs to be tested.

The used Fiji/ImageJ plugin was developed to detect either hollow spheres or compact structures which led to poor segmentation results if organoids changed their appearance from hollow to compact during acquisition. There is no direct option to circumvent this issue, but the steady decrease of the number of segmented organoids within a measurement interval can be interpreted as compacting of the organoids and therefore also as a result of a treatment as well.

#### 4.4.1. mPOs and hPOs show different growth behaviour – mPOs need less time to reach their final overall volume

The general growth of pancreas organoids is characterized by two steps: (1) the formation process which takes around one to twelve hours and leads to the establishment of a luminal structure; and (2) an overall increase of the volume accompanied by cell proliferation. Because the high-throughput pipeline is only able to segment the hollow structures of the already formed organoids, all analyses were made after a 12h formation phase to ensure the measurement of as many organoids as possible. Therefore, differences in the formation speed or formation behaviour were not addressed in this investigation.

The growth analysis of mPOs revealed that the overall volume of all measured organoids within a culture rapidly increased within the first 24 hours followed by a less strong increase in the following three days. The differences between mPOs and hPOs was significant since hPOs showed an overall higher constant volume increase over all 6 days in culture. Interestingly, the volume increase of the mPOs was higher in the first day in comparison to the hPOs. This observation led to the conclusion that mPOs reach their final volume much faster than the hPOs and then remain within a certain volume range and possibly enter a dormant stage. Whether this dormant stage is characterized only by keeping a constant organoid volume or also accompanied by a resting of cell proliferation cannot be answered with the conducted analysis. One possible theory is that the cells do not stop proliferating but the stop of volume increase leads to a more densely packed monolayer of cells. Because no investigation has been performed on that topic so far, this question remains open. In contrast to mPOs, the hPOs showed a more homogeneous rate of growth over all analysed days. Whether it is accompanied with a lower proliferation rate in comparison to mPOs needs to be addressed in future investigations.

#### 4.4.2. hPOs are highly DMSO sensitive

The use of organic solvents like DMSO for drug treatment approaches is widely accepted. However, it is also known that even in low concentrations DMSO is toxic to several cell lines (Brayton, 1986; Galvao et al., 2014; Pal et al., 2012). Therefore, a control measurement with 1 % (vol/vol) of DMSO within the growth medium was performed to investigate the influence of the solvent to the growth behaviour of mPOs and hPOs. Some of the components of the human organoid medium are already solved in DMSO (Forskolin, PGE2). The use of drugs solved in DMSO increases the overall DMSO concentration further. Therefore, influence of this compound needs to be clarified to interpret the obtained results in a right way. The experiments with mPOs treated with DMSO did not show a significant reduction of the growth of the organoids. In contrast, hPOs showed a significant reduction in growth when treated with 1 % (vol/vol) DMSO. Upon DMSO removal the volume increase was slightly higher compared to the control group without DMSO. This result shows that all investigations with drugs that are solved in DMSO need to be validated to the DMSO control group to gain robust and reliable data. Furthermore, the influence of the tested drugs always needs to be discussed in regard to the overall influence of DMSO to the growth hPOs. For that reason and to compare the results from mPO to hPO treatments, all experiments were made and interpreted relative to the DMSO control group. Additionally, the overall DMSO concentration was always lower than 1 % (vol/vol) in all conducted experiments.

Taking the results of the general growth observation and the DMSO treatment into account, it should be determined if and how the hPOs are influenced by DMSO which is present within the growth medium. As previously discussed, hPOs demonstrated a lower but more homogeneous volume increase over all days of growth in comparison to the mPOs. A possible reason for this observation could be the general higher concentration of DMSO in the growth medium. An overall reduction of DMSO within the culture by higher concentrations and multiple dilution steps of the corresponding medium supplements offers a solution to minimize the DMSO concentration. To investigate whether the lower DMSO concentration is accompanied with higher volume increasing rates, the brightfield pipeline can be used.

In conclusion, the high-throughput pipeline facilitates the record and analysis of multiple droplets containing hundreds of organoids in physiological conditions, and thus enables the extraction of general growth features and allows the analysis of the influence of drugs or other external stimuli. Furthermore, it reveals that mPOs and hPOs differ in their general growth behaviour, which is of major importance in future medical applications. In addition, it emphasises the need to investigate organoids not only on a macroscale but also on the level of the individual organoid (mesoscale) and on their single cells (microscale) to identify the reasons for the observed heterogeneity.

#### 4.5. Multiscale analysis of Organoid growth and behaviour by using light sheet and brightfield microscopy – Part II: the light sheet pipeline

The brightfield pipeline allows the observation and quantification of hundreds of organoids in terms of volume fluctuations on a macroscale (whole culture). However, to observe organoids on a microscale (single cell) and mesoscale (single organoid) level, another system is needed.

The most suitable microscope for this application is the light sheet microscope. It combines high temporal and spatial resolution with low phototoxicity and rapid image acquisition. It is therefore ideal for the observation of pancreas organoids in physiological conditions.

#### 4.5.1. The ultra-thin FEP-foil foil cuvette – adapted for the use in the Lightsheet microscope Z.1

The sample mounting in light sheet microscopy differs from the brightfield microscope. In order to enable the imaging of organoids, colleagues and I adapted a sample holder (Hötte et al., 2019) for the use in the mDSML to the use in the Zeiss Lightsheet Z.1. With this technique, the imaging and analysis of organoids in high temporal and spatial resolution is possible and allows the mesoscopic analysis as well the microscopic observation of organoids in controlled physiological conditions. Furthermore, the FEP-foil cuvette generates a closed and small chamber within the chamber of the microscope. Because the microscope itself is not sterile and the chamber is opened from the top the small chamber reduced the contamination risk. In addition, it is not necessary to fill the complete microscope chamber with the organoid growth medium but only the FEP-foil cuvette. This reduces the amount of medium from more than 20ml to approximated 500  $\mu$ l which significantly lowers the costs and enables the adoptability to industry and clinical research approaches. For additional information about handling and production of the FEP-foil cuvette please refer to Hof et al., 2020.

Generally, the FEP-foil cuvette is perfectly suitable to image organoids. However, some problems occurred during the use of the FEP-foil cuvette in the Z.1. First, the shrinkage tube which connects the FEP- foil cuvette with the glass capillary was not always completely tight. The leakage of medium from the cuvette to the chamber and *vice versa* can influence the growth of the organoids. To circumvent this, Parafilm can be wrapped around the connections before inserting the FEP- foil cuvette with the sample holder into the microscope. Second, the general leakage of the Z.1 microscope chamber is one major drawback. Ideally, all connections of the chamber are tight and the only way to lose liquid is by evaporation. In practice, the incubation system needs to be connected to the microscope chamber and the chamber itself is equipped with three windows for illumination and detection (Figure 12 A). The installation of all of these components is accompanied with a high risk of leakage. This problem is inherent in the setup and cannot be optimized. The risk of leakages can only be reduced by the careful handling of the mentioned parts and careful cleaning after each run. Furthermore, attention should be kept on the rubber parts that seal all connections (windows, illumination objective). With increasing age, usage, and cleaning cycles, they can partially lose their flexibility and lead to increasing the risk of leakage. A regular exchange of these parts can minimize this problem.

#### 4.5.2. Comparing the light sheet pipeline to other microscope systems

With a 30 minute recording interval, dynamic processes (e.g., budding or cell rearrangement, see (Serra et al., 2019)) can be temporally resolved and the acquired amount of data is suitable for long-term observations (e.g., to study cell differentiation, see Fatehullah et al., 2016; M. A. Lancaster et al., 2013). In organoid research, the observation of hundreds of organoids over long term periods in high temporal and spatial resolution has not been achieved so far. For example, in previous studies, organoids were monitored using a confocal microscopes in a z-range of 60  $\mu$ m in three to four minute intervals to study chromosomal segregation errors

(Bolhaqueiro et al., 2019). The developed FEP-foil cuvette allowed the observation, segmentation and tracking of single mitotic events (see Movie 5-11) in a high resolution as well. From the initial seeding to the growth plateau-phase and subsequent degeneration, the mitotic events of organoids can be imaged. This technique increases the throughput, allows the observation of larger organoids, and captures the organoid behaviour on a single cell level. The observation of developing organoids from a single cell level by using a LSM has been already achieved by (Serra et al., 2019). By image parallelisation they were able to image the development of multiple organoids separately. The developed light sheet pipeline does not need image parallelisation, and thus enables the observation of organoids in their environment as a culture (macroscale). In general, the analysis of mPOs revealed their high heterogeneity in growth patterns which matches observations in single intestine organoids. In particular, organoids form asymmetric structures and showed variable size and irregularly occurring rupture events (Mahe et al., 2013; Schlaermann et al., 2016; Schwank et al., 2013; Sebrell et al., 2018). As described, organoids can develop from single cells or cell clusters. Organoids grown from single cells display lower organoid formation efficiency which hampers the systematic analysis of cellular behaviour (Serra et al., 2019). In contrast, organoids grown from a cell cluster show higher survival rate. This leads to a higher multiplication-rate of cell material which can ensure the production of large amounts of material for a potential clinical application (Dossena et al., 2020). One drawback in starting from cell clusters is that both the heterogeneity of the culture and its dynamics increase. The light sheet pipeline captures this problematic as well. It supports the understanding of clonal formation as well as cell cluster formation and can help to generate quality control parameters for clinical applications as personalized cell therapy.

#### 4.6. Long-term imaging of pancreas organoids reveals high intercultural heterogeneity in growth behaviour

The experiments conducted in this work demonstrated that it is possible to culture pancreas organoids within the FEP- foil cuvette for multiple days. It enables the monitoring of dynamic processes at high temporal and spatial resolution for hundreds of organoids in one Z1-FEP-foil cuvette simultaneously (in Movie 5, a total volume of 5 mm<sup>3</sup> with a spatial resolution of 2 µm z-spacing and 1000 recorded z-planes is demonstrated).

#### 4.7. Organoids showed different sized cell nuclei – a classification

To use organoids in the clinic, they need to be completely characterized. The observation of different sized cell nuclei within a culture raises many questions about cellular identity. Moreover, single organoids were detected that consist of cells with either small nuclei or a heterogeneous distribution of big and small nuclei. This heterogeneity needs to be addressed to ensure that the organoids do not contain any already differentiated or mutated cells. On one hand, correlations between nuclear morphology and certain disease states have known for a while and many cancers are diagnosed based on increased nuclear size (Jevtić et al., 2014). On the other hand, nuclei size alterations are common during mitosis, development and cell differentiation processes and don't point towards diseases (Chow et al., 2012). Recently an investigation by our collaborators demonstrated that the pancreas organoids used in this study contain at least two populations of cells (Information obtained from cooperation partners Lorenza Lazzari and Matrixel Huch, manuscripts in review and in preparation). By

using flow cytometry and real time PCR, the studies demonstrated that ductal cells account for the majority of the culture but that acinar precursor cells were present as well. These two results provide a possible explanation for the observed heterogeneity within the organoid culture. A combination of the light sheet-based pipeline with single cell sequencing would be suitable to connect the cell nucleus size to the cell transcriptome and genome and thereby close the gap between molecular analysis and microscopic observations. The results can help to identify different cell types within one culture and connect it to its behaviour. With this technique the organoids can be defined in more detail and advance testing the suitability of pancreas organoids in clinical application approaches.

#### 4.7.1. Identifying dynamic organoid behaviours – fragment migration

In addition to the general cellular heterogeneity of the pancreas organoid systems, we also identified highly dynamic organoid behaviour. While the brightfield pipeline enables a general overview, the light sheet-based pipeline enables a detailed view on the organoid behaviour. The rendering and tracking of cell fragments revealed that they migrate with an average speed of 10  $\mu\text{m}/\text{hour}$  and a maximum speed of 23  $\mu\text{m}/\text{hour}$ . In 2D cell culture, fibroblasts are able to migrate with an average speed of 60  $\mu\text{m}/\text{hour}$  whereas in 3D cell culture no statement can be made because the migration speed is highly dependent on the topology of the surrounding ECM. (Trepats et al., 2012; Yamada et al., 2019; J. Zhu et al., 2016). Furthermore, 3D cell migration is far less understood due to the complexity of migratory behaviour. Cell migration can be separated in mesenchymal, amoeboid and lobopodial. In all three mechanisms, different levels of actin in connection with focal adhesions (constructed by integrin clusters) are the major components (Yamada et al., 2019). The data presented in this work demonstrates that the FEP-foil cuvette with the light sheet pipeline in combination with inhibition studies (e.g., inhibition of integrins) using the brightfield pipeline can be used to investigate 3D organoid migration in detail and shed light on the underlying mechanisms. The use of this technique may establish which of the possible mechanisms is responsible for the migration of organoid fragments.

#### 4.7.2. Identifying dynamic organoid behaviours – fusion of organoids

The fusion of two or more organoids is also an example of dynamic behaviour. This process has never been described in 3D in a compatible temporal and spatial resolution. Interestingly, this process shows similarities to several mammalian embryonic development and organ maintenance processes (Kim et al., 2015, Bruens et al., 2017). Kim and colleagues analysed the fusion of the palatal shelves during craniofacial development. They identified three stages for the fusion of the tissue: first, it is initialised by the convergence of the two epithelial layers; second, the cells migrate towards one epithelial layer; third, a subsequent rupture occurs of the single cell layer between the two layers. Dumortier et al. investigated the formation of the blastocoel during mouse pre-implantation. They identified multiple, highly dynamic processes of cell-cell rupture and fusion events which finally lead to a large lumen (Dumortier et al., 2019). As one result, they predicted that hydraulic fracturing of the cell-cell contacts guides the cell-cell rupture processes. These two processes are highly similar to the observations in this study. This suggests that the fusion of organoids can be used for wide-ranging research applications to gain more insight into the process of cell layer rearrangement, fusion and tissue formation. In conclusion, the observation of size oscillation, fusion and reorganisation

processes of organoids in a high temporal and spatial resolution offer a promising *ex vivo* model to investigate highly dynamic events in mammalian developmental processes.

#### 4.7.3. Identifying dynamic organoid behaviours – rotation of organoids

An overall rotation of the organoids was also identified. It was shown that the rotation speed and the rotation direction can differ within the culture and within the organoids themselves and that not all organoids demonstrate rotational behaviour. Histologically, organoid rotation has not been thoroughly investigated directly, but comparable mechanisms have been described in other 3D cell culture systems. In gastric epithelial organoids, Sebrell and colleagues related the rotation to the passage number and the patient/donor history (Sebrell et al., 2018). Wang et al. used mammary epithelial acini to investigate rotation. They identified that cell polarity and MTs are essential for the rotational motion (Wang et al., 2013). This aspect can be investigated in detail by using the light sheet pipeline. To this point, it remains unknown why only a portion of the organoids in a culture demonstrate rotation. Additionally, the underlying mechanism responsible for this process remains to be determined.

#### 4.7.4. Identifying dynamic organoid behaviours – size oscillation

The experiments in this work illustrate that frequent size oscillation in mPOs and hPOS are common during the period of growth. The quantification of these events with the light sheet pipeline showed that it occurs more often in smaller organoids. This observation demonstrates that the initial size of the cell cluster is a critical factor. Interestingly, this is in strong contrast to results from Sebrell et al. They observed more size oscillations in large organoids (>200  $\mu\text{m}$ ) (Sebrell et al., 2018). In their investigation they used human gastric epithelial organoids which were cultivated under the same conditions as hPOs and were also of epithelial origin. The higher oscillation rate of the gastric organoids raises the question how the pancreas organoid system differs from that. Additionally, this highlights the heterogeneity of organoid systems in general and the need to analyse them on multiple scales to define core regulatory principles. In this work, the segmented organoids illustrate a high diversity in their proliferation capacity. Whether this behaviour is somehow related to the organoid donor (as is presumed in the work of Sebrell and colleagues) needs to be analysed in the future. Aside from issues related to the donor background, the other possible difference in this work is that the organoids derived from mice.

In conclusion, organoids show highly dynamic and diverse behaviours. Several different behavioural patterns were identified on the macroscale by using the brightfield pipeline and on the meso- and microscale by using the light sheet pipeline. A complete overview is visualized in Figure 30.

### 4.8. Data handling

The imaging of three-dimensional objects like organoids on multiple scales in a high temporal and spatial resolution comes along with a high amount of produced data. Data handling and processing is one bottle neck in extracting relevant data and generating a reliable and robust readout which can be used for clinical evaluation. The brightfield pipeline used in this work is able to handle the large amount of data by sampling it step-by-step in an automated process

(see 2.21). Originally, the data is constructed in tiles that comprises a stack of z-planes per time point. Each stack is processed as a maximum projection to one z-plane per time point and fused with the projected z-planes of the other tiles to form one complete image. This process reduces the data storage demands tremendously (from hundreds of gigabytes to less than one gigabyte) and allows subsequent segmentation over all time points. The light sheet pipeline goes one step further. Depending on the settings for tiles and views, the produced data ranges from hundreds of gigabytes to tens of terabytes. To process such amounts of data, high computational power is necessary to extract relevant and statistically usable data. To circumvent long processing runs, regions of interest were extracted directly from the obtained data (by using ZEN blue). With this step, the amount of data was reduced from tens of terabytes to tens of gigabytes and it was possible to process them in a reasonable time (for details, see Hof et al., 2020). This step both enables the processing and handling of the data as well as reduces it to the important regions as interpreted by the viewer. One possible improvement would be to reduce the amount by data compression without losing information (e.g., JPEG2000, JP3D, Rossinelli et al., 2020).

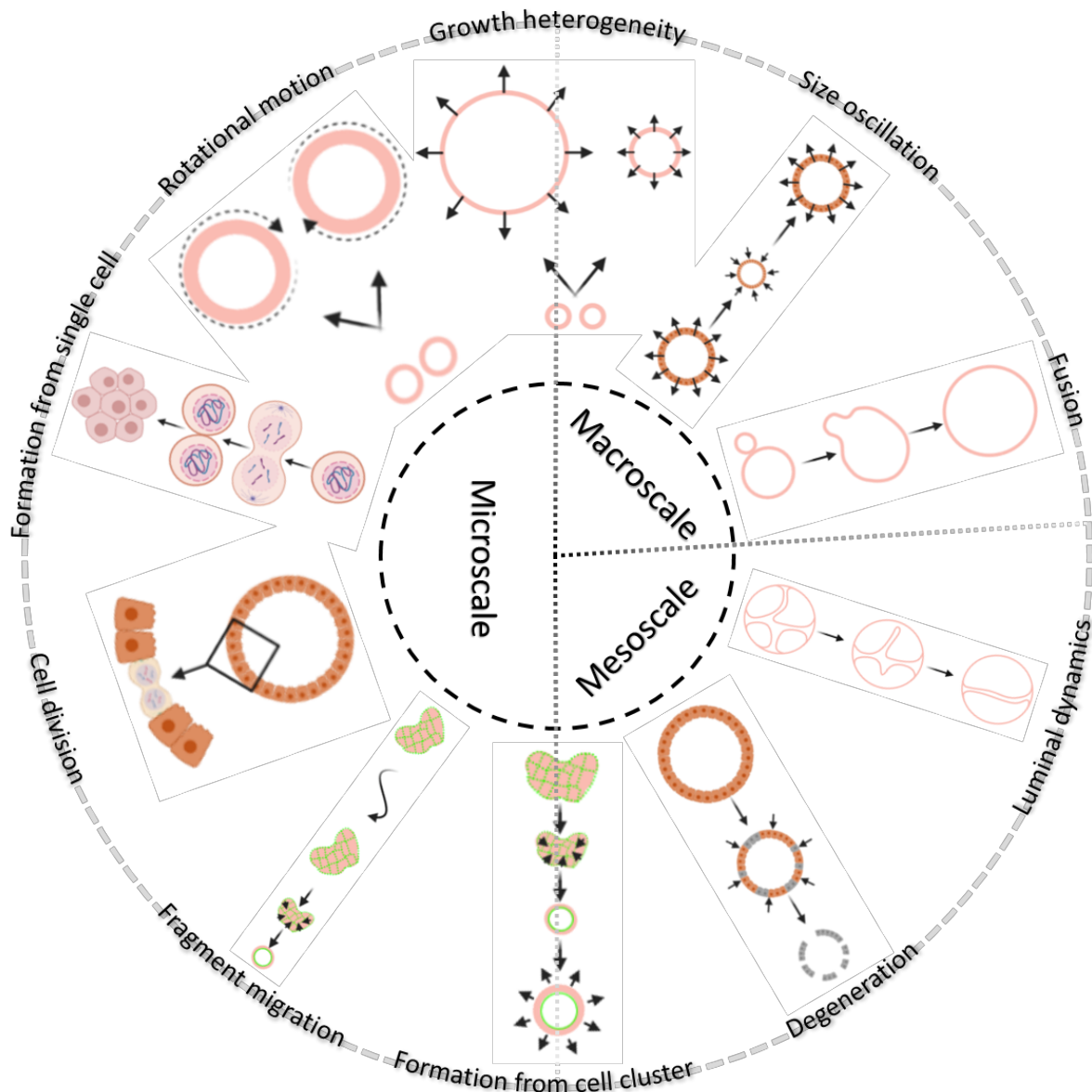


**Figure 30: Graphic illustration of organoid growth, heterogeneity and its corresponding detection on multiple scales with the brightfield and light sheet pipelines..** The middle sphere illustrates the scale at which the corresponding process can be detected and analysed. The analysis on a macroscopic scale includes the detection of the size oscillation events, fusion and growth rate heterogeneity. The analysis on a mesoscopic scale detects and quantify luminal dynamics, degeneration processes of complete organoids and the quantification of the organoids formed out of a cell cluster. On a microscopic scale the formation processes out of a single cell as well as out of cell clusters, single cell division events within an organoid, rotational motion of complete organoids and the fragment migration prior formation can be analysed. Growth heterogeneity can be observed at the microscopic scale for multiple organoids within a culture (modified from Hof et al., 2020)

#### 4.9. Pancreas organoids can be cultivated in Hanging-drops – no ECM is needed

This work is the first to describe the general appearance, different behavioural patterns and overall high heterogeneity of pancreas organoids. With the presented pipelines, general parameters of growth were identified and helped to generate fundamental knowledge of the nature of organoids. However, reasons for this heterogeneity and an understanding of the organoid's phenotype maintenance is still lacking. In addition to cellular mechanisms, which will be addressed later in this work, the ECM is one important factor that needs to be



considered to influence the organoid appearance and heterogeneity. The method of cultivation is based on the culture of liver organoids. For the cultivation of pancreas organoids, Huch and colleagues adapted this technique. They included additional medium components and adapted the isolation protocol. However, the need for an ECM has never been addressed. Whether it is needed as physical scaffold or only as a provider of specific binding ligands to activate downstream pathways has never been investigated (Broutier et al., 2016; Georgakopoulos et al., 2020). The ECM plays a significant role in heterogeneity as it is poorly defined in its components and can vary in its stiffness. Therefore, the necessity and influence for the ECM was addressed in this work.

In 2013, Jin and colleagues published a method for culturing and establishing adult mouse pancreas ring colonies by using a semi-solid methylcellulose-based medium that contains 5 % (vol/vol) Matrigel®. Based on the observation this study, I adapted the HD culture technique to the culture of mPOs and hPOs at a minimum of 4 % (vol/vol) Matrigel®. The experiments demonstrated that mPOs and hPOs can be cultured long term in a hanging drop and maintain their phenotype. No aberrations in the expression of polarisation markers or stem cell markers were detected. Furthermore, the constant splitting ratios of the long-term culture showed that the organoids maintain their proliferation activity. Moreover, the results suggest that hPOs can be cultured longer in HD than in ECM droplets. The reasons for this observation were not addressed directly in this work, but in general two differences can be discussed.

First, in the HD culture it is not possible to change the medium every two to three days. To guarantee an optimal nutrition supply 10 µl medium are added to the drops every two days. This leads to a steady increase in the concentrations of the components within the medium since the overall drop-volume stays constant due to evaporation of the water content. Whether the increased concentration of the growth factors is accompanied by an increased cellular reaction and if this is the only reason for the observations needs to be addressed. Second, the Matrigel® solved in the growth medium as a semi-solid medium can account for the growth of the organoids in the HD-system. As a result of the procedure detailed above, the Matrigel® concentration steadily increases but never reaches the required 3mg/ml concentration to polymerize to a solid phase. (10 days in culture: 5 time Medium is added means 2mg/ml Matrigel® within one droplet) (<https://www.corning.com/catalog/cls/documents/faqs/CLS-DL-CC-026.pdf>, 2020.07.02, 1.40pm). Although the drops remain liquid throughout the experiment all the time and no solid structure can be visually detected, it is likely that a loosely packed network of polypeptides becomes present with increasing concentration of Matrigel®. Whether this is somehow connected to the organoids surface is not clear but can be investigated by adding ECM-binding fluorophore-tagged Antibodies (e.g., against Laminin, collagen or entactin) and imaging the drops with a fluorescence microscope.

As shown, organoids need 4 % (vol/vol) Matrigel® to grow but no solidified ECM as a physical scaffold. There is ongoing debate about the component, ligand and concentration that promotes organoid growth. In mammals nearly 300 proteins (Hynes et al., 2012) are known to build up the ECM *in vivo*. The so called matrisome comprises e.g., collagen, proteoglycans and glycoproteins. Moreover, cells can modulate their surrounding ECM by releasing metalloproteases which enzymatically digest the polymers into fragments. These fragments

can differ in their bioactive properties relative to the full-length polymers, and thus can change their bioavailability and the ECM properties (Bonnans et al., 2014; Hynes et al., 2012). Furthermore, cells are able to secrete ECM components by their own and thereby building their own ECM. The culture of organoids is a relatively new technique which means that little is known about the cell's activity in releasing ECM components or metalloproteases. However, in recent years, one key peptide binding motif, RGD (Arg-Gly-Asp), was identified to play a critical role in *in vitro* organoid development. RGD is an integrin-binding motif and promotes the growth of organoids (Blondel et al., 2019). Adding such motifs to the medium and analysing the growth of mPOs and hPOs may lead to improved understanding of the ECM-organoid interaction and will help to develop synthetic hydrogels with defined, xenograft-free and clinically applicable properties. In recent years, much research has been done in the field of hydrogel development but to date no commercial, ready-to-use hydrogel for human pancreas organoids has been developed (for additional research: Annabi et al., 2014; Jiang et al., 2016; Thiele et al., 2014; Yang et al., 2017). Organoid growth in HD can inform the development of such hydrogels and can further be used as an intermediate stage towards clinical application. Because it reduces the needed amount of Matrigel® it reduces not only the costs, but also the overall variability of the system itself. As described, organoids cultured in the HD-system demonstrated a more homogenous appearance which favours the hypothesis that the ECM itself is one source of the observed heterogeneity in organoid culture. The replacement of the ECM-droplet-based culture with the HD-system may lead to more reliable and robust data.

In summary, pancreas organoids can be cultured in hanging drops for long term culture, do not need the ECM as physical scaffold and can be used to further understand the cell-ECM interaction. Moreover, the use of liquified ECM leads to a more homogeneous organoid culture and promotes the long-term culture of hPOs. It is therefore perfectly suited to be an intermediate stage on the way to replace Matrigel® as an animal derived ECM.

#### 4.10. CRM reveals water as the main component of the liquid within organoids

One defining feature in organoid appearance is the hollow, liquid filled lumen. It is not known whether the liquid contains any specific substance or how the cells are able to generate it. One way to analyse the liquid would be to extract it with a micro injection and analyse it via high performance liquid chromatography (HPLC). All in this work made attempts to extract the liquid failed, since the penetration of the epithelium with a micro injection directly led to a bursting of the complete organoid (data not shown). To circumvent the penetration of the organoid, a method was needed that analyses the liquid components in their native environment non-invasively. For this reason, CRM was used. It allows the non-invasive identification of the chemical composition *in vitro*. In a cooperation with Nathalie Jung (BMLS, working group Prof. Maïke Windbergs) we were able to identify the cellular monolayer of the organoids and distinguish the inner luminal liquid from the surrounding medium in fixed as well as living mouse organoids. We identified four major features of the organoid inner liquid: (1) no specific differences in the substance composition between the surrounding and the inner liquid were measurable, (2) soluble ECM components were detected within the organoid, (3) the main component of the liquid is water, (4) the water/protein ratio of the organoid liquid decreases with increasing size of the organoid.

Taking these results into an account, several statements can be made. First, the cells do not secrete any specific substance into the lumen of the organoid. This supports the theory that the cells actively generate an osmotic gradient which promotes the passive transport of water into the lumen (from basal to apical). Second, the detection of ECM components within the organoid lumen shows that the organoids somehow encapsulate parts of the ECM during their growth. Whether this happens during the formation or during the size-oscillation by a rupture of the organoid monolayer is still unknown. Third, during organoid growth, the general volume increase is accompanied by the influx of water. If the organoid growth is also based on cell proliferation activity is highly likely but need to be validated. The third observation also supports the theory that organoids encapsulate ECM only during the formation and not during the observed size-oscillation because the concentration of the ECM components within the organoid did not change with increasing size of the organoid.

CRM is already used in clinical applications and as a quality control for many different applications (Pence et al., 2016). The clinical validation of an analytic method is highly cost intense and time consuming. To use already validated methods for the quality control of pancreas organoids can circumvent this bottleneck. Differentiated cells in the pancreas usually have the task to release specific substances (e.g., digestive enzymes – acinus cells, hormones like insulin –  $\beta$ -cells, bicarbonate-rich liquid - ductal cells). The release of this substances can be measured by CRM. The absence of these substances within the organoid lumen validates the status of the organoid cells as undifferentiated stem cells. To investigate this theory a positive control (e.g., differentiated ductal cells) should be imaged with CRM and the concentration of corresponding substances should be measured and validated against other measurement methods (like HPLC).

#### 4.10.1. Aquaporins are present within the cell membrane and presumably guide the water influx into the lumen

The presence of mainly water inside the lumen is in align with to the observation of AQP1, 5 and 8 in the membrane of the organoids. AQPs are small, membrane-spanning, pore forming channels that facilitates the water transport between cells and their environment (Hof et al., 2021). The basolateral and apical expression of AQP1, the mainly apical expression of AQP5 and the appearance of AQP8 at the apical side align with the physiological conditions in the adult pancreas. Other AQPs have not been screened for, but checking for all 133 known AQP would shed more light on their presents in pancreas organoids (Abir-Awan et al., 2019). The general expression of AQPs in ductal cells is not surprising. In their native surrounding, ductal cells secrete bicarbonate-rich mucus into the ductal tree that, together with the digestive enzyme from the acinar cells, form the pancreatic juice. Investigations showed that AQPs are involved in this process (Burghardt, 2003). It is highly likely that the detected AQPs in pancreas organoids are involved in the process of water transfer into the organoid lumen, but this was not addressed within this work. Another explanation could be that the AQPs are a prerequisite of the fully differentiated ductal cells and are not included in the process of organoid lumen establishment. An experimental trial by which the AQPs would consecutively be inhibited would answer this question.

In summary, the use of CRM helped to generate fundamental knowledge about the pancreas organoid phenotype and has high potential to be used to validate and generate quality

parameters for pancreas organoids. The identification of water as the main component in the organoid lumen and the presence of the AQPs in the apical and basal cell membrane provide additional information about the mechanisms of organoid lumen establishment and maintenance.

#### 4.11. Tubulin and the actin-myosin-axis are the main contributors for the phenotype maintenance of pancreas organoids.

To understand the behaviour and the phenotype of pancreas organoids, the system needs to be investigated *in toto*. To this point, experiments revealed that the organoid is water-filled and that it expresses AQPs which may promote the water flux. Furthermore, size oscillation and organoid motion was identified which cannot be explained by hydraulic dynamic processes solely. In general, dynamic cellular processes are always accompanied by strong cytoskeleton rearrangements (Serrador et al., 1999). To investigate these aspects also in organoids, the presented brightfield pipeline was used to analyse hundreds of organoids in regard to their overall size changes over several days in culture. With this setup, basic mechanisms were explored which help to understand pancreas organoid growth.

##### 4.11.1. Human and mouse organoid volume increase and growth is based on tubulin and the actin-myosin-axis

Pancreas organoid phenotype and growth behaviour has not been addressed so far. In respect to other cell-, spheroid- and organoid-lines, cell-ECM and cell-cell interactions have only been studied to a level of general knowledge. The cell-cell connection is based on tight- and adherence junctions as well as desmosomes. The cell-ECM interaction take place via integrins and their functional units of focal adhesions. Furthermore, a highly organized cytoskeleton and a dynamic interplay between all previously mentioned cell-cell and cell-ECM connections represent the structural basis of organized 3D cell aggregates (Balaban et al., 2001; Trepap et al., 2018). The results obtained in this work show a highly polarized actin structure of the organoid cell. On this basis, the assumption was made that the organoid phenotype is maintained by the polarized components of the cytoskeleton and an equilibrium of generated and actual forces. The pressure of the liquid filled lumen and its counterpart, the cell-cytoskeleton in connection with the ECM, constitute the main components which are needed to generate the organoid phenotype. To validate this hypothesis, human and mouse organoids were treated with drugs that inhibit corresponding components.

The experiments demonstrated that upon an inhibition of actin with Cytochalasin D, mPOs and hPOs collapsed and lost their hollow phenotype. Whether the organoids where dead was not addressed directly, but as they were not able to recover their phenotype after replacing the Cytochalasin D treated medium with normal medium, it can be hypothesized that the cells were dead. This result is not surprising, because it is known that actin is one main components in the cytoskeleton for generating forces and responsible for maintaining the overall stability of the cell. Furthermore, actin is connected to the adherence junctions which are responsible for the cell-cell connection. For this reason, an inhibition leads not only to overall instability of the single cell, but also a loss in the cell-cell connection which is essential for the maintenance of the monolayered organoid structure.

Myosin, esp. myosin II, is directly associated with the actin associated molecular machinery is myosin, esp. myosin II. It generates intercellular forces by moving along actin filaments and is connected to other adhesion proteins like cadherins which construct the adherence junctions. To investigate whether the function of myosin II is associated with the organoid phenotype and behaviour, it was inhibited using Para-Blebbistatin. Interestingly, the inhibition of myosin lead to a significant increase in the overall size of mPOs as well as hPOs. Actomyosin forces are transferred between cells through the adherence junctions. For this reason, the inhibition of myosin affects not only the force generation but also presumably leads to a less strong cell-cell connection. As a result, the still present luminal pressure combined with the less strong cell-cell connection can lead to the recorded inflation of the organoid. Whether it is accompanied by a flattening of the epithelium is highly possible. The established light sheet pipeline would be one option to investigate if the inflation of the organoid is accompanied with a flattening of the epithelium. Another interesting aspect in the treatment with Para-Blebbistatin is that it did not lead to a burst of the organoid during the myosin inhibition time of 24 hours. Two hypotheses can be given as explanation. First, the incubation time was not long enough to reach a critical point of extension. Second, the inhibition of myosin did not affect, or was partly compensated by desmosomes, which play a main role in providing mechanical resilience on cell layers (Garrod et al., 2008). The first theory can be easily answered by extending the incubation time with Para-Blebbistatin, the second theory can be answered by using inhibitors of desmosomes alone and in combination with Para-Blebbistatin.

The largest class of cytoskeleton filaments is the MTs. They are essential for the intracellular transport of vesicles, the cell division process, and they provide mechanical support to the cell cytoskeleton (Muroyama et al., 2017). To investigate their function in the maintenance of the organoid phenotype, two inhibitors were used. Paclitaxel was used to inhibit the disassembly of the MTs, which stabilizes the MTs. Nocodazole was used to depolymerize MTs. The stabilisation with Paclitaxel led to a significant reduction in growth the organoids, whereas the depolymerisation with Nocodazole led to the organoids collapse and presumably death. The stabilisation of MTs and the corresponding organoid size is due to the cells mechanism of maintaining their polarized structure mainly by steady directed transport of vesicles. These cargos contain and transfer corresponding cellular components from the basal to the apical side by the use of the motor proteins kinesin and dynein (Muroyama et al., 2017). This process is highly dynamic and needs steady adjustments. The interruption of the dynamic assembly of MTs can maintain the polarisation steady state but does not allow any adaptations. Hence, the dynamic behaviour of the organoid is interrupted. The disruption of MTs by Nocodazole displays a complete collapse of the directed vesicle transport meaning, the cells are not able to maintain their polarisation. Finally, the cells are no longer able to keep the luminal pressure and the organoid collapse. To further investigate the influence of the polarisation dynamics and their role in organoid phenotype maintenance, kinesin and dynein can be inactivated separately. By inhibiting kinesin, the anterograde transport of vesicles can be interrupted and by inhibiting dynein the retrograde transport can be analysed. Because the organoid cells show an apical polarisation, the anterograde transport of cytoplasmic proteins (e.g., G-actin, intermediate filament protein type I and II (keratins)) can be hypothesized to be of major importance in this process.

In summary, the conducted experiments illustrate that the maintenance of the luminal characteristic of pancreas organoids is highly dependent on the actin-myosin-axis as well as on

tubulin. However, many open questions remain and need to be clarified to understand the role of the cytoskeleton components in detail.

#### 4.11.2. Pancreas organoid luminal dynamics are controlled by the mechanosensitive channel Piezo-1 and dependent on the active regulation of Cl<sup>-</sup>-mediated conductance regulators like CFTR

The organoid phenotype maintenance is dependent on the cell cytoskeleton. In addition, CRM revealed that the inner liquid of the organoids is primarily water. These two pieces of information lead to uncertainties about how the organoid is able to control the force equilibrium between the water influx into the lumen and the force generated by the cytoskeleton components. Ion channels are probable candidates to create a gradient within the cells that favours the transport of water and other molecules from the basal to the apical side.

One ion channel that is known to control the volume maintenance in liver and intestine organoids by Cl<sup>-</sup> mediated conductance is the CFTR channel (Dekkers et al., 2016). To date, this channel has not been studied in the context of pancreas organoids but the experiments in this work illustrate that CFTR is present in the cells. The high-throughput pipeline was used to investigate the function of this channel. It is known that CFTR is influenced by the degree of cell cytoskeleton extension and the membrane voltage (Barman et al., 2011; Kelly et al., 2010; Melis et al., 2014). Since the organoid phenotype points towards a steady extended condition of the cell cytoskeleton, the assumption was made that CFTR is activated. An additional consideration is that the channel has multiple opening states which depend on the membrane potential. To ensure a complete voltage depended depletion of the channel, two CFTR-inhibitors were used. The results showed that the voltage dependent inhibition of the CFTR channel significantly reduced the organoid size. The combination of the inhibitors GlyH-101 and CFTRinh-172, and GlyH-101 alone led to a significant reduction in the overall size of the organoids. In contrast to GlyH-101, CFTRinh-172 treatment alone did not show any significant reduction in mPOs. Furthermore, it led to a significant increase of the overall organoid size in hPOs. The effect of GlyH-101 can be partly explained by its low sensitivity. Investigations revealed that this inhibitor is also highly sensitive to inhibit two other types of Cl<sup>-</sup> conductance regulators, namely VSORC and CaCC. In contrast, CFTRinh-172 alone blocks VSORC in higher concentrations (>5  $\mu$ M) and does not block CaCC (Melis et al., 2014). In conclusion, the conducted experiments revealed that the organoid volume maintenance is partly Cl<sup>-</sup>-conductance regulator dependent. Further investigations should consider whether the regulation is due to CFTR solely or other Cl<sup>-</sup> channels are involved.

The sensitivity for mechanical stimulation is an important regulatory mechanism in embryonic and organ development. The conversion of mechanical forces to a biological response (mechanotransduction) plays a fundamental role e.g., in vascular and tubular development. (Borbiro et al., 2017; Montal et al., 2015). The phenotype of hPOs and mPOs suggests that the liquid filled lumen is one requirement for the development of this system. Whether the generated luminal pressure is involved in this process by a mechanosensitive transduction to a cellular response has never been investigated. Piezo-1 is a mechanosensitive cation channel that plays multiple important roles in developmental processes. With a propeller like molecular construction, it is highly force sensitive and voltage dependent. This work discovered the

presents of Piezo-1 in hPOs and mPOs. Immunofluorescence staining illustrates that Piezo-1 localizes to the membrane of the organoid cells but does not show a clear tendency towards the apical or basal side. Its function was addressed with the high-throughput pipeline which was used specifically to analyse the inhibition and activation of Piezo-1. Interestingly, the inhibition with GsMTx-4 did not show any effect on the overall size of the organoids in mPOs but a significant increase in the size of hPOs. This suggests that the channel is expressed in the organoids but remains in an inactive state in mPOs but shows some activity in hPOs. To confirm this, the recently developed Piezo-1 activator Yoda 1 was used to activate the channel. Piezo-1 has only an open or close and no intermediate configuration (Lin et al., 2019). Practically, this means that the concentration of Yoda 1 needs to overcome a critical threshold to activate the channel. The experiments revealed that mPOs exhibited a reaction upon Yoda 1 treatment at 50  $\mu\text{M}$  and hPOs at a concentration of 25  $\mu\text{M}$ . The activation of the Piezo-1 channel in mPOs and hPOs led to a fast collapse of the organoids, which was recovered in normal conditions. In contrast to mPOs, hPOs showed a strong compensating reaction in normal conditions. Additionally, these results confirm that the cells are not damaged by the collapse. The activation of Piezo-1 led to an influx of  $\text{Ca}^{2+}$ -cations into the cytoplasm which was proven by Fluo-8am staining. The  $\text{Ca}^{2+}$  cation is known to be a potent second messenger and associated with several cellular mechanisms like proliferation and gene transcription regulation (Bootman et al., 2001). The role of  $\text{Ca}^{2+}$  is for this reason a potential additional influence. Furthermore, the direct influence on the electrical current of the cell polarity should be considered. As mentioned previously, we know that the cells have a clear polarity which is maintained by a steady gradient driven transport of vesicles from the basal to the apical side. A change of the ion concentrations within the cell can have a direct influence on this mechanism by interrupting this ion gradient driven transport. The experiments on the CFTR channel demonstrate that the volume maintenance is strongly ion gradient driven. The deactivation of CFTR stops the  $\text{Cl}^-$  influx that leads to a change in the osmotic gradient within the cells and favours the deflation of the luminal water into the organoid surrounding. The result is the measured shrinkage of the organoid. The reaction of the organoids upon Piezo-1 activation based on the same mechanism. The influx of the  $\text{Ca}^{2+}$  cations at the apical side of the cell interrupt the ion driven osmotic gradient dependent water influx into the organoid lumen. Once the Piezo-1 is not activated, the ion gradient is re-established within the cell and the organoid is able to recover its luminal phenotype as evidenced by the fast size increase in the recovery phase.

#### 4.11.3. Piezo-1 activation leads to repolarisation of the cell cytoskeleton in pancreas organoids and changes in the expression pattern of Yap

After the treatment with Yoda 1 for 24 hours, the organoids appeared compact. Immunofluorescence staining of the organoids revealed a different phenotype. The organoids lost their monolayered organisation and their lumen and were characterized by a dense, multi-layered and multi-luminal phenotype. It is important to mention that not all organoids showed multiple lumens. In general, the overall appearance was quite diverse and ranged from completely dense structures to organoids with several very small lumens. The only common thing was that they all showed multi-layered areas of cells. This diversity can be explained simply by the high diversity in organoid size and the position within the ECM droplet. The penetration of the drug through the gel depends on several factors like the chemical polarity and molecular size, which can lead to differences in the incubation time of the organoids with

the drug. A closer look at the movies of Yoda 1 treatments (Movie 4) showed that a shrinkage of organoids can be first observed at the droplet's border and last in the organoids located in the centre. To circumvent this inconsistency shrinkage, the incubation time should be increased to determine if all organoids show the same dense-packed phenotype at a certain time of the treatment.

Another interesting observation was made after the Yoda 1 treatment and subsequent immunostaining of actin. The compaction led to a re-localisation of actin from the apical to the basal side. Two possible explanations can be given for that: first, the re-localisation was directly associated with the loss of the lumen and was not due to the activation of Piezo-1; second, the activation of Piezo-1 was directly associated with changes of cytoskeleton components like actin which led to the compaction of the organoids. The first assumption is promoted by the observation that organoids which had at least one lumen also showed an apical actin polarisation. The latter assumption can be made since data emerged that Piezo-1 directly and actively modulates cytoskeletal dynamics. Investigations revealed that Piezo-1 modulates the focal adhesion zone dynamics and has important regulatory functions in epithelial barrier maintenance. In regard to the barrier function, it modulates both the proliferation of cells when the barrier is threatened by apoptotic cells as well as induces the exclusions of cells when the cell layer is too dense (Nourse et al., 2017). Taking this into an account, the activation of Piezo-1 may lead to the activation of several upstream pathways that regulate the cell density and proliferation activity which lead to the observed dense structures.

The lumen is one major characteristic of epithelial organoids. It is associated with the stem cell like character which means that compaction of the organoids can be the first sign of losing the fate and starting differentiation. To clarify this, Yoda 1 treated compact organoids were stained against Sox9. No clear differences between treated and untreated organoids on the level of Sox9 expression was detected. From this, it can be inferred that the cells maintain their fate and do not start to differentiate. An additional validation of the expression rate via western blot would be helpful to see slight alterations in the up- or down-regulation of differentiation-associated transcription factors. Yap is known to be associated to Piezo-1 via the Hippo signalling pathway and, in this way, associated to multiple pathways ranging from differentiation to proliferation (see Box.1). In addition, Yap nucleus expression is also used as a stem cell marker in ES and iPCS cells. For this reason, the observed shift of Yap expression from the nucleus to the cytosol suggests changes in the expression profile of the organoid cells.

In summary, it was illustrated that the organoid phenotype is highly dependent on tubulin and the actin-myosin-axis. Additionally, it was shown and that pancreas organoids express CFTR and Piezo-1 which led upon deactivation or activation to a shrinkage of the organoids respectively. By immunofluorescence staining a re-localisation of actin from an apical to a basal polarisation upon Piezo-1 activation was observed. Whether this is associated with cell fate changes still needs to be clarified as nucleus re-localisation of Yap but no alteration in Sox9 expression was observed.



#### 4.11.4. Alterations of CFTR and Piezo-1 expression in mouse pancreas organoids cultured in HD – possible CFTR-Piezo-1 coupled mechanism

The presence and function of CFTR and Piezo-1 has been addressed in this work. Furthermore, the possibility to grow pancreas organoids without a solid ECM raises questions about the functional connection of the ECM and the organoids. Immunostaining of mouse organoids grown in HD revealed a clear tendency of CFTR towards the basal side and punctuated expression of Piezo-1 on the apical side. This is in strong contrast to the observed cytosolic expression of CFTR and overall membrane expression of Piezo-1 in organoids grown following standard procedures.

A solid ECM provides a physical scaffold for cells. Organoids can connect to it via integrin directly or focal adhesions; thus, generating resting forces which can support the overall shape and appearance of the organoids (Balaban et al., 2001). Without the solid ECM, the organoids need to produce the corresponding forces on a different way. The polarized expression of Piezo-1 and CFTR can give insights in this mechanism. As explained above, CFTR is a anion channel which is able to transport anion (mainly Cl<sup>-</sup>) into the cytoplasm, in contrast, Piezo-1 is a mechanosensitive channel which is able to transport cations (Ca<sup>2+</sup>) along the cell membrane into the cytoplasm and is connected to the cytoskeleton (Nourse et al., 2017). Without a solid ECM, the organoids need to generate more luminal pressure to maintain their structure. The required energy to transport liquid through the cell into the lumen can be provided by the osmotic gradient generated by CFTR. The higher degree of generated pressure may explain the stronger expression of Piezo-1 at the apical side.

Additionally, in the comparison of organoids in ECM droplets and organoids in HD (by eye), organoids in HD appeared smaller, more roundish and overall, more homogeneous in size. This observation supports the theory that the organoid volume is driven only by its luminal pressure in HD grown organoids whereas organoids embedded in an ECM droplet also use the ECM as a physical scaffold for growth. Because the surface area to volume ratio of the organoid is inversely proportional to its size ( $S/V = 3/R$ ,  $S$ = surface,  $V$ =volume,  $R$ =radius), the growth of organoids in HD is limited to the luminal pressure which can be generated by the cells. This means the organoids are smaller and because they are unaffected from external cues more roundish (Sutera et al., 1991)

In conclusion, the different expression patterns of CFTR and Piezo-1 in organoids cultured in HD additionally supports the theory that CFTR is involved in maintaining the organoid volume and that Piezo-1 may play a regulatory role by its ability to increase or decrease the gradient driven osmotic pressure.

#### 4.12. Two theories emerge from experimental evidence

In the following section, two theories are discussed which attempt to explain the observations made within this work. The first theory is supported by a mathematical model and explains the observed differences in organoid size oscillation. The second theory tries to explain the mechanism of organoid lumen maintenance by postulating a force-equilibrium between the organoid lumen and the cytoskeleton. This second theory is highly speculative and should be treated more sceptically.

#### 4.12.1. Organoid size oscillation is dependent on the surface-to-volume ratio

One major goal in this work was to gain deeper insight into the mechanism of organoid lumen development and maintenance. We showed that tubulin and the actin-myosin-axis are two major players in maintaining the luminal structure and that the lumen is established by the help of the ion channels CFTR and may be controlled by Piezo-1. This leads to the assumption that these ion channels are occasionally involved in the establishment of an ion gradient within the cell which causes the influx of water from the basal to the apical side (Figure 31). Although this hypothesis needs to be further validated, it is supported by the finding that no specific substance was detected within the lumen by CRM and that the protein-to-water ratio decreases with the increasing organoid size. This experimental evidence can be used to explain the observed heterogeneity in mPOs behaviour (e.g., frequent size oscillation). The analysis of the three representative organoids on a single cell level illustrates that size oscillation was more prominent in small organoids that demonstrated a slower cell division rate than the large organoids. Furthermore, the analysis showed that the organoid with the highest PCG value showed the lowest size oscillation frequency. All of these experimental outcomes lead to three assumptions: (1) organoid size oscillation depends on the surface-to-volume ratio (the cell density in relation to organoid size); (2) this ratio is dependent on cell proliferation, indicating that small organoids built up by a low number of cells show more frequent size oscillation; (3) the general organoid size increase is limited by the cytoskeleton force and not by the water influx (osmotic pressure generation).

Project collaborators Tim Liebisch and Mariana Kurtz (FIAS, Goethe-University Frankfurt) designed an agent-based mathematical model that uses the assumption that were made in this work to simulate the organoid size oscillation (for a detailed description take a look at Hof et al., 2020). With the model they were able to qualitatively reproduce the size oscillation of the three mPOs analysed in this work. They indicated that the two large organoids do not show a size oscillation event between the start of their initial growth phase and up to the point the cell growth rate reaches a plateau phase. At this linear growth phase, the organoids show size oscillation patterns that fit to the experimental results. Furthermore, their results agree with the made assumption that small organoids with a lower number of cells exhibit size oscillation as early as the initial growth phase. The modelling cannot be used as a proof of the assumptions, but it suggests that modelling can be a useful tool for understanding organoid size oscillation and that the acquired experimental data can be used to simulate the organoid growth behaviour. The simulation is only based on three representative organoids and many more organoids need to be analysed to validate the mathematical model. Specifically, more data related to the enormous growth heterogeneity would aid in understanding the accuracy of the mathematical model.

#### 4.12.2. The organoid size is dependent on the force-equilibrium generated between the organoid lumen and the cytoskeleton

This work also provides evidence for a mechanism that underlies the size oscillation: a misbalance of forces generated by the luminal pressure, the cell internal forces from tubulin and the actin-myosin-axis, and the resting forces generated by the interplay with the cell and the ECM via e.g., integrin, which leads to a rupture of the monolayer. As a result, water is released into the organoid surrounding, the luminal pressure decreases, and the monolayer

collapses. Because CRM demonstrated that only a minor number of ECM-components are located within the organoid lumen, no physical scaffold can keep the monolayer in its position. This suggests that the cell monolayer collapses until the ruptured cells can reconnect and close the leakage by themselves. As the cells are still polarized, the cell internal forces generated by myosin can be re-generated, and the needed ion gradient to rearrange the water influx into the lumen can be directly re-established by the interplay of ion channels like CFTR and Piezo-1.

The fast-organoid luminal recovery and the swelling experiments conducted with CFTR inhibition and Piezo-1 activation supports the assumptions of a force-equilibrium between the organoid lumen and the cytoskeleton. The observation of the higher degree of polarized actin as a cytoskeleton component and the higher expression of CFTR at the basal side and Piezo-1 at the apical side in the hanging drop culture system points in the same direction. The fact that the HD system contains no solid ECM that can serve as a physical scaffold leads to different growth conditions for the organoids. The organoid cells cannot generate integrin-related resting forces. As a compensatory mechanism they need a higher degree of polarized cytoskeleton components. To construct the luminal phenotype without the integrin-related resting forces, the organoid cells also need to generate a relatively higher degree of luminal pressure (to reach the same dimensions as with ECM). To generate this pressure, a higher degree of an osmotic gradient within the cells is needed. One possible mechanism is to generate this gradient is by expressing more ion channels within the cell membrane such as CFTR and Piezo-1. All of these explanations aim at fact that organoids growing in HD show in general a more homogeneous appearance and overall smaller size in comparison to organoids grow in an ECM droplet. This explanation can be explained by the missing ECM as a counterpart for the intracellular force generation. This absence results in a homogeneously formed sphere in accordance with the shape of a sphere having the lowest possible surface area-to-volume ratio ( $S = 4\pi r^2$ ,  $V = (4/3)\pi r^3$ ,  $S/V = 3/r$ ;  $S$  = surface,  $V$  = volume,  $r$  = radius). Because of that, the cells require the least energy to maintain it. Interestingly, this mathematical consideration also explains why small organoids tend to rupture more often than big organoids. The surface-to-volume is inversely proportional to the organoid size, which means more energy is needed to maintain a small sphere in comparison to a large one (for the small sphere the surface-to-volume ratio becomes larger). One approach to evaluate these mathematical assumptions would be to analyse the growth of organoids in the HD system with the brightfield pipeline. With this experiment, the general organoid size and the size oscillation frequency can be investigated and compared to organoids grown under normal conditions. Furthermore, the mean thickness of the organoids monolayer in comparison to organoids growing within a droplet of ECM would give insights into the organoid biophysical properties. A thicker and more densely packed monolayer of cells in the HD system would support the theory that the organoids maintain their shape in absence of a solid ECM solely by the cytoskeleton forces and the generated osmotic pressure.

In conclusion, the conducted experiments and the data presented in this work provide the first overview of the heterogeneity in behaviour and appearance of pancreas organoids (Figure 30). Furthermore, the fundamentals of the biophysical and biochemical background of pancreas organoids were experimentally understood. This study and the produced experimental evidence at least partially explain organoid's dynamics in growth and behaviour (Figure 31). However, extensive work is still needed to understand the cellular and biophysical reasons for the pancreas organoid appearance. The made assumptions about the influence of ECM to the

growth, the involved cytoskeleton components and ion channels as well as the observed dynamics in growth and cellular behaviour can be used as guidelines for targeted experiments which are elaborated in the following paragraph.

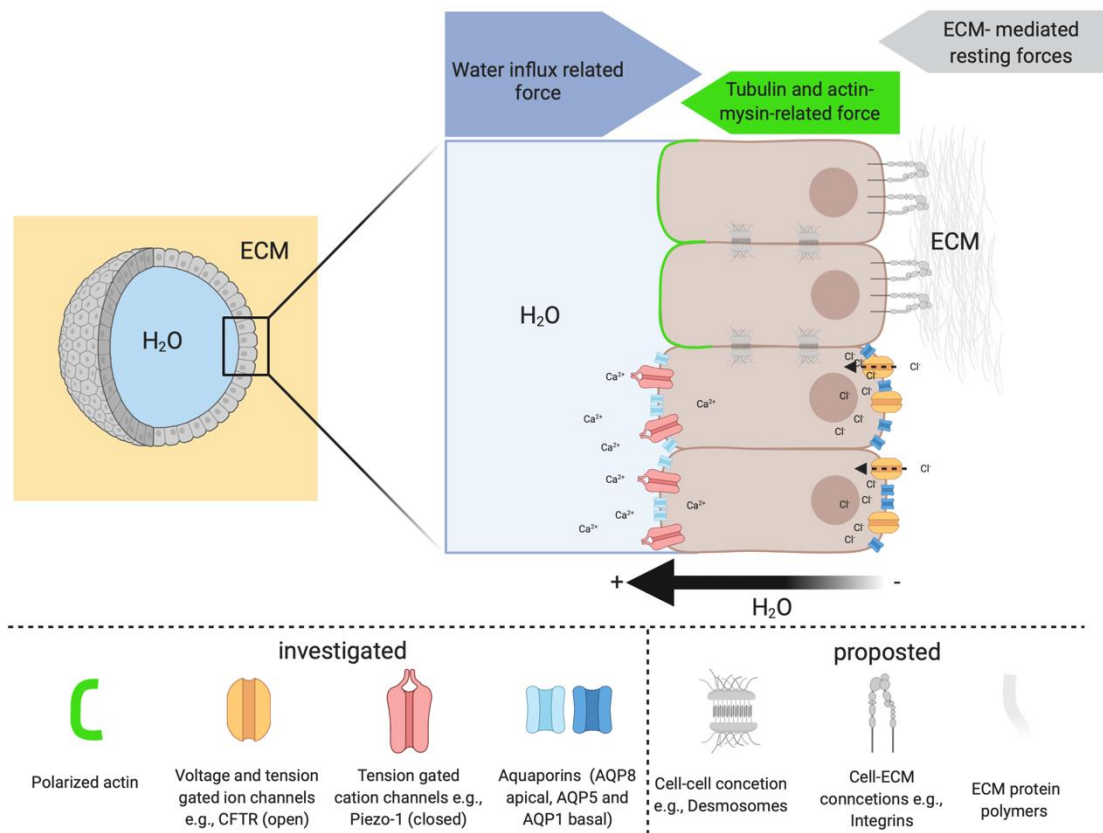


**Figure 31: Illustration of the hypothesis of the organoid lumen maintenance based on the results obtained in this work.** The close-up shows four representative cells of the organoid epithelium. The coloured components were investigated in this work, the greyish parts illustrate the postponed components. The water influx (blue arrow) and the actin-myosin-related forces (green arrow) in combination with the integrin-ECM mediated forces (grey arrow) build up a pressure and force equilibrium which maintains the organoid luminal structure. The water influx is regulated by voltage and tension gated ion channels (e.g., CFTR) and cation channels (e.g., mechanosensitive ion channel Piezo-1) which establishes an ion dependent osmotic gradient. The influx of water into the lumen is further fostered by aquaporins at the cell's membrane. (Graphic designed with www.BioRender.com)

## 5. Outlook and future research areas

### 5.1. Generate a donor bank to analyse donor related differences in the culture of pancreas organoids

Pancreas organoids offer promising perspectives not only in clinical application approaches, but also as a model to understand development and disease progression *ex vivo*. In this work, it is shown that organoids have a high heterogeneity in terms of behaviour, development and appearance. Therefore, it is of major importance to generate a comprehensive overview of donor related differences to classify possible outcomes of further investigations.

In terms to understand development and disease progression *ex vivo*, pancreas organoids derived from mouse can be used to optimize experimental procedures. In order to generate reliable and robust data, human donors need to be analysed. The protocol developed from Dossena and colleagues allows the generation of hPOs from the islet transplantation therapy and therefore offers a way to generate a pancreas organoid donor bank without the need for volunteers (Dossena et al., 2020). Using this and the analysis pipelines presented in this work, a database can be generated which comprises donor-related proliferation capacities, volume and size information and differences in the overall phenotype and expression patterns of key transcription factors. Additionally, the organoids can be further analysed on a molecular level. Georgakopoulos and colleagues conducted a study with some donors and extract genome sequencing data, mRNA expression levels of key genes such as Pdx 1 or Ngn3 and chromosomal aberrations (Georgakopoulos et al., 2020; Huch, Dorrell, et al., 2013). Furthermore, the hPOs from different donors can be used to develop a fully defined hydrogel for the clinical application.

### 5.2. Optimize hPO growth conditions for the long-term culture

This work and other studies (Broutier et al., 2016; Georgakopoulos et al., 2020) demonstrated that hPOs have a less long-term culture capacity in comparison to mPOs. The reason for this is not known so far but the results in this work illustrate that hPOs need more time to reach the final size and that the overall growth is more constant in comparison to mPOs. Further, it was shown that hPOs can be cultured longer in the HD-system than in the ECM droplets. One possible reason is that hPOs grown in HD receive a constant increase in growth factors over time. These observations point in the direction of the absence of perfectly adjusted growth conditions and illustrate the need for further optimization. Therefore, the brightfield pipeline can be used to analyse the growth in regard to different growth factors concentrations and help to optimize the overall conditions. The light sheet pipeline can be used to analyse the growth of the organoids with different growth factor concentrations in regard to the proliferation activity, luminal dynamics and neighbourhood relations. Thus, understand if the cells show higher proliferation rates at some point of the growth and if it is related to the volume increase or if it is associated with resting phases.

### 5.3. Validate and establish the HD-culture technique as an alternative to the normal culture

This work shows that the culture of pancreas organoids in HD is possible and that the organoids keep their fate also in long term. Further it proves that the organoid does not need an ECM as a physical scaffold. However, additional steps to validate the clinical usage need to be performed. First, only two human and mouse donors were tested. Additional donors need to be tested in order to validate the usage. Further, analysis should be conducted, whether the patient's background is reflected in the growth of organoids within the HD system (e.g., gender, age, medical history). For the usage in basic research as well as clinical applications the possibility to cryopreserve the organoids grown in HD needs to be tested to generate organoid databanks. All organoid HD lines generated in this work were extracted from an existing normal culture. One bottleneck in generating organoid cultures is the generation from fresh primary donor material. Due to these limitations, it is inevitable to establish a protocol to generate organoids from fresh donor material directly in the HD-system. Furthermore, a detailed molecular analysis which investigate the chromosomal stability, mRNA expression levels of key genes and the usability for transplantation approaches is needed to ensure the cell identity as MPCs (as references, the following publications can be use: (Broutier et al., 2016; Georgakopoulos et al., 2020; Greggio et al., 2013).

### 5.4. Use the HD-system to develop a fully synthetic hydrogel

For clinical use, to reduce the overall organoid heterogeneity and to generate robust and valid data, Matrigel® or BME needs to be replaced by a fully defined hydrogel. The culture of pancreas organoids in the HD-system demonstrated that the organoids do not need the ECM as a physical scaffold but as an interaction partner. To define the components of a liquid culture without Matrigel®, a systematic investigation of epitopes for the surface binding proteins (e.g., RGD, IKVAV, CBMS) can be conducted. The components can be easily solved in different concentrations and combinations and analysed in regard to the organoid growth in general and compared to organoid growth in Matrigel® in detail (e.g., volume increasing rate, size oscillation frequency). Additional IF screenings in regard to differentiation markers (e.g, Pdx 1, Nkx 6.1, Ngn3 and Sox9) define the cell's fate and help to identify the ECM key components which are needed for pancreas organoid growth.

### 5.5. Transfer the generated knowledge to organoids of different origin

The observation that organoids grow in a liquid interface is in contrast to several recently published articles with organoids of different origin (e.g., lung intestine, (Blondel et al., 2019; Gjorevski et al., 2017). The authors of these articles emphasize that the organoids need a solid ECM and that its rigidity plays a significant role in the organoid growth. Further, they observe differentiation upon ECM rigidity changes. However, none of them tried to culture the organoids in a liquid interphase with solved ECM as an interaction partner. The ability of other organoid lines to grow in the HD-system can generate fundamental knowledge and can be easily conducted.

### 5.6. Use CRM to investigate the organoid luminal liquid

The non-invasive chemical selective method of CRM was introduced within this work and used for the first time to analyse fixed and live pancreas organoids. A newfound understanding was archived regarding the liquid configuration within the organoid lumen. It was possible to detect ECM components within the organoid lumen. To investigate whether the ECM components were encapsulated only in the formation processes or also during the size oscillations of the organoids, a substance (e.g., FIT-Dextran) which is not cell-permeable but ECM-permeable and detectible with CRM, can be added to the medium after the organoids have been formed. When this substance is detectible within the organoid after a defined time of growth the only way to enter the organoid is within a size-oscillation.

### 5.7. Validating the CRM technique to generate a robust readout which can be used to determine the cell status

As already mentioned, CRM has high potential to be used in clinical applications to validate the organoid fate. To generate a robust readout, reference parameters need to be defined. For this reason, native material (e.g., islets of Langerhans, ductal cells, acinar cells,  $\beta$ -cells upon glucose stimulation) need to be measured and analysed. Each of those cells secrete defined substances in their environment (e.g., ductal cells secrete bicarbonate-rich mucus, acinar cells secrete digestion enzymes,  $\beta$  cells secrete insulin) (Grapin-Botton, 2005; Remedi et al., 2016; Williams, 2010). Using CRM, corresponding reference values should be measured and further used as quality parameters of the differentiation status of the pancreas organoids.

### 5.8. Investigating the function of Aquaporins in the organoid phenotype establishment and maintenance

The presents of mainly water in the lumen of the organoids led to the assumption that water channels within the cells guides it. For the first time, the presents of AQP1, 5 and 8 was shown in this work. Their presence alone does not mean that they also fulfil a function. The inhibition of the AQP and simultaneous observation of the luminal organoid behaviour should be further investigated. Heavy metal compounds (e.g., nickel chloride) have been shown to be effective in AQP inhibition. However, their highly toxic nature renders their use in organoid research unlikely (Abir-Awan et al., 2019). Small molecular inhibitors are the most promising candidates to block AQPs. For example, Tetraethylammonium (TEA) and Acetazolamide are known to block AQP1 (Detmers et al., 2006; Pastorekova et al., 2004) and Anti-epileptic drugs (AEDs) to block AQP5. Furthermore, a relatively new approach is to use antibodies. These antibodies bind to the corresponding channel and block them physically. So far, it has been tested only in mouse, but in vivo studies show already promising results (Jha et al., 2019). However, the use of the mentioned substances needs to be validated for the use in organoid culture because the ECM displaying a physical barrier and offer many possible epitopes the substances can bind on. To circumvent it, the HD-system offers an option to investigate the influence of the named substances without these problems.

### 5.9. Shed light on the organoid ECM interaction by modulating integrin

The interaction of the organoid cells with the ECM was not addressed directly in this work. However, it is known that integrins are a major player in the cell-ECM connection and that the focal adhesions are essential for the polarization of cells by providing the counterpart of the exerted pushing force to the plasma membrane. It is highly likely that they are important for the organoid's formation and phenotype maintenance. An experimental trial similar to the inhibition of Actin and MTs by using the brightfield pipeline can be used to generate fundamental knowledge about the influence of integrins to the organoid luminal dynamics.

As an additional experimental setup, the investigation of an integrin inhibition on organoids grown in the HD-system can be performed. The interaction of the organoids without a solid surrounding ECM and simultaneously inhibited integrin signalling generates advanced knowledge about their physiological role.

### 5.10. Analysing the effect of Myosin-II inhibition

To understand the organoid phenotype as a monolayered liquid filled lumen, organoids were treated with different substances and analysed with the brightfield pipeline. One important aspect in this observation was the organoid deflation upon Myosin-II inhibition. Two aspects need to be addressed in this regard. The measurement of the organoid volume cannot give information about the organoid on a cellular level. The question that arises is whether the organoid volume increase is associated with either, a flattening of the epithelium alone or with an increase in proliferation activity. The epithelium size can be analysed by fixing the organoids after the treatment and without the treatment, followed by an immunolabelling in regard to the organoid cytoskeleton (e.g., Phalloidin to label actin or antibody staining against the MTs or INFs). Subsequently, the organoids can be imaged, and the epithelium thickness can be measured and compared to the control group. Information about the proliferation activity can be given by using the light sheet pipeline.

### 5.11. The third cytoskeleton component: the intermediate filaments

One focus of this work was to investigate the function of the cytoskeleton components for the maintenance of the luminal structure of pancreas organoids. Therefore, actin and MTs were inhibited or stabilized. However, INFs were not addressed directly but display one major component of the cytoskeleton. Therefore, a drug-treatment-trial, similar to the already performed once should be conducted. Possible drug candidates are puromycin (Aviner, 2020) and cycloheximide (Eldeeb et al., 2019). Furthermore, the inhibition of INFs also influences the cell-cell connections via desmosomes and thereby can provide additional information about their role in the maintenance of the monolayered structure of the organoids. To additionally investigate the desmosomes and the influence of the INF-inhibition, the immunolabeling of cadherin upon INF inhibition can be conducted. Cadherin are the main components in desmosomes and adherence junctions, and it can be expected that upon cell-cell contact inhibition, the expression pattern is changed from the membrane into the cytosol.

One additional step in this regard would be to inhibit Myosin-II with Para-Blebbistatin in combination with one mentioned INFs inhibitor. With the combined application the Actin-



myosin related force generation is inhibited simultaneously with a weakening of the cell-cell interaction due to desmosome inhibition. The expected result would be (1) an inflation of the organoids due to myosin inhibition followed by (2) a burst of the organoid at one point due to less strong cell-cell connection.

#### 5.12. Investigating the polarisation dynamics of pancreas organoids

One outcome of this work is that the MTs dynamic plays a fundamental role in the organoid phenotype maintenance. Based this result, it can be assumed that the MTs are essential for the polarisation of the cells. To validate this assumption, the dynamic transport of cytoskeleton components via kinesin and dynein can be investigated separately. By inhibiting kinesin (e.g., Inspinesib (Blagden et al., 2008) or Monoastrol (El-Hamamsy et al., 2020), the anterograde transport of vesicles can be interrupted and by inhibiting dynein (e.g., Dynarrestin (Höing et al., 2018) or Ciliobrevin (Firestone et al., 2012), the retrograde transport can be interrupted. The organoids' reactions in terms of volume fluctuations can be measured by using the brightfield pipeline.

#### 5.13. Clarify the influence of GlyH101 and CFTRinh- 172

One aim of this work was to understand the cellular mechanisms of organoid phenotype development and maintenance. One main result was that the ion channel CFTR and the cation channel Piezo-1 were identified. To investigate the CFTR-channel the two inhibitors GlyH101 and CFTRinh-172 were used. Interestingly, the reaction upon CFTRinh-172 did not show a reduction in organoid size. As discussed, GlyH101 is able to block CFTR and two additional CL-channel namely VSORC and CaCC. CFTRinh-172 is only able to block VSORC but not CaCC. Based on the results the question rised if the organoid reaction is due to CFRT inhibition solely or also to the inhibition of the CaCC-channel. To test this, an additional drug treatment trail can be conducted that uses CaCCinh-A01 (De La Fuente et al., 2008), MONNA (Boedtkjer et al., 2015) or NPPB (Malekova et al., 2007) to inhibit CaCC solely.

#### 5.14. Clarify the role of Piezo-1 in pancreas organoid development and phenotype maintenance

The identification of Piezo-1 in pancreas organoids opens up the question of its function within the organoid development and maintenance. The activation of Piezo-1 led to a rapid deflation of the organoid whereas deactivation had no effect in mPOs. These two observations can be explained by the hypothesis that Piezo-1 is present in a mainly inactive form in the organoid cells. However, the strong and reversible effect upon its activation point towards a regulatory function within the organoid luminal maintenance. To investigate this further, a knockdown by using siRNA of the Piezo-1 related genes can be performed. In a first approach, mPOs should be used to validate the vitality and the general organoid formation ability upon Piezo-1 knockdown, because mPOs are more robust and easier to handle. If the organoids are still able to grow, the growth rate should be measured and compared with a control group by using the brightfield pipeline. To validate the influence of Piezo-1 in hPOs, the same experiments should be conducted and compared to the results obtained with mPOs.

### 5.15. Treatment of Pancreas organoids with Yoda 1 to initiate EMT-like processes – first step towards optimized $\beta$ -cell differentiation

The observation that pancreas organoids collapse and stay compact during Piezo-1 activation by Yoda 1 treatment and the associated repolarisation of actin from the apical to the basal side can be a first hint towards differentiation processes. As described the embryonic development of the islets of Langerhans is initiated with an epithelial-to mesenchymal transition (EMT) of the endocrine progenitor cells from the trunk regions of the plexus. The EMT is always accompanied by fundamental remodelling processes of the cytoskeleton. It is characterized by decreased and subsequent loss of cytokeratin, E-cadherin and  $\beta$ -catenin as well as the increased expression of mesenchymal proteins like Vimentin (Cole et al., 2009; Mastracci et al., 2012; Pan et al., 2014). In this work, beside the cytoskeleton component actin, the expression of adhesion proteins like E-cadherin or  $\beta$ -catenin after Yoda 1 treatment were not addressed but can be easily immunolabelled to gain information about the status of the cells. Aside from this, markers for mesenchymal cells like Vimentin or for endocrine differentiation like Ngn3, should be stained or measured via Western Blot to see if any changes in the expression patterns occur. The initiation of an EMT-like process before using already established differentiation protocols can potentially lead to a higher yield in  $\beta$ -cell production which is needed for personalised cell therapeutic approaches like Diabetes 1 (Aguayo-Mazzucato et al., 2018; Chakravarthy et al., 2017; Xu et al., 2008). Interestingly, to this point, no research group tried to initialize EMT before initializing the differentiation or trans-differentiation in vitro. One attempt has been made with intestine organoids to study EMT associated intestinal fibrosis. By using transformation growth factor- $\beta$  (TGF- $\beta$ ) and Tumour necrosis factor- $\alpha$  (TNF- $\alpha$ ), Hahn et al. were able to generate an organoid-based EMT model (Hahn et al., 2017). The use of these two components leads to a collapse and a restructuring of the cytoskeleton comparable to the observation made in this work. Whether these components also support the EMT in pancreas organoids or may be an option in combination with Yoda 1 treatment needs to be addressed.

In conclusion, one limit of personalized cell therapeutic approaches to treat Diabetes 1 is the low yield in the differentiation of  $\beta$ -cells. To overcome this, one promising option would be first to initiate EMT and then force the differentiation towards  $\beta$ -cells. Whether the treatment of pancreas organoids with Yoda 1 leads to an initiation of EMT could be one option.

### 5.16. Universal applicability of the FEP-foil cuvette in different research fields

In this work the FEP-foil cuvette was successfully used for the analysis of human and murine pancreas organoids on a microscale i.e., cellular level. However, during this work, the FEP-foil cuvette was also used within many different biological systems. Next to pancreas organoids, it was also used to image, analyse and define behaviour patterns in human cholangiocarcinoma-derived organoids (Hof et al., 2020) and dense structured spheroids (Hötte et al., 2019). Furthermore, it was used to image complete cleared tissue sections which helped to define the position, the appearance, and the fate of metastatic cancer cells within an affected organ (Gupta et al. 2020, under review). The imaging of complete organs has always been a challenge. With the help of the FEP-foil cuvette coupled with the use of light sheet microscopy, millimetre sized sections of mouse brains as well as whole murine ovaries can be imaged and analysed

(Hötte et al., 2019). The FEP-foil cuvette can help to generate fundamental understanding of cellular organisation and help to understand complex cellular interactions. For example, in a cooperation with University of Cambridge, the FEP-foil cuvette was used to image islets of Langerhans *in toto*. The results of this study helped to develop, optimized and validate an isolation and cryopreservation protocol. Using this protocol, the islet overall vitality was increased, which can potentially enhance the transplantation success rate. Because the availability of suitable donor material is the limiting factor in transplantation approaches for diabetic patients, the success rate becomes of extensive importance (Dolezalova et al 2020, in review).

The future use of the FEP-foil cuvette in other organoid cultures, (e.g., intestine, lung, brain) can help in understanding highly dynamic organoid developmental processes *in toto* and simultaneously provide fundamental information about single cell behaviour (e.g., migration, proliferation, cell fate changes, apoptosis, cell rearrangement processes). The use of the FEP-cuvette in cancer research offers promising perspectives in understanding metastatic cell behaviour in e.g., all modalities of tissue integrity or the influence of chemotherapeutic active ingredients.

In conclusion, all the present and future application fields of the FEP-foil cuvette show that it is universally applicable and has high potential to be used in different research areas.

## 6. Concluding remarks - what we now know

This thesis identified and characterized pancreas organoid phenotypes on multiple scales. In this work, an optimized isolation and staining protocol, a sample holder to image organoids in high temporal and spatial resolution and two processing pipelines which enable the analysis of complete cultures and single organoids on a cellular level has been developed. In addition, an alternative cultivation method to reduce the needed amount of ECM has been identified and helps to generate more robust and reliable datasets.

Applying these methodologies led to the following findings:

- Human as well as murine organoids show diverse behavioural patterns and a tremendous heterogeneity in terms of size and growth rates within a culture. Furthermore, a generally lower and time delayed growth rate was observed in human organoids.
- Neither murine nor human organoids need an ECM as a physical scaffold. However, they do require at least a low concentration of ECM ligands within the medium to establish their spherical structure.
- The cellular requirements for the phenotypic behaviour are at a minimum a polarized cytoskeleton, adhesion associated molecules and actively generated intracellular forces.
- The absence of characteristic molecules within the organoid luminal liquid shows (1) that the organoid cells do not actively secrete specific components inside the lumen and (2) that the spherical structure is established by water pressure from the lumen towards the surrounding medium or the ECM.
- The identification of specific water and ion channels point towards a process by which the cells actively generate an intracellular ion gradient that drives the water flux from the basal to the apical side. This water flux generates the spherical pressure.
- The regulatory mechanism of this process could not be clarified completely but experiments suggest that ion channels which are voltage- and/or mechano-sensitive are associated.

The ultimate goal of pancreas organoid research area is the clinical application for personalized cell therapeutic approaches. This thesis forms a basis for further investigations on pancreas organoid appearance and behaviour. It also identifies biochemical and biophysical regulatory mechanisms that provide wider perspectives and biological relevance. Furthermore, the need for an extracellular matrix is brought into question, which could have significant clinical implications.

## 7. Publication

- (1) Jung, N.\* and **Moreth, T.\*** (2021), 'First-time non-invasive analysis of pancreas organoids in defined hydrogels'. Application in process.
- (2) Hof, L., **Moreth, T.**, (2021). Long-term live imaging and multiscale analysis identify heterogeneity and core principles of epithelial organoid morphogenesis. BMC Biology, 19(1), 37. doi: 10.1186/s12915-021-00958-w
- (3) Gupta, J., Schmitt, M., Nicolas, A., Pesic, M., Pallangyo, C., Varga, J., Ramakrishnan, M., Ablasser, A., **Moreth, T.**, Stelzer, E.H.K., Karimova, M., Sato, T., J de Sauvage, F., Greten, F.R. (2020), 'Paracrine mTOR activation and BMP inhibition preserve colorectal tumor maintenance upon Lgr5+ cell loss'. Under review (Nature)
- (4) Dolezalova, N., Gruszczuk, A., Barkan, K., Gamble, K.J., Galvin, S., **Moreth, T.**, O'Holleran, K., Mahbubani, K.T., Higgins, J.A., Gribble, F.M., Reimann, F., Surmacki, K., Andrews, S., Casey, J.J., Pampaloni, F., Murphy, M.P., Ladds, G., Slater, N.K.H., Saeb-Parsy, K. (2020), 'Accelerating cryoprotectant diffusion kinetics improves cryopreservation of pancreatic islets'. Under review (Nature communications)
- (5) Dossena, M., Piras, R., Cherubini, A., Barilani, M., Dugnani, E., Salanitro, F., **Moreth, T.**, Pampaloni, F., Piemontj, L., Lazzari, L. (2020), 'Standardized GMP-compliant scalable production of human pancreas organoids', Stem Cell Research & Therapy. Stem Cell Research & Therapy, 11(1), p. 94. doi: 10.1186/s13287-020-1585-2.
- (6) Katharina, H., Michael, K., Lotta, H., Tuppi, M., **Moreth, T.**, Verstegen, M.M.A., van der Laan, L.J.W., Stelzer, E.H.K., Pampaloni, F. (2019), 'Ultra-thin fluorocarbon foils optimise multiscale imaging of three-dimensional native and optically cleared specimens', Scientific Reports, 9(1), pp. 1–13. doi: 10.1038/s41598-019-53380-2.

\*authors contribute equally

## 8. References

- Abir-Awan, M., Kitchen, P., Salman, M. M., Conner, M. T., Conner, A. C., & Bill, R. M. (2019). Inhibitors of mammalian aquaporin water channels. *International Journal of Molecular Sciences*, *20*(7). doi: 10.3390/ijms20071589
- Aguayo-Mazzucato, C., & Bonner-Weir, S. (2018). Pancreatic  $\beta$  Cell Regeneration as a Possible Therapy for Diabetes. *Cell Metabolism*, *27*(1), 57–67. doi: 10.1016/j.cmet.2017.08.007
- Alqahtani, F. Y., Aleanizy, F. S., El Tahir, E., Alkahtani, H. M., & AlQuadeib, B. T. (2019). Paclitaxel. *Profiles of Drug Substances, Excipients and Related Methodology*, *44*, 205–238. doi: 10.1016/bs.podrm.2018.11.001
- Andrei, S. R., & Gannon, M. (2020). Embryonic development of the endocrine pancreas. In *Transplantation, Bioengineering, and Regeneration of the Endocrine Pancreas*. Elsevier Inc. doi: 10.1016/b978-0-12-814831-0.00012-9
- Annabi, N., Tamayol, A., Uquillas, J. A., Akbari, M., Bertassoni, L. E., Cha, C., Camci-Unal, G., Dokmeci, M. R., Peppas, N. A., & Khademhosseini, A. (2014). 25th anniversary article: Rational design and applications of hydrogels in regenerative medicine. *Advanced Materials*, *26*(1), 85–124. doi: 10.1002/adma.201303233
- Aviner, R. (2020). The science of puromycin: From studies of ribosome function to applications in biotechnology. *Computational and Structural Biotechnology Journal*, *18*(April), 1074–1083. doi: 10.1016/j.csbj.2020.04.014
- Azzarelli, R., Rulands, S., Nestorowa, S., Davies, J., Campinoti, S., Gillotin, S., Bonfanti, P., Göttgens, B., Huch, M., Simons, B., & Philpott, A. (2018). Neurogenin3 phosphorylation controls reprogramming efficiency of pancreatic ductal organoids into endocrine cells. *Scientific Reports*, *8*(1), 1–12. doi: 10.1038/s41598-018-33838-5
- Balaban, N. Q., Schwarz, U. S., Rivelino, D., Goichberg, P., Tzur, G., Sabanay, I., Mahalu, D., Safran, S., Bershadsky, A., Addadi, L., & Geiger, B. (2001). Force and focal adhesion assembly: A close relationship studied using elastic micropatterned substrates. *Nature Cell Biology*, *3*(5), 466–472. doi: 10.1038/35074532
- Balls, M., Goldberg, A. M., Fentem, J. H., Broadhead, C. L., Burch, R. L., Festing, M. F. W., Frazier, J. M., Hendriksen, C. F. M., Jennings, M., van der Kamp, argot D. O., Morton, D. B., Rowan, A. N., Russell, C., Russell, W. M. S., Spielmann, H., Stephens, M. L., Stokes, W. S., Straughan, D. W., Yager, J. D., ... van Zutphen, B. F. M. (1995). The Three Rs: The Way Forward: The Report and Recommendations of ECVAM Workshop 111,2. *Alternatives to Laboratory Animals*, *23*(6), 838–866. doi: 10.1177/026119299502300614
- Bardeesy, N., & DePinho, R. A. (2002). Pancreatic cancer biology and genetics. *Nature Reviews Cancer*, *2*(12), 897–909. doi: 10.1038/nrc949

- Barker, N., van Es, J. H., Kuipers, J., Kujala, P., van den Born, M., Cozijnsen, M., Haegebarth, A., Korving, J., Begthel, H., Peters, P. J., & Clevers, H. (2007). Identification of stem cells in small intestine and colon by marker gene Lgr5. *Nature*, *449*(7165), 1003–1007. doi: 10.1038/nature06196
- Barker, T. H. (2011). The role of ECM proteins and protein fragments in guiding cell behavior in regenerative medicine. *Biomaterials*, *32*(18), 4211–4214. doi: 10.1016/j.biomaterials.2011.02.027
- Barman, P. P., Choisy, S. C. M., Gadeberg, H. C., Hancox, J. C., & James, A. F. (2011). Cardiac ion channel current modulation by the CFTR inhibitor GlyH-101. *Biochemical and Biophysical Research Communications*, *408*(1), 12–17. doi: 10.1016/j.bbrc.2011.03.089
- Baumgart, E., & Kubitscheck, U. (2012). Scanned light sheet microscopy with confocal slit detection. *Optics Express*, *20*(19), 21805. doi: 10.1364/oe.20.021805
- Bayguinov, P. O., Oakley, D. M., Shih, C. C., Geanon, D. J., Joens, M. S., & Fitzpatrick, J. A. J. (2018). Modern Laser Scanning Confocal Microscopy. *Current Protocols in Cytometry*, *85*(1), 1–17. doi: 10.1002/cpcy.39
- Beall, M. H., Van Den Wijngaard, J. P. H. M., Van Gemert, M., & Ross, M. G. (2012). Water Flux and Amniotic Fluid Volume: Understanding Fetal Water Flow. In *Nephrology and Fluid/Electrolyte Physiology* (Second Ed). Elsevier Inc. doi: 10.1016/B978-1-4377-2658-9.00001-7
- Bekiari, E., Kitsios, K., Thabit, H., Tauschmann, M., Athanasiadou, E., Karagiannis, T., Haidich, A. B., Hovorka, R., & Tsapas, A. (2018). Artificial pancreas treatment for outpatients with type 1 diabetes: Systematic review and meta-Analysis. *BMJ (Online)*, *361*. doi: 10.1136/bmj.k1310
- Benitez, C. M., Goodyer, W. R., & Kim, S. K. (2012). Deconstructing pancreas developmental biology. *Cold Spring Harbor Perspectives in Biology*, *4*(6), 1–17. doi: 10.1101/cshperspect.a012401
- Bernard-Kargar, C., & Ktorza, A. (2001). Endocrine pancreas plasticity under physiological and pathological conditions. *Diabetes*, *50*(Supplement 1), S30–S35. doi: 10.2337/diabetes.50.2007.S30
- Bissell, M. J., Hall, H. G., & Parry, G. (1982). How does the extracellular matrix direct gene expression? *Journal of Theoretical Biology*, *99*(1), 31–68. doi: 10.1016/0022-5193(82)90388-5
- Blagden, S. P., Molife, L. R., Seebaran, A., Payne, M., Reid, A. H. M., Protheroe, A. S., Vasist, L. S., Williams, D. D., Bowen, C., Kathman, S. J., Hodge, J. P., Dar, M. M., De Bono, J. S., & Middleton, M. R. (2008). A phase I trial of ispinesib, a kinesin spindle protein inhibitor,

- with docetaxel in patients with advanced solid tumours. *British Journal of Cancer*, 98(5), 894–899. doi: 10.1038/sj.bjc.6604264
- Blondel, D., & Lutolf, M. P. (2019). Bioinspired hydrogels for 3d organoid culture. *Chimia*, 73(1–2), 81–85. doi: 10.2533/chimia.2019.81
- Boedtkjer, D. M. B., Kim, S., Jensen, A. B., Matchkov, V. M., & Andersson, K. E. (2015). New selective inhibitors of calcium-activated chloride channels - T16Ainh-A01, CaCCinh-A01 and MONNA - What do they inhibit? *British Journal of Pharmacology*, 172(16), 4158–4171. doi: 10.1111/bph.13201
- Boj, S. F., Hwang, C. Il, Baker, L. A., Chio, I. I. C., Engle, D. D., Corbo, V., Jager, M., Ponz-Sarvisé, M., Tiriác, H., Spector, M. S., Gracanin, A., Oni, T., Yu, K. H., Van Boxtel, R., Huch, M., Rivera, K. D., Wilson, J. P., Feigin, M. E., Öhlund, D., ... Tuveson, D. A. (2015). Organoid models of human and mouse ductal pancreatic cancer. *Cell*, 160(1–2), 324–338. doi: 10.1016/j.cell.2014.12.021
- Bolhaqueiro, A. C. F., Ponsioen, B., Bakker, B., Klaasen, S. J., Kucukkose, E., van Jaarsveld, R. H., Vivié, J., Verlaan-Klink, I., Hami, N., Spierings, D. C. J., Sasaki, N., Dutta, D., Boj, S. F., Vries, R. G. J., Lansdorp, P. M., van de Wetering, M., van Oudenaarden, A., Clevers, H., Kranenburg, O., ... Kops, G. J. P. L. (2019). Ongoing chromosomal instability and karyotype evolution in human colorectal cancer organoids. *Nature Genetics*, 51(5), 824–834. doi: 10.1038/s41588-019-0399-6
- Bonnans, C., Chou, J., & Werb, Z. (2014). Remodelling the extracellular matrix in development and disease. *Nature Reviews Molecular Cell Biology*, 15(12), 786–801. doi: 10.1038/nrm3904
- Bonner-Weir, S. (2001).  $\beta$ -cell turnover: Its assessment and implications. *Diabetes*, 50(SUPPL. 1). doi: 10.2337/diabetes.50.2007.s20
- Bonner-Weir, S., & Weir, G. C. (2005). New sources of pancreatic  $\beta$ -cells. *Nature Biotechnology*, 23(7), 857–861. doi: 10.1038/nbt1115
- Bonnet, D. (2002). Adult stem cell plasticity. *Journal of Pathology*, 197(4), 441–456. doi: 10.1002/path.1176
- Bootman, M. D., Collins, T. J., Peppiatt, C. M., Prothero, L. S., MacKenzie, L., De Smet, P., Travers, M., Tovey, S. C., Seo, J. T., Berridge, M. J., Ciccolini, F., & Lipp, P. (2001). Calcium signalling - An overview. *Seminars in Cell and Developmental Biology*, 12(1), 3–10. doi: 10.1006/scdb.2000.0211
- Borbiro, I., & Rohacs, T. (2017). Regulation of Piezo Channels by Cellular Signaling Pathways. In *Current Topics in Membranes* (Vol. 79). Elsevier Ltd. doi: 10.1016/bs.ctm.2016.10.002



- Boyle, J. (2008). Molecular biology of the cell, 5th edition by B. Alberts, A. Johnson, J. Lewis, M. Raff, K. Roberts, and P. Walter. *Biochemistry and Molecular Biology Education*, 36(4), 317–318. doi: 10.1002/bmb.20192
- Brayton, C. F. (1986). Dimethyl sulfoxide (DMSO): a review. *The Cornell Veterinarian*, 76(1), 61–90.
- Brazovskaja, A., Treutlein, B., & Camp, J. G. (2019). High-throughput single-cell transcriptomics on organoids. *Current Opinion in Biotechnology*, 55, 167–171. doi: 10.1016/j.copbio.2018.11.002
- Broutier, L., Andersson-Rolf, A., Hindley, C. J., Boj, S. F., Clevers, H., Koo, B.-K., & Huch, M. (2016). Culture and establishment of self-renewing human and mouse adult liver and pancreas 3D organoids and their genetic manipulation. *Nature Protocols*, 11(9), 1724–1743. doi: 10.1038/nprot.2016.097
- Broutier, L., Mastrogiovanni, G., Versteegen, M. M., Francies, H. E., Gavarró, L. M., Bradshaw, C. R., Allen, G. E., Arnes-Benito, R., Sidorova, O., Gaspersz, M. P., Georgakopoulos, N., Koo, B.-K., Dietmann, S., Davies, S. E., Praseedom, R. K., Lieshout, R., IJzermans, J. N. M., Wigmore, S. J., Saeb-Parsy, K., ... Huch, M. (2017). Human primary liver cancer-derived organoid cultures for disease modeling and drug screening. *Nature Medicine*, 23(12), 1424–1435. doi: 10.1038/nm.4438
- Burghardt, B. (2003). Distribution of aquaporin water channels AQP1 and AQP5 in the ductal system of the human pancreas. *Gut*, 52(7), 1008–1016. doi: 10.1136/gut.52.7.1008
- Carafoli, E., & Krebs, J. (2016). Why calcium? How calcium became the best communicator. *Journal of Biological Chemistry*, 291(40), 20849–20857. doi: 10.1074/jbc.R116.735894
- Catoira, M. C., Fusaro, L., Di Francesco, D., Ramella, M., & Boccafoschi, F. (2019). Overview of natural hydrogels for regenerative medicine applications. *Journal of Materials Science: Materials in Medicine*, 30(10). doi: 10.1007/s10856-019-6318-7
- Cerf, M. E., Muller, C. J. F., Du Toit, D. F., Louw, J., & Wolfe-Coote, S. A. (2005). Transcription factors, pancreatic development, and  $\beta$ -cell maintenance. *Biochemical and Biophysical Research Communications*, 326(4), 699–702. doi: 10.1016/j.bbrc.2004.10.217
- Chakravarthy, H., Gu, X., Enge, M., Dai, X., Wang, Y., Damond, N., Downie, C., Liu, K., Wang, J., Xing, Y., Chera, S., Thorel, F., Quake, S., Oberholzer, J., MacDonald, P. E., Herrera, P. L., & Kim, S. K. (2017). Converting Adult Pancreatic Islet  $\alpha$  Cells into  $\beta$  Cells by Targeting Both Dnmt1 and Arx. *Cell Metabolism*, 25(3), 622–634. doi: 10.1016/j.cmet.2017.01.009
- Chang, A. C., Mekhdjian, A. H., Morimatsu, M., Denisin, A. K., Pruitt, B. L., & Dunn, A. R. (2016). Single Molecule Force Measurements in Living Cells Reveal a Minimally Tensioned Integrin State. *ACS Nano*, 10(12), 10745–10752. doi: 10.1021/acsnano.6b03314

- Chatterjee, K., Pratiwi, F. W., Wu, F. C. M., Chen, P., & Chen, B. C. (2018). Recent Progress in Light Sheet Microscopy for Biological Applications. *Applied Spectroscopy*, *72*(8), 1137–1169. doi: 10.1177/0003702818778851
- Chow, K. H., Factor, R. E., & Ullman, K. S. (2012). The nuclear envelope environment and its cancer connections. *Nature Reviews Cancer*, *12*(3), 196–209. doi: 10.1038/nrc3219
- Clevers, H. (2016). Review Modeling Development and Disease with Organoids. *Cell*, *165*(7), 1586–1597. doi: 10.1016/j.cell.2016.05.082
- Clevers, H., Loh, K. M., & Nusse, R. (2014). An integral program for tissue renewal and regeneration: Wnt signaling and stem cell control. *Science*, *346*(6205). doi: 10.1126/science.1248012
- Cohen, O., Filetti, S., Castaneda, J., Maranghi, M., & Glandt, M. (2016). When intensive insulin therapy (MDi) fails in patients with type 2 diabetes: Switching to GLP-1 receptor agonist versus insulin pump. *Diabetes Care*, *39*(August), S180–S186. doi: 10.2337/dcS15-3029
- Cole, L., Anderson, M., Antin, P. B., & Limesand, S. W. (2009). One process for pancreatic  $\beta$ -cell coalescence into islets involves an epithelial–mesenchymal transition. *Journal of Endocrinology*, *203*(1), 19–31. doi: 10.1677/JOE-09-0072
- Coons, A. H., & Kaplan, M. H. (1950). LOCALIZATION OF ANTIGEN IN TISSUE CELLS. *Journal of Experimental Medicine*, *91*(1), 1–13. doi: 10.1084/jem.91.1.1
- Da Silva Xavier, G. (2018). The Cells of the Islets of Langerhans. *Journal of Clinical Medicine*, *7*(3), 54. doi: 10.3390/jcm7030054
- Dassaye, R., Naidoo, S., & Cerf, M. E. (2016). Transcription factor regulation of pancreatic organogenesis, differentiation and maturation. *Islets*, *8*(1), 13–34. doi: 10.1080/19382014.2015.1075687
- De La Fuente, R., Namkung, W., Mills, A., & Verkman, A. S. (2008). Small-molecule screen identifies inhibitors of a human intestinal calcium-activated chloride channel. *Molecular Pharmacology*, *73*(3), 758–768. doi: 10.1124/mol.107.043208
- de Souza, N. (2009). Optical imaging in thick samples. *Nature Methods*, *6*(1), 35–35. doi: 10.1038/nmeth.f.241
- de Winter-De Groot, K. M., Janssens, H. M., van Uum, R. T., Dekkers, J. F., Berkers, G., Vonk, A., Kruisselbrink, E., Oppelaar, H., Vries, R., Clevers, H., Houwen, R. H. J., Escher, J. C., Elias, S. G., De Jonge, H. R., de Rijke, Y. B., Tiddens, H. A. W. M., van der Ent, C. K., & Beekman, J. M. (2018). Stratifying infants with cystic fibrosis for disease severity using intestinal organoid swelling as a biomarker of CFTR function. *European Respiratory Journal*, *52*(3). doi: 10.1183/13993003.02529-2017

- Debas, H. T. (1987). Gastrin. In *Clinical and Investigative Medicine* (Vol. 10, Issue 3). Elsevier Inc. doi: 10.1097/cej.0000000000000008
- Debnath, J., Muthuswamy, S. K., & Brugge, J. S. (2003). Morphogenesis and oncogenesis of MCF-10A mammary epithelial acini grown in three-dimensional basement membrane cultures. *Methods*, *30*(3), 256–268. doi: 10.1016/S1046-2023(03)00032-X
- Dekkers, J. F., Alieva, M., Wellens, L. M., Ariese, H. C. R., Jamieson, P. R., Vonk, A. M., Amatngalim, G. D., Hu, H., Oost, K. C., Snippert, H. J. G., Beekman, J. M., Wehrens, E. J., Visvader, J. E., Clevers, H., & Rios, A. C. (2019). High-resolution 3D imaging of fixed and cleared organoids. *Nature Protocols*, *14*(6), 1756–1771. doi: 10.1038/s41596-019-0160-8
- Dekkers, J. F., Berkers, G., Kruisselbrink, E., Vonk, A., De Jonge, H. R., Janssens, H. M., Bronsveld, I., Van De Graaf, E. A., Nieuwenhuis, E. E. S., Houwen, R. H. J., Vleggaar, F. P., Escher, J. C., De Rijke, Y. B., Majoor, C. J., Heijerman, H. G. M., De Winter-De Groot, K. M., Clevers, H., Van Der Ent, C. K., & Beekman, J. M. (2016). Characterizing responses to CFTR-modulating drugs using rectal organoids derived from subjects with cystic fibrosis. *Science Translational Medicine*, *8*(344). doi: 10.1126/scitranslmed.aad8278
- Dekkers, J. F., Wiegerinck, C. L., De Jonge, H. R., Bronsveld, I., Janssens, H. M., De Winter-De Groot, K. M., Brandsma, A. M., De Jong, N. W. M., Bijvelds, M. J. C., Scholte, B. J., Nieuwenhuis, E. E. S., Van Den Brink, S., Clevers, H., Van Der Ent, C. K., Middendorp, S., & Beekman, J. M. (2013). A functional CFTR assay using primary cystic fibrosis intestinal organoids. *Nature Medicine*, *19*(7), 939–945. doi: 10.1038/nm.3201
- Detmers, F. J. M., De Groot, B. L., Müller, E. M., Hinton, A., Konings, I. B. M., Sze, M., Flitsch, S. L., Grubmüller, H., & Deen, P. M. T. (2006). Quaternary ammonium compounds as water channel blockers: Specificity, potency, and site of action. *Journal of Biological Chemistry*, *281*(20), 14207–14214. doi: 10.1074/jbc.M513072200
- DiGruccio, M. R., Mawla, A. M., Donaldson, C. J., Noguchi, G. M., Vaughan, J., Cowing-Zitron, C., van der Meulen, T., & Huising, M. O. (2016). Comprehensive alpha, beta and delta cell transcriptomes reveal that ghrelin selectively activates delta cells and promotes somatostatin release from pancreatic islets. *Molecular Metabolism*, *5*(7), 449–458. doi: 10.1016/j.molmet.2016.04.007
- Dobrokhotov, O., Samsonov, M., Sokabe, M., & Hirata, H. (2018). Mechanoregulation and pathology of YAP/TAZ via Hippo and non-Hippo mechanisms. *Clinical and Translational Medicine*, *7*(1), 1–14. doi: 10.1186/s40169-018-0202-9
- Dolega, M. E., Delarue, M., Ingremeau, F., Prost, J., Delon, A., & Cappello, G. (2017). Cell-like pressure sensors reveal increase of mechanical stress towards the core of multicellular spheroids under compression. *Nature Communications*, *8*(May 2016), 1–9. doi: 10.1038/ncomms14056

- Donath, M. Y., & Shoelson, S. E. (2011). Type 2 diabetes as an inflammatory disease. *Nature Reviews Immunology*, *11*(2), 98–107. doi: 10.1038/nri2925
- Dorrell, C., Tarlow, B., Wang, Y., Canaday, P. S., Haft, A., Schug, J., Streeter, P. R., Finegold, M. J., Shenje, L. T., Kaestner, K. H., & Grompe, M. (2014). The organoid-initiating cells in mouse pancreas and liver are phenotypically and functionally similar. *Stem Cell Research*, *13*(2), 275–283. doi: 10.1016/j.scr.2014.07.006
- Dossena, M., Piras, R., Cherubini, A., Barilani, M., Dugnani, E., Salanitro, F., Moreth, T., Pampaloni, F., Piemonti, L., & Lazzari, L. (2020). Standardized GMP-compliant scalable production of human pancreas organoids. *Stem Cell Research & Therapy*, *11*(1), 94. doi: 10.1186/s13287-020-1585-2
- Doxey, A. C., Cheng, Z., Moffatt, B. A., & McConkey, B. J. (2010). Structural motif screening reveals a novel, conserved carbohydrate-binding surface in the pathogenesis-related protein PR-5d. *BMC Structural Biology*, *10*. doi: 10.1186/1472-6807-10-23
- Dupont, S., Morsut, L., Aragona, M., Enzo, E., Giulitti, S., Cordenonsi, M., Zanconato, F., Le Digabel, J., Forcato, M., Bicciato, S., Elvassore, N., & Piccolo, S. (2011). Role of YAP/TAZ in mechanotransduction. *Nature*, *474*(7350), 179–184. doi: 10.1038/nature10137
- Dutta, D., Heo, I., & Clevers, H. (2017). Disease Modeling in Stem Cell-Derived 3D Organoid Systems. *Trends in Molecular Medicine*, *23*(5), 393–410. doi: 10.1016/j.molmed.2017.02.007
- Edelblum, K. L., & Turner, J. R. (2015). Epithelial Cells: Structure, Transport, and Barrier Function. Structure, Transport, and Barrier Function. In *Mucosal Immunology: Fourth Edition (Fourth Edi, Vols. 1–2)*. Elsevier. doi: 10.1016/B978-0-12-415847-4.00012-4
- Edwards, M., Zwolak, A., Schafer, D. A., Sept, D., Dominguez, R., & Cooper, J. A. (2014). Capping protein regulators fine-tune actin assembly dynamics. *Nature Reviews Molecular Cell Biology*, *15*(10), 677–689. doi: 10.1038/nrm3869
- El-Gohary, Y., & Gittes, G. (2017). Structure of Islets and Vascular Relationship to the Exocrine Pancreas. *Pancreapedia: Exocrine Pancreas Knowledge Base*, *14*(1), 60–74. doi: 10.3998/panc.2017.10
- El-Hamamsy, M. H., Sharafeldin, N. A., El-Moselhy, T. F., & Tawfik, H. O. (2020). Design, synthesis, and molecular docking study of new monastrol analogues as kinesin spindle protein inhibitors. *Archiv Der Pharmazie*, *353*(8), 1–18. doi: 10.1002/ardp.202000060
- Eldeeb, M. A., Siva-Piragasam, R., Ragheb, M. A., Esmaili, M., Salla, M., & Fahlman, R. P. (2019). A molecular toolbox for studying protein degradation in mammalian cells. *Journal of Neurochemistry*, *151*(4), 520–533. doi: 10.1111/jnc.14838

- Fatehullah, A., Tan, S. H., & Barker, N. (2016). Organoids as an in vitro model of human development and disease. *Nature Cell Biology*, *18*(3), 246–254. doi: 10.1038/ncb3312
- Fedrizzi, L., Lim, D., & Carafoli, E. (2008). Calcium and signal transduction. *Biochemistry and Molecular Biology Education*, *36*(3), 175–180. doi: 10.1002/bmb.20187
- Fernández-Suárez, M., & Ting, A. Y. (2008). Fluorescent probes for super-resolution imaging in living cells. *Nature Reviews Molecular Cell Biology*, *9*(12), 929–943. doi: 10.1038/nrm2531
- Firestone, A. J., Weinger, J. S., Maldonado, M., Barlan, K., Langston, L. D., O'Donnell, M., Gelfand, V. I., Kapoor, T. M., & Chen, J. K. (2012). Small-molecule inhibitors of the AAA+ ATPase motor cytoplasmic dynein. *Nature*, *484*(7392), 125–129. doi: 10.1038/nature10936
- Foty, R. (2011). A simple hanging drop cell culture protocol for generation of 3D spheroids. *Journal of Visualized Experiments*, *51*, 2–6. doi: 10.3791/2720
- Fuchs, E., & Segre, J. A. (2000). Stem cells: A new lease on life. *Cell*, *100*(1), 143–155. doi: 10.1016/S0092-8674(00)81691-8
- Galvao, J., Davis, B., Tilley, M., Normando, E., Duchon, M. R., & Cordeiro, M. F. (2014). Unexpected low-dose toxicity of the universal solvent DMSO. *FASEB Journal*, *28*(3), 1317–1330. doi: 10.1096/fj.13-235440
- Garrod, D., & Chidgey, M. (2008). Desmosome structure, composition and function. *Biochimica et Biophysica Acta - Biomembranes*, *1778*(3), 572–587. doi: 10.1016/j.bbamem.2007.07.014
- Georgakopoulos, N., Prior, N., Angres, B., Mastrogiovanni, G., Cagan, A., Harrison, D., Hindley, C. J., Arnes-Benito, R., Liau, S., Curd, A., Ivory, N., Simons, B. D., Martincorena, I., Wurst, H., Saeb-Parsy, K., & Huch, M. (2020). Long-term expansion, genomic stability and in vivo safety of adult human pancreas organoids. *BMC Developmental Biology*, *20*(1), 4. doi: 10.1186/s12861-020-0209-5
- George, N. M., Day, C. E., Boerner, B. P., Johnson, R. L., & Sarvetnick, N. E. (2012). Hippo Signaling Regulates Pancreas Development through Inactivation of Yap. *Molecular and Cellular Biology*, *32*(24), 5116–5128. doi: 10.1128/MCB.01034-12
- Gjorevski, N., & Lutolf, M. P. (2017). Synthesis and characterization of well-defined hydrogel matrices and their application to intestinal stem cell and organoid culture. *Nature Protocols*, *12*(11), 2263–2274. doi: 10.1038/nprot.2017.095
- Gjorevski, N., Sachs, N., Manfrin, A., Giger, S., Bragina, M. E., Ordóñez-Morán, P., Clevers, H., & Lutolf, M. P. (2016). Designer matrices for intestinal stem cell and organoid culture. *Nature*, *539*(7630), 560–564. doi: 10.1038/nature20168

- Goldmann, W. H. (2018). Intermediate filaments and cellular mechanics. *Cell Biology International*, *42*(2), 132–138. doi: 10.1002/cbin.10879
- Gouzi, M., Kim, Y. H., Katsumoto, K., Johansson, K., & Grapin-Botton, A. (2011). Neurogenin3 initiates stepwise delamination of differentiating endocrine cells during pancreas development. *Developmental Dynamics*, *240*(3), 589–604. doi: 10.1002/dvdy.22544
- Gradwohl, G., Dierich, A., LeMeur, M., & Guillemot, F. (2000). Neurogenin3 Is Required for the Development of the Four Endocrine Cell Lineages of the Pancreas. *Proceedings of the National Academy of Sciences of the United States of America*, *97*(4), 1607–1611. doi: 10.1073/pnas.97.4.1607
- Grapin-Botton, A. (2005). Ductal cells of the pancreas. *International Journal of Biochemistry and Cell Biology*, *37*(3), 504–510. doi: 10.1016/j.biocel.2004.07.010
- Greggio, C., De Franceschi, F., Figueiredo-Larsen, M., Gobaa, S., Ranga, A., Semb, H., Lutolf, M., & Grapin-Botton, A. (2013). Artificial three-dimensional niches deconstruct pancreas development in vitro. *Development*, *140*, 4452–4462. doi: 10.1242/dev.096628
- Gu, D., & Sarvetnick, N. (1993). Epithelial cell proliferation and islet neogenesis in IFN- $\gamma$  transgenic mice. *Development*, *118*(1), 33 LP – 46.
- Guo, Y. R., & MacKinnon, R. (2017). Structure-based membrane dome mechanism for piezo mechanosensitivity. *eLife*, *6*, 1–19. doi: 10.7554/eLife.33660
- Gurung, S., Werkmeister, J. A., & Gargett, C. E. (2015). Inhibition of Transforming Growth Factor- $\beta$  Receptor signaling promotes culture expansion of undifferentiated human Endometrial Mesenchymal Stem/stromal Cells. *Scientific Reports*, *5*(October), 27–31. doi: 10.1038/srep15042
- Hahn, S., Nam, M. O., Noh, J. H., Lee, D. H., Han, H. W., Kim, D. H., Hahm, K. B., Hong, S. P., Yoo, J. H., & Yoo, J. (2017). Organoid-based epithelial to mesenchymal transition (OEMT) model: From an intestinal fibrosis perspective. *Scientific Reports*, *7*(1), 1–11. doi: 10.1038/s41598-017-02190-5
- Hanson, G., & Hanson, B. (2008). Fluorescent Probes for Cellular Assays. *Combinatorial Chemistry & High Throughput Screening*, *11*(7), 505–513. doi: 10.2174/138620708785204090
- Hatzfeld, M., Keil, R., & Magin, T. M. (2017). Desmosomes and intermediate filaments: Their consequences for tissue mechanics. *Cold Spring Harbor Perspectives in Biology*, *9*(6). doi: 10.1101/cshperspect.a029157
- Hecksher-Sørensen, J., Riedel, D., Krull, J., Herrera, P. L., Berger, J., Collombat, P., Mansouri, A., & Serup, P. (2007). Embryonic endocrine pancreas and mature  $\beta$  cells acquire  $\alpha$  and PP

- cell phenotypes upon Arx misexpression. *Journal of Clinical Investigation*, 117(4), 961–970. doi: 10.1172/JCI29115DS1
- Held, M., Santeramo, I., Wilm, B., Murray, P., & Lévy, R. (2018). Ex vivo live cell tracking in kidney organoids using light sheet fluorescence microscopy. *PLOS ONE*, 13(7), e0199918. doi: 10.1371/journal.pone.0199918
- Heller, R. S., Jenny, M., Collombat, P., Mansouri, A., Tomasetto, C., Madsen, O. D., Mellitzer, G., Gradwohl, G., & Serup, P. (2005). Genetic determinants of pancreatic  $\epsilon$ -cell development. *Developmental Biology*, 286(1), 217–224. doi: 10.1016/j.ydbio.2005.06.041
- Herrera, P. L., Huarte, J., Zufferey, R., Nichols, A., Mermillod, B., Philippe, J., Muniesa, P., Sanvito, F., Orci, L., & Vassalli, J. D. (1994). Ablation of islet endocrine cells by targeted expression of hormone-promoter-driven toxigenes. *Proceedings of the National Academy of Sciences of the United States of America*, 91(26), 12999–13003. doi: 10.1073/pnas.91.26.12999
- Hill, J. T., Mastracci, T. L., Vinton, C., Doyle, M. L., Anderson, K. R., Loomis, Z. L., Schrunk, J. M., Minic, A. D., Prabakar, K. R., Pugliese, A., Sun, Y., Smith, R. G., & Sussel, L. (2009). Ghrelin is dispensable for embryonic pancreatic islet development and differentiation. *Regulatory Peptides*, 157(1–3), 51–56. doi: 10.1016/j.regpep.2009.02.013
- Hof, L., Moreth, T., Koch, M., Liebisch, T., Kurtz, M., Tarnick, J., Lissek, S. M., Verstegen, M. M. A., van der Laan, L. J. W., Huch, M., Matthäus, F., Stelzer, E. H. K., & Pampaloni, F. (2021). Long-term live imaging and multiscale analysis identify heterogeneity and core principles of epithelial organoid morphogenesis. *BMC Biology*, 19(1), 37. doi: 10.1186/s12915-021-00958-w
- Hof, L., Moreth, T., Koch, M., Liebisch, T., Kurtz, M., Tarnick, J., Lissek, S., Verstegen, M., van der Laan, L., Huch, M., Matthäus, F., Stelzer, E., & Pampaloni, F. (2020). Long-term live imaging of epithelial organoids and corresponding multiscale analysis reveal high heterogeneity and identify core regulatory principles. *BioRxiv*, 1–51. doi: 10.1101/2020.07.12.199463
- Höing, S., Yeh, T. Y., Baumann, M., Martinez, N. E., Habenberger, P., Kremer, L., Drexler, H. C. A., Küchler, P., Reinhardt, P., Choidas, A., Zischinsky, M. L., Zischinsky, G., Nandini, S., Ledray, A. P., Ketcham, S. A., Reinhardt, L., Abo-Rady, M., Glatza, M., King, S. J., ... Sternecker, J. (2018). Dynarrestin, a Novel Inhibitor of Cytoplasmic Dynein. *Cell Chemical Biology*, 25(4), 357–369.e6. doi: 10.1016/j.chembiol.2017.12.014
- Hötte, K., Koch, M., Hof, L., Tuppi, M., Moreth, T., Verstegen, M. M. A., van der Laan, L. J. W., Stelzer, E. H. K., & Pampaloni, F. (2019). Ultra-thin fluorocarbon foils optimise multiscale imaging of three-dimensional native and optically cleared specimens. *Scientific Reports*, 9(1), 1–13. doi: 10.1038/s41598-019-53380-2

- Huch, M., Bonfanti, P., Boj, S. F., Sato, T., Loomans, C. J. M., van de Wetering, M., Sojoodi, M., Li, V. S. W., Schuijers, J., Gracanin, A., Ringnalda, F., Begthel, H., Hamer, K., Mulder, J., van Es, J. H., de Koning, E., Vries, R. G. J., Heimberg, H., & Clevers, H. (2013). Unlimited in vitro expansion of adult bi-potent pancreas progenitors through the Lgr5/R-spondin axis. In *The EMBO journal* (Vol. 32, Issue 20, pp. 2708–2721). doi: 10.1038/emboj.2013.204
- Huch, M., Dorrell, C., Boj, S. F., Van Es, J. H., Li, V. S. W., Van De Wetering, M., Sato, T., Hamer, K., Sasaki, N., Finegold, M. J., Haft, A., Vries, R. G., Grompe, M., & Clevers, H. (2013). In vitro expansion of single Lgr5 + liver stem cells induced by Wnt-driven regeneration. *Nature*, 494(7436), 247–250. doi: 10.1038/nature11826
- Huch, M., Gehart, H., van Boxtel, R., Hamer, K., Blokzijl, F., Verstegen, M. M. A., Ellis, E., van Wenum, M., Fuchs, S. A., de Ligt, J., van de Wetering, M., Sasaki, N., Boers, S. J., Kemperman, H., de Jonge, J., Ijzermans, J. N. M., Nieuwenhuis, E. E. S., Hoekstra, R., Strom, S., ... Clevers, H. (2015). Long-Term Culture of Genome-Stable Bipotent Stem Cells from Adult Human Liver. *Cell*, 160(1–2), 299–312. doi: 10.1016/J.CELL.2014.11.050
- Hughes, C. S., Postovit, L. M., & Lajoie, G. a. (2010). Matrigel: a complex protein mixture required for optimal growth of cell culture. *Proteomics*, 10(9), 1886–1890. doi: 10.1002/pmic.200900758
- Huisken, J., Swoger, J., Del Bene, F., Wittbrodt, J., & Stelzer, E. H. K. (2004). Optical sectioning deep inside live embryos by selective plane illumination microscopy. *Science*, 305(5686), 1007–1009. doi: 10.1126/science.1100035
- Hynes, R. O., & Naba, A. (2012). Overview of the matrisome-An inventory of extracellular matrix constituents and functions. *Cold Spring Harbor Perspectives in Biology*, 4(1), 1–16. doi: 10.1101/cshperspect.a004903
- International Diabetes Federation. (2019). *IDF Diabetes Atlas, Ninth edition 2019*.
- Ivanov, A. I., Hopkins, A. M., Brown, G. T., Gerner-Smidt, K., Babbin, B. a, Parkos, C. a, & Nusrat, A. (2008). Myosin II regulates the shape of three-dimensional intestinal epithelial cysts. *Journal of Cell Science*, 121(Pt 11), 1803–1814. doi: 10.1242/jcs.015842
- Jaffe, A. B., Kaji, N., Durgan, J., & Hall, A. (2008). Cdc42 controls spindle orientation to position the apical surface during epithelial morphogenesis. *Journal of Cell Biology*, 183(4), 625–633. doi: 10.1083/jcb.200807121
- Jennings, R. E., Berry, A. A., Kirkwood-Wilson, R., Roberts, N. A., Hearn, T., Salisbury, R. J., Blaylock, J., Piper Hanley, K., & Hanley, N. A. (2013). Development of the Human Pancreas From Foregut to Endocrine Commitment. *Diabetes*, 62(10), 3514–3522. doi: 10.2337/db12-1479
- Jennings, R. E., Berry, A. A., Strutt, J. P., Gerrard, D. T., & Hanley, N. A. (2015). Human pancreas



- development. *Development*, 142(18), 3126–3137. doi: 10.1242/dev.120063
- Jevtić, P., Edens, L. J., Vuković, L. D., & Levy, D. L. (2014). Sizing and shaping the nucleus: Mechanisms and significance. *Current Opinion in Cell Biology*, 28(1), 16–27. doi: 10.1016/j.ceb.2014.01.003
- Jha, R. M., Kochanek, P. M., & Simard, J. M. (2019). Pathophysiology and treatment of cerebral edema in traumatic brain injury. *Neuropharmacology*, 145, 230–246. doi: 10.1016/j.neuropharm.2018.08.004
- Jiang, W., Li, M., Chen, Z., & Leong, K. W. (2016). Cell-laden microfluidic microgels for tissue regeneration. *Lab on a Chip*, 16(23), 4482–4506. doi: 10.1039/c6lc01193d
- Jørgensen, M. C., Ahnfelt-Rønne, J., Hald, J., Madsen, O. D., Serup, P., & Hecksher-Sørensen, J. (2007). An illustrated review of early pancreas development in the mouse. *Endocrine Reviews*, 28(6), 685–705. doi: 10.1210/er.2007-0016
- Kang, Y., Wang, Z., & Jin, P. (2017). Active DNA Demethylation in Neurodevelopment. In DNA Modifications in the Brain: Neuroepigenetic Regulation of Gene Expression. Elsevier Inc. doi: 10.1016/B978-0-12-801596-4.00003-4
- Kassis, T., Hernandez-Gordillo, V., Langer, R., & Griffith, L. G. (2019). OrgaQuant: Human Intestinal Organoid Localization and Quantification Using Deep Convolutional Neural Networks. *Scientific Reports*, 9(1), 1–7. doi: 10.1038/s41598-019-48874-y
- Keller, P. J., Schmidt, A. D., Santella, A., Khairy, K., Bao, Z., Wittbrodt, J., & Stelzer, E. H. K. (2010). Fast, high-contrast imaging of animal development with scanned light sheet-based structured-illumination microscopy. *Nature Methods*, 7(8), 637–642. doi: 10.1038/nmeth.1476
- Keller, P. J., Schmidt, A. D., Wittbrodt, J., & Stelzer, E. H. K. (2008). *Reconstruction of Zebrafish Early Light Sheet Microscopy*. 322(November), 1065–1069. doi: 10.1126/science.1162493
- Kelly, M., Trudel, S., Brouillard, F., Bouillaud, F., Colas, J., Nguyen-Khoa, T., Ollero, M., Edelman, A., & Fritsch, J. (2010). Cystic Fibrosis Transmembrane Regulator Inhibitors CFTR inh -172 and GlyH-101 Target Mitochondrial Functions, Independently of Chloride Channel Inhibition. *Journal of Pharmacology and Experimental Therapeutics*, 333(1), 60–69. doi: 10.1124/jpet.109.162032
- Kelm, J. M., Timmins, N. E., Brown, C. J., Fussenegger, M., & Nielsen, L. K. (2003). Method for generation of homogeneous multicellular tumor spheroids applicable to a wide variety of cell types. *Biotechnology and Bioengineering*, 83(2), 173–180. doi: 10.1002/bit.10655
- Kenyon, J., & Gerson, S. L. (2007). The role of DNA damage repair in aging of adult stem cells. *Nucleic Acids Research*, 35(22), 7557–7565. doi: 10.1093/nar/gkm1064

- Korinek, V., Barker, N., Moerer, P., Van Donselaar, E., Huls, G., Peters, P. J., & Clevers, H. (1998). Depletion of epithelial stem-cell compartments in the small intestine of mice lacking Tcf-4. *Nature Genetics*, *19*(4), 379–383. doi: 10.1038/1270
- Kretschmar, K., & Clevers, H. (2016). Organoids: Modeling Development and the Stem Cell Niche in a Dish. *Developmental Cell*, *38*(6), 590–600. doi: 10.1016/j.devcel.2016.08.014
- Ladoux, B., Nelson, W. J., Yan, J., & Mège, R. M. (2015). The mechanotransduction machinery at work at adherens junctions. *Integrative Biology (United Kingdom)*, *7*(10), 1109–1119. doi: 10.1039/c5ib00070j
- Ladoux, Benoit, & Mège, R. M. (2017). Mechanobiology of collective cell behaviours. *Nature Reviews Molecular Cell Biology*, *18*(12), 743–757. doi: 10.1038/nrm.2017.98
- Lancaster, M. A., & Huch, M. (2019). Disease modelling in human organoids. *Disease Models & Mechanisms*, *12*(7), dmm039347. doi: 10.1242/dmm.039347
- Lancaster, M. a., & Knoblich, J. a. (2014). Organogenesis in a dish: modeling development and disease using organoid technologies. *Science (New York, N.Y.)*, *345*, 1247125. doi: 10.1126/science.1247125
- Lancaster, M. A., Renner, M., Martin, C. A., Wenzel, D., Bicknell, L. S., Hurles, M. E., Homfray, T., Penninger, J. M., Jackson, A. P., & Knoblich, J. A. (2013). Cerebral organoids model human brain development and microcephaly. *Nature*, *501*(7467), 373–379. doi: 10.1038/nature12517
- Laurent, J., Blin, G., Chatelain, F., Vanneaux, V., Fuchs, A., Larghero, J., & Théry, M. (2017). Convergence of microengineering and cellular self-organization towards functional tissue manufacturing. *Nature Biomedical Engineering*, *1*(12), 939–956. doi: 10.1038/s41551-017-0166-x
- Legland, D., Arganda-Carreras, I., & Andrey, P. (2016). MorphoLibJ: Integrated library and plugins for mathematical morphology with ImageJ. *Bioinformatics*, *32*(22), 3532–3534. doi: 10.1093/bioinformatics/btw413
- Li, D. S., Yuan, Y. H., Tu, H. J., Liang, Q. Le, & Dail, L. J. (2009). A protocol for islet isolation from mouse pancreas. *Nature Protocols*, *4*(11), 1649–1652. doi: 10.1038/nprot.2009.150
- Li, J., Hou, B., Tumova, S., Muraki, K., Bruns, A., Ludlow, M. J., Sedo, A., Hyman, A. J., McKeown, L., Young, R. S., Yuldasheva, N. Y., Majeed, Y., Wilson, L. A., Rode, B., Bailey, M. A., Kim, H. R., Fu, Z., Carter, D. A. L., Bilton, J., ... Beech, D. J. (2014). Piezo1 integration of vascular architecture with physiological force. *Nature*, *515*(7526), 279–282. doi: 10.1038/nature13701
- Li, W., Gao, N., & Yang, M. (2017). The Structural Basis for Sensing by the Piezo1 Protein.

- Current Topics in Membranes*, 79, 135–158. doi: 10.1016/bs.ctm.2016.10.001
- Lian, I., Kim, J., Okazawa, H., Zhao, J., Zhao, B., Yu, J., Chinnaiyan, A., Israel, M. A., Goldstein, L. S. B., Abujarour, R., Ding, S., & Guan, K. L. (2010). The role of YAP transcription coactivator in regulating stem cell self-renewal and differentiation. *Genes and Development*, 24(11), 1106–1118. doi: 10.1101/gad.1903310
- Lin, Y. C., Guo, Y. R., Miyagi, A., Levring, J., MacKinnon, R., & Scheuring, S. (2019). Force-induced conformational changes in PIEZO1. *Nature*, 573(7773), 230–234. doi: 10.1038/s41586-019-1499-2
- Louchami, K., Best, L., Brown, P., Virreira, M., Hupkens, E., Perret, J., Devuyt, O., Uchida, S., Delporte, C., Malaisse, W. J., Beauwens, R., & Sener, A. (2012). A new role for aquaporin 7 in insulin secretion. *Cellular Physiology and Biochemistry*, 29(1–2), 65–74. doi: 10.1159/000337588
- Low, B. C., Pan, C. Q., Shivashankar, G. V., Bershadsky, A., Sudol, M., & Sheetz, M. (2014). YAP/TAZ as mechanosensors and mechanotransducers in regulating organ size and tumor growth. *FEBS Letters*, 588(16), 2663–2670. doi: 10.1016/j.febslet.2014.04.012
- Mahe, M. M., Aihara, E., Schumacher, M. A., Zavros, Y., Montrose, M. H., Helmrath, M. A., Sato, T., & Shroyer, N. F. (2013). Establishment of Gastrointestinal Epithelial Organoids. *Current Protocols in Mouse Biology*, 3(4), 217–240. doi: 10.1002/9780470942390.mo130179
- Maksimovic, S., Nakatani, M., Baba, Y., Nelson, A. M., Marshall, K. L., Wellnitz, S. A., Firozi, P., Woo, S. H., Ranade, S., Patapoutian, A., & Lumpkin, E. A. (2014). Epidermal Merkel cells are mechanosensory cells that tune mammalian touch receptors. *Nature*, 509(7502), 617–621. doi: 10.1038/nature13250
- Malekova, L., Tomaskova, J., Novakova, M., Stefanik, P., Kopacek, J., Lakatos, B., Pastorekova, S., Krizanova, O., Breier, A., & Ondrias, K. (2007). Inhibitory effect of DIDS, NPPB, and phloretin on intracellular chloride channels. *Pflugers Archiv European Journal of Physiology*, 455(2), 349–357. doi: 10.1007/s00424-007-0300-9
- Marunaka, Y. (2017). The mechanistic links between insulin and cystic fibrosis transmembrane conductance regulator (CFTR) Cl<sup>-</sup> channel. *International Journal of Molecular Sciences*, 18(8), 1–11. doi: 10.3390/ijms18081767
- Mastracci, T. L., & Sussel, L. (2012). The endocrine pancreas: Insights into development, differentiation, and diabetes. *Wiley Interdisciplinary Reviews: Developmental Biology*, 1(5), 609–628. doi: 10.1002/wdev.44
- Melis, N., Tauc, M., Cougnon, M., Bendahhou, S., Giuliano, S., Rubera, I., & Durantou, C. (2014). Revisiting CFTR inhibition: A comparative study of CFTRinh-172 and GlyH-101 inhibitors. *British Journal of Pharmacology*, 171(15), 3716–3727. doi: 10.1111/bph.12726

- Méndez-Giménez, L., Becerril, S., Camões, S. P., Da Silva, I. V., Rodrigues, C., Moncada, R., Valentí, V., Catalán, V., Gómez-Ambrosi, J., Miranda, J. P., Soveral, G., Frühbeck, G., & Rodríguez, A. (2017). Role of aquaporin-7 in ghrelin-and GLP-1-induced improvement of pancreatic  $\beta$ -cell function after sleeve gastrectomy in obese rats. *International Journal of Obesity*, *41*(9), 1394–1402. doi: 10.1038/ijo.2017.135
- Méndez-Giménez, Leire, Ezquerro, S., da Silva, I. V., Soveral, G., Frühbeck, G., & Rodríguez, A. (2018). Pancreatic Aquaporin-7: A Novel Target for Anti-diabetic Drugs? *Frontiers in Chemistry*, *6*(April), 1–10. doi: 10.3389/fchem.2018.00099
- Mitchison, T. J., Charras, G. T., & Mahadevan, L. (2008). Implications of a poroelastic cytoplasm for the dynamics of animal cell shape. *Seminars in Cell and Developmental Biology*, *19*(3), 215–223. doi: 10.1016/j.semcdb.2008.01.008
- Montal, M., Coste, B., Tully, D. C., Xu, J., Dubin, A. E., Engels, I. H., Schumacher, A. M., Mathur, J., Matzen, J., Bandell, M., Lao, J., Syeda, R., Huynh, T., Petrassi, H. M., & Patapoutian, A. (2015). Chemical activation of the mechanotransduction channel Piezo1. *ELife*, *4*, 1–11. doi: 10.7554/elife.07369
- Moroni, M., Servin-Vences, M. R., Fleischer, R., Sánchez-Carranza, O., & Lewin, G. R. (2018). Voltage gating of mechanosensitive PIEZO channels. *Nature Communications*, *9*(1), 1–15. doi: 10.1038/s41467-018-03502-7
- Morrone, L. A., Rombolà, L., Corasaniti, M. T., Bagetta, G., Nucci, C., & Russo, R. (2015). Natural compounds and retinal ganglion cell neuroprotection. In *Progress in Brain Research* (1st ed., Vol. 220). Elsevier B.V. doi: 10.1016/bs.pbr.2015.05.004
- Müller, T. D., Nogueiras, R., Andermann, M. L., Andrews, Z. B., Anker, S. D., Argente, J., Batterham, R. L., Benoit, S. C., Bowers, C. Y., Broglio, F., Casanueva, F. F., D'Alessio, D., Depoortere, I., Geliebter, A., Ghigo, E., Cole, P. A., Cowley, M., Cummings, D. E., Dagher, A., ... Tschöp, M. H. (2015). Ghrelin. *Molecular Metabolism*, *4*(6), 437–460. doi: 10.1016/j.molmet.2015.03.005
- Muroyama, A., & Lechler, T. (2017). Microtubule organization, dynamics and functions in differentiated cells. *Development (Cambridge)*, *144*(17), 3012–3021. doi: 10.1242/dev.153171
- Murtaugh, L. C. (2007). Pancreas and beta-cell development: from the actual to the possible. *Development (Cambridge, England)*, *134*(3), 427–438. doi: 10.1242/dev.02770
- Newell-Litwa, K. A., Horwitz, R., & Lamers, M. L. (2015). Non-Muscle myosin II in disease: Mechanisms and therapeutic opportunities. *DMM Disease Models and Mechanisms*, *8*(12), 1495–1515. doi: 10.1242/dmm.022103
- Nourse, J. L., & Pathak, M. M. (2017). How cells channel their stress: Interplay between Piezo1

- and the cytoskeleton. *Seminars in Cell and Developmental Biology*, 71, 3–12. doi: 10.1016/j.semcdb.2017.06.018
- Okamoto, R., Shimizu, H., Suzuki, K., Kawamoto, A., Takahashi, J., Kawai, M., Nagata, S., Hiraguri, Y., Takeoka, S., Sugihara, H. Y., Yui, S., & Watanabe, M. (2020). Organoid-based regenerative medicine for inflammatory bowel disease. *Regenerative Therapy*, 13, 1–6. doi: 10.1016/j.reth.2019.11.004
- Ovečka, M., von Wangenheim, D., Tomančák, P., Šamajová, O., Komis, G., & Šamaj, J. (2018). Multiscale imaging of plant development by light-sheet fluorescence microscopy. *Nature Plants*, 4(9), 639–650. doi: 10.1038/s41477-018-0238-2
- Pache, J. C. (2006). Epidermal Growth Factors. *Encyclopedia of Respiratory Medicine, Four-Volume Set, 2*, 129–133. doi: 10.1016/B0-12-370879-6/00138-1
- Pal, R., Mamidi, M. K., Das, A. K., & Bhonde, R. (2012). Diverse effects of dimethyl sulfoxide (DMSO) on the differentiation potential of human embryonic stem cells. *Archives of Toxicology*, 86(4), 651–661. doi: 10.1007/s00204-011-0782-2
- Pampaloni, F., Ansari, N., & Stelzer, E. H. K. (2013). High-resolution deep imaging of live cellular spheroids with light-sheet-based fluorescence microscopy. In *Cell and Tissue Research* (Vol. 352, Issue 1, pp. 161–177). doi: 10.1007/s00441-013-1589-7
- Pampaloni, F., Reynaud, E. G., & Stelzer, E. H. K. (2007). The third dimension bridges the gap between cell culture and live tissue. *Nature Reviews Molecular Cell Biology*, 8(10), 839–845. doi: 10.1038/nrm2236
- Pan, F. C., & Brissova, M. (2014). Pancreas development in humans. *Current Opinion in Endocrinology, Diabetes and Obesity*, 21(2), 77–82. doi: 10.1097/MED.0000000000000047
- Parker, K. H., Beury, D. W., & Ostrand-Rosenberg, S. (2015). Myeloid-Derived Suppressor Cells: Critical Cells Driving Immune Suppression in the Tumor Microenvironment. In *Advances in Cancer Research* (1st ed., Vol. 128). Elsevier Inc. doi: 10.1016/bs.acr.2015.04.002
- Pastorekova, S., Parkkila, S., Pastorek, J., & Supuran, C. T. (2004). Carbonic anhydrases: Current state of the art, therapeutic applications and future prospects. *Journal of Enzyme Inhibition and Medicinal Chemistry*, 19(3), 199–229. doi: 10.1080/14756360410001689540
- Pathak, M. M., Nourse, J. L., Tran, T., Hwe, J., Arulmoli, J., Le, D. T. T., Bernardis, E., Flanagan, L. A., & Tombola, F. (2014). Stretch-activated ion channel Piezo1 directs lineage choice in human neural stem cells. *Proceedings of the National Academy of Sciences*, 111(45), 16148–16153. doi: 10.1073/pnas.1409802111

- Pathak, V., Pathak, N. M., O'Neill, C. L., Guduric-Fuchs, J., & Medina, R. J. (2019). Therapies for Type 1 Diabetes: Current Scenario and Future Perspectives. *Clinical Medicine Insights: Endocrinology and Diabetes*, *12*. doi: 10.1177/1179551419844521
- Paul, A. S., & Pollard, T. D. (2009). Review of the mechanism of processive actin filament elongation by formins. *Cell Motility and the Cytoskeleton*, *66*(8), 606–617. doi: 10.1002/cm.20379
- Pećina-Šlaus, N. (2003). Tumor suppressor gene E-cadherin and its role in normal and malignant cells. *Cancer Cell International*, *3*, 1–7. doi: 10.1186/1475-2867-3-17
- Pence, I., & Mahadevan-Jansen, A. (2016). Clinical instrumentation and applications of Raman spectroscopy. *Chemical Society Reviews*, *45*(7), 1958–1979. doi: 10.1039/c5cs00581g
- Piccolo, S., Dupont, S., & Cordenonsi, M. (2014). The biology of YAP/TAZ: Hippo signaling and beyond. *Physiological Reviews*, *94*(4), 1287–1312. doi: 10.1152/physrev.00005.2014
- Pin, C., & Fenech, M. (2017). Development of the Pancreas 1 . Morphological development – from endoderm to definitive pancreas. *Pancreapedia: Exocrine Pancreas Knowledge Base*. doi: 10.3998/panc.2017.09
- Preibisch, S., Saalfeld, S., & Tomancak, P. (2009). Globally optimal stitching of tiled 3D microscopic image acquisitions. *Bioinformatics*, *25*(11), 1463–1465. doi: 10.1093/bioinformatics/btp184
- Prestwich, G. D. (2007). Simplifying the extracellular matrix for 3-D cell culture and tissue engineering: A pragmatic approach. *Journal of Cellular Biochemistry*, *101*(6), 1370–1383. doi: 10.1002/jcb.21386
- Prochazkova, M., Chavez, M. G., Prochazka, J., Felfy, H., Mushegyan, V., & Klein, O. D. (2015). Embryonic Versus Adult Stem Cells. In *Stem Cell Biology and Tissue Engineering in Dental Sciences*. Elsevier Inc. doi: 10.1016/B978-0-12-397157-9.00020-5
- Ranade, S. S., Qiu, Z., Woo, S. H., Hur, S. S., Murthy, S. E., Cahalan, S. M., Xu, J., Mathur, J., Bandell, M., Coste, B., Li, Y. S. J., Chien, S., & Patapoutian, A. (2014). Piezo1, a mechanically activated ion channel, is required for vascular development in mice. *Proceedings of the National Academy of Sciences of the United States of America*, *111*(28), 10347–10352. doi: 10.1073/pnas.1409233111
- Ranade, S. S., Woo, S. H., Dubin, A. E., Moshourab, R. A., Wetzel, C., Petrus, M., Mathur, J., Bégay, V., Coste, B., Mainquist, J., Wilson, A. J., Francisco, A. G., Reddy, K., Qiu, Z., Wood, J. N., Lewin, G. R., & Patapoutian, A. (2014). Piezo2 is the major transducer of mechanical forces for touch sensation in mice. *Nature*, *516*(729), 121–125. doi: 10.1038/nature13980
- Remedi, M. S., & Emfinger, C. (2016). Pancreatic  $\beta$ -cell identity in diabetes. *Diabetes, Obesity*

- and Metabolism*, 18(September), 110–116. doi: 10.1111/dom.12727
- Rosa, J. P., Raslova, H., & Bryckaert, M. (2019). Filamin A: Key actor in platelet biology. *Blood*, 134(16), 1279–1288. doi: 10.1182/blood.2019000014
- Rossinelli, D., Fourestey, G., Schmidt, F., Busse, B., & Kurtcuoglu, V. (2020). High-throughput lossy-to-lossless 3D image compression. *IEEE Transactions on Medical Imaging*, PP. doi: 10.1109/TMI.2020.3033456
- Rosso, F., Giordano, A., Barbarisi, M., & Barbarisi, A. (2004). From Cell-ECM Interactions to Tissue Engineering. *Journal of Cellular Physiology*, 199(2), 174–180. doi: 10.1002/jcp.10471
- Ructural, S. T., & Lo, B. I. O. (2018). Force-activated ion channels in close-up. *Nature*, 554, 469–470. doi: 10.1038/d41586-018-01631-z
- Rukstalis, J. M., & Habener, J. F. (2009). Neurogenin3: a master regulator of pancreatic islet differentiation and regeneration. *Islets*, 1(3), 177–184. doi: 10.4161/isl.1.3.9877
- Ryan, E. A., Lakey, J. R. T., Rajotte, R. V., Korbitt, G. S., Kin, T., Imes, S., Rabinovitch, A., Elliott, J. F., Bigam, D., Kneteman, N. M., Warnock, G. L., Larsen, I., & Shapiro, A. M. J. (2001). Clinical outcomes and insulin secretion after islet transplantation with the edmonton protocol. *Diabetes*, 50(4), 710–719. doi: 10.2337/diabetes.50.4.710
- Salinno, C., Cota, P., Bastidas-Ponce, A., Tarquis-Medina, M., Lickert, H., & Bakhti, M. (2019).  $\beta$ -Cell Maturation and Identity in Health and Disease. *International Journal of Molecular Sciences*, 20(21), 1–19. doi: 10.3390/ijms20215417
- Sanghvi-Shah, R., & Weber, G. F. (2017). Intermediate filaments at the junction of mechanotransduction, migration, and development. *Frontiers in Cell and Developmental Biology*, 5(SEP), 1–19. doi: 10.3389/fcell.2017.00081
- Santos, N. C., Figueira-Coelho, J., Martins-Silva, J., & Saldanha, C. (2003). Multidisciplinary utilization of dimethyl sulfoxide: Pharmacological, cellular, and molecular aspects. *Biochemical Pharmacology*, 65(7), 1035–1041. doi: 10.1016/S0006-2952(03)00002-9
- Sato, T., Vries, R. G., Snippert, H. J., van de Wetering, M., Barker, N., Stange, D. E., van Es, J. H., Abo, A., Kujala, P., Peters, P. J., & Clevers, H. (2009). Single Lgr5 stem cells build crypt-villus structures in vitro without a mesenchymal niche. *Nature*, 459(7244), 262–265. doi: 10.1038/nature07935
- Schlaermann, P., Toelle, B., Berger, H., Schmidt, S. C., Glanemann, M., Ordemann, J., Bartfeld, S., Mollenkopf, H. J., & Meyer, T. F. (2016). A novel human gastric primary cell culture system for modelling *Helicobacter pylori* infection in vitro. *Gut*, 65(2), 202–213. doi: 10.1136/gutjnl-2014-307949

- Schmitz, A., Fischer, S. C., Mattheyer, C., Pampaloni, F., & Stelzer, E. H. K. (2017). Multiscale image analysis reveals structural heterogeneity of the cell microenvironment in homotypic spheroids. *Scientific Reports*, 7(January), 43693. doi: 10.1038/srep43693
- Schwank, G., Andersson-Rolf, A., Koo, B. K., Sasaki, N., & Clevers, H. (2013). Generation of BAC Transgenic Epithelial Organoids. *PLoS ONE*, 8(10), 6–11. doi: 10.1371/journal.pone.0076871
- Sebrell, T. A., Sidar, B., Bruns, R., Wilkinson, R. A., Wiedenheft, B., Taylor, P. J., Perrino, B. A., Samuelson, L. C., Wilking, J. N., & Bimczok, D. (2018). Live imaging analysis of human gastric epithelial spheroids reveals spontaneous rupture, rotation and fusion events. *Cell and Tissue Research*, 371(2), 293–307. doi: 10.1007/s00441-017-2726-5
- Semino, C. E., Merok, J. R., Crane, G. G., Panagiotakos, G., & Zhang, S. (2003). Functional differentiation of hepatocyte-like spheroid structures from putative liver progenitor cells in three-dimensional peptide scaffolds. *Differentiation*, 71(4–5), 262–270. doi: 10.1046/j.1432-0436.2003.7104503.x
- Serban, M. A., Liu, Y., & Prestwich, G. D. (2008). Effects of extracellular matrix analogues on primary human fibroblast behavior. *Acta Biomaterialia*, 4(1), 67–75. doi: 10.1016/j.actbio.2007.09.006
- Serra, D., Mayr, U., Boni, A., Lukonin, I., Rempfler, M., Challet Meylan, L., Stadler, M. B., Strnad, P., Papasaikas, P., Vischi, D., Waldt, A., Roma, G., & Liberali, P. (2019). Self-organization and symmetry breaking in intestinal organoid development. *Nature*. doi: 10.1038/s41586-019-1146-y
- Serrador, J. M., Nieto, M., & Sánchez-Madrid, F. (1999). Cytoskeletal rearrangement during migration and activation of T lymphocytes. *Trends in Cell Biology*, 9(6), 228–233. doi: 10.1016/S0962-8924(99)01553-6
- Sharma, M., Reif, G. A., & Wallace, D. P. (2019). In vitro cyst formation of ADPKD cells. In *Methods in Cell Biology* (1st ed., Vol. 153). Elsevier Inc. doi: 10.1016/bs.mcb.2019.05.008
- Shi, Y., Inoue, H., Wu, J. C., & Yamanaka, S. (2017). Induced pluripotent stem cell technology: A decade of progress. *Nature Reviews Drug Discovery*, 16(2), 115–130. doi: 10.1038/nrd.2016.245
- Spurlin, J. W., & Nelson, C. M. (2017). Building branched tissue structures: From single cell guidance to coordinated construction. *Philosophical Transactions of the Royal Society B: Biological Sciences*, 372(1720). doi: 10.1098/rstb.2015.0527
- Stelzer, E. H. K. (2014). Light-sheet fluorescence microscopy for quantitative biology. *Nature Methods*, 12(1), 23–26. doi: 10.1038/nmeth.3219



- Storm, C., Pastore, J. J., MacKintosh, F. C., Lubensky, T. C., & Janmey, P. A. (2005). Nonlinear elasticity in biological gels. *Nature*, *435*(7039), 191–194. doi: 10.1038/nature03521
- Strobl, F., Schmitz, A., & Stelzer, E. H. K. (2015). Live imaging of *Tribolium castaneum* embryonic development using light-sheet-based fluorescence microscopy. *Nature Protocols*, *10*(10), 1486–1507. doi: 10.1038/nprot.2015.093
- Stylianopoulos, T. (2017). The Solid Mechanics of Cancer and Strategies for Improved Therapy. *Journal of Biomechanical Engineering*, *139*(2), 1–10. doi: 10.1115/1.4034991
- Stylianopoulos, T., Martin, J. D., Chauhan, V. P., Jain, S. R., Diop-Frimpong, B., Bardeesy, N., Smith, B. L., Ferrone, C. R., Hornicek, F. J., Boucher, Y., Munn, L. L., & Jain, R. K. (2012). Causes, consequences, and remedies for growth-induced solid stress in murine and human tumors. *Proceedings of the National Academy of Sciences of the United States of America*, *109*(38), 15101–15108. doi: 10.1073/pnas.1213353109
- Sun, Z., Costell, M., & Fässler, R. (2019). Integrin activation by talin, kindlin and mechanical forces. *Nature Cell Biology*, *21*(1), 25–31. doi: 10.1038/s41556-018-0234-9
- Sun, Z., Guo, S. S., & Fässler, R. (2016). Integrin-mediated mechanotransduction. *Journal of Cell Biology*, *215*(4), 445–456. doi: 10.1083/jcb.201609037
- Susaki, E. a, Tainaka, K., Perrin, D., Yukinaga, H., Kuno, A., & Ueda, H. R. (2015). Advanced CUBIC protocols for whole-brain and whole-body clearing and imaging. *Nature Protocols*, *10*(11), 1709–1727. doi: 10.1038/nprot.2015.085
- Sussel, L., Kalamaras, J., Hartigan-O'Connor, D. J., Meneses, J. J., Pedersen, R. A., Rubenstein, J. L. R., & German, M. S. (1998). Mice lacking the homeodomain transcription factor Nkx2.2 have diabetes due to arrested differentiation of pancreatic  $\beta$  cells. *Development*, *125*(12), 2213–2221.
- Sutera, S. P., & Krogstad, D. J. (1991). Reduction of the surface-volume ratio: A physical mechanism contributing to the loss of red cell deformability in malaria. *Biorheology*, *28*(3–4), 221–229. doi: 10.3233/BIR-1991-283-413
- Takahashi, K., & Yamanaka, S. (2006). Induction of pluripotent stem cells from mouse embryonic and adult fibroblast cultures by defined factors. *Cell*, *126*(4), 663–676. doi: 10.1016/j.cell.2006.07.024
- Takeda, N., Jain, R., Li, D., Li, L., Lu, M. M., & Epstein, J. A. (2013). Lgr5 Identifies Progenitor Cells Capable of Taste Bud Regeneration after Injury. *PLoS ONE*, *8*(6), 1–8. doi: 10.1371/journal.pone.0066314
- Takeichi, M. (2014). Dynamic contacts: Rearranging adherens junctions to drive epithelial remodelling. *Nature Reviews Molecular Cell Biology*, *15*(6), 397–410. doi:

10.1038/nrm3802

- Terai, T., & Nagano, T. (2008). Fluorescent probes for bioimaging applications. *Current Opinion in Chemical Biology*, *12*(5), 515–521. doi: 10.1016/j.cbpa.2008.08.007
- Thiele, J., Ma, Y., Bruekers, S. M. C., Ma, S., & Huck, W. T. S. (2014). 25th anniversary article: Designer hydrogels for cell cultures: A materials selection guide. *Advanced Materials*, *26*(1), 125–148. doi: 10.1002/adma.201302958
- Thomasy, S. M., Morgan, J. T., Wood, J. A., Murphy, C. J., & Russell, P. (2013). Substratum stiffness and latrunculin B modulate the gene expression of the mechanotransducers YAP and TAZ in human trabecular meshwork cells. *Experimental Eye Research*, *113*(June), 66–73. doi: 10.1016/j.exer.2013.05.014
- Trepat, X., Chen, Z., & Jacobson, K. (2012). Cell migration. *Comprehensive Physiology*, *2*(4), 2369–2392. doi: 10.1002/cphy.c110012
- Trepat, X., & Sahai, E. (2018). Mesoscale physical principles of collective cell organization. *Nature Physics*, *14*(7), 671–682. doi: 10.1038/s41567-018-0194-9
- Turunen, S. P., Tatti-Bugaeva, O., & Lehti, K. (2017). Membrane-type matrix metalloproteases as diverse effectors of cancer progression. *Biochimica et Biophysica Acta - Molecular Cell Research*, *1864*(11), 1974–1988. doi: 10.1016/j.bbamcr.2017.04.002
- Valdez, I. A., Teo, A. K. K., & Kulkarni, R. N. (2015). Cellular stress drives pancreatic plasticity. *Science Translational Medicine*, *7*(273), 273ps2. doi: 10.1126/scitranslmed.3010577
- Verkman, A. S. (2013). Aquaporins. *Current Biology*, *23*(2), 52–55. doi: 10.1016/j.cub.2012.11.025
- Vicente-Manzanares, M., & Horwitz, A. R. (2011). Adhesion dynamics at a glance. *Journal of Cell Science*, *124*(23), 3923–3927. doi: 10.1242/jcs.095653
- Vinet, L., & Zhedanov, A. (2019). Mechano-modulatory synthetic niches for liver organoid derivation. *Journal of Physics A: Mathematical and Theoretical*, *44*(8), 1–13. doi: 10.1101/810275
- Wang, Y., Dorrell, C., Naugler, W. E., Heskett, M., Spellman, P., Li, B., Galivo, F., Haft, A., Wakefield, L., & Grompe, M. (2018). Long-Term Correction of Diabetes in Mice by In Vivo Reprogramming of Pancreatic Ducts. *Molecular Therapy*, *26*(5), 1327–1342. doi: 10.1016/j.ymthe.2018.02.014
- Warshauer, J. T., Bluestone, J. A., & Anderson, M. S. (2020). New Frontiers in the Treatment of Type 1 Diabetes. *Cell Metabolism*, *31*(1), 46–61. doi: 10.1016/j.cmet.2019.11.017

- Werb, Z. (1997). ECM and cell surface proteolysis: Regulating cellular ecology. *Cell*, *91*(4), 439–442. doi: 10.1016/S0092-8674(00)80429-8
- Williams, J. A. (2010). Regulation of acinar cell function in the pancreas. *Current Opinion in Gastroenterology*, *26*(5), 478–483. doi: 10.1097/MOG.0b013e32833d11c6
- Winograd-Katz, S. E., Fässler, R., Geiger, B., & Legate, K. R. (2014). The integrin adhesome: From genes and proteins to human disease. *Nature Reviews Molecular Cell Biology*, *15*(4), 273–288. doi: 10.1038/nrm3769
- Woo, S. H., Ranade, S., Weyer, A. D., Dubin, A. E., Baba, Y., Qiu, Z., Petrus, M., Miyamoto, T., Reddy, K., Lumpkin, E. A., Stucky, C. L., & Patapoutian, A. (2014). Piezo2 is required for Merkel-cell mechanotransduction. *Nature*, *509*(7502), 622–626. doi: 10.1038/nature13251
- Xu, X., D'Hoker, J., Stangé, G., Bonn e, S., De Leu, N., Xiao, X., Van De Castele, M., Mellitzer, G., Ling, Z., Pipeleers, D., Bouwens, L., Scharfmann, R., Gradwohl, G., & Heimberg, H. (2008).  $\beta$  Cells Can Be Generated from Endogenous Progenitors in Injured Adult Mouse Pancreas. *Cell*, *132*(2), 197–207. doi: 10.1016/j.cell.2007.12.015
- Yamada, K. M., & Sixt, M. (2019). Mechanisms of 3D cell migration. *Nature Reviews Molecular Cell Biology*, *20*(12), 738–752. doi: 10.1038/s41580-019-0172-9
- Yang, J., Zhang, Y. S., Yue, K., & Khademhosseini, A. (2017). Cell-laden hydrogels for osteochondral and cartilage tissue engineering. *Acta Biomaterialia*, *57*, 1–25. doi: 10.1016/j.actbio.2017.01.036
- Zaret, K. S., & Grompe, M. (2008). Generation and regeneration of cells of the liver and pancreas. *Science*, *322*(5907), 1490–1494. doi: 10.1126/science.1161431
- Zhang, J., McKenna, L. B., Bogue, C. W., & Kaestner, K. H. (2014). The diabetes gene Hhex maintains  $\delta$ -cell differentiation and islet function. *Genes and Development*, *28*(8), 829–834. doi: 10.1101/gad.235499.113
- Zhou, H., Wu, S., Joo, J. Y., Zhu, S., Han, D. W., Lin, T., Trauger, S., Bien, G., Yao, S., Zhu, Y., Siuzdak, G., Sch oler, H. R., Duan, L., & Ding, S. (2009). Generation of Induced Pluripotent Stem Cells Using Recombinant Proteins. *Cell Stem Cell*, *4*(5), 381–384. doi: 10.1016/j.stem.2009.04.005
- Zhu, J., & Mogilner, A. (2016). Comparison of cell migration mechanical strategies in three-dimensional matrices: A computational study. *Interface Focus*, *6*(5). doi: 10.1098/rsfs.2016.0040
- Zhu, Y., Liu, Q., Zhou, Z., & Ikeda, Y. (2017). PDX1, Neurogenin-3, and MAFA: Critical transcription regulators for beta cell development and regeneration. *Stem Cell Research*

*and Therapy*, 8(1), 1–7. doi: 10.1186/s13287-017-0694-z

Zihni, C., Mills, C., Matter, K., & Balda, M. S. (2016). Tight junctions: From simple barriers to multifunctional molecular gates. *Nature Reviews Molecular Cell Biology*, 17(9), 564–580. doi: 10.1038/nrm.2016.80

## 9. Supplement

### 9.1. Movie description

**Movie 1: Growth of mPOs and hPOs recorded with the brightfield microscope.** Murine and human pancreas organoids were recorded over 6 days and 120 hours respectively. The formation of organoids from the initial seeded cell clusters, including cell cluster contraction, followed by lumen formation and expansion can be followed. After about 75 hours of observation the murine organoids reached their plateau-phase. The human organoids showed a constant growth over the complete recorded time. Microscope: Zeiss Cell Observer Z.1; objective: Plan-Apochromat 5x/0.16; voxel size: 1.29 x 1.29  $\mu\text{m}^2$ ; recording interval: 30 min; scale bar: 1000  $\mu\text{m}$ ; tile scan 3x3, 10 planes with a z-distance of 120  $\mu\text{m}$ , the tiles were fused with ImageJ/Fiji plugin (Preibisch et al., 2009) and subsequent maximum intensity projected (ImageJ/Fiji).

**Movie 2: MPO growth heterogeneity recorded with the brightfield microscope.** From left to right, four different growth behaviours were recorded: the contraction, subsequent lumen formation and expansion of a cell cluster, the behaviour of a dense and debris filled organoid that did not show a lumen formation or growth, a cell cluster which presents a fragment migration prior lumen formation, a fusion of three organoids and the subsequent luminal dynamics to merge to one organoid. The first two right sets show organoids recorded over 68 hours and the left two sets show organoids that were recorded for 35 hours. Microscope: Zeiss Cell Observer Z.1; objective: Plan-Apochromat 5x/0.16; voxel size: 1.29 x 1.29  $\mu\text{m}^2$ ; recording interval: 10 min; scale bar: 100  $\mu\text{m}$ , sets show close ups of a multi-position image series of 4 positions, 34 planes with a distance of 14  $\mu\text{m}$  and a total observation time of 433 time point (72 hours).

**Movie 3: One mPO that shed presumably dead cells into its lumen, recorded with the brightfield microscope.** One murine pancreas organoid was recorded that sheds cells from its epithelial layer into its lumen (indicated by the black arrows). This process was observed several times during the growth of the organoid. The excluded cell conglomerated at the bottom of the organoid. During the exclusion from the epithelial layer, the cells rounded up and decreased in size which is a common indicator of cell death. Microscope: Zeiss Cell Observer Z.1; objective: Plan-Apochromat 5x/0.16; voxel size: 1.29 x 1.29  $\mu\text{m}^2$ ; recording interval: 10 min; scale bar: 100  $\mu\text{m}$ , sets show close ups of a multi-position image series of 4 positions, 34 planes with a distance of 14  $\mu\text{m}$  and a total observation time of 433 time point (72 hours). Movie modified from (Jung and Moreth et al. 2021 (1))

**Movie 4: MPOs were treated with 5 different drugs and segmented with the brightfield segmentation pipeline.** 6 exemplary wells of murine organoids are shown that were recorded before (normal growth, 24 hours), during (treatment, 24 hours), and after the treatment (recovery, 24 hours) and subsequently segmented and tracked with the brightfield pipeline. From left to right, the control group without a treatment, Cytochalasin D, Para-Blebbistatin, Nocodazole, Paclitaxel and Yoda 1 treated organoids are shown. Each coloured circle indicates one segmented organoid. Organoids that were treated with Cytochalasin D, Nocodazole and Yoda 1 showed a fast size decrease. In the recovery phase, organoids treated with Nocodazole and Yoda1 showed a recover of its luminal phenotype whereas organoids treated with Cytochalasin D were not able to recover their luminal phenotype. Microscope: Zeiss Cell Observer Z.1; objective: Plan-Apochromat 5x/0.16; voxel size: 1.29 x 1.29  $\mu\text{m}^2$ ; recording interval: 30 min; scale bar: 1000  $\mu\text{m}$ ; tile scan 3x3, 10 planes with a z-distance of 120  $\mu\text{m}$ , Images were processed with the brightfield pipeline.

**Movie 5: Time-resolved observations of mPOs growing in the Z1-FEP- foil cuvette.** The organoids expressed Rosa26-nTnG (grey) as nuclei marker and were imaged over 6 days. The formation of organoids from the initially seeded cell clusters, including cell cluster contraction, cell polarisation, lumen formation and expansion can be followed. After about 100 hours of observation some mPOs begin to display signs of degeneration due to starvation. This process is indicated by overall shrinking of the organoid, followed by nuclear condensation and fading of the nuclei signal. Microscope: Zeiss Lightsheet Z.1; detection objective: W Plan-Apochromat 20x/1.0, illumination objective: Zeiss LSFM 10x/0.2; laser line: 561 nm; filters: laser block filter (LBF) 405/488/561; voxel size: 1.02 x 1.02 x 2.00  $\mu\text{m}^3$ ; complete FEP- foil cuvette is imaged by 2 tiles that were fused by hand. Shown is a Maximum Intensity projection (ImageJ/Fiji) of 871 z-slices per tile; recording interval: 30 min; total recorded intervals: 288; scale bar: 50  $\mu\text{m}$ .

**Movie 6: Time-resolved 3D volume rendering of the formation process of mPO.** One murine organoid expressed Rosa26-nTnG (grey) as nuclei marker was imaged during the formation process. The movie shows an excerpt of the first 10 hours from a recorded data set of 6 days. Cells were 3D-rendered, segmented and tracked with Arivis Vision4D. The initial processes of cell cluster contraction followed by the initiation and establishment of a lumen is shown. The segmentation and tracking of the cell nuclei revealed that not all cells of the initial cell cluster participated in the lumen formation. Further, it is shown that the contraction is a highly dynamic process in which all cells of the developing organoid are involved. Microscope: Zeiss Lightsheet Z.1; detection objective: W Plan-Apochromat 20x/1.0, illumination objective: Zeiss LSFM 10x/0.2; laser line: 561 nm; filters: laser block filter (LBF) 405/488/561; voxel size: 1.02 x 1.02 x 2.00  $\mu\text{m}^3$ ; recording interval: 30 min; 3D rendering and tracking software: Arivis Vision4D.

**Movie 7: Time-resolved 3D volume rendering of the fusion process of two organoids.** Two murine organoids expressing Rosa26-nTnG (grey) as nuclei marker were imaged during the fusion process. The movie shows an excerpt of 4 hours from a recorded

data set of 6 days. Cells were 3D-rendered with Arivis Vision4D to enable a detailed inspection of the fusion process. After the epithelial monolayers of both organoids touched, they began to form an opening that connects lumen within one hour. This opening then expanded while cells migrated into one connected monolayer. Short after the connection is established one cell nuclei became visible which travelled from the small organoid into the big organoid. This proof that the connection enables the exchange of material. Microscope: Zeiss Lightsheet Z.1; detection objective: W Plan-Apochromat 20x/1.0, illumination objective: Zeiss LSFM 10x/0.2; laser line: 561 nm; filters: laser block filter (LBF) 405/488/561; voxel size: 1.02 x 1.02 x 2.00  $\mu\text{m}^3$ ; recording interval: 30 min; 3D rendering software: Arivis Vision4D.

**Movie 8: Time resolved observation of two mPOs that showed different cell densities and nucleus sizes.** Both organoids expressed Rosa26-nTnG (grey) as nuclei marker and were imaged over 91 hours within the FEP-foil cuvette. The initial formation from the seeded cell clusters, the subsequent lumen establishment and the final expansion of both organoids are shown. While both organoids showed comparable cell nuclei sizes at the beginning, the right organoid became dense packed, and the left organoid became loose packed with increasing time. After 91 hours, both organoids differed only slightly in the overall size, but the dense packed organoid showed small and homogeneous sized cell nuclei whereas the loose packed organoid show big variations in the cell nuclei sizes. Furthermore, the loose packed organoid showed a high mobility of the cell nuclei within the organoid and a rotatory movement of the complete organoid. The dense packed organoid showed a high mobility and overall rotational movement only in the first 48 hours and stood more static with increased time. Microscope: Zeiss Lightsheet Z.1; detection objective: W Plan-Apochromat 20x/1.0, illumination objective: Zeiss LSFM 10x/0.2; laser line: 561 nm; filters: laser block filter (LBF) 405/488/561; voxel size: 1.02 x 1.02 x 2.00  $\mu\text{m}^3$ ; Shown is a Maximum Intensity projection (ImageJ/Fiji) of 170 z-slices; recording interval: 30 min; scale bar: 100  $\mu\text{m}$

**Movie 9: MPOs showed collective cell rotation.** The video shows one murine organoid as an excerpt from an entire culture grown within one Z1-FEP-foil cuvette. The organoids expressed Rosa26-nTnG (grey) as nuclei marker and were imaged over 17 hours. During the recorded time, the organoid showed a steady rotation of all cells. Cell segmentation and tracking revealed a rotational motion of all cells in the same direction. Microscope: Zeiss Lightsheet Z.1; detection objective: W Plan-Apochromat 20x/1.0, illumination objective: Zeiss LSFM 10x/0.2; laser line: 561 nm; filters: laser block filter (LBF) 405/488/561; voxel size: 1.02 x 1.02 x 2.00  $\mu\text{m}^3$ ; recording interval: 30 min; 3D rendering and tracking software: Arivis Vision4D.

**Movie 10: Alterations in rotational motion of two organoids in close neighbourhood.** The movie shows two mPOs grown within one Z1-FEP-foil cuvette as an excerpt from an entire culture. The organoids expressed Rosa26-nTnG (grey) as nuclei marker. Differences in cell nuclei size and overall behaviour are shown. Cell segmentation revealed that the small organoid (diameter at end of observation: 100  $\mu\text{m}$ ) with large nuclei (longest axis: 52  $\mu\text{m}$ ) show less cell divisions and less cell movement than larger organoids (diameter at end of observation: 180  $\mu\text{m}$ ) with smaller nuclei (longest axis: 32  $\mu\text{m}$ ). Further, the organoid with small nuclei showed more rotational motion and an overall tightly packed cell nuclei positioning in comparison to the organoid with the big nuclei. Microscope: Zeiss Lightsheet Z.1; detection objective: W Plan-Apochromat 20x/1.0, illumination objective: Zeiss LSFM 10x/0.2; laser line: 561 nm; filters: laser block filter (LBF) 405/488/561; voxel size: 1.02 x 1.02 x 2.00  $\mu\text{m}^3$ ; recording interval: 30 min; 3D rendering and tracking software: Arivis Vision4D.

**Movie 11: Organoids cell fragment motion prior formation.** The movie shows one murine organoid as an excerpt of an entire culture grown within one Z1-FEP-foil cuvette. The organoids expressed Rosa26-nTnG (grey) as nuclei marker. Before the organoid established its luminal character, the initially seeded organoid cell fragment migrates through the ECM for about 25 hours. Thereby it migrated about a 250  $\mu\text{m}$  distance with an average speed of 10  $\mu\text{m}$  (from green/minimum to red/maximum: 2.5  $\mu\text{m}/\text{h}$  – 23  $\mu\text{m}/\text{h}$ ). Microscope: Zeiss Lightsheet Z.1; detection objective: W Plan-Apochromat 20x/1.0, illumination objective: Zeiss LSFM 10x/0.2; laser line, 561 nm; filters: laser block filter (LBF) 405/488/561; voxel size: 1.02 x 1.02 x 2.00  $\mu\text{m}^3$ ; recording interval: 30 min; 3D rendering and tracking software: Arivis Vision4D.

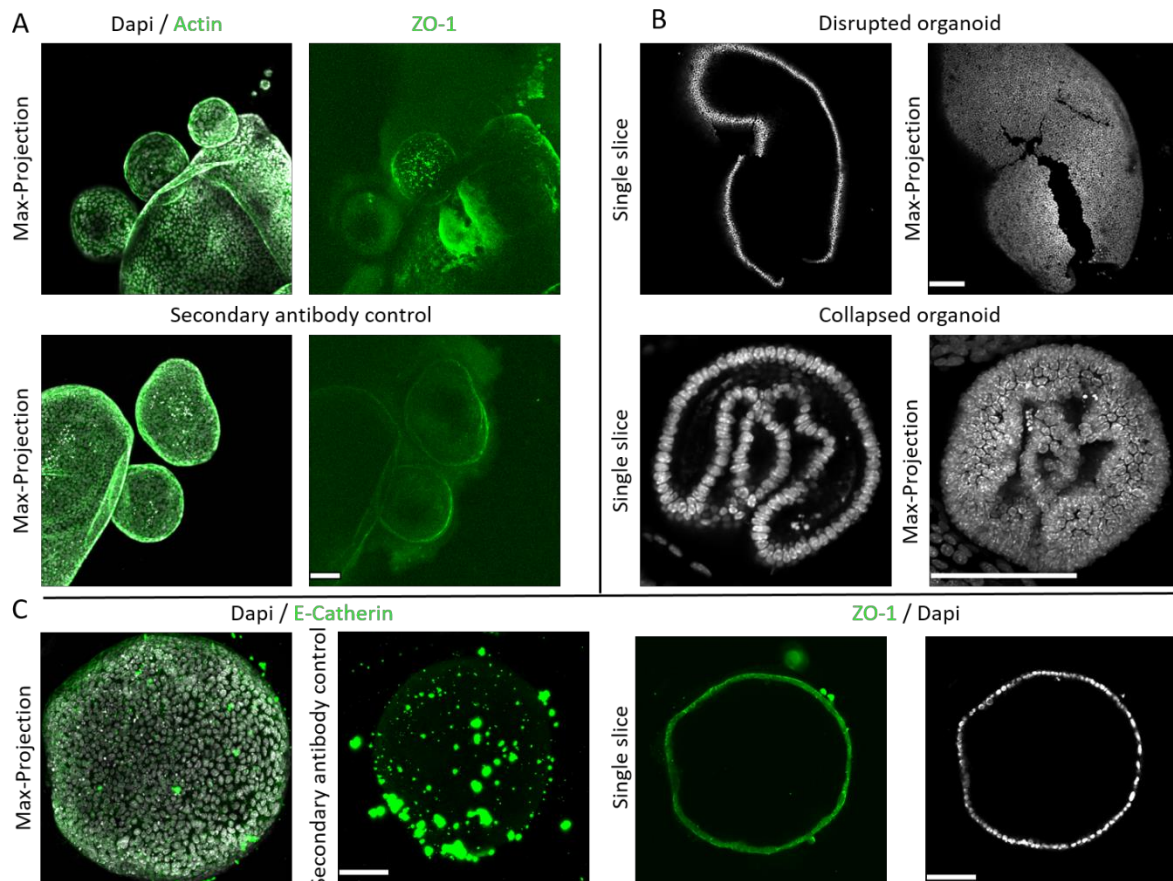
**Movie 12: MPO development from single, two and three cells within the FEP-foil cuvette.** From left to right, the organoid formation from one, two and three cells are shown. The organoid cells expressed Rosa26-nTnG (grey) as nuclei marker. The single cell showed one cell division after 4h whereas the two cells needed about 27 hours before on cell fulfilled one division. The organoid that started the formation out of three cells showed the first division event after 7 hours. All three organoids developed a lumen and showed a high dynamic in cell behaviour. Microscope: Zeiss Lightsheet Z.1; detection objective: W Plan-Apochromat 20x/1.0, illumination objective: Zeiss LSFM 10x/0.2; laser line, 561 nm; filters: laser block filter (LBF) 405/488/561; voxel size: 1.02 x 1.02 x 2.00  $\mu\text{m}^3$ ; recording interval: 30 min; scale bar: 10  $\mu\text{m}$

**Movie 13: Three representative mPOs processed with the Lightsheet segmentation pipeline.** The movie shows three murine organoids as an excerpt of an entire culture grown within one Z1-FEP-foil cuvette. The organoids expressed Rosa26-nTnG (grey) as nuclei marker. From top to bottom and left to right, the raw image and the segmented image sets of a small, middle and large organoids are shown. The colours are chosen randomly and represent one cell nuclei per time point. The corresponding processed data sets are shown in Figure 18. Microscope: Zeiss Lightsheet Z.1; detection objective: W Plan-Apochromat 20x/1.0, illumination objective: Zeiss LSFM 10x/0.2; laser line, 561 nm; filters: laser block filter (LBF) 405/488/561; voxel size: 1.02 x 1.02 x 2.00  $\mu\text{m}^3$ ; recording interval: 30 min; scale bar: 10  $\mu\text{m}$

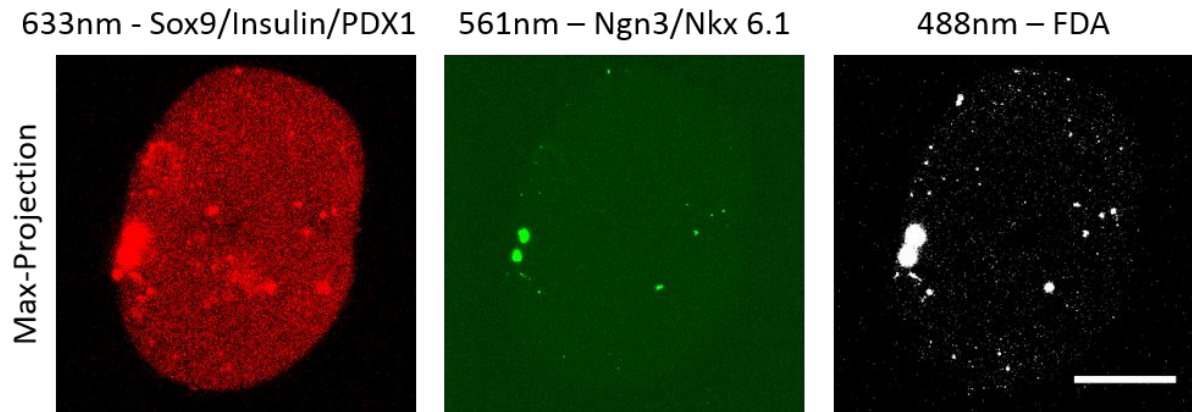
**Movie 14: One Organoid imaged for 48 hours, tracked and segmented in regard to single cells expansion agility and phylogeny.** The movie shows one big and many small murine organoids as an excerpt of an entire culture grown within one Z1-FEP-foil cuvette. The organoids expressed Rosa26-nTnG (grey) as nuclei marker and are imaged in total for 48 hours (interval 30 min). In the first part of the movie, the cells are segmented and tracked in regard to their speed of expansion (from green to red).

It becomes visible that not all cells within the organoid showed the same expansion speed and the same expansion agility. In the second part of the movie, the cells are tracked in regard to its phylogeny. It became visible that most the daughter cells stay in close contact to each other and stayed as clusters during the development of the organoid (cells with the same mother cells have the same colour, colours are chosen randomly). Microscope: Zeiss Lightsheet Z.1; detection objective: W Plan-Apochromat 20x/1.0, illumination objective: Zeiss LSM 10x/0.2; laser line, 561 nm; filters: laser block filter (LBF) 405/488/561; voxel size: 1.02 x 1.02 x 2.00  $\mu\text{m}^3$ ; recording interval: 30 min; scale bar: 10  $\mu\text{m}$

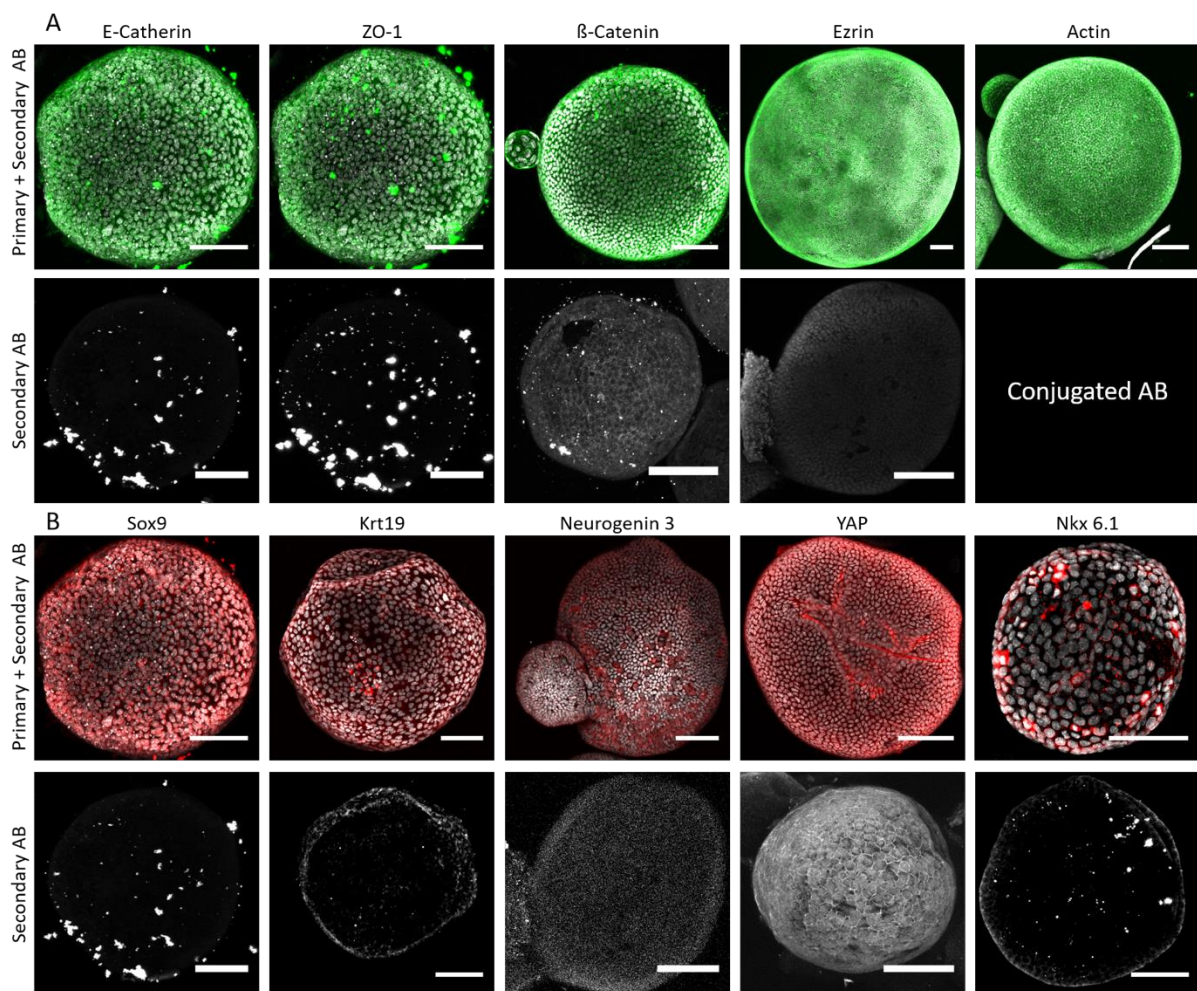
## 9.2. Supplemental material



**Supplemental Figure 1: Illustration of the challenges in organoid imaging** In (A) several mPOs are shown which were directly stained within the ECM. On the left side, a mPO which were directly labelled with Alexa Fluor® Phalloidin 488 against Actin (green) and Dapi against the cell nuclei (grey) are shown. A clear staining was archived without a high background signal. In contrast, (B) shows mPOs which were indirectly immunolabeled with a primary and secondary antibody against ZO-1 within the ECM. It became clear that a high background noise was present and that no specific signal was detectible. In (B) several mPOs stained with Dapi (grey) to illustrate the cell nuclei. After several washing and up-and-down pipetting steps with ice-cold PBS that served to degenerate the ECM, alterations in the phenotype in terms of collapsed and disrupted mPOs became present. In (C) results of the improved immunofluorescence labelling protocol are shown. On the left side, a Max-Projection of an organoid immunolabeled with an antibody against E-Catherin, and the corresponding control are shown. Only a minor number of residues of the ECM became visible and the secondary antibody control showed that no ECM surrounded the organoid. On the left side is a ZO-1 antibody labelled organoid illustrated. With the improved protocol a clear and specific signal was detected. Microscope: Zeiss LSM780, Objectives: Plan-Apochromat 20x/0.8, Plan-Apochromat 10x/0.3). Ex/Em: Dapi 405/462; ZO-1, 488/553; E-catherin, 633/699. Scale bar: 100  $\mu\text{m}$



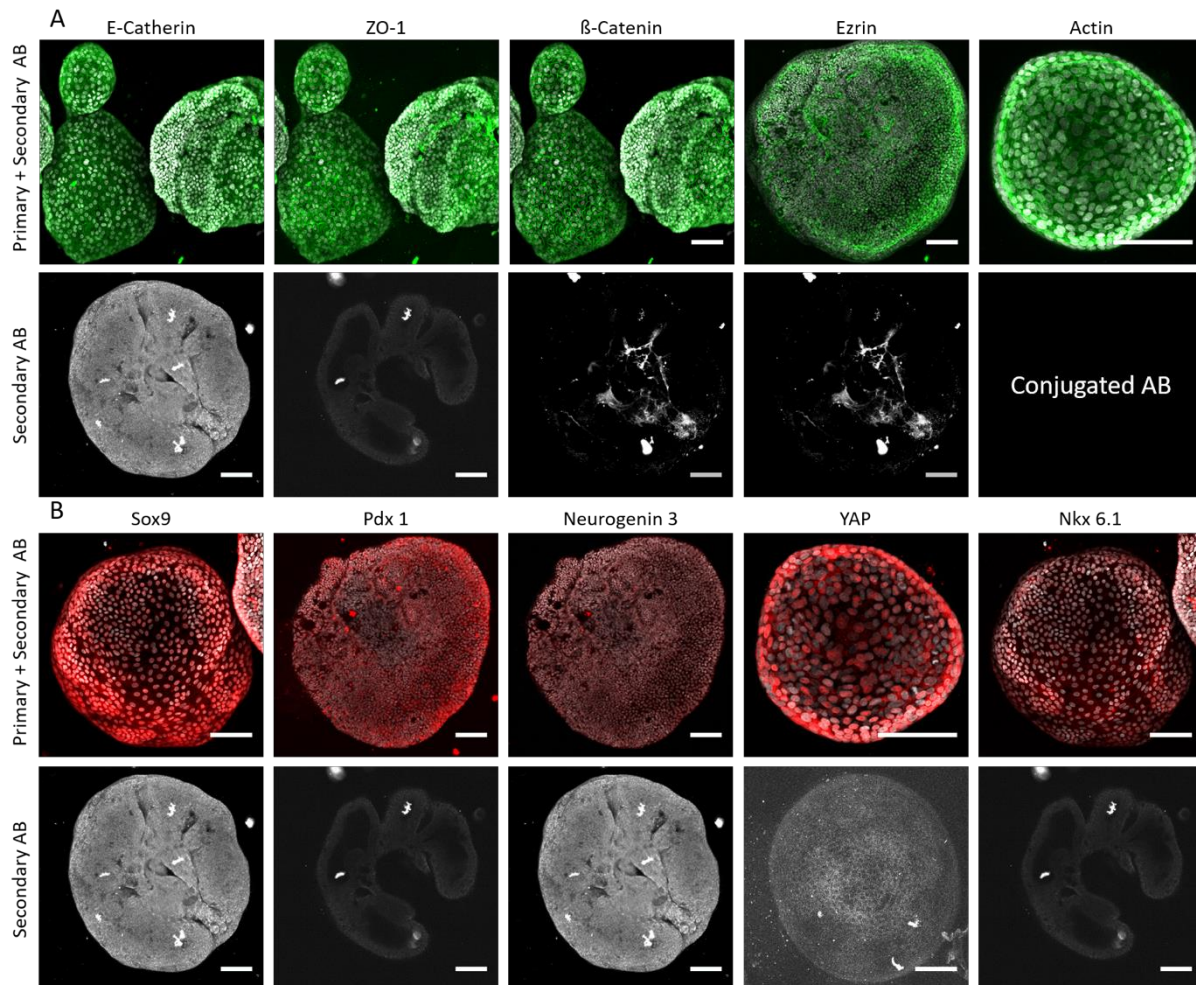
**Supplemental Figure 2: Secondary antibodies controls of immunolabeled islets of Langerhans.** Illustrated are the Max-Projection of the secondary antibody controls for the wavelength of 488 nm, used for FDA, 561 nm, used for the primary antibodies against Ngn3 and Nkx 6.1 as well as for 633 nm which was used for the primary antibodies against Sox9, Insulin and Pdx 1. The brightness was increased to display the scheme of the organoid, but no specific binding was detected. Microscope: Zeiss LSM780:EC-Plan Neofluar 40x/0.75, FDA 488/553, Sox9, Ngn3, Nkx 6.1 3 561/633; Insulin, Pdx 1 633/699. Scale bar: 100  $\mu$ m



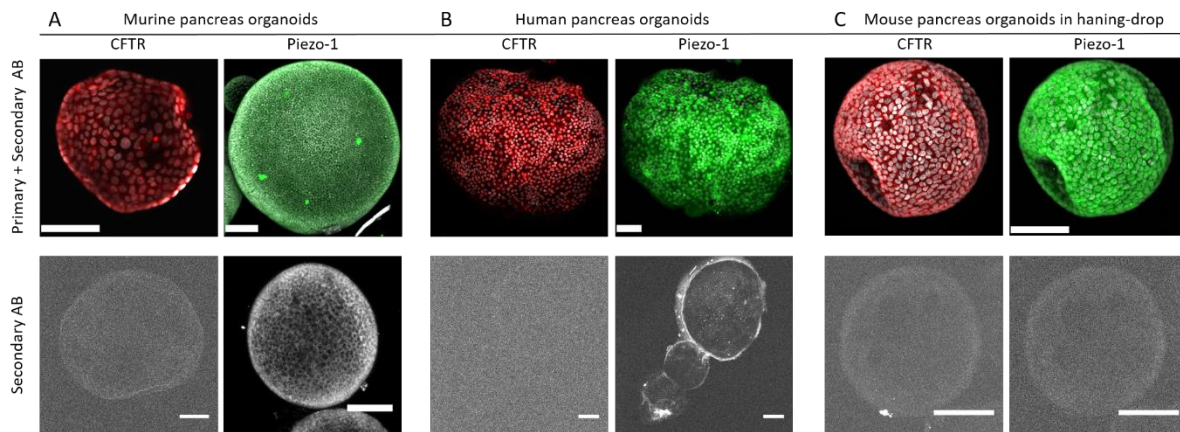
**Supplemental Figure 3: Secondary antibody controls of immunolabeled mPOs.** In (A) the Max-Projections of the immunolabeled mPOs with primary, secondary antibody and Dapi (cell nuclei, top row) and labelled with the secondary AB solely (lower row) are shown. The brightness is increased up to a point the scheme of the organoid becomes visible. No specific signal was observed at some of the used antibodies which illustrate the overall polarized and highly organized phenotype of



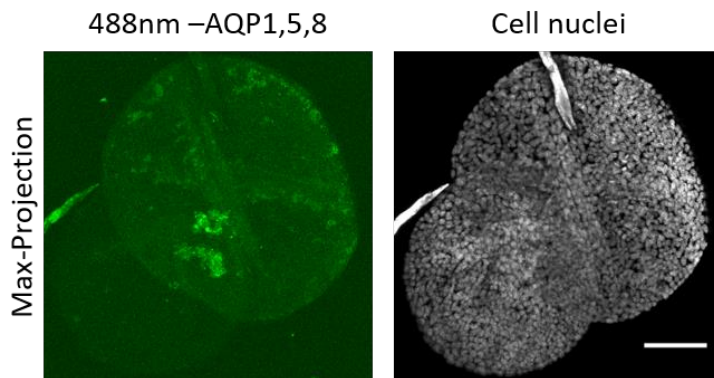
the mPOs. In (B) the Max-Projections of the immunolabeled mPOs with primary and secondary antibody (AB, top row) and labelled with the secondary AB solely (lower row) are shown. The brightness is increased up to a point the scheme of the organoid becomes visible. No specific signal was observed at some of the used antibodies which illustrate stem cell like fate of the mPOs. Microscope: Zeiss LSM780, Objectives: Plan-Apochromat 20x/0.8, Plan-Apochromat 10x/0.3 (Ezrin). Ex/Em: Dapi 405/462; Krt19, ZO-1, YAP, Nkx 6.1:  $\alpha$ -goat Alexa Fluor 488; Actin: Alexa Fluor<sup>®</sup> 546 Phalloidin; Sox9, Ezrin:  $\alpha$ -mouse Alexa Fluor 568; E-catherin,  $\beta$ -catenin, Ngn3:  $\alpha$ -rat Alexa Fluor 633. Scale bar: 100  $\mu$ m



**Supplemental Figure 4: Secondary antibody controls for immunolabeled hPOs.** In (A) the Max-Projections of the immunolabeled hPOs with primary, secondary antibody and Dapi (cell nuclei, top row) and labelled with the secondary AB solely (lower row) are shown. The brightness is increased up to a point the scheme of the organoid becomes visible. No specific signal was observed at some of the used antibodies which illustrate the overall polarized and highly organized phenotype of the hPOs. In (B) the Max-Projections of the immunolabeled hPOs with primary and secondary antibody (AB, top row) and labelled with the secondary AB solely (lower row) are shown. The brightness is increased up to a point the scheme of the organoid becomes visible. No specific signal was observed at some of the used antibodies which illustrate stem cell like fate of the hPOs. Microscope: Zeiss LSM780, Objectives: Plan-Apochromat 20x/0.8, Plan-Apochromat 10x/0.3 (Ezrin, CXCR4). Ex/Em (nm): Dapi: 405/462; Pdx 1, ZO-1, YAP, Nkx 6.1:  $\alpha$ -goat Alexa Fluor 488; Actin: Alexa Fluor<sup>®</sup> 546 Phalloidin; Sox9, Ezrin, Ngn3:  $\alpha$ -mouse Alexa Fluor 568; E-catherin,  $\beta$ -catenin, :  $\alpha$ -rat Alexa Fluor 633. Scale bar: 100  $\mu$ m



**Supplemental Figure 5: Secondary antibody control of the immunolabeled channel proteins CFTR and Piezo-1 in mPOs, hPOs and mPOs grown in HD.** In (A) the Max-Projections of the immunolabeled mPOs with primary and secondary antibody against CFTR ( $\alpha$ -mouse Alexa Fluor 568) and Piezo 1 ( $\alpha$ -rabbit Alexa Fluor 488) (top row) and labelled with the secondary AB solely (lower row) are shown. The brightness is increased up to a point the scheme of the organoid becomes visible. The secondary AB control of Piezo-1 appears bright, but a direct comparison with the primary antibody illustrates clear differences which shows the specific binding of the primary Ab conjugated with the secondary. In (B) the Max-Projections of the immunolabeled hPOs with primary and secondary antibody against CFTR and Piezo 1 (AB, top row) and labelled with the secondary AB solely (lower row) are shown. In both cases neither a signal at all (CFTR) nor a specific signal (Piezo-1) was detected. In (C) the Max-Projections of the immunolabeled mPOs grown in the HD system with primary and secondary antibody against CFTR and Piezo 1 (AB, top row) and labelled with the secondary AB solely (lower row) are shown. The brightness is increased up to a point the scheme of the organoid becomes visible. No specific signal was detected in the secondary AB control. Microscope: Zeiss LSM780, Objectives: Plan-Apochromat 20x/0.8. Ex/Em: Dapi 405/462; Piezo-1 488/553; CFTR 561/633. Scale bar: 100  $\mu$ m



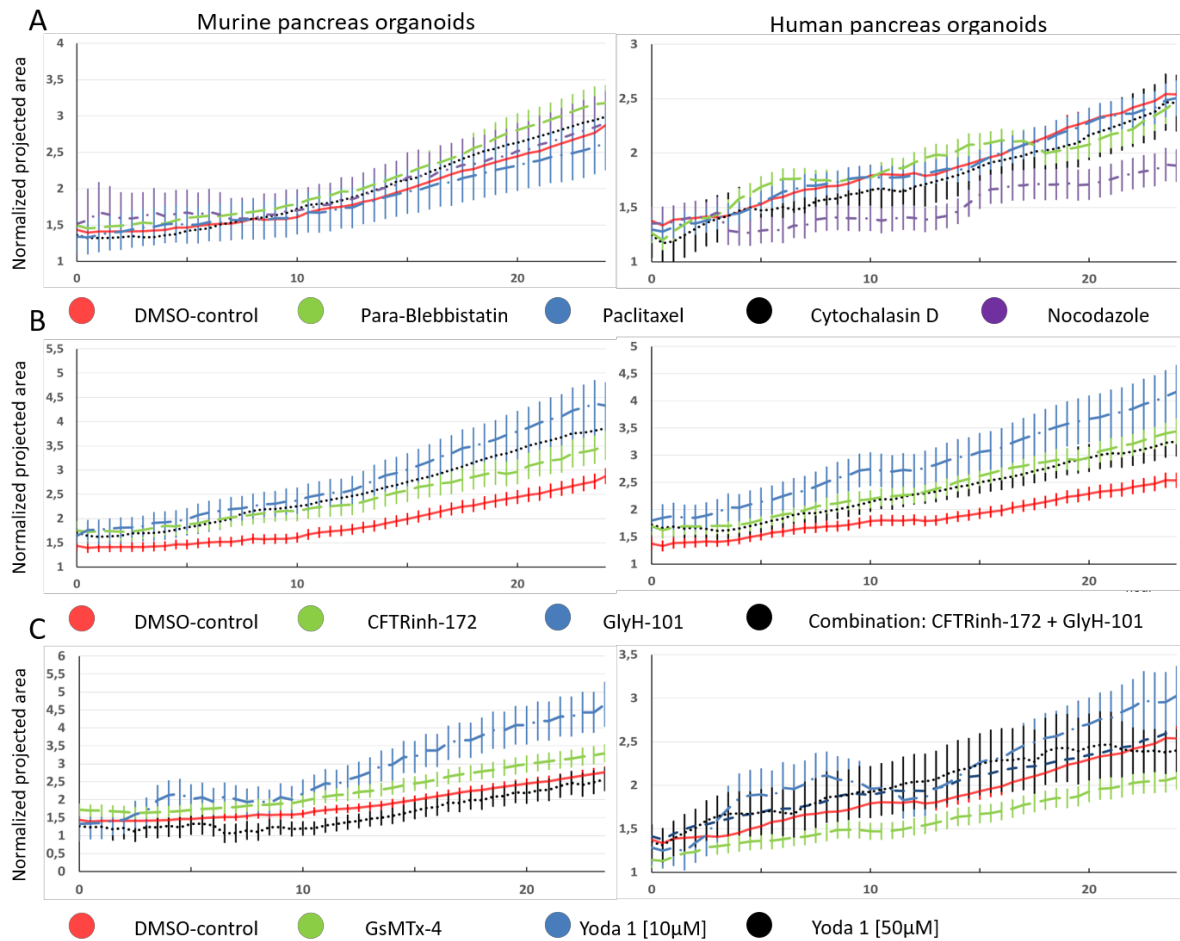
**Supplemental Figure 6: Secondary antibody control of the immunolabeled channel proteins Aquaporin 1, 3 and 8 in mPOs.** Illustrated are the Max-Projections of the immunolabeled mPOs with the secondary antibody against AQP 1,3 and 8 ( $\alpha$ -rabbit Alexa Fluor 488) and Dapi to illustrate the cell nuclei. The brightness is increased up to a point the scheme of the organoid becomes visible. No specific signal was detectible. Microscope: Zeiss LSM780, Objectives: Plan-Apochromat 20x/0.8. Ex/Em: Dapi 405/462; Piezo-1 488/55. Scale bar: 100  $\mu$ m

**Supplemental table 1: Splitting data of two mPO organoid lines grown in the HD.** Illustrated are the date of splitting, the number of days between the splitting, the corresponding splitting ratio, the calculated splitting factor with the theoretical number of generated drops based on the real splitting ratio (starts with one drop), the total days in culture and the overall passage number of the culture.

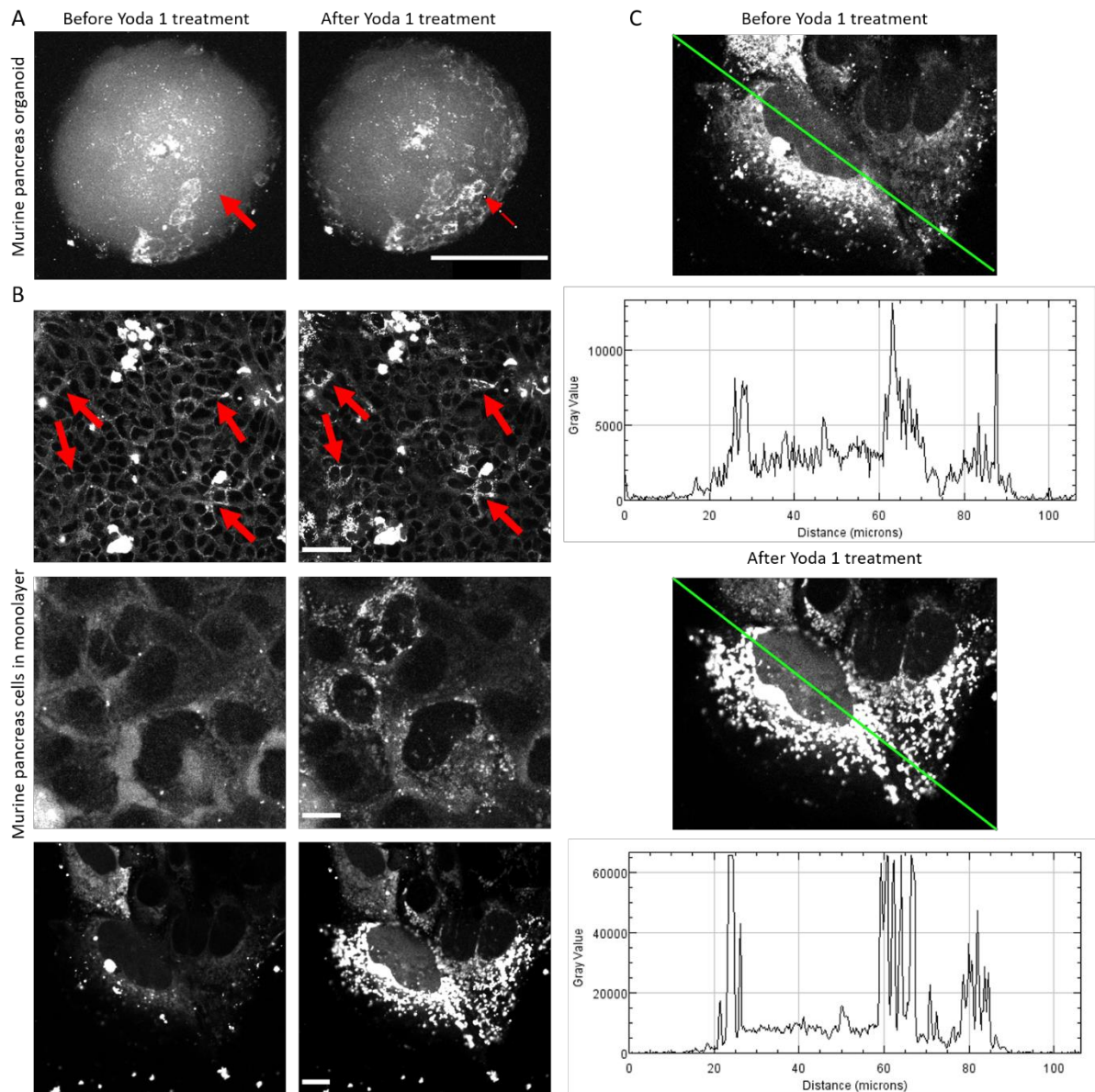
**Culture 1**

<i>Day of splitting</i>	Days between splitting	Splitting ratio	Splitting factor	Theoretical number of drops based on the splitting factor	Days in culture	Passage number
04.01.2018		01:06	6,00	1,00	1,00	55
11.01.2018	7,00	01:04	4,00	4,00	7,00	56
23.01.2018	12,00	02:03	1,50	6,00	19,00	57
01.02.2018	9,00	01:05	5,00	30,00	28,00	58
08.02.2018	7,00	01:04	4,00	120,00	35,00	59
16.02.2018	8,00	01:05	5,00	600,00	43,00	60
26.02.2018	10,00	01:05	5,00	3000,00	53,00	61
06.03.2018	8,00	01:05	5,00	15000,00	61,00	62
13.03.2018	7,00	09:20	2,20	33000,00	68,00	63
20.03.2018	7,00	02:05	2,50	82500,00	75,00	64
27.03.2018	7,00	02:05	2,50	206250,00	82,00	65
03.04.2018	7,00	07:16	2,28	470250,00	89,00	66
10.04.2018	7,00	01:03	3,00	1410750,00	96,00	67
17.04.2018	7,00	01:03	3,00	4232250,00	103,00	68
24.04.2018	7,00	01:03	3,00	12696750,00	110,00	69
02.05.2018	8,00	01:03	3,00	38090250,00	118,00	70
09.05.2018	7,00	01:03	3,00	114270750,00	125,00	71
15.05.2018	6,00	01:03	3,00	342812250,00	131,00	72
22.05.2018	7,00	01:03	3,00	1028436750,00	138,00	73

29.05.2018	7,00	01:01	1,00	1028436750,00	145,00	74
05.06.2018	7,00	01:03	3,00	3085310250,00	152,00	75
14.06.2018	9,00	01:03	3,00	9255930750,00	161,00	76
21.06.2018	7,00	01:03	3,00	27767792250,00	168,00	77
28.06.2018	7,00	01:03	3,00	83303376750,00	175,00	78
05.07.2018	7,00	01:02	2,00	166606753500,00	182,00	79
12.07.2018	7,00	01:03	3,00	499820260500,00	189,00	80
<b><u>Culture 2</u></b>						
23.04.2018		2x50 µl		1,00	1,00	1
07.05.2018	14,00	01:01	1,00	1,00	15,00	2
14.05.2018	7,00	01:02	2,00	2,00	22,00	3
18.05.2018	4,00	01:03	3,00	6,00	26,00	4
24.05.2018	6,00	03:05	5,00	30,00	32,00	5
29.05.2018	5,00	01:04	4,00	120,00	37,00	6
05.06.2018	7,00	01:02	2,00	240,00	44,00	7
12.06.2018	7,00	01:02	2,00	480,00	51,00	8
19.06.2018	7,00	01:02	2,00	960,00	58,00	9
26.06.2018	7,00	01:03	3,00	2880,00	65,00	10
03.07.2018	7,00	01:03	3,00	8640,00	72,00	11
09.07.2018	6,00	01:02	2,00	17280,00	78,00	12
16.07.2018	7,00	01:04	4,00	69120,00	85,00	13
23.07.2018	7,00	01:04	4,00	276480,00	92,00	14
30.07.2018	7,00	02:09	4,50	1244160,00	99,00	15



**Supplemental Figure 7: MPO and hPO pre-treatments to identify that the lumen maintenance is tubulin-, actin-myosin, CFTR and Piezo-1-dependent.** Illustrated are the imaged and analysed 24 h pre-treatments of murine (left) and human (right) organoids as a control to guarantee normal and comparable growth rates before the treatments against specific cytoskeleton and channel proteins were conducted. The different colours illustrate the analysed organoids 24 h before medium was replaced with the corresponding conditioned medium to inhibit MT, Actin, Myosin (purple dashed line (mPO: n~15, hPO: n~120): Nocodazol (1 µM), blue dashed line (mPO: n~65, hPO: n~189): Paclitaxel (100 µM), black pointed line (mPO: n~100, hPO: n~40): Cytochalasin D (10 µM), green interrupted line (mPO: n~100, hPO: n~115): Para-Blebbistatin (50 µM) and the channel protein CFTR (green interrupted line (mPO: n~250, hPO: n~210): CFTR-172 (50 µM), blue dashed line (mPO: n~220, hPO: n~160): GlyH-101: 50 µM, black pointed line Combination (mPO: n~200, hPO: n~170): 50 µM CFTR-172 + 50 µM GlyH-101). Further, the growth curves of the pre-treatments to block and activate Piezo-1 are shown (green interrupted line (mPO: n~240, hPO: n~345): GsMTx (10 µM), blue dashed line (mPO: n~100, hPO: n~110): Piezo-1 (10 µM), black pointed line (mPO: n~50, hPO: n~60): Piezo-1 (mPO: 50 µM, hPO: 25 µM). No significant differences were detected between the DMSO control group and the different organoids that were later on treated with the corresponding substances (Mann-Whitney  $p < 0.05$ ).



**Supplemental Figure 8: Illustration of the  $Ca^{2+}$  influx in mPO cells upon Yoda 1 ( $50 \mu\text{m}$ ) treatment measured with Fluo8-AM.** In (A) one organoid is shown which was stained with Fluo8-AM ( $5 \mu\text{m}$ ) for one hour and imaged with confocal microscopy before (left) and after (right) the treatment with  $50 \mu\text{m}$  Yoda 1 solution to activate Piezo-1. All images were conducted with the same settings. An overall increase of the fluorescence signal was detected whereas depicted organoid cells show local differences in the reaction (red arrow). In (B) the same setup as in (A) was used to illustrate and measure the influence of Yoda 1 treatment to a monolayer of mPO cells. Again, an overall increase of fluorescence signal was detected upon Yoda 1 treatment (left). The upper lane illustrates an overview of the monolayer of cells and the red arrows indicate clusters of cells which shows an increase in the Fluo8-AM signal after the treatment. The middle and bottom lane shows two additional tests and the corresponding close-ups of a cell cluster (mid-lane) and a single cell (bottom-lane) upon Yoda 1 treatment. A punctuated and strong increase of the signal was detected. In (C) the fluorescence single from the single cell from (B) was measured. The corresponding histograms (compute along the green line) showed a massive increase in the fluorescence signal value of Fluo8-AM after the treatment with Yoda 1. Microscope: Zeiss LSM780, Objectives: (A) Plan-Apochromat 20x/0.8. (B and C) Plan-Apochromat 63x/1.40 Oil DIC, Ex/Em: 488/559.

Treatment



Supplemental Figure 9: Illustration of the Mann-Whitney-U test of data obtained with the brightfield pipeline for mPOs. Illustration of the Mann-Whitney-U test of the Data obtained with the brightfield pipeline for organoids treated with different drugs to inhibit the cytoskeletal components Actin (Cytochalasin D), MTs (Nocodazole, Paclitaxel), the motor protein Myosin II (Para-Blebbistatin), the channel protein CFTR (CFTRinh-172 and GlyH101) and to block (GsmTx) and activate (Yoda 1) the mechanosensitive cation channel Piezo-1 are shown. The lower right data illustrate the Mann-Whitney-U test to the data of the recovery potential of the organoids size after the treatment with 50 µM CFTRinh-172 and GlyH-101.

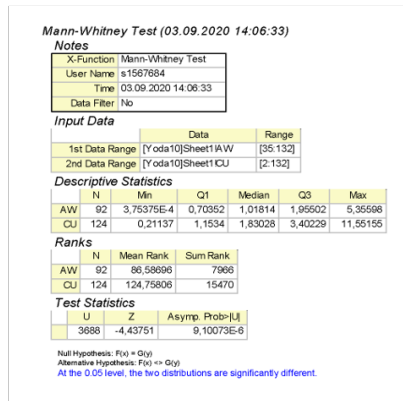
Treatment



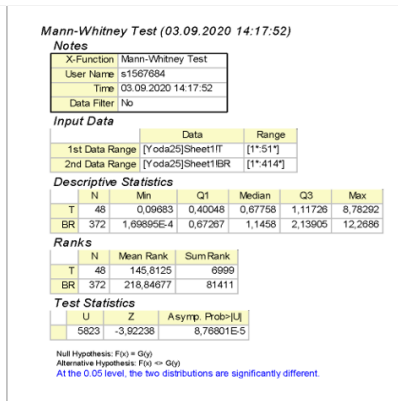
Supplemental Figure 10: Illustration of the Mann-Whitney-U test of the data obtained with the brightfield pipeline for hPOs. From left to right the results of the Mann-Whitney-U tests to the data obtained from the brightfield pipeline for organoids treated with different drugs to inhibit the cytoskeletal components Actin (Cytochalasin D), MTs (Nocodazole, Paclitaxel), the motor protein Myosin II (Para-Blebbistatin), the channel protein CFTR (CFTRinh-172 and GlyH101) and to block (GsmTx) and activate (Yoda 1) the mechanosensitive cation channel Piezo-1 (referee Figure XX.) are shown (referee to Figure XX.).



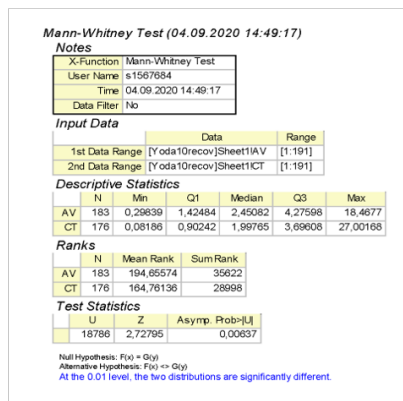
Treatment: 10µM Yoda 1



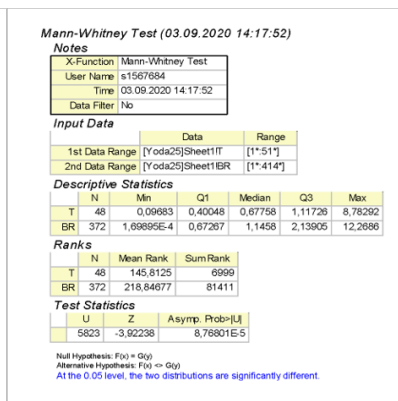
Treatment: 25µM Yoda 1



Recovery: 10µM Yoda 1



Recovery: 25µM Yoda 1



**Supplemental Figure 11: Illustration of the Mann-Whitney-U test for the data obtained with the pipeline for hPOs from the treatment with Yoda 1.** The upper row shows the results of the Mann-Whitney-U-test to the data obtained from the brightfield pipeline for organoids treated with Yoda 1 to inhibit the mechanosensitive channel Piezo-1. The lower row shows the results of the test for the recovery potential of the organoids after the treatment with Yoda 1 (referee to Figure XX.).

## 10. Curriculum Vitae

Name	Till Seeberger (geb. Moreth)
Adresse	Arndtstraße 44 60325 Frankfurt am Main
E-Mail	Till.Seebeger@gmx.de
Telefon	0171/1782127
Geburtsdatum / -ort	8. August 1988 / Darmstadt



### Berufserfahrung

---

08/2016-06/2020

#### **Wissenschaftlicher Mitarbeiter (Promotion)**

Physical Biology Group, Prof. Dr. Ernst H.K Stelzer, Goethe Universität Frankfurt a. M.,  
Buchmann Institute for Molecular Life Science

05/2015-12/2015

#### **Junior Consultant**

BCNP-Consultant GmbH, Frankfurt a. M.

12/2014-05/2015

#### **Wissenschaftliche Hilfskraft**

Physical Biology Group, Prof. Dr. Ernst H.K Stelzer, Goethe Universität Frankfurt a. M.,  
Buchmann Institute for Molecular Life Science

### Ausbildung

---

Seit 08/2016

#### **Promotion an der Goethe Universität Frankfurt a. M.**

Physical Biology Group, Prof. Dr. Ernst H.K Stelzer, Buchmann Institute for Molecular Life  
Science

10/2012-11/2014

#### **Master of Science, Interdisciplinary Neuroscience, Goethe Universität Frankfurt a. M.**

Physical Biology Group, Prof. Dr. Ernst H.K Stelzer, Buchmann Institute for Molecular Life  
Science, Goethe-Universität

- Masterthesis: "High resolution imaging of single cell migration in 3D-glioma cell spheroids during autophagy"
- Abschlussnote: 1,6 (Masterthesis: 1,3)

10/2009-07/2012

#### **Bachelor of Science, Biowissenschaften, Goethe Universität Frankfurt a.M.**

Institut für Bienenkunde, Prof. Dr. Bernd Grünewald

- Bachelorthesis: „Einfluss von Koffein auf die Mobilität von *Apis mellifera* (Honigbiene) in einer optimierten Versuchsanordnung“
- Bachelorthesis: 1,3

## Publikationen

---

Jung, N.\* and **Moreth, T.\*** (2021), 'First-time non-invasive analysis of pancreas organoids in defined hydrogels'. Application in process.

Hof, L., **Moreth, T.**, (2021). Long-term live imaging and multiscale analysis identify heterogeneity and core principles of epithelial organoid morphogenesis. *BMC Biology*, 19(1), 37. doi: 10.1186/s12915-021-00958-w

Hof, L.\* and **Moreth, T.\*** (2020), 'Long-term image-based multiscale analysis of live epithelial organoids reveals high heterogeneity and identifies core regulatory principles'. Under review (BMCB). BioRxiv: 10.1101/2020.07.12.199463

Gupta, J., Schmitt, M., Nicolas, A., Pesic, M., Pallangyo, C., Varga, J., Ramakrishnan, M., Ablasser, A., **Moreth, T.**, Stelzer, E.H.K., Karimova, M., Sato, T., J de Sauvage, F., Greten, F.R. (2020), 'Paracrine mTOR activation and BMP inhibition preserve colorectal tumor maintenance upon Lgr5+ cell loss'. Under review (Nature)

Dolezalova, N., Gruszczuk, A., Barkan, K., Gamble, K.J., Galvin, S., **Moreth, T.**, O'Holleran, K., Mahbubani, K.T., Higgins, J.A., Gribble, F.M., Reimann, F., Surmacki, K., Andrews, S., Casey, J.J., Pampaloni, F., Murphy, M.P., Ladds, G., Slater, N.K.H., Saeb-Parsy, K. (2020), 'Accelerating cryoprotectant diffusion kinetics improves cryopreservation of pancreatic islets'. Under review (Nature communications)

Dossena, M., Piras, R., Cherubini, A., Barilani, M., Dugnani, E., Salanitro, F., **Moreth, T.**, Pampaloni, F., Piemonti, L., Lazzari, L. (2020), 'Standardized GMP-compliant scalable production of human pancreas organoids', *Stem Cell Research & Therapy*. *Stem Cell Research & Therapy*, 11(1), p. 94. doi: 10.1186/s13287-020-1585-2.

## Talks

---

- |                                   |  |
|-----------------------------------|--|
| November 2019, LFSM2019:<br>Milan | In toto analyses of epithelial organoids reveal high intracultural heterogeneity                                     |
| September 2019, EARC:<br>Berlin   | Behind the scenes – PIEZO1 and CFTR mediate the cystic structure of pancreatic organoids                             |
| März 2019, Leopoldina:<br>Venice  | Using light sheet-based fluorescence microscopy: from thick histological sections to observations of live organoids. |

## Poster

---

- Lausanne 2017, Engineering multicellular self-organization, EPFL:  
Multiscale light microscopy analysis of pancreatic organoid cultures
- Heidelberg 2018, Organoids 2018, EMBL:  
The traction force linker PIEZO1 and the CFTR ion channel are key transducers of mechanical forces in growing pancreatic organoid

Milan 2019, European Organoid Symposium 2019:

Behind the scenes – PIEZO1 and CFTR mediate the cystic structure of pancreatic organoids

Berlin 2019, Goodbye Flat Biology 2019:

Behind the scenes – PIEZO1 and CFTR mediate the cystic structure of pancreatic organoids

## Lehre

---

Kurse: Organisation und Betreuung von Großpraktika des Master-Studiengangs *Physical Biology of Cells and Cell Interaction* (früher „*Cell Biology and Physiology*) und *Interdisciplinary Neuroscience* von 2014 bis 2020

Studenten: Spezialisierungsmodul IV Neurobiologie II des Bachelorstudiengangs Biowissenschaften WS 2016/2017 und WS 2017/2018

Betreuung des Methodenpraktikums im Masterstudiengang *Physical Biology of Cells and Cell Interaction* (Bianca Rodrigues, Christopher Raab, Maximilian Brückner, Sertap Öztürk, Yi-Hsuan Lin)

Betreuung Schülerpraktikum (Tina Baharloo)

Betreuung der Masterarbeit im Masterstudiengang *Cell Biology and Physiology* (Julia Tarnick)

Betreuung der Current Concepts und der Masterarbeit im Masterstudiengang *Physical Biology of Cells and Cell Interaction* (Kaja Nicole Wächtershäuser)

## Sprachen

---

German (native), English (fluent)

## Ehrenamtliche Tätigkeiten

---

01/2017-06/2020

### **PhD-Repräsentant des Buchmann Institute for Molecular Life Science**

- Organisation von drei BMLS Student & Postdoc – Symposien (2017-2019) und dem BMLS Career-day (2019) sowie die Initiierung der BMLS PhD-Gartens
- Gestaltung und Initiierung des IQBio-Programms der Goethe-Universität
- Mitstimm- und Gestaltungsrecht bei institutsinternen Beschlüssen
- Repräsentation des Institutes bei universitären und öffentlichen Veranstaltungen

03/2005-10/2012

### **Hockeytrainer von Kindern und Jugendmannschaften, Tennis und Eis Club (TEC) Darmstadt**

## 11. Erklärung

Ich erkläre hiermit, dass ich mich bisher keiner Doktorprüfung im Mathematisch-Naturwissenschaftlichen Bereich unterzogen habe.

Frankfurt am Main, den 13.4.2021



Till Seeberger

## 12. Versicherung

Ich erkläre hiermit, dass ich die vorgelegte Dissertation über „Pancreas organoid development, behaviour and structural maintenance: a multiscale analysis“ selbständig angefertigt und mich anderer Hilfsmittel als der in ihr angegebenen nicht bedient habe, insbesondere, dass alle Entlehnungen aus anderen Schriften mit Angabe der betreffenden Schrift gekennzeichnet sind.

Ich versichere, die Grundsätze der guten wissenschaftlichen Praxis beachtet, und nicht die Hilfe einer kommerziellen Promotionsvermittlung in Anspruch genommen zu haben.

Frankfurt am Main, den 13.4.2021



Till Seeberger